NOTICE

The quality of this microform is heavily dependent upon the quality of the original thesis submitted for microfilming. Every effort has been made to ensure the highest quality of reproduction possible.

If pages are missing, contact the university which granted the degree.

Some pages may have indistinct print especially if the original pages were typed with a poor typewriter ribbon or if the university sent us an inferior photocopy.

Reproduction in full or in part of this microform is governed by the Canadian Copyright Act, R.S.C. 1970, c. C-30, and subsequent amendments.

AVIS

La qualité de cette microforme dépend grandement de la qualité de la thèse soumise au microfilmage. Nous avons tout fait pour assurer une qualité supérieure de reproduction.

S'il manque des pages, veuillez communiquer avec l'université qui a conféré le grade.

La qualité d'impression de certaines pages peut laisser à désirer, surtout si les pages originales ont été dactylographiées à l'aide d'un ruban usé ou si l'université nous a fait parvenir une photocopie de qualité inférieure.

La reproduction, même partielle, de cette microforme est soumise à la Loi canadienne sur le droit d'auteur, SRC 1970, c. C-30, et ses amendements subséquents

ISBN 0-315-53227-0

Canada

UNIVERSITÉ D'OTTAWA
UNIVERSITY OF OTTAWA

To my Wife Wegesa

PREFACE

The study of upd of metal and H adatom arrays on metal electrode surfaces has provided an area of major interest in surface science in general and electrochemical surface science in particular because of its importance in understanding a wide variety of electrochemical phenomena such as adsorption, charge-transfer, surface diffusion and electrocatalysis. Using cyclic-voltammetry or single-sweep potentiodynamic methods, the i vs E profiles for the upd of metal or H adatom on electrode surfaces are characterized by multiple-state adsorption below the monolayer limit of coverage. In the case of the upd of Pb on Au, from aq. $HClO_4$, up to seven distinguishable submonolayer states are observed. Even on well prepared single crystal surfaces, multiple-state adsorption arises indicating successive development of lattice arrays that can be commensurate or non-commensurate with the substrate electrode lattice.

Although the upd of metal and H adatom arrays on foreign metal substrates has been studied extensively over a number of years, the role that the solvent may play in modifying the upd profiles has received little attention todate.

Studying the upd of Pb at Au in various solvents therefore provides the means of comparison with the well recognized results obtained in aqueous media. Solvent effects in the upd profiles of metal adatoms can arise due to: a) Competition between electrodeposition of metal adatoms and desorption of solvent molecules. The upd process is thus a replacement reaction and its energetics depend on the difference between adsorption energy of the adatoms and the desorption energy of the appropriate number of the solvent molecules; b) An indirect effect due to solvent-dependent anion adsorption.

Solvent effects will be most pronounced for the initial stages of Pb adatom deposition, as is found experimentally, because most of the electrode surface will be covered by the solvent molecules. The former effect will be significant when the solvent interaction with the outside of the upd array is different from that initally at the metal substrate surface. Also, changes of potential of zero charge upon upd of e.g. Pb at Au can lead to changes of electrolyte anion adsorption and of

solvent dipole orientation.

Interest in upd behaviour in non-aqueous systems arises for three reasons: (i) The deposition profile may be solvent-dependent if solvent displacement by the deposited adatom introduces an irreversible process in the upd; (ii) The upd profiles and the kinetics of the upd processes can be studied down to quite low temperatures, especially in MeOH, and the kinetics may be solvent-dependent; (iii) Anion adsorption effects are solvent-dependent on account of varying strength of solvation in media of differing dielectric constant and electron donicity or accepting power; and (iv) From the change of peak potentials with temperature, the entropies of upd states, relative to the bulk state, can be determined.

Previous studies have shown that usually co-adsorbed anions (Cl^-, Br^-, I^-) have marked effects on the i vs E upd profiles of H at Pt, Pb at Au and the initial stages of surface oxidation of Pt or Au. In the case of Pb at Au the effects of co-adsorbed anions from very low concentrations (10^{-7} or 10^{-6}M) have not hitherto been investigated . One of the aims of the work decribed in this thesis is to study in detail the effect of co-adsorbed anions and thiourea (a neutral molecule which behaves like an ion) on the i vs E upd profile over a wide concentration range, starting with very low concentrations. Effects for the different anions are expected to be different since anion adsorption is solvent-dependent and different adsorbabilities will be manifested. It is also interesting to compare the effect of a strongly adsorbing neutral molecule (thiourea) with those of anions.

In addition to the thermodynamic behaviour of 2-d upd array formation processes, the kinetics of electrodeposition and desorption can also be evaluated for each distinguishable state by measurement of the peak potentials in linear potential-sweep experiments as a function of the log of the sweep-rate, s, giving the s_o value, the maximum sweep-rate for which the surface process just remains reversible. The s_o value characterizes the kinetics of a surface process (analogous to the exchange current-density, i_o, for a regular continuous Faradaic process) at the equilibrium potential, $E_{p,o}$, for each distinguishable array. It has the advantage over i_o for kinetic evaluations in that the real area of the electrode surface is not a required parameter.

When the entropy of the particles in a monolayer can be determined, information is given

about the nature and states of the adsorbed layer, e.g. mobility or immobility of the particles in the ad-layer can be distinguished. The distinguishable submonolayer states, e.g. 4 or 5 for H at Pt or 6 to 7 for Pb at Au have temperature-dependent standard free energies of electrodeposition and ionization which enable the corresponding standard entropies of adsorption, $\Delta\bar{S}^{\circ}$, to be evaluated.

Most of the work described in this thesis is in preparation for publication as follows:

1. Characterization of UPD Processes in Pb Deposition from Non-aqueous Protic and Aprotic Solvents. J.S. Chacha and B.E. Conway, and K. Tellfesen, Extended Abstract No. 483, Electrochemical Society Symposium, Philadelphia, Pennsylvania, May 10 - 15, 1987.

2. Temperature and Anion Effects on the UPD of Pb on Au. J.S. Chacha and B.E. Conway, Extended Abstract No. 496, Electrochemical Society Symposium, Atlanta, Georgia, May 15 - 20, 1988.

ACKNOWLEDGEMENTS

I wish to express my sincere gratitude to my research supervisor, Prof. Brian E. Conway, for his help and guidance throughout this study. The fruitful discussions with Prof. Conway, his valuable comments and the assistance during the preparation of thesis are highly acknowledged.

My thanks are also to Dr. H. Angerstien-Kozlowska for occasional help and discussions in the course of this study.

I would like to thank all my colleagues in the electrochemistry laboratory with whom I have worked over the past years for their support, advice, discussions and the many enjoyable and memorable moments we shared. My special thanks are to K. Tellfesen, who introduced me to cyclic-voltammetry experiments and D.P. Wilkinson for his advice on non-aqueous work, at the initial stages of this work. My thanks are also to my friends and others who supported me in one or the other during this study.

My sincere thanks are to Mr. Egon Kristof for the assitance in designing and construction of the glass-ware used in the present study and Ms. Eva Szabo for assitance in the preparation of the diagrams. My thanks are also extended to Mr. Joseph Halpern for sovling some of the electrical problems. The assistance of the other members of the support staff is also acknowledged.

The award of Commonwealth Scholarship by the Canadian Government for this graduate work and the Study Leave granted by Kenyatta University are greatly acknowledged.

Above all, I am greatly indebted to my wife, Wegesa, for her love, patience, encouragement and support throughout this work.

TABLE OF CONTENTS

	Page No.
PREFACE	i
ACKNOWLEDGEMENTS	iv
TABLE OF CONTENTS	v
LIST OF FIGURES	xiii
LIST OF TABLES	xxvi
ABSTRACT	xxvii

CHAPTER 1

GENERAL INTRODUCTION		1
1.1	Underpotential Deposition (UPD) of Atomic Monolayers on Metal Electrodes	1
	1.1.1 Introduction	1
	1.1.2 Previous Studies of UPD Processes	2
	1.1.3 UPD Studies in Non-aqueous Solvents	5
	1.2 Previous Studies of the UPD of Pb at Au	6
1.3	Specular Reflectance Studies of Surface Films	9
	1.3.1 Introduction	9
	1.3.2 Theory	10
	1.3.3 Specular Reflectance Studies of Pb Adatoms on Au	11
1.4	UPD of Pb on Au Single crystals: Effect of Crystallographic Orientation	13
1.5	Multiple-State Adsorption in UPD	13
	1.5.1 Origin of Multiple-State Adsorption	13

		Page No.
1.6	Chemisorption on Metals	16
	1.6.1 Adatom-Adatom Interactions among Adsorbates	18
	1.6.2 Simple Chemisorption Theory	19
1.7	Adsorption Isotherms for Atoms in Monolayers	20
	1.7.1 Langmuir Isotherm	21
	1.7.2 Frumkin Isotherm	22
	1.7.3 Adsorption Pseudocapacitance for a (UPD) Surface Process	22
1.8	2-Dimensional Array Structures on Substrate Surfaces	24
1.9	Effects of Co-adsorbed Anions	25
1.10	Substitutional Adsorption at Electrodes	27
1.11	Double-layer Structure in Non-aqueous Media and the Role of Solvent Orientation	27
1.12	Models for Solvent Dipole Orientation at charged Interfaces	30
	1.12.1 Introduction	30
	1.12.2 The Two-State Model	31
	1.12.3 The Three-State Model	32
	1.12.4 The Four-State Model	34
	1.12.5 The Multi-State Model	35
1.13	The Nature of the Metal Surface Itself at the Electrode/Solution Interface	35
	1.13.1 Metal/Vacuum Interface	35
	1.13.2 Metal/Solution Interface	36
1.14	Effects of Competitive Adsorption with Solvent Molecules on Kinetic parameters for Electrode Reactions	36

		Page No.
1.14.1	Introduction	36
1.15	Entropy of Electrodeposited Species in a Monolayer	39
1.16	Aims of the Present Work	41

CHAPTER 2

EXPERIMENTAL		43
2.1	Introduction and Choice of Methods	43
2.2	Experimental Method	44
2.2.1	Cyclic-Voltammetry	44
2.2.2	Electrical Circuitry	44
2.3	Purity and Purification of Solvents	46
2.3.1	Water Purity	46
2.3.2	Non-aqueous Solvents	50
2.4	Gases	50
2.5	Cleaning of Glassware	51
2.6	Electrodes	51
2.6.1	Working Electrodes	51
2.6.2	Reference Electrodes	52
2.6.2.1	Hydrogen Reference Electrodes	52
2.6.2.2	Lead Reference Electrodes	53
2.6.2.3	Counter-Electrodes	53
2.7	Choice of Electrolytes	54
2.7.1	Anions	54
2.7.2	Supporting Electrolyte	55
2.8	Salts and Solutions	55
2.9	Cells	57

		Page No.
2.9.1	Electrochemical Cells	57
2.9.2	Non-Isothermal Cell	57
2.10	Temperature Control	61
2.11	Determination of Real Surface Area of Au Electrodes	63

CHAPTER 3

THE METHOD OF CYCLIC-VOLTAMMETRY AND ITS APPLICATIONS TO ELECTRODE SURFACE PROCESSES		65
3.1	Introduction	65
3.2	Method	65
3.3	Kinetic Conditions	67
3.4	Sweep-rate Dependence of Current: Diffusion Control	68
3.5	Peak Potential and Peak Current for Surface Process Control	69
3.6	Determination of the s_o Parameter	72
3.7	General Form of the i vs E Profiles	76

CHAPTER 4

SOLVENT AND ANION EFFECTS ON THE i vs E UPD PROFILES FOR Pb AT Au		79
4.1	Introduction: Factors Characterizing i vs E Profiles for UPD of Pb at Au	79
4.2	Origin of Solvent Effects on UPD Profiles for Pb at Au	80

		Page No.
4.3	Comparison of UPD Profiles for Pb Adatom Deposition on Au in Five Solvents	81
4.4	Comparison of Potentials of Corresponding Peaks in Various Solovents	87
	4.4.1 Basis for Copmparisons	87
	4.4.2 Values of Peak Potential Shift with Change of Solvent	89
4.5	Commentary on Behaviour in Individual Solvent Systems	95
4.6	Influence of Ions of the Supporting Electrolyte on the i vs E Profiles for UPD of Pb at Au: Ion Adsorption Effects	100
	4.6.1 Cation Effects	100
	4.6.2 Anion Effects	102
4.7	The Effect of the Anion of the Pb Salt	107
4.8	Effects of Added Water on the UPD i vs E Profiles for Pb at Au in the Four Non-aqueous Solvents	113

CHAPTER 5

COMPETITIVE ADSORPTION EFFECTS OF HALIDE IONS (X^-) AND THIOUREA (TU) ON THE UPD OF Pb AT Au		118
5.1	Micrometer Titration Procedure	118
5.2	Effects of Adsorption of halide Ions on the i vs E Profiles for UPD of Pb at Au	119
	5.2.1 The Effects of Cl^- Ion	119

			Page No.
	5.2.2	The Effects of Cl^- on the Double-layer Charging Region at Au in 1M aq. $HClO_4$	129
	5.2.3	The Effects of Br^-	129
	5.2.4	The Effects of Br^- on the i vs E Profile in the Double-layer Charging Region at Au in 1M aq. $HClO_4$	131
	5.2.5	The Effect of I^-	133
	5.2.6	The Effects of I^- on the i vs E Profile in the Double-layer Charging Region at Au in 1M aq.$HClO_4$	134
	5.2.7	The Effects of Temperature on the Co-adsorption of Anions	134
5.3		Adsorption of Thiourea (TU)	138
	5.3.1	Introduction and Previous Studies of TU Adsorption	138
	5.3.2	Summary about TU Adsorption	139
	5.3.3	Effects of Adsorbed Thiourea on the i vs E UPD Profile for Pb at Au	139
	5.3.4	Effects of TU on the Double-layer Charging Behaviour at Au in 1M aq. $HClO_4$	141
5.4		Competitive Adsorption Isotherms for Co-adsorption of Halide Ion (X^-) or Thiourea (TU) with Electrodeposited Pb Adatoms	143
5.5		Discussion and Conclusions on the effects of Anions	152

Page No.

CHAPTER 6

KINETICS OF Pb UPD PROCESSES AT Au IN VARIOUS NON-AQUEOUS SOLVENTS 155

6.1 Methods Used in the Investigation of Kinetics of Electrochemical Surface Processes 155

6.2 Distinguishable States of the UPD of Pb at Au in the Monolayer Region 157

6.3 Sweep-rate Dependence of the Anodic and cathodic Peak Potentials in UPD of Pb at Au 157

6.4 Effects of Sweep-rate on the Anodic Peaks 158

6.5 Effects of Sweep-rate on the Processes Associated with Cathodic Peaks 161

6.6 Effect of Temperature 167

6.7 Tafel-type Plots: Evaluation of the s_o parameter 167

6.8 Slopes of the Tafel-type Relations 178

CHAPTER 7

TEMPERATURE EFFECTS ON THE UPD OF Pb AT Au 181

7.1 Entropy of 2-Dimensional Array States of UPD Adatoms 181

7.2 Problems in Measurement of dE_p/dT in Relation to Derivation of the ΔS_{Pb} Quantities 181

7.3 Tempearature Effects on the i vs E UPD Profiles 183

7.4 Procedure for Evaluation of True dE_p/dT Values and the Corresponding ΔS's 190

		Page No.
7.5	Correction of the Observed dE_p/dt Values to Absolute Values Using the Temperature-Dependence of the Reference Electrode Potential	191
7.6	Tempereature-Dependence of the Peak Potentials	195
	7.6.1 General Significance	195
	7.6.2 Experimental Behaviour of E_p Values with Temperature	196
7.7	Evaluation of Entropy Changes in the Electrodeposition and Desorption of Pb at Au	197
APPENDIX I		210
CONTRIBUTIONS TO ORIGINAL RESEARCH		215
REFERENCES		218

LIST OF FIGURES

Figure		Page No.
1.1	Potentiodynamic i vs E profile for Pb upd at Au in aq. 1M $HClO_4$ + 10^{-3}M $Pb(NO_3)_2$ solution at 298K showing the various distinguishable Pb ad-states developed in a formation of a monolayer region. s = 50 mV s^{-1}.	7
1.2	Potentiodynamic i vs E profile (upper) and relative reflectivity vs potential (lower) curves of Au in 1M $HClO_4$ both in the absence (-----) and in the presence (____) of 1.0 x 10^{-3}M Pb^{2+} at 299K. s = 51.3 mV s^{-1}; $\Delta R/R_o$ obtained with perpendicular polarization, Ø = 60°. (From ref. 41).	12
1.3	Cyclic-voltammograms for Pb upd on Au single-crystal surfaces. Potentials are shown as the upd shift ΔE relative to the bulk Pb^{++}/Pb reversible potential. (From ref. 39).	15
1.4	Plots of the C vs E profiles for reaction (1.13) for various positive and negative g values for: a) reversible conditions b) irreversible conditions. (From ref. 150).	23
1.5	The three-state model of the solvent monolayer at the electrode/solution interface illustrating the orientation of molecular dipoles in the up (↓), down (↑) and parallel (→ ←) positions. (From ref. 99).	33
1.6	Schematic diagram of the complex interphase at a metal/electrolyte boundary with solvent molecules and ions present. (From ref. 6).	37

Figure		Page No.
2.1	Electrical circuitry employed in potentiodynamic sweep experiments.	45
2.2	Apparatus for the pyrodistillation of water.	47
2.3	(a) Schematic diagram of the two-compartment electrochemical cell employed for experiments conducted in aqueous medium.	58
2.3	(b) Schematic diagram of the one-compartment electrochemical cell employed for experiments conducted in non-aqueous media.	59
2.4	Water jacketed, non-isothermal reference electrode cell with provision for a salt-bridge in the region of the thermal liquid-junction.	60
2.5	Non-isothermal cell potentials for the H^+/H_2 reference electrode in 0.1M HCl in CH_3OH with and without a salt-bridge, referred to 298 K. (From ref. 149).	62
2.6	The anodic i vs E profile for Au in 0.5M H_2SO_4 at 298 K used in the evaluation of the Au electrode real surface area. $s = 50\ mV\ s^{-1}$.	64
3.1	Schematic diagram of: a) Cyclic potential sweep; b) Resulting cyclic-voltammogram for a reversible surface process.	66
3.2	Sweep-rate dependence of peak currents for a surface reaction and a diffusion-controlled electrochemical reaction.	71
3.3	Schematic plots of variation of peak potential with sweep-rate, s, for an ad-layer in which interactions are of	74

Figure		Page No.
	various strengths determined by the g value. (From ref. 127).	
3.4	Some peak potential vs log s plots for states of H electrosorption at Pt. (From ref. 127).	74
3.5	Shapes of i vs E profile with increasing s for a surface process involving: a) a 2-d array of adatoms on an electrode e.g. Pb on Au b) consumption of a 2-d surface phase on an electrode.	77
4.1	Cyclic-voltammetry i vs E profile for Pb upd at Au from 0.1M $NaClO_4$ + 10^{-2}M $Pb(CF_3SO_3)_2$ solution in acetonitrile (AN) at 298 K. s = 50 mV s^{-1}.	82
4.2	Cyclic-voltammetry i vs E profile for Pb upd at Au from 0.1M $NaCLO_4$ + 10^{-2}M $Pb(CF_3SO_3)_2$ solution in methanol (MeOH) at 298 K. s = 50 mV s^{-1}.	83
4.3	Cyclic-voltammetry i vs E profile for Pb upd at Au from 0.1M $NaClO_4$ + 10^{-2}M $Pb(CF_3SO_3)_2$ solution in dimethylformamide (DMF) at 298 K. s = 50 mV s^{-1}.	84
4.4	Cyclic-voltammetry i vs E profile for Pb upd at Au from 0.1M $NaClO_4$ + 10^{-2}M $Pb(CF_3SO_3)_2$ solution in propylene carbonate (PC) at 298 K. s = 50 mV s^{-1}.	85
4.5	Cyclic-voltammetry i vs E profile for Pb upd at Au in aq. 1M $HClO_4$ + 10^{-3}M $Pb(NO_3)_2$ solution at 298 K. s = 50 mV s^{-1}.	86
4.6	Background cyclic-voltammograms for Au in 0.1M $NaClO_4$ solution at 298 K in a) acetonitrile (AN) and b) dimethylformamide (DMF). s = 50 mV s^{-1}.	88

Figure		Page No.
4.7	Plots of variation of the individual anodic peak potentials in the i vs E upd profiles for Pb at Au in various solvents.	90
4.8	Plots of variation of the individual cathodic peak potentials in the i vs E upd profiles for Pb at Au in various solvents.	91
4.9	Model for competitive adsorption between solvent molecules (S) and Pb metal adatoms on Au electrode surface. a) Initial substrate; solvent-to-Au interactions. b) Substrate partially covered by upd Pb adatom film; mixed interactions. c) Substrate completely covered by Pb adatom film (p.z.c. changed): solvent-to-Pb adatom interactions.	94
4.10	Cyclic-voltammetry i vs E profile for Pb upd at Au in 0.1M TEAP + 10^{-2}M $Pb(CF_3SO_3)_2$ solution in acetonitrile at 298 K. s = 50 mV s^{-1}.	101
4.11	Cyclic-voltammogram for the upd of Cd on Ag(111) in an aqueous solution containing 0.2M TEAP and $5x10^{-3}$M $Cd(ClO_4)_2$. s = 10 mV s^{-1}. (From ref. 37).	103
4.12	Cyclic-voltammogram for the upd of Cd on Ag(111) in an aqueous solution containing 0.1M $LiClO_4$ and $5x10^{-3}$M $Cd(ClO_4)_2$. s = 10 mV s^{-1}. (From ref. 37).	103
4.13	Cyclic-voltammetry i vs E profile for Pb upd at Au from 0.1M $NaNO_3$ + 10^{-2}M $Pb(CF_3SO_3)_2$ solution in methanol at 298 K. s = 50 mV s^{-1}.	105

Figure		Page No.
4.14	Cyclic-voltammetry i vs E profile for Pb upd at Au from 0.1M $NaCF_3SO_3$ + 10^{-2}M $Pb(CF_3SO_3)_2$ solution in methanol at 298 K. s = 50 mV s^{-1}.	106
4.15	Cyclic-voltammetry i vs E profile for Pb upd at Au in aq. 1M $HClO_4$ + 10^{-2}M $Pb(CF_3SO_3)_2$ solution at 298 K. s = 50 mV s^{-1}.	108
4.16	Cyclic-voltammetry i vs E profile for Pb upd at Au in aq. 1M $HClO_4$ + 10^{-3}M $Pb(NO_3)_2$ solution at 298 K. s = 50 mV s^{-1}.	109
4.17	Cyclic-voltammetry i vs E profile for Pb upd at Au from 0.1M $NaClO_4$ + 10^{-2}M $Pb(ClO_4)_2$ solution in methanol at 298 K. s = 50 mV s^{-1}.	111
4.18	Cyclic-voltammetry i vs E profile for Pb upd at Au from 0.1M $NaClO_4$ + 10^{-2}M $Pb(NO_3)_2$ solution in methanol at 298 K. s = 50 mV s^{-1}.	112
4.19	Series of superimposed potentiodynamic i vs E profiles for Pb upd at Au from 0.1M $NaClO_4$ + 10^{-2}M $Pb(CF_3SO_3)_2$ solution in acetonitrile at 298 K with successive additions of water from ca. 5.5 x 10^{-5} to 2M. Arrows show directions of change of curves with increasing water content. s = 50 mV s^{-1}.	115
4.20	Series of superimposed potentiodynamic i vs E profiles for Pb upd at Au from 0.1M $NaClO_4$ + 10^{-2}M $Pb(CF_3SO_3)_2$ solution in propylene carbonate at 298 K with successive additions of water from ca. 5.5 x 10^{-3} to 5M. Arrows show directions of change of curves with increasing water content. s = 50 mV s^{-1}.	116

Figure		Page No.
5.1	Series of superimposed cyclic-voltammetry i vs E profiles for Pb upd at Au in aq. 1M $HClO_4$ + 10^{-3}M $Pb(NO_3)_2$ with successive additions of Cl^- ion from 2.5 x 10^{-7} to 9.25 x 10^{-2} mol dm^{-3}. Arrows show directions of change of curves with increasing [Cl^-]. s = 50 mV s^{-1}.	120
5.2	Series of superimposed cyclic-voltammetry i vs E profiles for Pb upd at Au in aq. 1M $HClO_4$ + 10^{-3}M $Pb(NO_3)_2$ with successive additions of Br^- ion from 1.25 x 10^{-7} to 2.5 x 10^{-4} mol dm^{-3}. Arrows show directions of change of curves with increasing [Br^-]. s = 50 mV s^{-1}.	121
5.3	Series of superimposed cyclic-voltammetry i vs E profiles for Pb upd at Au in aq. 1M $HClO_4$ + 10^{-3}M $Pb(NO_3)_2$ with successive additions of I^- ion from 1.25 x 10^{-8} to 5 x 10^{-5} mol dm^{-3}. Arrows show directions of change of curves with increasing [I^-]. s = 50 mV s^{-1}.	122
5.4	Series of superimposed cyclic-voltammetry i vs E profiles for Pb upd at Au from 0.1M $NaClO_4$ + 10^{-2}M $Pb(CF_3SO_3)_2$ solution in MeOH with successive additions of Cl^- ion from 10^{-6} to 3.4 x 10^{-4} mol dm^{-3}. Arrows show directions of change of curves with increasing [Cl^-]. s = 50 mV s^{-1}.	123
5.5	Series of superimposed cyclic-voltammetry i vs E profiles for Pb upd at Au from 0.1M $NaClO_4$ + 10^{-2}M $Pb(CF_3SO_3)_2$ solution in MeOH with successive additions of Br^- ion from 10^{-5} to 10^{-4} mol dm^{-3}. Arrows show directions of change of curves with increasing [Br^-]. s = 50 mV s^{-1}.	124

Figure		Page No.
5.6	Series of progressively restricted cyclic-voltammetry i vs E profiles for Pb upd at Au in aq. 1M $HClO_4$ + 10^{-3}M $Pb(NO_3)_2$ containing 5×10^{-5} mol dm^{-3} of Cl^- ion. s = 50 mV s^{-1}.	126
5.7	Series of superimposed cyclic-voltammetry i vs E profiles for Pb upd at Au in aq. 1M $HClO_4$ with successive additions of Cl^- ion from 2.5×10^{-7} to 2.74×10^{-2} mol dm^{-3}, without a Pb salt being present. Arrows show directions of change of curves with increasing [Cl^-]. s = 50 mV s^{-1}.	130
5.8	Series of superimposed cyclic-voltammetry i vs E profiles for Pb upd at Au in aq. 1M $HClO_4$ with successive additions of Br^- ion from 2.5×10^{-7} to 3.14×10^{-4} mol dm^{-3}, without a Pb salt being present. Arrows show directions of change of curves with increasing [Br^-]. s = 50 mV s^{-1}.	132
5.9	Series of superimposed cyclic-voltammetry i vs E profiles for Pb upd at Au in aq. 1M $HClO_4$ with successive additions of I^- ion from 2.5×10^{-7} to 3.875×10^{-5} mol dm^{-3}, without a Pb salt being added. Arrows show directions of change of curves with increasing [I^-]. s = 50 mV s^{-1}.	135
5.10	Shift in peak potential of the first cathodic peak (C_{Pb1}) in the i vs E profile for Pb upd at Au in aq. 1M $HClO_4$ + 10^{-3}M $Pb(NO_3)_2$ as a function of log [NaCl] at three temperatures: 278.5, 295 and 318 K.	136
5.11	Shift in peak potential of the first cathodic peak (C_{Pb1}) in the i vs E profile for Pb upd at Au in aq. 1M $HClO_4$ + 10^{-3}M $Pb(NO_3)_2$ as a function of log [NaBr]	137

Figure		Page No.
	at three temperatures: 278.5, 295 and 318 K.	
5.12	Series of superimposed cyclic-voltammetry i vs E profiles for Pb upd at Au in aq. 1M $HClO_4$ + 10^{-3}M $Pb(NO_3)_2$ with successive additions of TU from 1.25×10^{-6} to 1.6×10^{-5} mol dm^{-3}. Arrows show directions of change of curves with increasing [TU]. s = 50 mV s^{-1}.	140
5.13	Series of superimposed cyclic-voltammetry i vs E profiles for Pb upd at Au in aq. 1M $HClO_4$ with successive additions of TU from 2.5×10^{-7} to 3.75×10^{-6} mol dm^{-3}, without a Pb salt being added. Arrows show directions of change of curves with increasing [TU]. s = 50 mV s^{-1}.	142
5.14	Shift in peak potential of the first cathodic peak (C_{Pb1}) in the i vs E profile for Pb upd at Au in aq. 1M $HClO_4$ + 10^{-3}M $Pb(NO_3)_2$ as a function of log [Cl^-]. (Data from curves shown in Fig. 5.1).	144
5.15	Shift in peak potential of the first cathodic peak (C_{Pb1}) in the i vs E profile for Pb upd at Au in aq. 1M $HClO_4$ + 10^{-3}M $Pb(NO_3)_2$ as a function of log [Br^-]. (Data from curves shown in Fig. 5.2).	145
5.16	Shift in peak potential of the first cathodic peak (C_{Pb1}) in the i vs E profile for Pb upd at Au in aq. 1M $HClO_4$ + 10^{-3}M $Pb(NO_3)_2$ as a function of log [I^-]. (Data from curves shown in Fig. 5.3).	146
5.17	Shift in peak potential of the first cathodic peak (C_{Pb1}) in the i vs E profile for Pb upd at Au in aq.	147

Figure		Page No.
	1M $HClO_4$ + 10^{-3}M $Pb(NO_3)_2$ as a function of log [TU]. (Data from curves shown in Fig. 5.12).	
5.18	Percentage blocking of Pb upd on Au in aq. 1M $HClO_4$ + 10^{3}M $Pb(NO_3)_2$, measured as its charge reduction by Cl^- ion as a function of log [Cl^-]. (Data from curves shown in Fig. 5.1).	148
5.19	Percentage blocking of Pb upd on Au in aq. 1M $HClO_4$ + 10^{3}M $Pb(NO_3)_2$, measured as its charge reduction by Br^- ion as a function of log [Br^-]. (Data from curves shown in Fig. 5.2).	149
5.20	Percentage blocking of Pb upd on Au in aq. 1M $HClO_4$ + 10^{3}M $Pb(NO_3)_2$, measured as its charge reduction by I^- ion as a function of log [I^-]. (Data from curves shown in Fig. 5.3).	150
5.21	Percentage blocking of Pb upd on Au in aq. 1M $HClO_4$ + 10^{3}M $Pb(NO_3)_2$, measured as its charge reduction by TU as a function of log [TU]. (Data from curves shown in Fig. 5.12)	151
6.1	Series of superimposed cyclic-voltammetry i vs E profiles for Pb upd at Au from 0.1M $NaClO_4$ + 10^{-2}M $Pb(CF_3SO_3)_2$ solution in AN for variable low sweep-rates. Sweep-rate varied from 60 to 150 mV s^{-1}.	159
6.2	Series of superimposed cyclic-voltammetry i vs E profiles for Pb upd at Au from 0.1M $NaClO_4$ + 10^{-2}M $Pb(CF_3SO_3)_2$ solution in MeOH for variable low sweep-rates.	160

Figure		Page No.
	Sweep-rate varied from 10 to 150 mV s^{-1}.	
6.3	Series of cyclic-voltammetry i vs E profiles for Pb upd at Au from 0.1M $NaClO_4$ + 10^{-2}M $Pb(CF_3SO_3)_2$ solution in DMF at various higher sweep-rates at 298 K: a) 1 V s^{-1} b) 5 V s^{-1} c) 10 V s^{-1} and d) 20 V s^{-1}.	162
6.4	Series of cyclic-voltammetry i vs E profiles for Pb upd at Au from 0.1M $NaClO_4$ + 10^{-2}M $Pb(CF_3SO_3)_2$ solution in DMF at various higher sweep-rates at 318 K: a) 5 V s^{-1} b) 10 V s^{-1} c) 20 V s^{-1} and d) 50 V s^{-1}.	163
6.5	Cylic-voltammetry i vs E profiles for Pb upd at Au in aq. 1M $HClO_4$ + 10^{-3}M $Pb(NO_3)_2$ solution at two low sweep-rates: 1. 10 mV s^{-1} and 2. 50 mV s^{-1}. T: 298 K.	164
6.6	Series of cyclic-voltammetry i vs E profiles for Pb upd at Au from 0.1M $NaClO_4$ + 10^{-2}M $Pb(CF_3SO_3)_2$ solution in DMF at low sweep-rates at 298 K: 1) 5 mV s^{-1} and 2) 10 mV s^{-1}.	166
6.7	Variations of peak potentials vs log s for desorption of Pb ad-states at Au in 0.1M $NaClO_4$ + 10^{-2}M $Pb(CF_3SO_3)_2$ solution in MeOH at 298 K.	168
6.8	Variations of peak potentials vs log s for desorption of Pb ad-states at Au in 0.1M $NaClO_4$ + 10^{-2}M $Pb(CF_3SO_3)_2$ solution in DMF at 298 K.	169
6.9	Variations of peak potentials vs log s for desorption of Pb ad-states at Au in 0.1M $NaClO_4$ + 10^{-2}M $Pb(CF_3SO_3)_2$ solution in PC at 298 K.	170

Figure		Page No.
6.10	Dependence of apparent peak potential on log s for various values of R_u. (From ref. 200).	171
6.11	Variations of peak potentials vs log s for deposition of Pb ad-states at Au in 0.1M $NaClO_4$ + 10^{-2}M $Pb(CF_3SO_3)_2$ solution in AN at 298 K.	172
6.12	Variations of peak potentials vs log s for deposition of Pb ad-states at Au in 0.1M $NaClO_4$+ 10^{-2}M $Pb(CF_3SO_3)_2$ solution in MeOH at 298 K.	
6.13	Variations of peak potentials vs log s for deposition of Pb ad-states at Au in 0.1M $NaClO_4$ + 10^{-2}M $Pb(CF_3SO_3)_2$ solution in PC at 298 K.	174
7.1	Series of superimposed i vs E upd profiles for Pb upd at Au from 0.1M $NaClO_4$ + 10^{-2}M $Pb(CF_3SO_3)_2$ solution in AN with increasing temperature in the range 280 to 340 K.	184
7.2	(a) Series of superimposed i vs E upd profiles for Pb upd at Au from 0.1M $NaClO_4$ + 10^{-2}M $Pb(CF_3SO_3)_2$ solution in DMF in with increasing temperature in the range 233 to 293 K. Arrows indicate the direction of the shift of the curves with increasing temperature.	185
7.2	(b) Series of superimposed i vs E upd profiles for Pb upd at Au from 0.1M $NaClO_4$ + 10^{-2}M $Pb(CF_3SO_3)_2$ solution in DMF with increasing temperature in the range 298 to 333 K. Arrows indicate the direction of the shift of the curves with increasing temperature.	186

Figure		Page No.
7.3	Series of superimposed i vs E upd profiles for Pb upd at Au in aq. 1M $HClO_4$ + 10^{-3}M $Pb(NO_3)_2$ solution with increasing temperature in the range 278 to 358 K. Arrows indicate the direction of the shift of the curves with increasing temperature.	187
7.4	Non-isothermal cell potentials for the Pb^{++}/Pb reference electrode in 0.1M $NaClO_4$ + 10^{-2}M $Pb(CF_3SO_3)_2$ in various non-aqueous solvents referred to 298 K.	193
7.5	Temperature dependence of Pb apparent peak potentials in the i vs E upd profile for Pb at Au from 0.1M $NaClO_4$ + 10^{-2}M $Pb(CF_3SO_3)_2$ solution in AN.	198
7.6	Temperature dependence of Pb apparent peak potentials in the i vs E upd profile for Pb at Au from 0.1M $NaClO_4$ + 10^{-2}M $Pb(CF_3SO_3)_2$ solution in MeOH.	199
7.7	Temperature dependence of Pb apparent peak potentials in the i vs E upd profile for Pb at Au from 0.1M $NaClO_4$ + 10^{-2}M $Pb(CF_3SO_3)_2$ solution in DMF.	200
7.8	Temperature dependence of Pb apparent peak potentials in the i vs E upd profile for Pb at Au from 0.1M $NaClO_4$ + 10^{-2}M $Pb(CF_3SO_3)_2$ solution in PC.	201
7.9	(a) Temperature dependence of Pb apparent peak potentials in the i vs E upd profile for Pb at Au in aq. 1M $HClO_4$ + 10^{-3}M $Pb(NO_3)_2$.	202
7.9	(b) Temperature dependence of Pb apparent peak potential with temperature in the i vs E upd profile for Pb at Au in aq. 1M $HClO_4$ + 10^{-3}M $Pb(NO_3)_2$.	203

Figure		Page No.
7.9	(c) Temperature dependence of Pb apparent peak potentials in the i vs E upd profile for Pb at Au in aq. 1M $HClO_4$ + 10^{-3}M $Pb(NO_3)_2$.	204

LIST OF TABLES

Table		Page No.
3.1	Critical Parameters of Cyclic-voltammetry Experiments on Monolayers at Electrodes.	75
4.1	Possible Origins of Solvent Effect on UPD Metal Adatom Profiles.	81
4.2	Peak Potentials of the Anodic Peaks Relative to Pb/Pb^{++} of the UPD i vs Profiles of Pb at Au in Various Solvents.	92
4.3	Peak Potentials of the Cathodic Peaks Relative to Pb/Pb^{++} of the UPD i vs Profiles of Pb at Au in Various Solvents.	92
5.1	Shifts in Peak Potential of the Peak A_{Pb1} in the Presence of added Cl^-.	128
5.2	Maximum Shift of the Peak Potentials of the First Cathodic Peak (C_{Pb1}) in the Presence of Added Anions or Thiourea.	141
6.1	Estimated s_o Parameters for the Deposition and Desorption of Pb at Au in Various Non-aqueous Solvents and at Different Temperatures.	176
6.2	Estimated Slopes from the Tafel-type Plots for the Adsorption/desorption of Pb at Au in Various Non-aqueous Solvents and at Different Temperature.	179
7.1	Temperature Coefficients of Non-isothermal Cell Potentials Pb/Pb^{++} and H_2/H^+ Reference Electrodes at 298 K.	194
7.2	dE_p/dT, $(dE_pdT + dE_{Cell}/dT)$ and Estimated ΔS^o Values for Pb Adatom States on Au in Various Solvents.	206

ABSTRACT

In the present work, the upd of Pb at polycrystalline Au from aqueous and non-aqueous solvents (acetonitrile, methanol, dimethylformamide and propylene carbonate) has been investigated by means of cyclic-voltammetry. Results obtained from aqueous medium are used for comparative reference purposes. Experiments on upd of Pb at polycrystalline Au electrodes have been conducted with respect to: a) the form of the i vs E upd profiles for multiple-state adsorption below a monolayer as a function of solvent; b) the effects of co-adsorbed anions (Cl^-, Br^-, I^-) and thiourea(TU) on the i vs E upd profiles starting from very low concentrations ($\cong 10^{-7}$M) which can affect the apparent entropies of upd states; c) the kinetics of the deposition and desorption processes in various non-aqueous solvents by evaluation of the s_o parameter; and d) the determination of the entropy of distinguishable upd adatom arrays by evaluating the temperature-derivatives of the peak potentials.

It has been found in the present study that i vs E upd profiles of Pb at Au obtained in various solvents (aqueous and non-aqueous) under conditions that were kept identical as far as possible (e.g. the same concentration of Pb^{2+} ions, same sweep-rate, same potential range scanned) are characteristically different. For example, the i vs E upd profile obtained in MeOH resembles that found for aqueous solutions in terms of resolution of multiple-states of adsorption and peak shapes, while for that in AN the profile is least resolved.

The i vs E upd profiles also demonstrate that the first cathodic peak, desgnated C_{Pb1}, is the one most affected by solvent change. Its relative peak potential and shape is found to be solvent-dependent. Solvent effects in the upd profiles of metal adatoms can arise due to competition between electrodeposition of the metal adatoms and desorption of a corresponding volume of solvent molecules. The upd process is thus a replacement reaction and its energetics depend on the desorption energy of the appropriate number of solvent molecules. Solvent effects will therefore be most pronounced for the initial stages of adatom deposition, as is found in the present work because most of the electrode surface will be covered by the solvent molecules initially. Various ions have

also been found to have marked effects on the upd i vs E profiles.

When TEA^+ is used as the cation of the supporting electrolyte, the upd profile obtained in AN is found to be distorted. The first cathodic peak is shifted to less positive potentials, indicating that TEA^+ is strongly adsorbed at the Au electrode. Similar results are also obtained when NO_3^- is used as the anion of the supporting electrolyte. When NO_3^- is used as the anion of the Pb salt, upd profiles obtained in MeOH are distorted and different from the usual profiles obtained in aq. $HClO_4$ with $Pb(NO_3)$ as the Pb salt. This clearly demonstrates that anion adsorption is solvent-dependent. Both ClO_4^- and $CF_3SO_3^-$ give similar results, when used as anions of the supporting electrolyte in H_2O or MeOH.

In the presence of specifically adsorbed anions (Cl^-, Br^-, I) and thiourea, it has been found that the peaks for the initial process of Pb adatom deposition are substantially shifted to less positive potentials. Depending on the species, the effects on the upd profiles are different but it is generally observed that the effects are significant already at high dilutions of the added species. For example, in the case of I^- or thiourea, the effects are already discernable already at about 10^{-7}M. Saturation effects for the different species are also attained at different concentrations.

The most striking and interesting effect of added Cl^-, not observed in the case of Br^- or I^-, is the appearance of an extra peak in the anodic sweep at the most positive potential of the sweeps (ca. 0.40 to 0.55 V/E_H). A corresponding peak is not observed on the cathodic sweep of the profile, neither is it in the case of experiments done in methanolic 0.1M $NaClO_4$ solution. Examples are discussed with Pb adatom blocking isotherms for a range of adsorbed anion or thiourea concentrations; the type of competitive adsorption isotherm depends appreciably on the identity of the anion involved.

The electrochemical kinetics of electrodeposition and desorption for two distinguishable states in the multi-state adsorption of Pb at Au are evaluated by measuring the peak potentials as a function of log s over a wide range of sweep-rate in which the peak potentials can be followed. The determined kinetic parameter s_o, the maximum sweep-rate for which a surface process ceases to be kinetically reversible, in non-aqueous solvents is lower than that obtained in aqueous solution for

the similar process. It is also found that at substantially higher sweep-rates ($\equiv$ 50 V s^{-1}) there is deviation from linearity in the plots of peak potentials vs log s. This deviation is attributed to irreversibility of the Pb upd process an effect which begins to become significant at these high sweep-rates, especially in non-aqueous solutions.

The highest s_o values are obtained in AN as a solvent. It is also found that the apparent values of s_o values increase with temperature since the solution resistance and diffusion-influence is decreased with increase in temperature.

In the present work, the apparent entropies of the distinguishable states, corresponding to multiple-state adsorption of Pb adatoms on Au, are determined by evaluating the temperature-derivatives of the peak potentials (dE_p/dT) which are proportional to the entropies, at half-coverage for each of the resolved adsorption states, relative to the entropy of deposition of the bulk metal. Since the peak potentials determined were referred to the reference electrode in the same solution at the given experimental temperature, the experimentally determined dE_p/dT is corrected using the experimentally determined dE_{cell}/dT of the reference electrode from non-isothermal cell measurements. The estimated entropy values are found to be solvent-dependent and differ significantly for the various solvents used in the present study. The estimated entropy changes corresponding to the various states of adsorbed Pb at Au for various solvents are discussed in relation to the standard entropy of Pb in the bulk which, for the crystalline solid (298 K), is 64.85 J mol^{-1} K^{-1}, while that of Pb^{++} in water is -21.3 J mol^{-1} K^{-1}.

CHAPTER 1

GENERAL INTRODUCTION

1.1 Underpotential Deposition (UPD) of Atomic Monolayers on Metal Electrodes

1.1.1 Introduction

The work described in this thesis is concerned with the characterization of so-called "underpotential deposition" ("upd") processes in the deposition of Pb atoms on polycrystalline Au from non-aqueous protic and aprotic solvents for which the situation in aqueous medium is now well established, e.g. [1,2,3] and provides a system for comparison and reference.

"Underpotential deposition" is a term that has been adopted to describe the situation where an adatom species is electrodeposited in a monolayer or submonolayer below the potential for deposition of the same element in bulk-phase form. When this situation obtains, it follows that the Gibbs energy of electrodeposition of the deposited M on a substrate S is lower (more negative) than the Gibbs energy for bulk-phase formation of M. It therefore follows approximately, for many cases, that the M-S bond is then stronger than the M-M bond in phase of M and this provides a semi-quantitative description of the condition for upd of M on S to be observed. More precisely, the condition

$$G^{\circ}_{M\text{-}S} < G^{\circ}_{M\text{-}M}$$

is required with respect to the Gibbs energies involved.

The underpotential deposition of M species takes place in a 2-dimensional lattice structure usually up to one or sometimes two atomic diameters thick. The electrodeposition of M species on the metal substrate S in the upd region takes place over a range of reversible potentials which depend thermodynamically on the coverage θ_M, of M on S, when the process is conducted slow enough for it to remain kinetically reversible. Usually the coverage is in the range $0 < \theta_M < 1$ but sometimes a second or a further half monolayer can be deposited before bulk-phase formation of M starts, e.g. as in the case of deposition of Cu on Pt; then the nominal value of θ_M may be significantly greater

than 1 but not corresponding to a multilayer.

Previously upd processes for H, Pb and other metal adatoms have been studied by various workers, mainly from the aqueous medium. The earliest example of upd that was characterized was that of H on Pt [4]. In the present work, attention is directed towards the upd behaviour of metal adatoms, Pb in particular, in non-aqueous media with regard to the role of solvent adsorption and competition by anions.

Interest in upd behaviour in non-aqueous media arises mainly for the following reasons:

a) The deposition profile may be solvent-dependent if solvent displacement and interchange caused by the deposited adatom introduces a significant component of the Gibbs energy of the upd process.

b) The upd profiles and the kinetics of the upd processes can be studied down to quite low temperatures, especially in MeOH and acetonitrile (AN), and the kinetics, which may be solvent-dependent, can therefore be examined over a wide range of temperature.

c) Anion adsorption effects are dependent on solvent on account of varying strength of the anion's solvation in media of differing dielectric constant and electron donicity or accepting power [5].

d) From the dependence of peak potentials on temperature, the entropies of upd states, relative to the bulk state, can be evaluated, and thus the states of arrays of upd adatoms determined e.g. with respect to their 2-dimensional mobility or otherwise.

1.1.2 Previous Studies of UPD Processes

The study of metal and H adatom arrays on metal electrode surfaces has provided an area of major interest in electrochemical surface science and surface chemistry (e.g. ref. 6). These topics have been studied extensively in recent years because of their importance in understanding a wide variety of electrochemical phenomena such as adsorption, charge transfer and, by contrast, nucleation and growth, as well as surface diffusion and also because of their practical importance in electrocatalysis [7].

Historically, the investigation of metal ion deposition in monolayers was carried out by means of measurements at very low metal-ion concentrations, with emphasis on the applicability of stripping analysis for analytical purposes at low concentration levels of metal ions.

The earliest adsorption studies, perhaps, were those by Hevesy [8] who reported a deviation from the reversible Nernst potential when radioactive metals were deposited onto Cu. Later Herzfeld [9] explained Hevesy's [8] result by assuming, essentially correctly, that the activity of the deposited solid in the monolayer is less than unity and is a function of coverage, θ. Rogers and co-workers [10] studied the deposition and stripping of trace amounts of radioactive Cu and Ag onto Pt, Au and Pd. They extended Herzfeld's [9] ideas in explaining their own results. Besides the activity of the deposited metal being a function of coverage, they introduced an additional term, E_a, to account for any specific interaction between the deposited and the substrate species. The modified Nernst equation, which correlated the electrode potential and the coverage then had the form:

$$E_r = E_o + E_a + RT/zF \ln C_{ox} / \theta \qquad (1.1)$$

After the pioneering study of upd by Haissinsky [11,12], Nicholson investigated the deposition of Ag, Pb and Cu on Pt [13] and Ni on Pt and Au [14]. The first results of electrolytic deposition of the first atomic layer of a metal on a foreign metal substrate seem to be those reported by Mills and Wills [15] in their investigation of the monolayer electrodeposition of Pb, Tl , Sb and Ni on Au and of Pb on Ag.

On the basis of these early investigations [10], the study of upd both experimentally and theoretically has received much attention over the last twenty years by various groups using different techniques. Schmidt and co-workers [16,17,18] have extensively studied monolayer formation of metal adatoms on various metal substrates using a twin electrode, thin-layer technique. The cell employed consisted of two plane-parallel electrodes, closely spaced, the potentials of which could be regulated independently. The generator electrode was composed of the same metal as that to be underpotential-deposited at the second, working electrode. Their studies revealed that there were several distinguishable stages in the adsorption (electrodeposition) process which could be quantitatively characterized.

Bruckenstein and his co-workers [19,20,21] have studied upd using the rotating ring-disk electrode (rrde). While the potential of the disk electrode is scanned at a constant rate, dE/dt, the potential of the ring electrode is held constant at certain controlled values. The surface concentration of the deposited metal, $\Gamma(E)$ on the disk electrode can be calculated by measuring the charge due to redeposition at the ring during stripping from the disk, allowing for the hydrodynamic "collection efficiency" of the ring. The rotating ring-disk technique also yields, under appropriate analysis, kinetic parameters such as the exchange-current density, adsorption and charge-transfer rate coefficients and the electrosorption valency [22].

Vetter and Schultze [23,24] also used potentiostatic and galvanostatic pulse measurements to study mainly upd kinetics and, in a limited way, also the relevant thermodynamic data. For example, in the adsorption of Cu^{2+} ion onto polycrystalline Pt, the rate-determining step was found to be the reduction of Cu^{2+} ions to Cu^{+} ions [25].

Cyclic- or linear-sweep voltammetry was used by Lorenz and co-workers [26] in the investigation of upd. The potential of the working electrode was changed continuously at a constant sweep-rate (dE/dt) by a ramp potential supplied from a function generator. The reaction at the surface of the working electrode in relation to the states of upd adatoms, is characterized by the current-potential profiles. Since this is the technique that has been mainly employed in the present investigations, it will be discussed in more detail in Chapter 3. Bowles [27], using a different approach, studied the deposition of metal monolayers by means of a radioactive tracer technique.

Optical methods have also been used to detect and characterize the formation of submonolayers or monolayers of metal adatoms on metal electrode sub-states. For example, Yeager and co-workers [28,29] and Kolb [30] have applied the specular reflectance technique to investigations of upd and showed that, although the metal adsorption changed the reflectivity in a definite way, the reflectivity change was also wavelength-dependent, indicating the role of optical absorption effects amongst other factors that determine the reflectivity.

1.1.3 UPD Studies in Non-aqueous Solvents

There is a growing interest in the study of upd in non-aqueous solvents. Besides the metal pairs which can be studied in aqueous solutions, non-aqueous media provide alternative solvents or solution for studying a larger variety of metal pairs such as Li, Al, Sb, Cd and Sn which, in water, would react strongly to form hydroxides. Also it is now possible to investigate the electrodeposition of alkali metals [31] e.g. Na, Li, which obviously cannot be studied in aqueous solutions.

Fried and Barak [32] and Kolb and Gerischer [33] have studied the upd of alkali metals onto noble or semi-noble metals. However, Li, was found to have a substantial alloying tendency in the upd region. Li monolayers have, nevertheless, been electrodeposited on metals such as Au, Ag, Cu and Pt [32,33]. Also, the upd of Li at Mg [34] and Sb [35] results in alloy formation.

Non-aqueous solvents also provide an opportunity of carrying out measurements over a wider range of temperatures than is usually possible in water. For example, propylene carbonate and methanol have liquid ranges of 289 and 159 K, respectively. This is important because measurements of the temperature-dependence of peak potentials enables evaluations to be made of the apparent entropy of the adlayer (see Section 7.7). Conway et al. [36] reported preliminary results of this kind for the entropy of the monolayer of Pb on Au deposited in non-aqueous media in their exploratory studies of the upd of Pb at polycrystalline Au in AN and MeOH.

Since the upd behaviour of several metal pairs in aqueous medium is now well understood [1,2,3], upd studies in other solvents should form an interesting basis for comparison with the well-known results in aqueous medium. Such comparisons should prove valuable in understanding the role of the solvent molecules in modifying the characteristics of metal ion deposition in monolayers onto suitable metal substrates. So far, this has been addressed only by Conway et al. [36] and Xue-Kun Xing et al. [37]. The latter authors investigated the upd of Cd on Ag(111) in PC and compared their results with those in aqueous medium. There were differences in the cyclic-voltammetry curves for Cd upd on Ag(111) in PC and in water, the peaks being sharper than those in water. These authors [37] explained these differences as being probably due to the competitive adsorption of ionic species other than the metal being electrodeposited on the electrode

surface and/or to interactions of the solvent molecules with the metal substrate, as will be discussed later in Chapter 4.

The most commonly used solvents are MeOH, PC, AN, DMF and DMSO. However, their applicability is restricted by the rather low solubility of many inorganic salts of suitable metals in such media and the high-purity requirements for satisfactory work in most non-aqueous solvents, a matter to be discussed later in Chapter 2, Section 2.3.2.

1.2 Previous Studies of the UPD of Pb at Au

The upd of Pb on Au provides an excellent system for study because it gives rise to several distinct adsorption/desorption peaks at different underpotentials on a dynamic cyclic-voltammetry i vs E profile which demonstrate the existence of several different types of adsorbed state (Fig. 1.1), or stages in the formation of a Pb monolayer on Au.

Mills and Wills [15] were the first to report results on electrodeposition of Pb on Au in their work on monolayer formation of metal adatoms on foreign-metal substrates. Using alkaline lead acetate solutions, they found that Pb deposition occurred at two distinct potentials before the reversible potential of bulk Pb was attained. Later, various workers using different techniques extensively studied the upd phenomenon. Using a more sosphiscated twin-electrode thin layer technique, Schmidt and Gygax [38] later investigated monolayer formation of Pb on Au. The adsorption of Pb occurred mainly at two potentials, giving rise to two upd peaks at potentials more positive than the Nernst reversible potential for bulk Pb. The charge equivalent to monolayer formation was between 420 - 460 μC per real cm^2, compared to the value of 347 μC per real cm^2 reported by Schmidt and Wüthrich [17] using a similar technique. However, later Engelsmann, Lorenz and Schmidt [39], using well prepared Au(111), (100) and (110) single-crystal Au surfaces, found multiple-state adsorption of Pb on Au still with 3 to 5 distinguishable states at each monocrystal surface indicating that multiple-state upd below a monolayer is not due to trivial effects of polycrystallinity or surface heterogeneity.

Vicente and Bruckenstein [21] investigated the adsorption of Pb on Au from a slightly

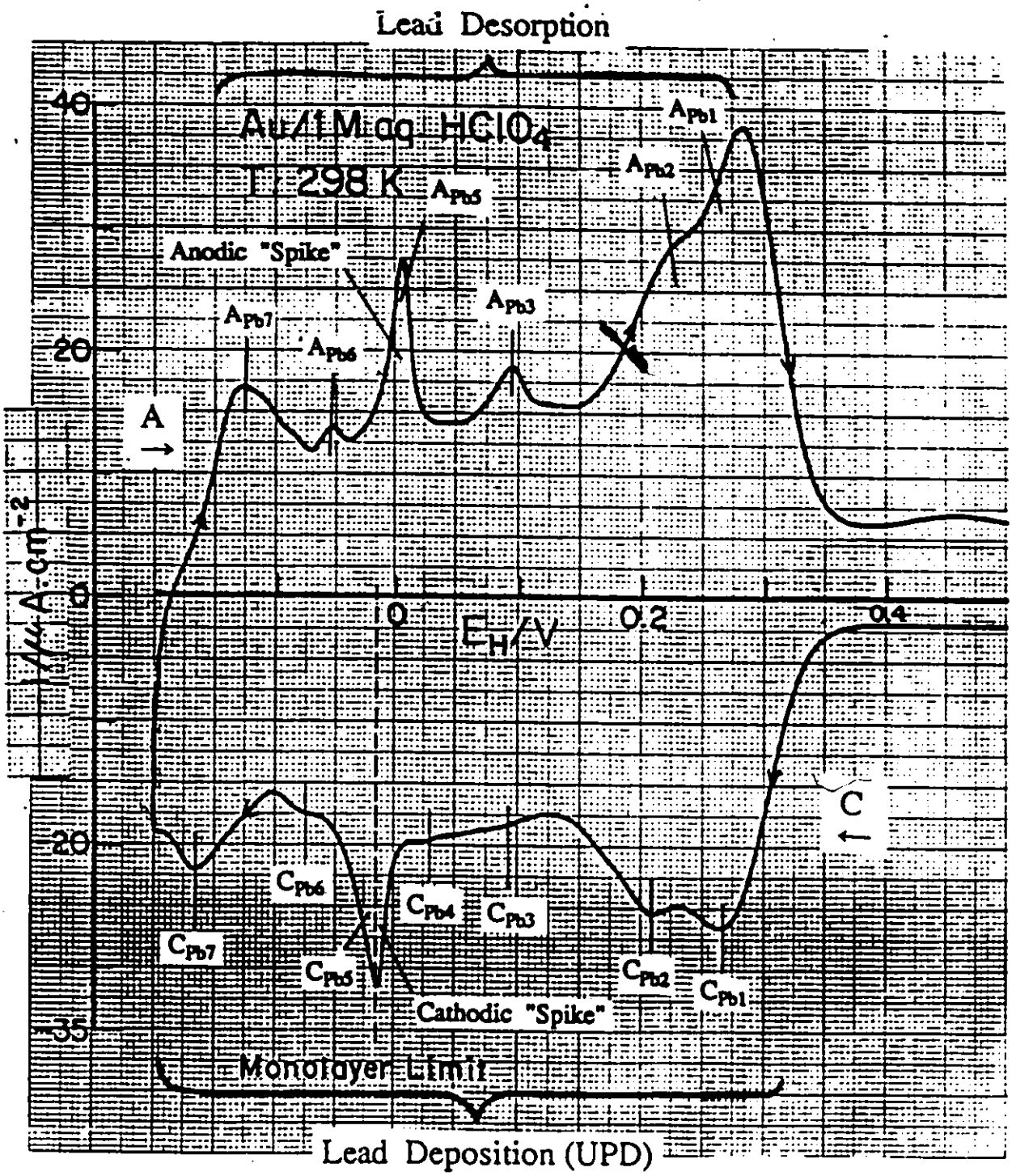

Fig. 1.1 Potentiodynamic i vs E profile for Pb upd at Au in aq. 1M $HClO_4$ + 10^{-3}M $Pb(NO_3)_2$ solution at 298K showing the various distinguishable Pb ad-states developed in a formation of a monolayer region. s = 50 mV s^{-1}.

acidified 0.5M KCl solution using the rotating ring-disk electrode technique. They found that adsorption took place over a wide potential range, increasing with cathodic potential. The charge corresponding to a monolayer of Pb was about 420 μC per geometric cm^2 or 247 μC per real cm^2. The formation of the monolayer was characterized principally by two adsorption but three anodic desorption stripping peaks. In the work of Schmidt and Gygax [38] a third peak was not, however, recorded because they used higher concentrations of Pb^{++} ion and very low scan-rates, conditions which are now known to be favourable for bulk Pb formation at the potential of this third peak.

Takamura and Sakamoto [40] also studied the upd of Pb on Au but from aqueous 1M $HClO_4$ solution using the cyclic-voltammetry technique. Both the cathodic and anodic i vs E profiles showed four peaks, including one which later has been referred to as the "spike" [29]. The nearly symmetrical i vs E profiles for the cathodic and anodic peaks suggested that the Pb adsorption and dissolution due to the reactions

$$Pb^{2+}_{(aq)} + 2e \rightleftharpoons Pb_{ads} \qquad (1.2)$$

is reversible. The charge corresponding to the four cathodic peaks was again found to be about 452 μC per geometric cm^2, an indication of monolayer formation as previously suggested by the results of Vicente and Brunkenstein [21] and Takamura and co-workers [41].

The investigation of Schmidt and Wüthrich using the twin-electrode, thin-layer technique [17] showed that Pb adsorbs on polycrystalline Au in up to 5 states before completion of a monolayer. The currents of the indicator and generator electrodes are about the same in opposite directions indicating that the system follows the metal monolayer deposition model, with virtually complete discharge of Pb^{++} ions to Pb adatoms, i.e. with an electrosorption valency [22] near 1. The exchange current-density for the adsorption process was determined, using curve-fitting methods, to be 6.3 A cm^{-2} which is very high compared, for example to a value of 10^{-3} for the system Au/0.1M Cu^{2+} [26].

Kolb, Przasnyski and Gerischer [31] investigated the upd of many couples including Au/Pb^{2+} in order to establish a correlation between the difference in deposition potentials of the bulk phase and states of the monolayer. To describe the upd behavior quantitatively, the peak potentials "of the

monolayer" and bulk stripping peaks were chosen as the most suitable parameters for characterizing the difference in chemical potentials of the monolayer and the bulk deposit. The underpotential shift, ΔE_p, is the potential difference between the bulk deposition potential (i.e. the Nernst equilibrium potential) and the monolayer stripping potential. (They took mean potentials for the upd envelope of states; it would have been better to refer to individual sub-monolayer states). They also evaluated the half-width, $\Delta E_{1/2}$, of the monolayer stripping peak. For the system Au/Pb^{2+}, the values of ΔE_p and $\Delta E_{1/2}$ are 0.40 and 0.12 V, respectively.

For most of the couples studied, a linear relationship was found to hold between ΔE_p and the difference in the work functions, $\Delta\phi$, of the substrate (ϕ_o) and the bulk value (ϕ_1) of the monolayer materials by the equation:

$$\Delta E_p = \alpha\Delta\phi, \qquad (1.3)$$

where $\alpha \equiv 0.5\ V\ eV^{-1}$ and $\Delta\phi$ is $\phi_1 - \phi_0$. For couples where there was a deviation from the above linear relationship, e.g. Hg, Ag and Tl on Au, it was attributed to "specific interaction" between the adsorbate and the substrate, an unclear explanation.

1.3 Specular Reflectance Studies of Surface Films

1.3.1 Introduction

The specular reflectance technique has been extensively employed for in situ characterization of electrode surfaces. Various workers [29,42,43] have shown that specular reflectance at an electrode surface is very sensitive to the electrochemical surface state of the electrode. It is currently employed to investigate optical properties of solids, in situ studies of the formation and optical properties of monolayer and sub-monolayer coverages of ad-species on electrode surfaces, and to detect intermediates and products of heterogeneous chemical and electrochemical reactions.

Reflectance change produced by adsorbates on an electrode surface depends on the film thickness, surface coverage, wavelength of incident light, the dielectric constants of the adsorbate and the substrate, the adsorption and orientation of solvent dipoles, adsorption of ions of the electrolyte and the electron charge-density at the electrode/solution interface, related to the

electronic refractive index of the metal surface region.

1.3.2 Theory

The details of the theory of reflectance changes at an electrode have been dealt with elsewhere [44], so will not be given here, especially as the method was not used in the present work.

McIntyre and Aspnes [42] derived an equation which expresses the proportionality between reflectivity change, $\Delta R/R$, and the surface coverage, θ, by ad-species.

$$(\Delta R / R_o)_\theta = (\Delta R / R_o)_{\theta=1} \times \theta \qquad (1.4)$$

where

$$\theta = Q / Q_{\theta=1}, \qquad (1.5)$$

is the surface coverage, $Q_{\theta=1}$ is the monolayer charge, and $(\Delta R/R_o)_\theta$ and $(\Delta R/R_o)_{\theta=1}$ are the reflectivity changes at θ and $\theta = 1$, respectively. For light at normal incidence, the change in reflectance is also given [42] more informatively by

$$\Delta R / R = (8\pi n_s m d_o \theta / \lambda)\ \mathrm{Im}\ (\epsilon_2 - \epsilon_3) / (\epsilon_1 - \epsilon_3) \qquad (1.6)$$

where n_s is the refractive index of the electrolyte, d_o is the monolayer thickness, θ is the surface coverage and m is an integral multiplier of d_o, ϵ_1 is the real part of the dielectric constant of the adsorbate, ϵ_2 and ϵ_3 are the complex dielectric constants of the adsorbate and the metal (substrate), respectively. Provided that ϵ_2 and ϵ_3 remain unchanged during adsorption, $\Delta R/R$ is then proportional to the surface coverage for an experiment conducted at constant λ. The main assumption in the derivation of eqn. (1.6) is that the reflectivity changes will be proportional to the fractional surface coverage if the polarizabilities of the isolated atoms are not too different from those in the bulk phase. This assumption is not entirely satisfactory when chemisorption with charge-transfer arises, as usually the degree of charge-transfer varies appreciably or significantly with coverage so that the electronic state of the adsorbate (and hence its absorption coefficient or polarizability, etc.) may actually depend on its coverage. More detailed analysis takes into account changes of the refractive index of the metal surface region and changes of solvent polarization at the interface with changing potential.

1.3.3 Specular Reflectance Studies of Pb Adatoms Electrodeposited on Au

Since ordinary electrochemical techniques provide only limited information at the atomic level concerning upd, the specular reflectance technique [28] has been used to provide more information about the upd phenomenon, in general, and the state of Pb adatoms at Au in particular.

In upd studies using cyclic-voltammetry or the linear potential-sweep method, the electronic properties of the adsorbed layer change with increasing coverage and can be monitored continuously from monolayer to multilayer coverages by means of reflectance measurements, as illustrated in Fig. 1.2. Relative reflectivity results were first obtained by Takamura, Takamura et al. [29] in their studies of the specular reflectance changes of a Au electrode during the course of electrodeposition of Cd and Pb on Au. The specular reflectance of an electrode surface changes when a metal film is deposited on it but the magnitude and sign of change are wavelength-dependent [43].

Although there are regions of reflectance change that vary with coverage, there is a change in slope corresponding to the "spike" [29]. This change was explained by Takamura et al. [43] as due to the formation and oxidation of another state of the Pb film, different from that adsorbed at more positive potentials (lower coverage). However, according to Adzic and co-workers [29], this change is due to a large change in the electronic structure of the adsorbed Pb on the surface, associated with a 2-dimensional phase transition in the adsorbed layer.

Takamura, Watanabe and Takamura [41] have shown that the adsorbed Pb layer has similar optical properties to those of metallic Pb except for the adatoms deposited or desorbed at the most positive potentials. This is probably because they are located at the shortest distance from the surface Au atoms, and therefore experience the strongest interaction with the surface. Reflectance spectra also show the existence of adsorbed Pb in sites having different optical properties, indicating multiple state adsorption in the formation of the monolayer or submonolayer of Pb on Au electrodes.

The wavelength-, and potential-dependence of the optical constants of the adsorbed Pb layer are appreciable as found in work by Horkans, Cahan and Yeager [45], using the ellipsometric technique. Such a large dependence as is observed would not arise if the state of the adsorbed film resembled that of bulk Pb metal.

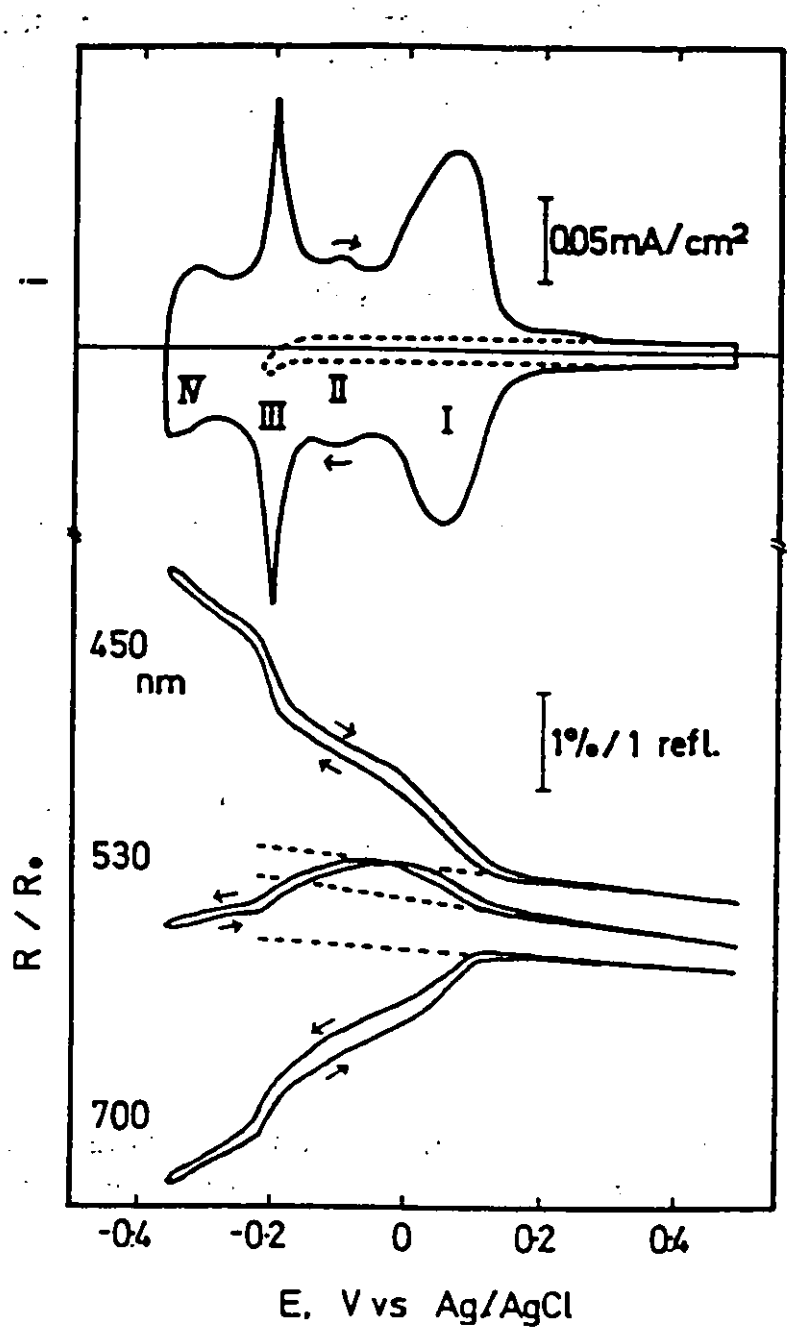

Fig. 1.2 Potentiodynamic i vs E profile (upper) and relative reflectivity vs potential (lower) curves of Au in 1M $HClO_4$ both in the absence (———) and in the presence (——) of 1.0×10^{-3}M Pb^{2+} at 299 K. s = 51.3 mV s^{-1}; $\Delta R/R_o$ obtained with perpendicular polarization, $\varnothing = 60°$. (From ref. 41).

1.4 UPD of Pb on Au Single-Crystals: Effect of Crystallographic Orientation

Differential reflectance spectroscopy, combined with cyclic-voltammetry, has been applied by Yeager and co-workers [29] in order to study the upd of Pb on Au single-crystal faces. Schultze and Dickertmann [46], Schmidt and co-workers [39] and Hamelin [47] have also studied the upd of Pb on Au single-crystal faces using the cyclic-voltammetry technique. In all cases, the cyclic-voltammograms are characterized by several peaks indicating multiple-state adsorption on the three low-index faces [(100), (110) and (111)] of Au single-crystals, including a "spike" (also seen at polycrystalline Au) which is less pronounced for the (110) face. The i vs E profiles are characteristically different for the three faces, i.e. they depend on the crystallographic orientation of the substrate surface. Coverage isotherms, of course, also depend on the crystallographic orientation and, in the case of Au(111) face, the peak structures are influenced by the pre-polarization procedure.

The upd profile for Pb on the Au (110) face closely resembles that on polycrystalline Au (Fig. 1.3). Schmidt et al. [39], therefore, suggested that polycrystalline Au predominantly exhibits (110) faces. It was pointed out by Yeager et al. [29] that the strong dependence of the "spike" on the crystallographic orientation is not surprising since the 2-d phase transition which is believed to arise at the "spike", leading to a metallic type layer, should be dependent on crystallographic orientation.

Schmidt et al. [39] found the Kolb-Gerischer [1] relation to hold for the three low-index faces but Schultze and Dickertmann [46] found it to hold for only the Au(110) face. This is not surprising because the work function values used are for polycrystalline substances and the Au(110) face evidently closely resembles in structure the main fraction of the surface of polycrystalline Au.

1.5 Multiple-State Adsorption in UPD

Nearly all i vs E profiles for the upd of H or metal adatoms on foreign metal substrates below the level of monolayer coverage are characterized by multiple-state adsorption as is clearly seen in the cyclic-voltammetry curves. Two states of adsorbed H on Pt were distinguished in the early work of Frumkin and Slygin [48] and Will and Knorr [49]. Later, working in clean and dilute solutions,

Conway et al. [50,51] were able to resolve 4 to 5 adsorbed states of H on Pt. Previous work had also shown multiple-state adsorption of Pb on Pt and Au [52]. As was mentioned previously, early studies showed two states of Pb on Au but later [40] four states and in this laboratory [52] even up to seven states have been observed, including a "spike" at $\theta_{Pb} \equiv 68\%$ that corresponds to the 2-dimensional phase transition referred to above.

1.5.1 Origin of Multiple-State Adsorption

It is now clear that multiple-state adsorption in upd is a general phenomenon. Because the early studies were carried out using polycrystalline electrode surfaces, multiplicity of upd peaks was first attributed to heterogeneity of the electrode surfaces, including principally the effects of polycrystallinity. However, even on single-crystal faces, it is now clear that the i vs E upd profiles indicate multiple-state adsorption as exemplified in the work of Schmidt et al. [39] as illustrated in Fig. 1.3.

Clavilier [53] has reported multiple-state adsorption of H on well prepared single-crystals of Pt. On the three low-index faces of Au single-crystals, Schmidt et al. [39] have shown that the upd i vs E profiles are characteristically different for the three surfaces and again multiple-state adsorption also arises. It is clear from the above examples that multiple-state adsorption is not solely due to the presence of a variety of crystal planes on which atoms are deposited with different energies of adsorption but in a much more fundamental phenomenon.

Briefly, multiplicity may arise on account of the following factors [2]:

(i) Polycrystallinity (and hence surface heterogeneity) of the electrode surface - a relatively trivial effect, referred to above.

(ii) Adsorption of atoms occupying geometrically distinguishable sites (which exist even on single-crystal principal index planes) having different binding energies for, and coordinations of, the adatoms as the monolayer is built up.

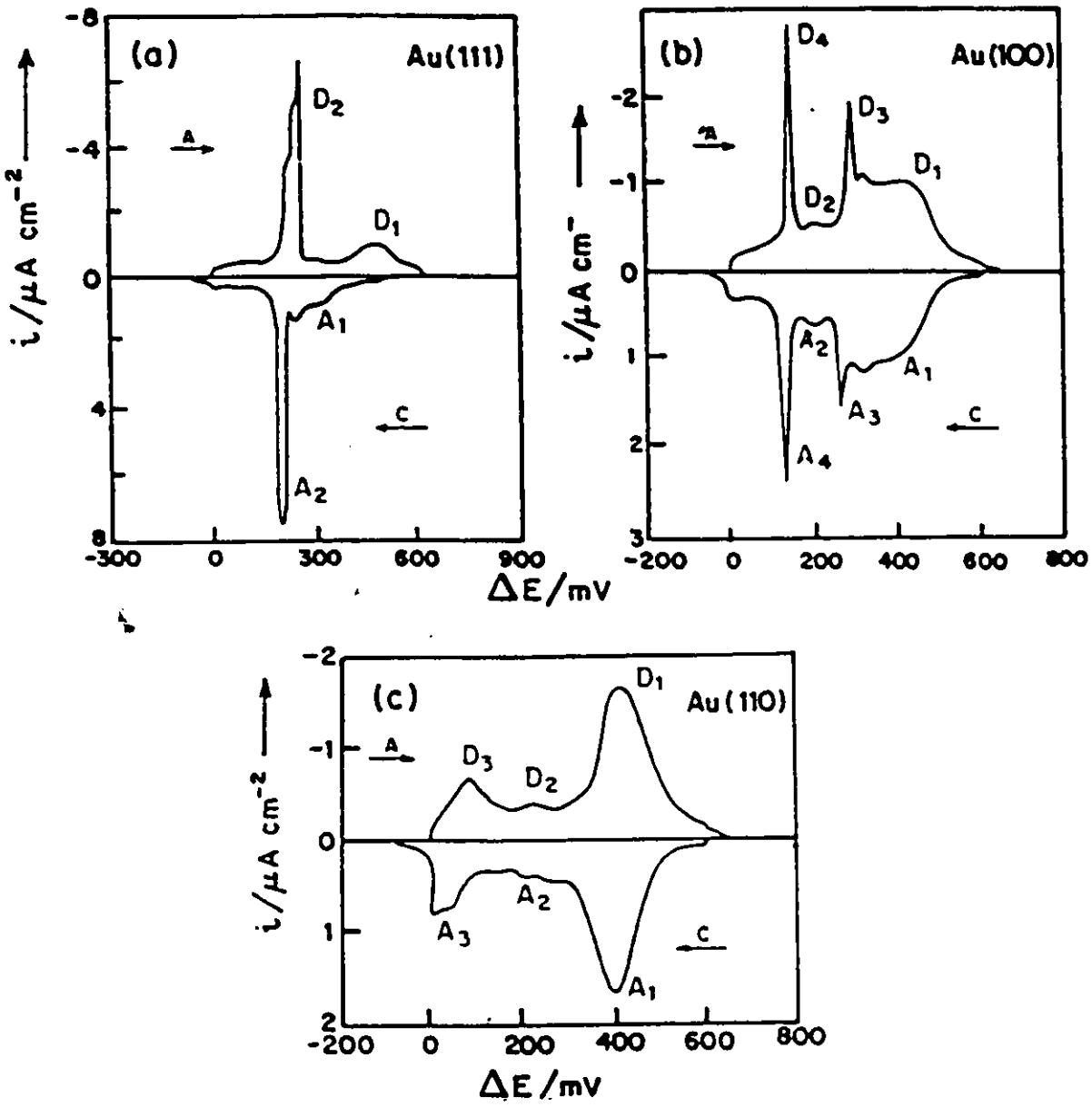

Fig. 1.3 Cyclic-voltammograms for Pb upd on Au single-crystal surfaces. Potentials are shown as the upd shift ΔE relative to the bulk Pb^{++}/Pb reversible potential. (From ref. 39).

(iii) Use of the various hybrid surface orbitals of the transition metals could lead to electronic interaction effects in deposited adatom arrays which could result in adsorption energy which is dependent on coverage.

(iv) Long-range electronic interactions between the atoms of the adsorbate [54,55,56] as the monolayer is built up (cf. (iii) above).

(v) Local influence of adsorbed ions of the electrolyte, especially anions, may induce an heterogeneity effect at the surface of the substrate.

(vi) The interaction of adsorbed atoms with oriented solvent molecules may induce an heterogeneity effect, as recently pointed out by Bewick et al. [57].

(vii) Reconstruction of the adsorbate/substrate layer may take place in some systems as the coverage increases, giving rise to various overlay structures [58] in domains whose geometries depend on coverage and potential.

1.6 Chemisorption on Metals

Adsorbate species usually become bound to a surface of the substrate metal in two ways. One is referred to as physisorption (physical adsorption), in which case the interaction between the adsorbate molecule and the substrate is weak. The interaction is due to the weak van der Waals forces which arise from mutually induced dipoles involving quantum-mechanical London dispersion forces produced by the responce of polarizable electrons to the instantaneous dipoles created by nearby electrons. These attractive forces are usually weak, long range and the enthalpy of adsorption rarely exceeds -25 kJ mol^{-1}. Additionally, physical interaction between permanent dipoles and the interfacial field at surfaces gives rise to another component of the physical adsorption energy.

In chemisorption (chemical adsorption) the adsorbate interacts with the substrate through overlap of its electronic orbitals with those of the metal surface and this usually leads to the formation of a chemical bond, usually of a covalent polar type, having an energy comparable with that of a regular chemical bond. In fact, chemisorption can, in a sense, be thought of a 2-dimensional surface compound formation and it usually occurs with some degree of charge-transfer between the

substrate and the adsorbate, that in electrochemical experiments can actually be measured [22].

The enthalpy change due to chemisorption is usually substantially more negative than - 40 kJ mol^{-1}. Chemisorption, which results in the formation of real bonds, thus produces in 2-dimensions new "chemical compounds" at the substrate surface.

It should be pointed out that the nature of chemisorption bonds is not at all so well understood as are normal molecular bonds because the state and stoichiometry of the adsorbate-adsorbent complex is often not well characterized; thus it is usual that the adsorbate is sometimes bonded to more than one atom on the substrate surface. Also some adsorbates can alter the energetics of the substrate surface which will influence the bonding of further adsorbate molecules and also lead to reconstruction of the surface of the adsorbate.

Chemisorption on noble and other transition metals has received greater attention than on any other class of solid surfaces as evidenced by the great quantity of experimental data for such surfaces. Transition and noble metals are of interest because their surfaces are chemically stable, relatively easy to clean and these metals are technologically important. Of especial chemical interest in catalysis is that the properties of transition and noble metals are dominated uniquely by the d-electrons, leading to complex electronic band structures. Their surfaces and hence their chemisorptive properties are thus of special interest.

Electrons in solids can usefully be classified into "valence" (or bonding) and so-called "core" electrons. The core electrons are tightly bound to their nuclei and hence are less affected by the presence of other atoms in the solid. Valence electrons, which are usually the s and p electrons of the outermost shell, or with transition metals, hybridized d-orbitals, exhibit different behaviour. They overlap strongly from one atom to another so they cannot be identified so specifically with any particular atom. In a metal, some fraction of the valence electrons (ca. 1 per atom) behave as "itinerant" or free-running plane waves traversing the whole solid. This delocalized character is treated in terms of metal electron band concepts such as the "jellium" model, the "nearly-free-electron" approximation and the "array of pseudopotentials".

The d-electrons have wave functions with maxima " well inside" the atom and their

amplitudes decay rapidly further out, which is a core-electron-like behaviour. However, the tails on the neighbouring atoms overlap considerably and are thus significantly modified on going from isolated atoms to the solid state, and this corresponds to valence-electron-like behaviour. The d-electrons therefore exhibit intermediate behaviour between that of valence electrons and core electrons.

The various techniques and models used in calculating the effects of chemisorption on the electronic structure of d-band metals have been described and reviewed in various articles and monographs (e.g. ref. 59) but are outside the scope of the present thesis.

1.6.1 Adatom-Adatom Interactions among Adsorbates

Many real situations involve a large 2-dimensional number-density of adsorbed species on metal substrates. When substantial charge-transfer occurs between substrate and adsorbate, a surface dipole moment arises, usually normal to the substrate surface. For any two parallel-oriented dipoles, a lateral interaction will arise with an energy given by:

$$\Delta E = 625 \text{ meV} \times \mu^2 / r^3 \qquad (1.7)$$

where μ is the moment of the surface dipoles in Debyes and r is the lateral separation in Ångstroms. At low coverages, especially in the case of gaseous adsorbates, the adatoms are sufficiently separated so that there is negligible adatom-adatom overlap. In such circumstances and the fact that induced dipole moments are small, the only interaction is an indirect coupling via the substrate electronic states. Depending on whether the two "impurity" states [60] are bonding or antibonding, the coupling can be attractive or repulsive. It was also shown that the pair interaction energy depends on the binding site symmetry, both in strength and in sign.

Interaction energy is a function of separation and typical values are 0.6, 0.12 and 0.05 in the units of the substrate bandwidths (typically 6 to 12 eV) for nearest, next-nearest and third-nearest neighbour pairs, respectively. These values were obtained in calculations made for the case of the (100) face of a single-band, simple cubic crystal. Similar results were obtained by Burke [61] from calculations for a model study of the (100) and (110) faces of W.

Attractive and repulsive interactions can be involved in the formation of ordered overlayers on substrate surfaces. For example, a centred (2x2) adlayer might be a product of a repulsive nearest-neighbour and attractive next-neighbour interaction. When predominantly attractive forces arise, they can result in the formation of islands or domains of the ordered phase at low coverages, and 2-d phase transitions can sometimes be observed, including situations at electrodes, e.g. in the underpotential-deposition of Pb on Au. This kind of case is very important both in surface science and electrochemical surface science.

1.6.2 Simple Chemisorption Theory

Desjonqueres and Spanjaard [62] developed a simple chemisorption theory and applied it in their investigation of transition metal adatoms on transition metals. It was observed that the bond length increases with the coordination number of the adsorbate, so that the most stable adsorbate position is at the site with the largest coordination number available on the surface. It has been shown by Marcus et al. [63], Demuth et al. [64] and Van Hore and Tong [65] that, for example, O and S occupy a centred threefold site on Ni(111) and a centred fourfold site on Ni(100), the bond length of O (S) increases from 1.88 Å to 1.98 Å (2.02 Å to 2.19 Å) when going from Ni(111) to Ni(100). This trend is also obeyed by surface atoms of transition metals.

The model of Desjonqueres and Spanjaard [62] was used to calculate the potential energy of the adatom as a function of position. They assumed that, due to symmetry, all bonds are equivalent and the binding energy involves the sum of two terms, i.e.

$$E_L = \Delta E_{rep} + \Delta E_{band} \qquad (1.8)$$

where ΔE_{rep} is the variation of the repulsive energy of the system due to the bonding of the adatom. It is described by

$$\Delta E_{rep} = Z\, A \exp(-pR) \qquad (1.9)$$

where Z is the coordination number of the adatom in the surface and R is bond length.

The variation of the band energy term, ΔE_{band}, is also given by two terms

$$\Delta E_{band} = \Delta E_a + \Delta E_s \qquad (1.10)$$

where ΔE_a is the energy gain of an adatom when going from vacuum to the position R on the surface and ΔE_s is the change of the substrate energy when the bond is formed.

The derived expression for the binding energy then has the form

$$E_L = ZA \exp(-pR) - \sqrt{Z}\, B\, (N_s) \exp(-qR) \qquad (1.11)$$

where $N_s(Na) = -La(\beta_{os}^2/2\pi)^{1/2} \exp(-x^2)$ and $x = erf^{-1}(2Na/La - 1)$ where La is the degeneracy of the adatom level, β_{os}^2 is the average of the square of hoping integrals between adsorbate and substrate and Na is the number of adatom electrons involved in the bonding. The equilibrium distance is given by

$$R_o = 1/[2(p-q)] \log Z + 1/(p-q) \log p^A/q^B \qquad (1.12)$$

Equations (1.11) and (1.12) show that the binding energy and the bond length increase with coordination number of the adatom. One of the most important conclusions of Desjonqueres and Spanjaard [62] was, as mentioned above, that the most stable site is one with maximum coordination (as might intuitively be anticipated), although there are exceptions as discussed by these authors [62].

These effects give rise to significant and practically interesting variations of the binding energy with the crystallographic orientation of the substrate surface. Electronic correlation effects, however, decrease the influence of the geometry and of the chemical nature of the substrate.

1.7 Adsorption Isotherms for Atoms in Monolayers

Several types of adsorption isotherms have been used to describe the adsorption behaviour of an array of metal, H atoms or OH which can be electrodeposited uniformly over a surface up to approximately a monolayer before the deposition of the bulk form of the species.

The general reaction equation for a simple, 1 e , single-state surface process involving a charge-transfer reaction where species A is electrodeposited on a metal substrate M can be written as follows:

$$\underset{1-\theta_A}{M} + \underset{C_A^{\pm}}{A^{\pm}} \underset{k_{-1}}{\overset{k_1}{\rightleftharpoons}} \underset{\theta_A}{MA_{ads}} \pm \underset{E}{e} \qquad (1.13)$$

where (1 - θ) is the fraction of the surface on M that are unoccupied by A (proportional to the free area), $C_A\pm$ is the concentration of the reactant $A^{\pm}$ species in solution, θ_A is the fractional coverage of A on M, $k_1/k_{-1} = K$ is the electrochemical adsorption equilibrium constant and E is the electrode potential related to the Fermi level of electrons in the above equation.

When a surface process described by eqn. (1.13) is at equilibrium, the forward and reverse rates, expressed in terms of current-densities are

$$i = zFk_1(1 - \theta_A)C_A\pm \exp \pm\beta EF/RT \qquad (1.14a)$$

and

$$i = zFk_{-1}\,\theta_A \exp \pm(1-\beta)EF/RT \qquad (1.14b)$$

where E is the metal/solution potential difference and β (≅ 0.5) is the well known Brønsted or energy-barrier symmetry factor for the charge-transfer process [66].

The adsorption equations commonly used to describe adsorption behaviour in upd are: (i) the Langmuir isotherm or (ii) the Frumkin isotherm, each of which is described further below.

1.7.1 Langmuir Isotherm

The Langmuir isotherm is based on two main assumptions:

(a) The substrate surface provides a homogeneous distribution of adsorption sites and lateral interactions between the adsorbate species are negligible;

(b) The adsorbate species occupy the substrate sites at random, i.e. every adsorption site is equivalent.

When the process in eqn. (1.13) is at equilibrium, i.e. $i = i$ or $i = 0$, we have

$$\theta_A/(1-\theta_A) = KC_A\pm \exp \pm EF/RT \qquad (1.15a)$$

or

$$\theta_A = [KC_A\pm \exp(\pm EF/RT)] / [1 + KC_A\pm \exp(\pm EF/RT)] \qquad (1.15b)$$

which is the electrochemical Langmuir adsorption equation for an upd surface process involving charge transfer. Eqn. (1.15) indicates that θ_A is a function of E with θ_A in the range $0 < \theta_A < 1$; thus at any E, corresponding to states within this range, there is a characteristic and definite value of θ_A

that is established which is thermodynamically determined by the value of E.

1.7.2 Frumkin Isotherm

In general, when interaction effects between the adsorbate species cannot be neglected, the adsorption isotherm must be written in the form

$$\theta_A / (1-\theta_A) = KC_A \pm \exp(-g\theta_A) \exp(\pm EF/RT) \qquad (1.16)$$

where g is a 2-dimensional lateral interaction parameter [67]. The same configurational factor, $\theta_A / (1-\theta_A)$ as in the Langmuir case, is assumed to arise. The Langmuir isotherm is evidently a special case of the Frumkin isotherm above, when $g = 0$. Eqn. (1.16) represents the situation where the adsorption equilibrium constant is a $f(\theta)$, viz. $K_\theta = K_{\theta=0} \exp(-g\theta_A)$.

The condition $g < 0$, represents the situation when attractive interactions are operative in the ad-layer. Attractive interactions arise, for example, in the upd of Pb on Au [29] leading to the 2-dimensional phase transition in the ad-layer referred to earlier in terms of the "spike". The condition $g > 0$ corresponds to the effect of repulsive interactions.

When $g \neq 0$, the differential coefficient of the adsorption isotherm can only be explicitly expressed as a function of coverage θ_A. Then the so-called adsorption pseudocapacitance, C_ϕ, is given explicitly by [67]

$$C_\phi = q_1 \, d\theta/dE = q_1 F/RT \, . \, \theta(1-\theta) / [1 + g\theta(1-\theta)] \qquad (1.17)$$

C_ϕ as f(E) when $g \neq 0$ must be evaluated numerically from the above equation using $\theta(E)$ from eqn. (1.16). Examples are shown in Fig. 1.4.

1.7.3 Adsorption Pseudocapacitance for a UPD (Surface) Process

The isotherms for potential-dependence of coverage, such as the Langmuir adsorption equation, can be differentiated with respect to potential E to yield differential or "capacitance" isotherms which can be determined experimentally.

If q_1 is the charge required to for the deposition or desorption of the monolayer, the charge corresponding to a change of coverage $d\theta$ can be written as

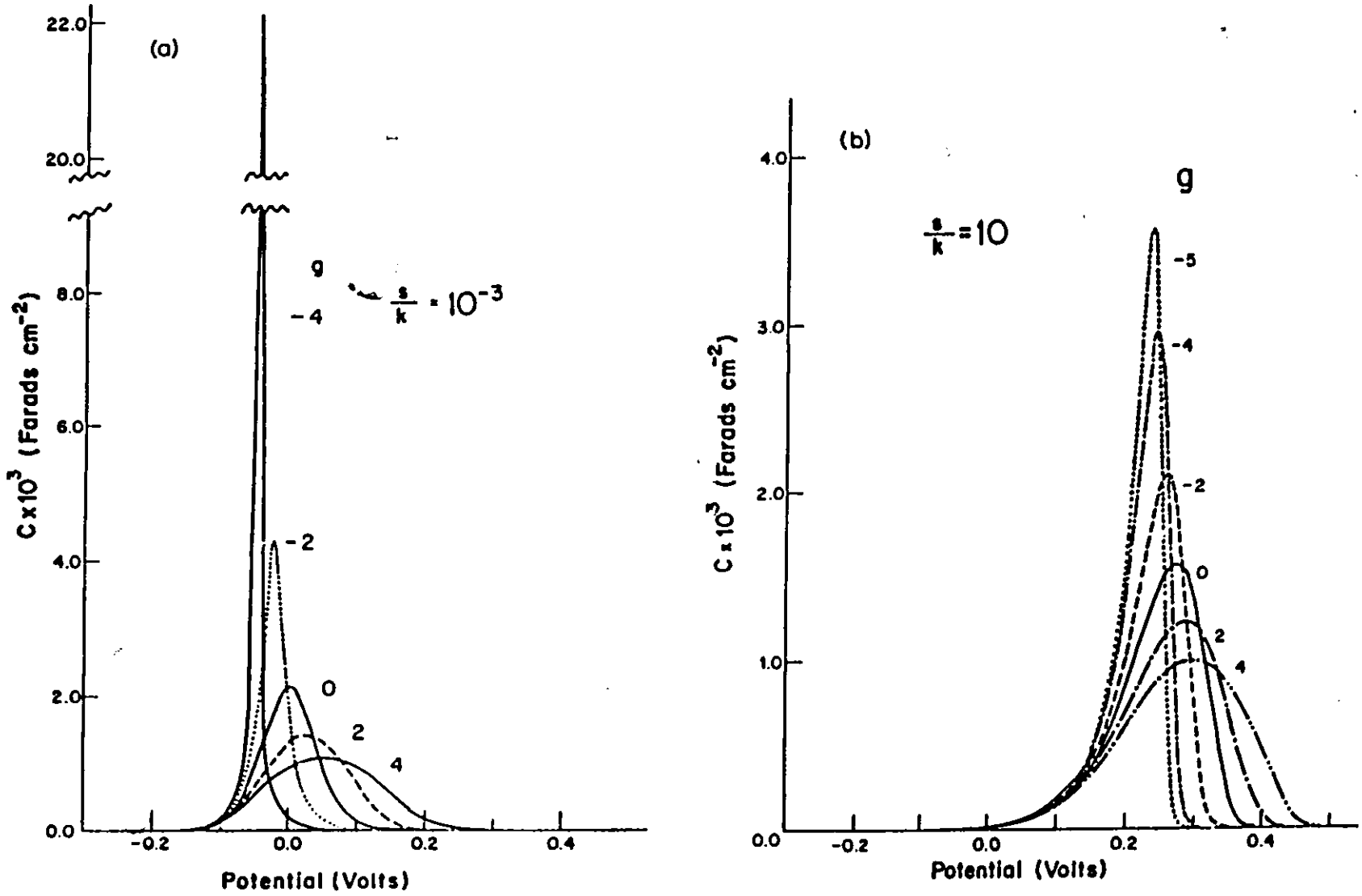

Fig. 1.4 Plots of the C vs E profiles for reaction (1.13) for various positive and negative g values for: a) reversible conditions b) irreversible conditions. (From ref. 150).

$$dq = q_1 \, d\theta \qquad (1.18)$$

The differential coefficient of the adsorption isotherm eqn. (1.15) is then given by the expression:

$$C_\phi = dq/dE = q_1 d\theta/dE$$

$$= q_1 F/RT \, . \, [KC_A \pm \exp(\pm EF/RT)] \, / \, [1 + KC_A \pm \exp(\pm EF/RT)]^2 \qquad (1.19)$$

where, again, C_ϕ is the so-called the adsorption pseudocapacitance for the surface process.

In the linear potential sweep or so-called potentiodynamic method, E varies linearly with time at a constant sweep-rate $s = dE/dt$ and the corresponding response current is measured and is a function of the varying potenial. In general, since $i = dq/dt$, where dq is the charge passed by the current i in time dt, i can be written as

$$i = dq/dt \equiv dq/dE \, . \, dE/dt = (dq/dE) \, s \qquad (1.20)$$

It is seen that the quantity dq/dE is a capacitance, C, for the surface process and can be determined experimentally as

$$C = i/s \qquad (1.21)$$

Eqn. (1.21) forms the basis for distinguishing a simple surface process from one, say, which is diffusion-controlled for which

$$i \propto s^{1/2} \qquad (1.22)$$

It is to noted that although the C in eqn. (1.21) arising from (1.20) has the proper units of a capacitance, it does not behave as an electrostatic capacitance; it arises physically only when charge is transferred in the upd process giving rise to change of θ, but since the resulting variation of θ depends on E, a capacitance quantity C arises and can be measured as such in transient or a.c. impedance experiments.

1.8 2-Dimensional Array Structrures on Substrate Surfaces

Low Energy Electron Diffraction (LEED) and other UHV techniques have been used to study several vapour/solid systems to determine surface structures of metal monolayers deposited on metal single-crystal surfaces [68]. In almost all cases the formation of a 2-dimensional ordered structures is a general phenomenon. At low coverages, ordered structures exist, as revealed by LEED. This suggests that significant repulsive interactions arise between the adsorbate atoms on the surface. Also, at low coverages, the orientation of the metal substrate largely determines the structural

properties of the monolayer.

The interaction between the adsorbate and the substrate particles is a major factor in determining the ordering observed. At low coverages, the crystallographic orientation of the metal substrate largely determines the structural properties of the monolayer array as the dimensions of the two unit cells are closely related. At high coverages, the surface structures of the monolayer array are sometimes rather complex and do not correspond to the structure of the substrate lattice (a so-called non-commensurate array). The structures are determined by a combination of many factors such as the relative atomic sizes of the adsorbate and the substrate, and the relative magnitudes of the adsorbate-substrate, adsorbate-adsorbate and substrate-substrate interactions.

Despite the complex adsorbate ordering at high coverages, a 1x1 structure is often observed, (commensurate array) showing nearly identical adsorbate and substrate lattice parameters. Such a situation arises when the bulk interatomic distances of the two metals are similar, for example when Pt is deposited on Au(100) [69]. When the interatomic distances in the bulk are different, coincidence structures are observed, as found for example, when Pb is deposited on Au(100) [70]. A model proposed by Huber and Oudar [71] requires that the adsorbate and the substrate layers have the highest possible symmetry, corresponding to minimization of Gibbs energy.

At the vapour/metal interface, thermal desorption spectra (TDS) [72] have been determined in order to indicate multiple-state adsorption in 2-dimensional structures. At the electrode/solution interface, the analogue of this technique is cyclic-voltammetry, as was described above for characterization of distinguishable states of chemisorption of adatoms, for example, on single-crystal, low-index planes.

1.9 Effects of Co-adsorbed Anions

Co-adsorbed anions usually have marked effects on the i vs E upd profiles of H at Pt [73,74,75], Pb at Au [26] or of the initial stages of surface oxidation of Pt or Au [75,76]. Competitive adsorption effects between anions and H, or OH and O species are usually involved, so that (as with H) the same quantity of H is eventually deposited but over a different range of

potentials and in different sub-states from those in the absence of the competitively co-adsorbed species.

The specific adsorption of anions at Au increases in the order $F^- < ClO_4^- = SO_4^{2-} < Cl^- < OH^- < Br^- < I^-$ [77]. Schmidt and co-workers [78] found that in the upd of Pb on Au, the monolayer cathodic peak was shifted to more cathodic potentials by adsorbed anions in the increasing order $NO_3^- < CH_3COO^- < Cl^- < Br^-$. Kolb et al. [31] also found that the monolayer cathodic peak in the upd of Pb on Au from solutions containing Cl^- or Br^- is shifted to more cathodic potentials in the increasing order $Cl^- < Br^-$.

Schmidt and Wüthrich [79] have also discussed the adsorption of halides on Au in terms of competitive adsorption. Using the thin-layer technique, they determined the surface concentration of adsorbed halides and found that it corresponded to a coverage of more than 50% of the monolayer at positive potentials. They also proposed that since, electrostatically, halide adsorption should yield a maximum coverage of about 20%, it is probable that the halide is not adsorbed as an ion but forms a compound with the substrate, i.e. charge- transfer from the anion to adatom of the substrate occurs.

However, Kolb et al. [31] argued that the amount of adsorbed halide ion on Au in the underpotential region is less than 20% of the monolayer coverage in order to account for competitive adsorption. It is likely, of course, that the adsorbed anions change the surface properties of the substrate, for example, its effective electronegativity.

Vicente and Bruckenstein [21] found in their investigations that Cl^- ion enhances the adsorption of Pb on Au. In the presence of Cl^-, the monolayer cathodic peak is sharper, although it was slightly shifted to more negative potentials, as expected for competitive adsorption by an anion. The cathodic charge increased with Cl^- concentration. The apparently incomplete desorption of Pb^{2+} at positive potentials in Cl^- solution does not seem to be related to the surface coverage of Cl^-. The adsorbed species existing in the upd region is probably a chloride complex of lead, such as $PbCl^+$, which is first decomplexed before Pb^{2+} deposition occurs.

In the upd of Pb on Au, aliphatic amines also shift the monolayer cathodic peak to more negative potentials with increasing concentration of the amines [40]. Competitive adsorption takes

place because the amount of charge (q_C) for Pb deposition remains nearly constant with increasing amine concentration. For primary amines, the strength of adsorbability increases with increasing number of C-atoms in the molecule. Tertiary amines were found to be only weakly adsorbed.

1.10 Substitutional Adsorption at Electrodes

Thermodynamic studies show that solvent molecules adsorb at charged metal electrodes, as may be expected. Adsorption of other species, especially during upd, will therefore always be competitive with the charge-dependent adsorption and orientation of solvent molecules that are present initially at the surface. The solvent molecules initially at the surface will have to be replaced by the adsorbing species and the solvent effects will tend to be most pronounced for the initial stages of adatom deposition. Hence a situation of "substitutional adsorption" will arise and therefore solvent effects are important in upd and will be considered in detail in Chapter 4.

Since solvent adsorption energy and degree of orientation in the case of polar solvent molecules, tends to become larger at higher surface charges or interfacial fields (cf. refs. [80 - 83]), the solvent will become more difficult to displace in competitive substitutional adsorption by anions as surface charge increases. However, for anions, their own adsorption energy will tend to increase as q_M becomes more positive (see discussion later).

1.11 Double-Layer Structure in Non-Aqueous Media and the Role of Solvent Orientation

Much of the present work has been carried out in non-aqueous solutions, so it is appropriate here to summarise the results of some previous researches on metal electrode (mainly Hg)/non-aqueous solution interfaces. Systematic study of the double-layer in non-aqueous solvents began with the work of Frumkin [84] in 1923 when he showed that the capacity of the double-layer for the Hg/solution interface, determined in different solvents, did not correlate with the bulk dielectric constant of the medium. After the work of Grahame [85], various capacity measurements have been carried out in several non-aqueous solvents at polarizable interfaces and this work is well covered in a review by Payne [86].

Knowledge of the structure of the double-layer provides the basis for understanding solvent structure at the electrode interface and other related processes such as adsorption of simple ions, non-electrolytes and metal adatoms.

Based on the characteristic shapes of the differential capacity curves observed for Hg in various solvents, Parsons [87] classified the behaviour in various solvents into three groups:

Type I: Capacity curves having a hump and minima on each side. These are water-like, associated solvents and include formamide, DMSO and N-substituted formamide.

Type II: Capacity curves exhibiting only one hump but with no minimum on either side. These examples arise for polar cyclic compounds, including ethylene cabonate, propylene cabonate and sulpholane.

Type III: Capacity curves having the form of an inverted parabola. These examples arise for non-aqueous systems including solvents such as alcohols, ammonia, DMF and acetonitrile.

The differential capacity curves for the Hg/AN interface have been measured in solutions of different electrolytes of non- or weakly adsorbing ions [88,89]. The differential capacity curves, unlike those for other non-aqueous solvents [86], do not exhibit the so-called capacity hump.

Fawcett and Loutfy [90] have studied the double-layer capacity at the Hg/AN interface in alkali metal ion and tetraalkylammonium perchlorate solutions. There was no evidence for specific adsorption of TEA^+ or alkali metal cations although, in solutions of alkali metal cations, the inner-layer capacity, C_i, increases in the order $C_i(Li^+) < C_i(Na^+) < C_i(K^+) < C_i(Cs^+)$ at more negative potentials. Similar ordering has been observed in water [91] methanol [92] and ethylene carabonate [93], and this was explained as due to the decrease in solvation as the cation size increases.

In tetraalkyammonium perchlorate solutions, for cathodic potentials, the capacity decreases with increasing cationic size because as the cationic size increases, more solvent molecules are displaced from the inner-layer. Consequently the dielectric constant in the inner-layer increases.

The sharp increase in the differential capacity at potentials positive to the p.z.c. is mainly

attributed to solvent reorientation. This means that, like other aprotic solvents, AN is strongly adsorbed on Hg with the positive end of its dipole towards the Hg.

Borkowska and Fawcett [94] have studied the differential capacity of the Hg/MeOH interface in KF, $NaClO_4$ and $LiBF_4$ solutions. The capacity curves exhibit a deep minimum which is independent of the nature of the electrolyte, with no other extrema. At more positive potentials, the inner-layer capacity is found to increase in the order $C_i(BF_4^-) < C_i(ClO_4^-) < C_i(F^-)$. A similar order has been observed for other solvents such as DMSO [95], PC [96] and EN [93]. Since specific adsorption from these solutions was shown to be absent, the above ordering is due to variation in ionic size and the effeects of the anions on the dipole interactions in the solvent monolayer at the electrode surface.

The entropy of formation of the Hg/MeOH interface in 0.1M $NaClO_4$ solutions has been studied as a function of electrode surface charge-density [97]. The entropy maximum occurs at a positive charge density (0.05 C m^{-2}) which indicates maximum disorder of MeOH (least orientation polarization and greatest librational entropy).

Gordon and Conway [98], calculated the entropy of the electrostatistically adsorbed water molecules in the double-layer based on the up (↓) and down (↑) orientations (with the B.D.M. [81] model) and the dependence of the librational frequency of the oriented dipoles in the electric field, on the surface charge-density. The three-state model of Fawcett [99] gives related results.

The Hg/DMF interface gives capacity curves with no definite capacity hump of the kind that is observed at negative potentials in the case of protic amide solvents and is generally attributed to solvent reorientation.

Payne [100], and Bezugly and Korshikov [101], studied the adsorption of DMF at Hg from aqueous electrolyte solutions. The maximum adsorption occurs over a range of negative charge density depending on the concentration of DMF. They concluded that the DMF molecule is predominantly adsorbed on Hg at the p.z.c. with the orientation of its dipole parallel to the metal/solution interface. The preferential adsorption of the DMF molecule was interpreted as a "squeezing out" effect on water molecules rather than to specific interaction with the electrode metal

itself.

Payne [89] was the first to study the interfacial capacity of the Hg/PC interface in 0.1M KPF_6 solutions. The capacity curves exhibit the so-called capacity hump at positive potentials.

Nguyen et al. [102] have reported data from their capacity measurements at the Hg/PC interface in KPF_6 solutions as a function of temperature, and no specific adsorption on Hg from PC is indicated using this solution. The inner-layer differential capacity as a function of charge exhibits a capacity hump on the positive side of the C_i vs charge-density profile.

The adsorption entropy of PC at the Hg/PC interface is positive and the entropy curve passes through a maximum at a negative charge density [102], an indication that, at least in the region of p.z.c., the molecular arrangement of the solvent is more disordered in the adsorbed layer than in the bulk, and/or the intermolecular frequencies (librational modes at the charged surface) are "looser". The fact that the maximum entropy of adsorption occurs at a negative charge-density suggests that, at the p.z.c., the PC dipoles are preferentially oriented with their negative ends nearest to the electrode, as in the case with H_2O.

1.12 Models for Solvent Dipole Orientation at Charged Interfaces

1.12.1 Introduction

Knowledge of the solvent structure at the charged electrode/solution interface is desirable for understanding the role of the solvent in the electrode processes such as upd, electrosorption and electrocatalysis.

The orientation of solvent dipoles creates a surface-dipole layer potential difference, $\Delta\chi_d$, which is a function of the potential and hence of the electrode charge, q_M. The differential coefficient $d(\Delta\chi_d)/dq_M$ gives the reciprocal of the inner-layer differential capacitance, $1/C_i$, which is due to the dipole orientation at the electrode interface. Its effect and contribution to the overall capacitance will depend on how small it is, since it is in a series relation with other capacitance components of the overall double-layer capacitance.

Recently, several molecular models have been developed to describe the solvent structure at

the electrode/solution interface and will be briefly described below since they are relevant to the question of solven displacement by upd adatoms.

1.12.2 The Two-State Model

The first basic model used to describe the solvent orientation and hence the dielectric properties at the electrode interface was developed by Watts-Tobin [80] and Mott (W-T M model) [103]. In this model the inner-layer region is represented by an array of dipoles of the solvent in a monolayer at the electrode interface that can be aligned into two limiting directions of orientation: 2-state model, with dipoles having vectors parallel to the electrode field (normal to the surface) with the positive end pointing towards the metal, ↓ ("up" dipole) or away from it, ↑ ("down" dipole).

The W-T M model [103] can account qualitatively for the capacitance hump on the capacity-potential curves for the Hg-aqueous system and other solvents. However, lateral dipole-dipole interaction effects are neglected and it is also assumed that the dipoles at the interface have a high permittivity equal to that in the bulk solvent.

The two-state model was developed further in an important way by Bockris, Devanathan and Müller (BDM model) [81], taking into account the lateral interactions between oriented solvent dipoles, as this effect would be expected to be important in determining the rate of change of dipole orientation with electrode charge, q_M , or interfacial field.

N↓ and N↑ are the number of dipoles per cm^2 oriented with and against the field E, respectively, and N_T is the total number of dipoles, i.e. $N_T = N\uparrow + N\downarrow$ ($\equiv 10^{15}$ water molecules cm^{-2}). For N↑ dipoles, taking into account the lateral interaction energy that will be related to the fraction oriented in one way or the other,

$$\text{energy} = \mu E + (C_n/2\ U\ N\downarrow/N_T) - (C_n/2\ U\ N\uparrow/N_T) \qquad (1.23)$$

where μ is the solvent dipole moment, C_n is the 2-d coordination number in the double-layer (= 6), U is the pairwise interaction energy (ca. 48 to 64 kJ mol^{-1} for -OH dipoles).

According to the BDM model [81], the net (non-electronic) polarization of the dipoles is then given in terms of an orientation distribution function:

$$(N\uparrow - N\downarrow)/N_T = \tanh [\mu E/kT - C_i/2\ U/kT(N\uparrow - N\downarrow)/N_T)] \quad (1.24)$$

The surface dipole potential is related to the net orientation and is therefore given by

$$\chi_d = 4\pi (N\uparrow - N\downarrow)\mu / \epsilon_s \quad (1.25)$$

where ϵ_s is the dielectric constant in the intephase which will be smaller than in the bulk because of orientation dielectric saturation (for H_2O, ϵ_s was taken as 6 while in the bulk, $\epsilon = 78$).

In the BDM model [81] C_i is a maximum when $q_M = 0$, i.e. when $N\uparrow = N\downarrow$. However, the interaction energy factor is not zero but is attractive (due to H-bonding between water dipoles) and therefore the interaction effect term is incorrect. In general, the BDM model [81] does not offer a fully satisfactory explanation of the dielectric properties of the Hg/water interface.

Levine, Bell and Smith (LBS) [104] later developed a statistical-mechanical 2-state model which was discussed by Conway and Dhar [83], who avoided the introduction of a dielectric constant for the inner layer but considered the molecular polarizability. In their treatment, it is recognized that the two dipole vectors for the two possible orientations are not exactly equal and opposite but can be represented by two vectors, $P\uparrow$ and $P\downarrow$.

These models [80,81,103,104] predict inner-layer capacity vs electrode charge-density curves that have a single maximum. These, according to Parsons' classification, therefore represent behaviour of the type II solvents, which exhibit, in their capacity curves, a single maximum with no other extrema apparent in the polarizable range of the electrode. These models have been applied to data obtained for Hg/aqueous, Hg/NMF and Hg/EC interfaces.

In the W-TM and LBS models [103,104] the anodic capacitance hump is attributed to dielectric saturation at the interface but H-bonded structures in the interface were neglected.

1.12.3 The Three-State Model

Bockris and Habib [105] developed a 3-state model by considering the solvent in terms of "monomers" as in the W-TM 2-state model [103], and "dimers" with no net dipole moment in the direction of the electrode as a third state. This model [105] could only account for the behaviour of the differential inner-layer capacity curves for aqueous systems and especially for systems that give

rise to a solvent contribution to the interfacial entropy. They concluded that the solvent made a negligible contribution to the interfacial capacitance because their estimated solvent contribution to C_i was very high (note the "series" contributions of capacitance components).

A much improved 3-state model for non-associated solvents (monomers) was developed by Fawcett [99]. Besides the up (↓) and down (↑) orientations in the 2-state model, a third orientation with dipole vectors parallel (→ ←) to the electrode surface was considered, as illustrated in Fig. 1.5. below.

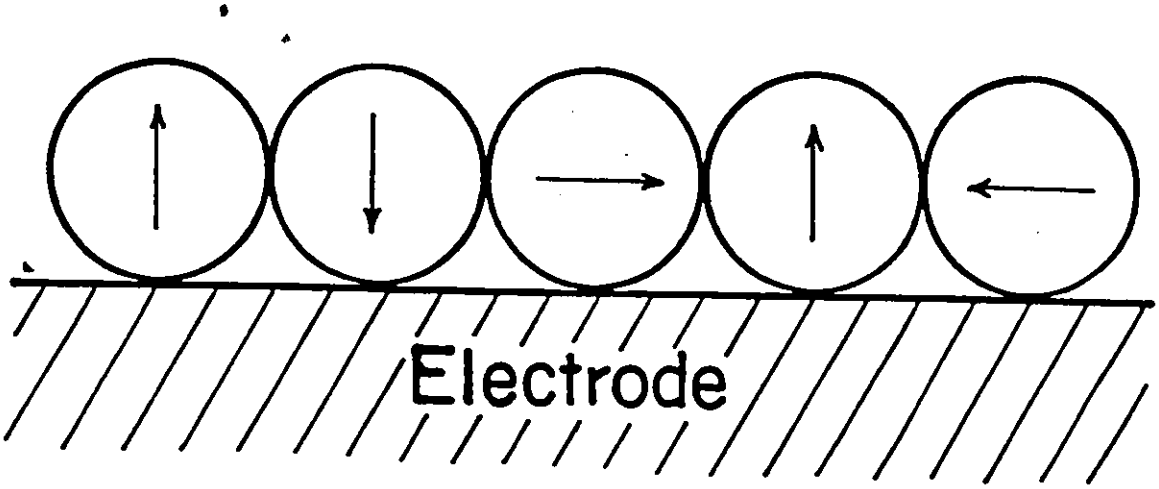

Fig. 1.5 The three-state model of the solvent monolayer at the electrode/solution interface illustrating the orientation of molecular dipoles in the up (↓), down (↑) and parallel (→ ←) positions. (From ref. 99).

The third orientation (number density = N_o) makes no orientational contribution to the polarization of the monolayer in a direction perpendicular to the interface but it has a different residual energy of interaction with substrate metal and neighbouring dipoles and occupies surface sites at the interface.

The differential capacity for the inner layer in the above model, which is similar to that of LBS [104], is

$$1/C_i = (4\pi d + 4\pi N_T d^3)/c_n(\partial\chi_d/dq_M) \qquad (1.26)$$

where d is the molecular diameter, c_n is the effective coordination number and $N_T = N\uparrow + N\downarrow + N_o$.

The 3-state model for "monomers" gives a good qualitative account of the differential capacity curves for both type I and type III solvents which exhibit a simple maximum or minimun as a $f(q_M)$. This model has been used rather successfully to describe the differential capacity curves for the Hg/MeOH, Hg/EC and Hg/DMF interfaces.

1.12.4 The Four-State Model

With the possibility that water clusters [106,107] could be present at the electrode/electrolyte interface, Damaskin and Frumkin [108] (DF model) proposed a "4-state" model to describe the dielectric properties of an interphase in associated solvents like water. In this model, two types of solvent particles are regarded as existing in the interphase: associated water molecules, freely oriented along the electric field and chemisorbed water dipoles in the down (↓) orientation.

Parsons [109] improved the DF model [108] by developing a more detailed treatment of the state of a solvent at an electrode interface in terms of a "primitive" 4-state model. In particular, this [109] took into account the total number of molecules in the monolayer in various states, and the concentration of so-called chemisorbed water molecules. Solvent molecules in the monolayer at the interface were regarded as existing in small clusters together with free "monomeric" molecules, each of which could have two possible orientations as in the 2-state model [80,81,103,104]. Parsons [109] suggested that the most stable orientation of dipoles at the p.z.c. ($q_M = 0$) is not in fact ↑↓↑↓↑↓ (the antiferromagnetic orientation) but preferably ⇄ ⇄ ⇄ parallel to the surface, as recognized in the Fawcett model [99].

These models can qualitatively describe the dielectric properties of the metal/solution interface for associated solvents like water, F and NMF, but their employment to treat experimental results is semi-empirical owing to the necessity for assigning values to several parameters, e.g. cluster size, etc.

1.12.5 The Multi-state Model

From the molecular two-state model [80,81] which was extended to the three-state model [99,105] and later to the four-state model [108,109], Macdonald and Barlow [110] and Fawcett and de Nobriga [111] have developed a more realistic multistate model for interfacial solvent structure and dielectric properties. In this model, all possible orientations of the solvent molecules are realistically considered, once again neglecting the dipole-dipole interactions.

The multistate model provides an explanation for the asymmetry observed experimentally in plots of the inner-layer capacity against surface charge-density. In addition it allows one to introduce specific effects due to the presence of counter-ions on the solution side of the inner-layer.

1.13 The Nature of the Metal Surface Itself at the Electrode/Solution Interface

1.13.1 Metal/Vacuum Interface

The discontinuity of a metal at its interface leaves unused orbitals in various electron-density distributions depending on the index of the crystal face. These unused orbitals are available for chemisorption of various adsorbates at metal surfaces and sometimes lead to surface reconstruction of the surface layer of a solid, e.g. Pt [58], into a different geometrical coordination structure.

The sudden interruption of the positive field due to ion cores at the interface causes the distributed electrons to "overspill" the edge of the lattice [112]. This creates an excess of negative charge outward from the nominal metal surface and an excess of positive charge inward from that surface. This separation of charges gives rise to the intrinsic surface potential, χ_m, of the metal in contact with a vacuum. The field created by χ_m can polarise adsorbate molecules. Thus, noble gases physically adsorbed on the metal are known to change substantially the surface potential, but they themselves do not undergo any charge-transfer with the metal but rather suffer polarization by the metal's surface field. The electron overspill effect is potential dependent.

1.13.2 Metal/Solution Interface

Frumkin [84] was the first to point out that the solvent properties at the metal/solution interface were different from those in the bulk even at $q_M = 0$, in reference to interpretation of capacity measurements in various solvents.

Capacity measurements for adsorbed water on solids [113] and density measurements of water at interfaces [114] indicate that the water usually is in a more ordered and structured state at most interfaces than in the bulk. The metal surface, he pointed out, might cause this difference in properties of solvent molecules at the interface and in the bulk.

The metal/solvent interface determines in important ways the behaviour of solid/electrolyte interfaces when the electrolyte is a liquid ionic solution. The adsorption at the electrode, whether specifically a chemisorption process or electrostatically charge-dependent, will involve the displacement of initially oriented water molecules. The existence of solvent molecules at the electrode interface and the presence of solvated ions introduces major complexities at the metal/solution interface compared with the situation in vacuum (Fig. 1.6), such as:

(a) The orientation of the solvent dipoles;

(b) Specific and electrostatic adsorption of ions at the charged interface; and

(c) Ion-adsorption in relation to ion-solvation and lateral interactions at the metal/electrolyte interface.

1.14 Effect of Competitive Adsorption with Solvent Molecules on the Kinetic Parameters for Electrode Reactions

1.14.1 Introduction

Solvent molecules constitute an important component of the electrode/solution interface. Adsorption of ions or neutral molecules, e.g. organic compounds, will be greatly influenced by the solvent structure at the interface and the energy of adsorption and orientation of solvent. In the case of any metal/solution interface, solvent molecules will have to be displaced from the electrode surface by any adsorbate becoming bound there.

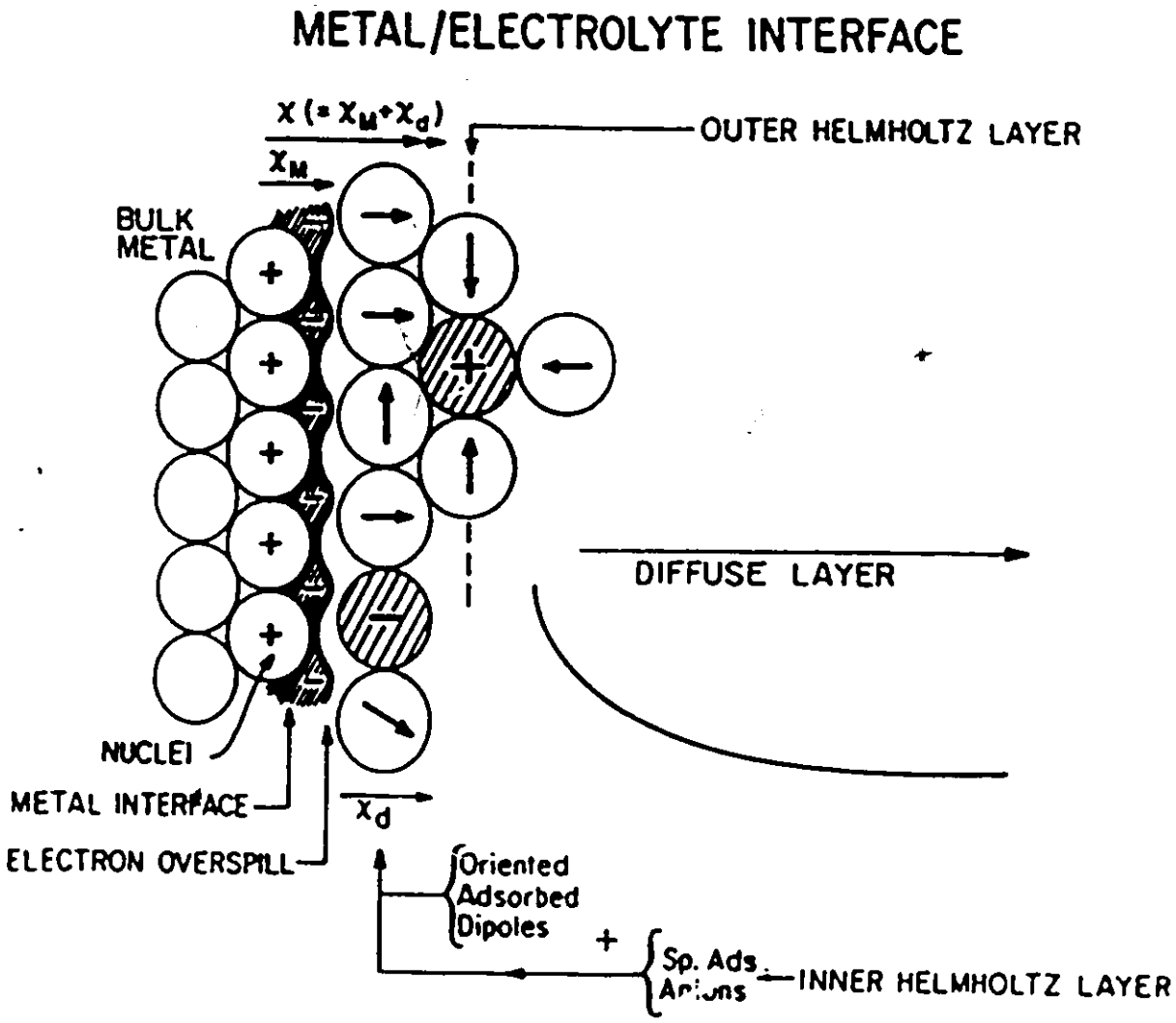

Fig. 1.6 Schematic diagram of the complex interphase at a metal/electrolyte boundary with solvent molecules and ions present. (From ref. 6).

Electrodeposition is the process of adsorption with charge-transfer on the electrode surface from solution (under controlled-current or-potential conditions) of species such as ions, neutral moleculess and intermediates formed in charge-transfer reactions [115]. The importance of the role of the energy of adsorbed water molecules in the energetics of adsorption processes was recognized by Butler [116] in 1932. Barradas and Conway [117] discussed the replacement of water molecules adsorbed on solid electrodes by adsorbed organic species. Electrodeposition of metal adatoms is also a "replacement reaction" or "subtitutional adsorption" process and its energetics depend on the difference between the adsorption energy of the adsorbate species and desorption energy of the appropriate number of solvent molecules [118] depending on the size (area) of the species being adsorbed. Hence this matter is relevant in the present work on upd of Pb at Au.

Gileadi and co-workers [119] and Gileadi [120] developed a combined isotherm which takes into account both the potential-dependence of adsorption due to charge transfer and due to replacement of solvent molecules from the interface; in an earlier treatment [121], these features were discussed separately. However, the treatment of Gileadi involves adsorbed intermediates that are involved in a continous Faradaic reaction but the case considered illustrates the importance of competitive adsorption with solvent replacement depending on the field-dependent energy of polarization of solvent dipoles in the inner-layer. Competitive adsorption between an adsorbed intermediate in a Faradaic electrode process and adsorbed oriented solvent molecules can affect the kinetics of the reaction in two ways:

1. The degree of coverage by adsorbed intermediates and the rate of change of their coverage with potential $d\theta/d(\Delta E)$, becomes changed due to the field dependence of electrostatic polarization of oriented solvent dipoles; and

2. The rate constant for the rate-determining step increases in the case of a desorption step but decreases in the case of an adsorption step due to the effect in (1).

Gileadi and Stoner [122] established a Tafel slope relation which takes into account these charge transfer and the competitive polarization effects of field-dependent water adsorption.

The basis of the effect introduced by Gileadi and co-workers [119] is that solvent dipoles of

will interact with the electrode, through the electrode field $\Delta E/\delta$, where δ is the interfacial thickness of the double-layer with an energy $\mu\,\Delta E/\delta$. If m molecules of solvent must be displaced for each act of deposition of an intermediate, the energy change is $m\mu\Delta E/\delta$. (In this treatment it is assumed that the potential is already sufficient to cause virtual orientation saturation). Then the energy of activation for the deposition process will be modified from its value $\Delta G_0^{\#}$, when no solvent displacement arises, to the value

$$\Delta G^{\#} = \Delta G_0^{\#} + \beta m\mu(\Delta E/\delta) \qquad (1.27)$$

Including additionally the conventional effect of potential on $\Delta G^{\#}$, then

$$\Delta G^{\#} = \Delta G_0^{\#} + \beta(m\mu\,\Delta E/\delta - \Delta Ee) \qquad (1.28)$$

is obtained for a charge transfer, electrodeposition step; its Tafel slope then

$$b = RT/\beta F\,(m\mu/\delta e - 1) \qquad (1.29)$$

which is to be compared with the normal slope where for a simple discharge step of $b = RT/\beta F$.

For a such solvent replacement process, the Tafel slope will therefore depend on the size of the adsorbed intermediate in relation to that of the solvent, as this will determine the number of solvent molecules displaced from the electrode surface for each act of deposition of the intermediate.

It was shown that the Tafel slope varies substantially with variation in molecular size of the adsorbed intermediate. Hence experimental results can only be properly interpreted if the water or solvent competition effect is taken into account using the "combined adsorption isotherm" treatment i.e. taking into account competitive solvent displacement when electrosorption of deposited species takes place. We shall show that this effect can be important in underpotential deposition of Pb on Au in various solvents.

1.15 Entropy of Electrodeposited Species in a Monolayer

Evaluation of the entropy of adsorbed species in a monolayer can give information about the state of the adsorbed layer and also indicates the mobility or immobility of the particles in the ad-layer.

Quantitative results on adsorption at the vapour/Hg interface were reported by Kemball

[123,124] in his work on the standard entropy and heat of adsorption of vapours of non-polar and polar substances on mercury. In both cases, the adsorption was reversible and, with the exception of water, adsorbed films in a 2–d gaseous state were formed at low pressures. Since the nature of the force field at the mercury was not known, the exact entropy values could not be obtained. The entropies were however, calculated from translational and rotational partition functions of adsorbed particles (assumed immobile) and compared with the experimental values.

The limitation of this method is that the influence of the force field on population of rotational states is ignored. The calculated entropies compared well with the experimental values and this gave a fairly good indication of the extents of translational and rotational freedom possessed by the particles on the surface of mercury.

For polar substances, the entropies of adsorption were negative. For the primary adsorbed layer, acetone had the least value ($\Delta S^\circ \equiv$ -20 J mol^{-1} K^{-1}) and water had the highest value ($\Delta S^\circ \equiv$ -15 J mol^{-1} K^{-1}). Higher alcohols (n-butyl, n-amyl and n-hexyl) showed two-dimensional condensation to liquid films at higher pressures. This phase change was accompanied by an increase of entropy which led to a decrease of the surface vapour pressure with rise of temperature. The large negative adsorption entropy of water is an indication that probably the water molecules become immobile and/or H-bonded on the Hg surface. Kemball [124] suggested, however, that probably any particular water molecule remained in contact with the same mercury atoms for a relatively long period and the water-mercury complex thus formed that was mobile within the mercury surface.

The entropy of monolayer particles can also be determined for underpotentially deposited species. In the case of the underpotential deposition of H or metal adatoms, it has been remarked earlier that the adlayer is usually formed in several electrochemically distinguishable sub-monolayer states, e.g. 4 or 5 for H on Pt [50,51] or up to 7 for Pb on Au [52]. These states of chemisorbed H or metal atoms have temperature-dependent standard Gibbs energies of electrodeposition and ionization which enable the corresponding standard entropies of adsorption, ΔS°, to be evaluated, as described in later sections of this thesis.

Detailed information on the relative Gibbs energies of the resolvable electrodeposited

submonolayer states of H or metal adatoms can be obtained from the peak potentials of the i vs E profiles derived in potentiodynamic sweep experiments [49,51].

For the purpose of obtaining ΔS° values for upd states, cyclic-voltammetry experiments are conducted at various temperatures, using the reference electrode in the same solution. The apparent entropies of the distinguishable states are determined by evaluating the temperature derivatives of the peak potentials (dE_p/dT) which represent the Gibbs energies of electrodeposition in standard states of half coverage for each resolved adsorption state. By extra-thermodynamic means [5,125], a series of values of single-ion partial molar entropies have been evaluated which enable the absolute temperature coefficients of half-cell reversible electrode potentials to be derived relatively reliably, so that the ΔS° values for upd states can be evaluated, as in the case of H on Pt [126].

This approach has been applied in the present work to the evaluation of the standard entropies of upd Pb adatoms in various states relative to the standard entropy of Pb in the bulk crystalline state.

1.16 Aims of the Present Work

Although much work has been reported in previous papers [1,2,3] on upd investigations, especially from aqueous medium, it is evident from this literature that hitherto little attention has been focused on the role of the solvent in influencing upd processes. Electrodeposition of ions, neutral atoms or molecules is greatly affected by the structure of the solvent molecule inner-layer at the electrode/solution interface. Also, the states of upd adatom arrays have been little characterized with respect to their entropies in relation to mobility or otherwise of the adatoms.

In the present work, the upd of Pb at polycrystalline Au has been studied in various protic and aprotic solvents with respect to:

1) Characterizing the i vs E upd profiles for multiple-state adsorption below a monolayer with regard to their dependence on the solvent. (The deposition profile may be solvent-dependent if the displacement of the solvent by the deposited adatom introduces an irreversible process or otherwise a change of the states of the adatoms in the upd process).

2) Investigation of the kinetics of the deposition and desorption processes by means of

cyclic-voltammetry. The peak potential for each distinguishable state is measured as a function of the log of the sweep-rate, s, giving the s_o value [127] characteristic of the kinetics of the surface electrodeposition process. (cf, i_o, the exchange current-density for a regular Faradaic process).

3) Examination of the effect of temperature on the peak potentials corresponding to sub-monolayer ad-atom states. From the changes of the peak potentials with temperature, the standard entropies of the upd states, relative to the entropy of the bulk state can be determined and interpreted in terms of the mobilities of adatoms in arrays.

4) Investigation of the effect of co-adsorbed anions and the supporting electrolyte on the upd i vs E profiles for Pb on Au. Anion adsorption effects are expected to be dependent on solvent on account of varying strength of ionic solvation in media of differing dielectric constant and electron donicity or accepting power [5], as well as on account of the strength of solvent dipole polarization at the electrode interface itself.

These investigations have been carried out in the following solvents: acetonitrile (AN), methanol (MeOH), dimethylformamide (DMF) and propylene carbonate (PC), with water as the reference solvent.

CHAPTER 2

EXPERIMENTAL

2.1 Introduction and Choice of Methods

In the present work, the underpotential deposition (upd) of Pb at polycrystalline Au has been studied in various protic and aprotic non-aqueous solvents, over a range of temperatures and in the presence of various electrolyte anions. The i vs E upd profiles for multiple-state adsorption of Pb, and the kinetics of Pb deposition and desorption into upd monolayers at Au electrodes, have been evaluated as a function of solvent and temperature.

The phenomenon of so-called upd is a surface process in which virtually only non-continuous currents pass as the available surface of the electrode is either filled to the limit of full coverage ($\theta = 1$) or the monolayer deposited is stripped to zero coverage ($\theta = 0$). Methods used in the study of electrochemical surface processes must therefore be of non-continuous, transient kind and include cyclic-voltammetry, galvanostatic charging/discharging, a.c. impedance, usually used in a complementary manner for better understanding of any electrochemical reaction. These methods can also be coupled with the rotating-disk electrode technique when controlled mass-transfer conditions are required. In the present work, the preferred technique, used throughout, was cyclic-voltammetry because it is the most powerful and sensitive tool for electrochemical study of surface processes where small, time-dependent current-densities are involved, and where resolution of multiple-states of adsorption in a monolayer is required.

Electrochemical surface processes are basically reactions occurring on the surface of electrodes. It is now recognized that the behaviour of an electrode is sensitive to factors such as: preparation and cleaning of the electrode, the level of the purity of the solutions and other experimental conditions. It has been found in this laboratory [128] that e.g. trace concentrations (10^{-8} - 10^{-7}M) of SO_4^{2-} and halide ions have marked effects on the initial stages of surface oxidation of Au and, in the present work, Pb at Au. Surface processes are also very dependent on the state of the electrode metal interface and are susceptible to any changes in it, e.g. due to adsorption

of impurities, crystal face orientation (i.e. crystal face lattice geometry) morphology changes, etc. Therefore great care must be exercised in the treatment of electrodes, i.e. their preparation and cleaning, cleaning of the electrochemical cells, preparation of solutions by using, where possible, the purest solvents available. For better comparison between the experimental results for various conditions under which upd of Pb at Au was studied, experiments were carried out under instrumental conditions that were kept, as far as possible, identical, e.g. ranges of potential scanned, values of sweep-rates used, as well as constancy of Pb^{++} ion concentration.

The details of the experimental method, preparation and cleaning of electrochemical cells and electrodes, preparation of salts and solutions, and other aspects of the experimental techniques used in the present work, are described below.

2.2 Experimental Method

2.2.1 Cyclic-voltammetry

The cyclic-voltammetry technique has become increasingly useful in electrochemical surface-science studies, especially upd, and provides a wealth of information about a particular surface process by the dynamical examination of the i vs E upd profile. Usually the potential of the working electrode is varied linearly with time at a constant sweep-rate, s, to a limit and then the direction of the sweep is reversed in a continuous repetitive manner ("cyclic-voltammetry"). During the potential cycling, the current is simultaneously recorded as a function of the potential. This is achieved by feeding into the potentiostat a pre-arranged, linearly-varying, time-dependent program, controlled by an electronic function generator. The electrical circuitry used in the present work is described below and schematically shown in Fig. 2.1, as was also recorded in some previous theses from this laboratory [52,128].

2.2.2 Electrical Circuitry

The basic electrical circuit used in this work is well known and is shown in Fig. 2.1. The potential of the working electrode was controlled by a high output-voltage Wenking potentiostat

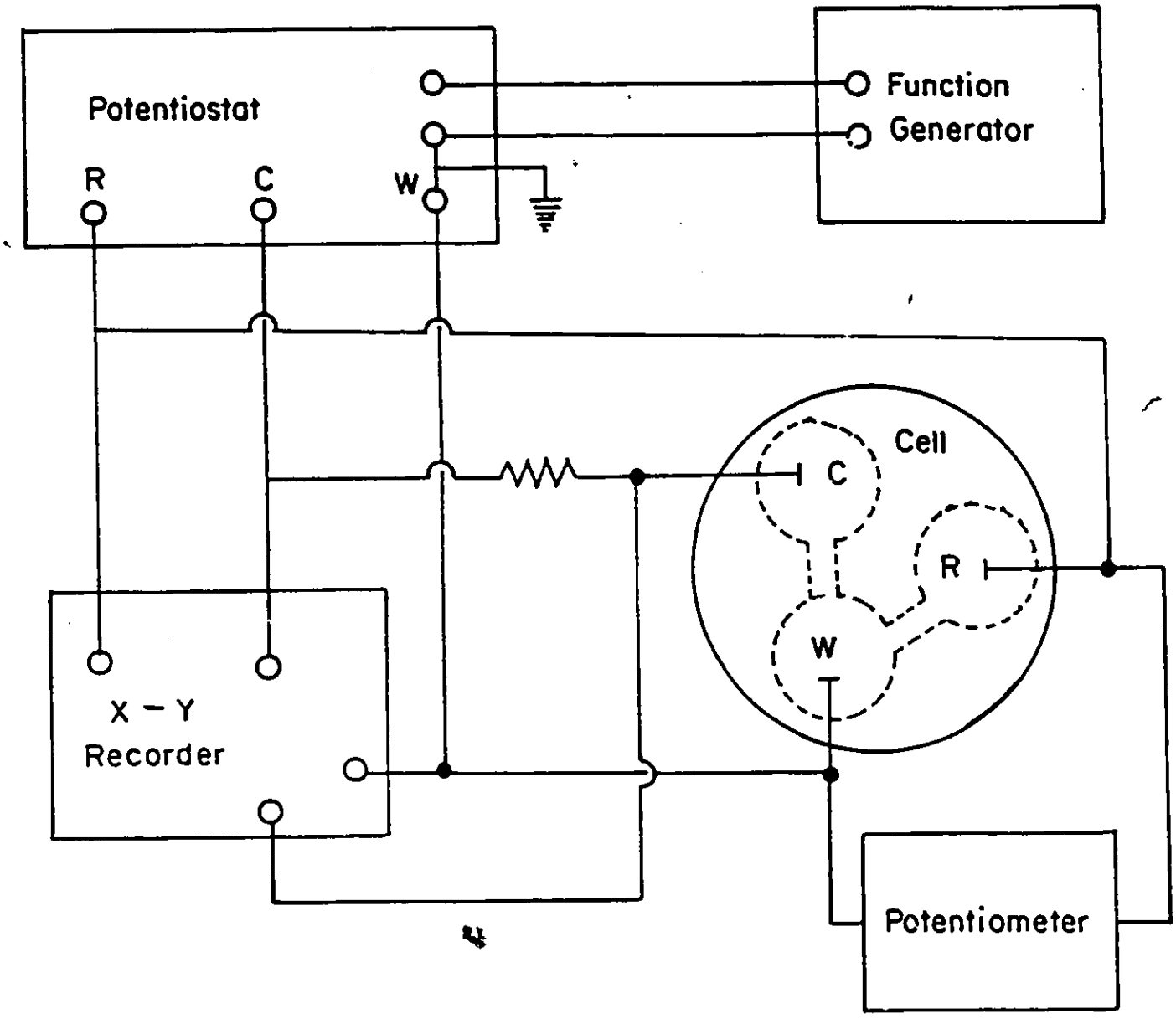

Fig. 2.1 Electrical circuitry employed in potentiodynamic sweep experiments.

which was programmed by a Tacussel GSATP function generator. The currents passed between the working electrode and the counter-electrode were measured as potentials across a decade resistance box (Leeds and Northrup Co.) connected in series with the counter-electrode. Experimental current (i) vs potential (E) profiles were recorded by means of a Houston (type 2000) or a Hewlett-Packard (Moseley Model 7001 AM) X-Y recorder in the case of slow sweep-rates ($\leq$ 150 mV/s) or were monitored on a Nicolet digital oscilloscope (Model 206) for higher sweep-rates (> 150 mV/s). Continuous read-out of the working electrode potential was available on a digital multimeter (Racal-Dana type 4002).

2.3 Purity and Purification of Solvents

2.3.1 Water Purity

In the early seventies it was found difficult, in this laboratory, to prepare highly pure water free from organic and other impurities by means of distillation, even followed by distillation from alkaline $KMnO_4$. Solutions prepared with this water exhibited stray impurity currents in electrochemical surface science-studies at Pt at which selective blocking of currents for surface reactions of O and H species took place. The organic impurities commonly present in domestic and industrial water supplies sometimes cannot be removed by simple distillation if they are steam-volatile. Although the actual chemical nature of the new impurity(ies) could not be established, Conway and co-workers [50] developed a new method to remove these impurities by "catalytic-pyrodistillation". The water thus obtained is virtually free from organic impurities and is then suitable for use in demanding electrochemical studies, particularly those in which surface processes that are very sensitive to adsorption of impurities, are to be examined.

The apparatus developed and now routinely used in this laboratory is shown schematically in Fig. 2.2. About 1.5 ℓ of fresh, doubly-distilled water is boiled in the 2 ℓ flask and stirred with purified O_2 entering the flask at about 1 $cm^3\ s^{-1}$. The steam rises through an 18 mm diameter silica tube which is heated to about 1023 K. The hot column contains a closely-packed, 90% Pt–10% Rh gauze for catalytic oxidation of organic trace impurities in the water vapour, to gaseous oxidation products

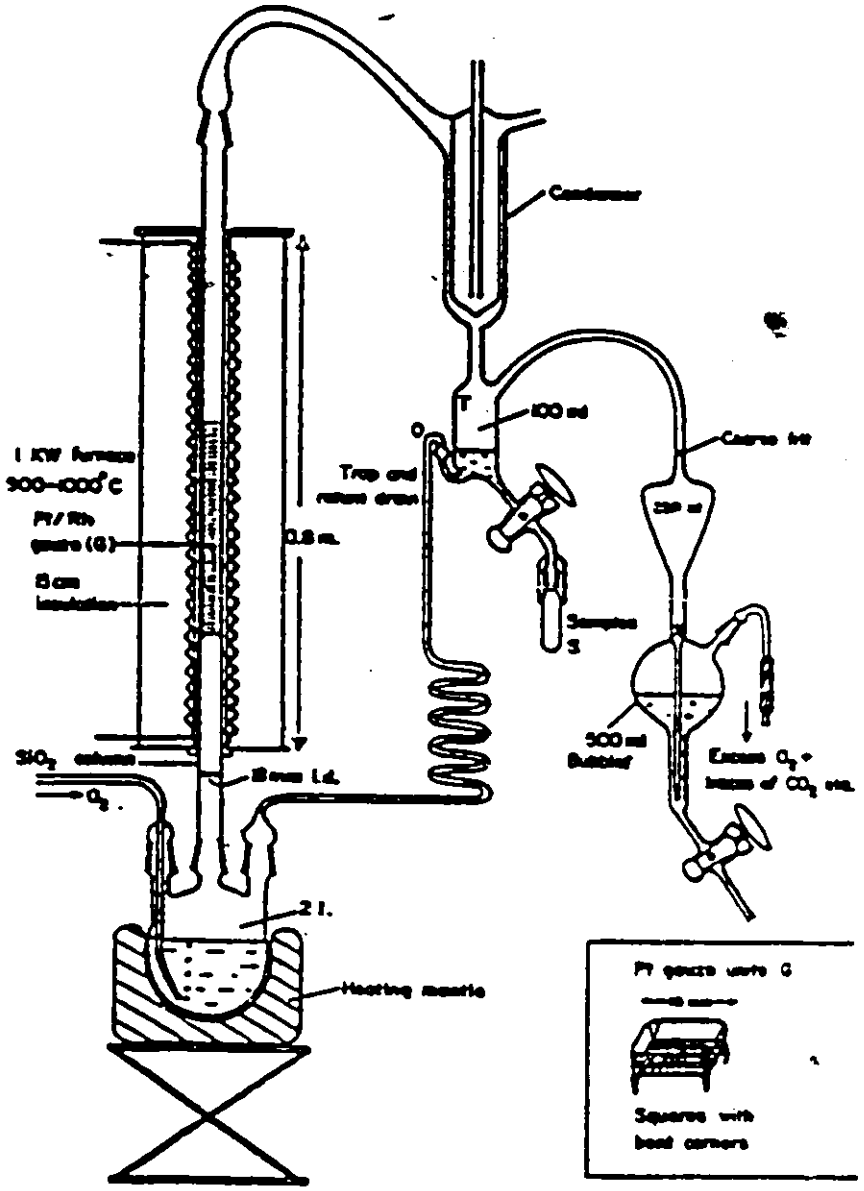

Fig. 2.2 Apparatus for the pyrodistillation of water.

(e.g. CO_2, NO_2). The apparatus has a Soxhlet-type overflow syphon which sequentially returns about 100 cm^3 volumes of condensed, pyro-distilled water back to the distilling flask every 1/3 hour for recycling in the distillation process which is continued for at least 48 hours before aliquots of purified water are collected in a specially-cleaned flask or in the electrochemical cell for use in experiments.

The pyrodistillation process is thought to be substantially superior to other methods developed elsewhere, based on the adsorption of impurities on activated charcoal [129] or platinized Pt sponge potentiostated at 0.005 to 0.350 V [130]. Especially at charcoal, other impurities can be adventitiously introduced.

Adsorption methods involve the difficulty of maintaining the adsorbent material itself in an ultrapure condition, especially with charcoal, and the assumption that any new impurities that may appear in the water supply will still be removed by the adsorbent.

The use of catalytically pyrodistilled water and "AristaR" (BDH) grade acids eliminates the need for potentiodynamic or potentiostatic pre-electrolysis [131 - 133] involving high anodic potentials, required to obtain the "clean" i vs E profiles, unchanging and independent of solution agitation. Satisfactory results could usually be obtained at Pt after about 10 cycles, normally over the potential range 0.07 – 1.32 V E_H in a fresh solution; however, under optimum conditions, it was found that they could be obtained even on the second or third cycle after the electrode has been left on open-circuit for some hours in a deaerated solution [134]. This important result incidentally eliminates the objection that has sometimes been raised that the "structure" of the cyclic-voltammetry i vs E profile for Pt or Au in aqueous solution is an artefact arising from multiple potential cycling.

The use of pyrodistilled water, AristaR grade acids and recrystallized salts combined with the special cleaning procedures (see Section 2.5) has made it possible to obtain "clean" (oxidation/reduction) i vs E profiles for Au under optimal conditions in 5 cycles or less.

Experience gained from studies of surface processes at Pt [52] and Au [52,128,135] in this laboratory in both clean and impure solutions has been utilized to formulate the following general

guiding principles for diagnosing the cause of impurity effects on the i vs E profiles:

	Effect on i vs E Profile	Source of Problem
1.	Solution agitation distorts the i vs E profile.	Presence of reactive impurities under diffusion control.
2.	Solution agitation improves or restores the "clean" i vs E profile.	Impurities leaking from inside electrode through an imperfect glass/metal seal.
3.	Profile "dirty" but not affected by agitation.	Impurities strongly adsorbed or deposited on electrode surface.
4.	Profile "dirty" as in 3, but improves with anodic/cathodic cycling.	Oxidizable or reducible impurities weakly adsorbed on the electrode surface.
5.	Peak currents do not increase linearly with sweep-rate, s.	Presence of reactive impurities in solution.
6.	Overall slant or shift in the profile with respect to the baseline.	Very leaky electrode or electronic artefact; high resistance in solution or circuit.

Consequently, the following criteria were developed for cleaniliness which are required to establish the purity of Pt and Au electrode-solution systems:

1. Absence of any agitation effects on the i vs E profile.
2. Maintainance of resolution of the multiple H (at Pt) and O states, and peaks in the i vs E profile down to sweep-rates as low as 0.005 $V\ s^{-1}$.
3. Equality of anodic and cathodic charge in the i vs E profile for oxide formation and reduction.
4. Constancy of the H deposition and removal charge at Pt to within 5% of its original value for at least 1h, while the potential range used excludes the region for deposition of O-species which otherwise re-activate the electrode surface by oxidative desorption of any impurities adsorbed or electro-desorbed.
5. Absence of any slant in the profile's baseline.

2.3.2 Non-aqueous Solvents

With the exception of methanol, preliminary upd experiments indicated no difference between results of experiments conducted in high-purity solvents (see below) as received and solvents further purified by drying, followed by distillation. Therefore, the following all-glass distilled, Burdick and Jackson, spectroscopically high-purity solvents (the levels of water being determined by Karl Fischer titrations) were used without further purification: acetonitrile (AN) (0.001% H_2O), dimethylformamide (DMF) (0.02% H_2O) and propylene carbonate (PC) (0.02% H_2O).

Methanol (Burdick and Jackson 0.02% H_2O or BDH analytical grade 0.1% H_2O) was further purified by refluxing ca. 800 ml over freshly prepared AgO (1 g $AgNO_3$ and 0.2 g NaOH added to MeOH) for 12 h with N_2 bubbling. The MeOH was then distilled into a second 1 ℓ flask and refluxed over 10 g Mg metal in a N_2-atmosphere for 24 h and finally carefully distilled into a collecting flask. Solvent purity was also checked by IR analysis and by recording and inspection of the cyclic-voltammetry for the supporting electrolyte without a lead salt being present. Satisfactory behaviour was achieved as shown in the examples illustrated in Fig. 4.6, Chapter 4.

2.4 Gases

Electrolytic H_2 and N_2 gases, used for the Pt/H_2 reference electrode and for deoxygenation of the solutions respectively, were purified in a conventional gas train [136] before use mainly to remove traces of O_2 since it (O_2) is chemically reactive with many substances and electrochemically reducible.

Hydrogen was passed through a gas train consisting of $Mg(ClO_4)_2$ as a desiccant, molecular sieves (BDH type 4A), an oven containing palladized asbestos and Cu turnings at 623 K, and finally activated charcoal traps cooled by liquid N_2.

N_2 gas was passed through an identical purification train except that only Cu turnings were used in the oven. The metallic surface of the Cu turnings at 623 K was periodically regenerated by passing H_2 through the oven until Cu turnings regained their bright metallic state.

2.5 Cleaning of Glassware

Before performing electrochemical experiments, the electrochemical cell and its glass component parts were soaked in fresh, concentrated chromic-sulphuric acid solution for ca. 12 h. They were then rinsed several times with doubly-distilled water and finally soaked in doubly-distilled water overnight to leach off any adsorbed chromate ions. Prior to use, the cell was rinsed thoroughly with very hot pyrodistilled water then filled with hot pyrodistilled water and left to stand for about 20 minutes. The assembled cell was then rinsed again and filled with the experimental solution.

For the experiments conducted in non-aqueous media, the cell and component parts were dried in an oven at 402 K, or higher, for at least 12 h in order to remove any residual water. To minimize moisture uptake, the cell was assembled a few minutes after removal from the oven and then flushed out with dry, purified H_2 or N_2 for about 30 minutes before the cell was rinsed and then filled with the experimental non-aqueous solution.

After the experiment, the solution was poured out and the cell immediately filled again with fresh, concentrated H_2SO_4.

Identical cleaning procedures were applied to the ancillary glassware for preparing salts or solutions, or for storing doubly-distilled and pyrodistilled water.

2.6 Electrodes

2.6.1 Working Electrodes

Working electrodes were made from Au wires of 99.999% purity, using Johnson Matthey "Grade 1" polycrystalline Au. Suitable lengths of these wires, usually of diameter 0.51 mm (0.02"), were first degreased overnight in refluxing acetone in a Soxhlet extractor. The Au wires were then flame-welded to much longer pieces of Ag wire to provide electrical contact and a droplet of (Pb-free) soft-glass was then melted on to the wire and then sealed into the end of a soft-glass tube (6 mm in diameter), leaving between 15 and 20 mm of wire protruding beyond the end of the tube. The Au-Ag contact was at least 15 mm above the glass seal. The soft glass had been previously cleaned

in fresh chromic acid solution and rinsed several times, first with doubly-distilled water, then followed by pyrodistilled water (see Section 2.5). The completed electrodes were then washed and stored in fresh, concentrated H_2SO_4, as indicated earlier.

Before each experiment in non-aqueous media, the working electrode was electrocleaned in aqueous 0.1M $HClO_4$ solution by applying a few anodic/cathodic cycles involving anodic oxidation of the surface and subsquent reduction of the surface oxide film produced in the anodic half-cycle. This procedure was performed until the usual "clean" i vs E profile (see criteria described earlier) was obtained. The electrode was then rinsed with the appropriate solvent, followed by the working electrolyte solution, and then immediately transferred to the cell.

2.6.2 Reference Electrodes

2.6.2.1 Hydrogen Reference Electrode

The hydrogen reference electrodes, which were used in all experiments conducted in aqueous medium, were prepared according to the procedure given by Ives and Janz [137]. The platinum wire and gauze used for their construction were degreased under reflux with acetone in a Soxhlet apparatus for ca. 12 h. The gauze was spot-welded to the short wire and sealed in glass in the usual way.

Prior to platinization, the electrodes were cleaned by briefly immersing them in a warm cleaning mixture of 50% aqua-regia (three volumes of 12M HCl, one volume of 16M HNO_3 and four volumes of distilled water). This mixture also can be used to remove the platinum black from used platinized electrodes which need to be replatinized. The electrodes were then briefly immersed in 16M HNO_3, rinsed thoroughly with pyrodistilled water and cathodically cleaned. The cleaning consisted of a cathodic electrolysis in 0.01M H_2SO_4 solution for ten minutes in order to remove any surface oxides. After this treatment, the electrodes were washed with pyrodistilled water and platinized without delay.

The platinizing solution was 2% H_2PtCl_6 in 2N HCl free from lead acetate (cf. the recipe of ref. [138]) because of the possibility of introducing undesirable impurities into the working

electrode electrolyte. Platinization was carried out for 10 to 20 minutes at a current-density of 10 to 20 mA cm^{-2}. Two electrodes (operated as anode and cathode) could be platinized simultaneously by reversing the direction of the current between them until a moderately thick coating of greyish-black platinum was obtained. Thick deposits of platinum black were avoided because they lead to sluggish, erratic behaviour. The finished electrodes were rinsed several times with doubly-distilled water and stored under pyrodistilled water. Potentials were checked from time to time against similar electrodes to detect appearance of any potential drift.

2.6.2.2 Lead Reference Electrode

For the experiments in non-aqueous media, lead wires (Aldrich Chemical Company, "Gold label" 99.9995% pure) 2.0 mm diameter were first degreased overnight in refluxing acetone in a Soxhlet extractor. The Pb wires were flame-welded to longer Ag wires to provide electrical contact. Prior to starting an experiment the lead wire was cleaned by immersing it in a glacial acetic acid-hydrogen peroxide solution (20 volumes glacial acetic acid to one volume of hydrogen peroxide). It was rinsed with the appropriate solvent, immersed in the electrolyte solution and immediately transferred to the electrochemical cell.

2.6.2.3 Counter Electrodes

The counter-electrode, whose only function is to allow the passage of the electric current, should be carefully chosen so that it does not introduce any high resistance in the circuit or impurities by side reaction(s) (e.g. from its own oxidation) which could interfere with the study of the process at the working test electrode. An ideal counter-electrode would, therefore, be one made from the same material as the working electrode and would transfer current by the reverse of the investigated reaction. In this way, no contaminants would originate from the counter-electrode and, under such conditions, the test electrolyte concentration in the cell would remain constant.

Although the choice and application of such an electrode is limited, counter-electrodes made from relatively inert materials such as Pt can usually be used with various working electrode materials if such an electrode is placed in a separate compartment. However, Pt counter-electrodes

used with Au working electrodes have been found [52] to cause contamination of the Au electrode by traces of Pt [139,140]; presumably Pt dissolves to a small extent at the counter-electrode (depending on anions of the electrolyte and temperature) and redeposits at the working electrode [141,142].

When the working and the counter-electrodes are placed in the same compartment, as is usually the case in most electrochemical surface studies, both the working and the counter-electrodes should be made of the same material. Therefore, with metals other than Pt, a Pt counter-electrode should not be used owing to the possibility of contaminating the working electrode, in the present work, Au. Large surface area counter-electrodes should be used because the large area minimizes the reaction resistance and the polarization of the electrode.

In the present work, counter-electrodes were made from Au wires (similar to those used for the working electrodes) and Au sheets (Johnson Matthey "Grade 1" Au 99.999% pure in the case of large counter-electrodes). The Au sheets, ca. 3 - 4 cm^2 geometric area, were spot-welded to the exposed Au wire. They were prepared, cleaned and stored in the same manner as that described for the working electrodes.

2.7 Choice of Electrolytes

When choosing an electrolyte in electrochemical studies where there is to be passage of current, the following properties of the salt must be considered: its solubility, dissociation constant, equivalent conductance and electrochemical stability. Therefore a suitable salt is one with high solubility, complete dissociation, high conductance and a numerically high discharge (decomposition) potential.

2.7.1 Anions

The choice of anion of the electrolyte is important in anodic reactions. Unless an anion is desired that is to be itself directly oxidised (e.g. Cl^- for Cl_2 evolution), difficulty oxidizable anions such as perchlorate, trifluoromethanesulfonate ($CF_3SO_3^-$), tetrafluoroborate, hexafluorophosphate or

nitrate should be chosen. For example, trifluoromethanesulfonate anion was selected as the anion of the Pb salt that was used in all the non-aqueous solution experiments reported in the present work. The salts of $CF_3SO_3^-$ are non-explosive, have excellent solubilities in commonly used non-aqueous solvents and dissociate to give solutions having high electrical conductivity (dependent on concentration) comparable with, or better than, that of perchlorates and tetrafluoroborates. $CF_3SO_3^-$ is also a thermally stable, and difficulty oxidizable anion, and is highly resistant to hydrolysis. Specific adsorption of the $CF_3SO_3^-$ anion on Hg in DMF and AN is similar to that for perchlorate [143] and nitrate anions [144,145] in aqueous solutions. Metal salts of $CF_3SO_3^-$ are easily prepared by reacting the corresponding metal carbonate or hydroxide with CF_3SO_3H (see Section 2.8).

2.7.2 Supporting Electrolyte

$NaClO_4$ was used throughout the work as the supporting electrolyte in the non-aqueous systems. It is soluble in many organic solvents and its ClO_4^- anion has a high discharge potential. Although the salt is hygroscopic, it can be vacuum dried at 383 K.

Quaternary ammonium salts, such as tetrabutyl-ammonium perchlorate (TBAP), the tetrafluoroborate (TBAT), the halides (TBAC, TBAB, TBAI) and the corresponding tetraethylammonium salts, e.g. TEAP etc., have been used as supporting electrolytes in non-aqueous systems. They were not, however, suitable in the present work because the tetraalkylammonium ions are themselves quite strongly adsorbed at the electrode where, in water, they form a region at the electrode interface with a low proton activity. The strength of adsorption of these cations also depends on the electrode potential relative to the p.z.c. of the electrode material itself and the size of the cation.

2.8 Salts and Solutions

Trifluoromethanesulfonic acid (3M Company), used to prepare trifluoromethanesulfonate salts, was purified by double distillation at atmospheric pressure (b.p. 435 K) in a nitrogen stream with trifluoromethanesulfonic anhydride added before the second distillation to remove any traces of water. The anhydride (b.p. 357 K) was prepared by distillation of the acid in a nitrogen stream over

P_2O_5 [146]. The so-called "monohydrate", really the H_3O^+ salt CF_3SO_3-H_3O^+, was prepared and purified as previously described [147]. A stoichiometric quantity of pyrodistilled water was added to the purified acid and the "monohydrate" formed was vacuum-distilled twice (355 K, $\leq$ 1 torr) in an all-glass apparatus. The distilled acid was collected in Pyrex collection ampoules which were immediately sealed under vacuum.

$Pb(CF_3SO_3)_2$ and $NaCF_3SO_3$ salts were prepared by neutralizing the corresponding metal carbonate with the purified CF_3SO_3H [148]. A suitable amount of the metal carbonate was added to about 100 ml pyrodistilled water to form a slurry. To the solution in an ice-bath, a sufficient quantity of CF_3SO_3H was added dropwise with stirring. The solution was evaporated to dryness and the white solid obtained was recrystallized first from acetone and then from ethanol. These trifluoromethanesulfonates were finally vacuum dried at 423 K for several days and then stored in a desiccator.

Other salts used in the present work were purified from the following starting materials: $Pb(NO_3)_2$, NaI (Fischer reagent grade material); NaCl, $NaNO_3$ and $NaClO_4$ (BDH AnalaR grade); NaBr ('Baker Analyzed' reagent). $Pb(ClO_4)_2.3H_2O$ (Aldrich 95% pure) and RbCl (Aldrich 99.99% pure) were used without further purification. These salts were recrystallized twice from pyrodistilled water and vacuum dried. In the case of NaI, the recrystallizations were performed under N_2 and the resulting crystals were kept in a dark vessel under N_2. Thiourea, also used as an additive in the present work, was the Fischer reagent grade material.

Non-aqueous solutions were prepared and kept in a N_2 tent. It was discovered in the early stages of the present work that reliable and satisfactory experimental results could only be obtained using freshly prepared non-aqueous solutions.

All aqueous solutions were prepared using pyrodistilled water [50]. H_2SO_4 and $HClO_4$ aqueous solutions were made using the purest commercially available acids (BDH AristaR grade) which, as noted previously [2,51], had been found to be of sufficiently high purity to be used directly, as demonstrated by highly sensitive cyclic-voltammetry results conducted at Pt electrodes (tests based on forms of the H and surface oxidation/reduction regions of the cyclic-voltammograms

and time effects thereon - see list of criteria in Section 2.3.1).

2.9 Cells

2.9.1 Electrochemical Cells

From previous experience gained in this laboratory with cells of different designs and sizes, it has been realized that a desirable cell should be of a suitably small size and simple design because it is then much easier to clean, and maintain in a clean state, and this then minimizes the possibility of impurity effects.

A conventional two-compartment cell, as shown in Fig. 2.3(a), was used in the case of experiments conducted in aqueous medium. The reference-electrode compartment is separate but it is connected to the solution and electrode in the working-electrode compartment by a Luggin capillary whose tip is placed close to the working electrode in order to minimize the "iR" drop in thesolution between the tip of the Luggin capillary and the working electrode. H_2, used in the reference-electrode compartment, was purified as described in Section 2.4.

For experiments conducted in non-aqueous media, a conventional one-compartment cell was used, as shown in Fig. 2.3(b) . The counter-electrode was placed close to the working electrode because of the unavoidable high solution resistance in such media and the reference electrode, bulk lead, was placed in the same compartment as the working electrode in order to minimize resistance between the working and the reference electrodes. This is necessary when high sweep-rates are to used in cyclic-voltammetry in resistive non-aqueous solutions.

Solutions in the working-electrode compartment were deoxygenated by bubbling a slow stream of purified N_2 (see Section 2.4), which was first pre-saturated with appropriate solvent vapour through them for 20 - 30 minutes before the experimental measurements were commenced.

2.9.2 Non-Isothermal Cell

The cell shown in Fig. 2.4 was used for non-isothermal, reference electrode measurements. A suitable thermostated fluid was circulated through each jacket. For non-isothermal measurements,

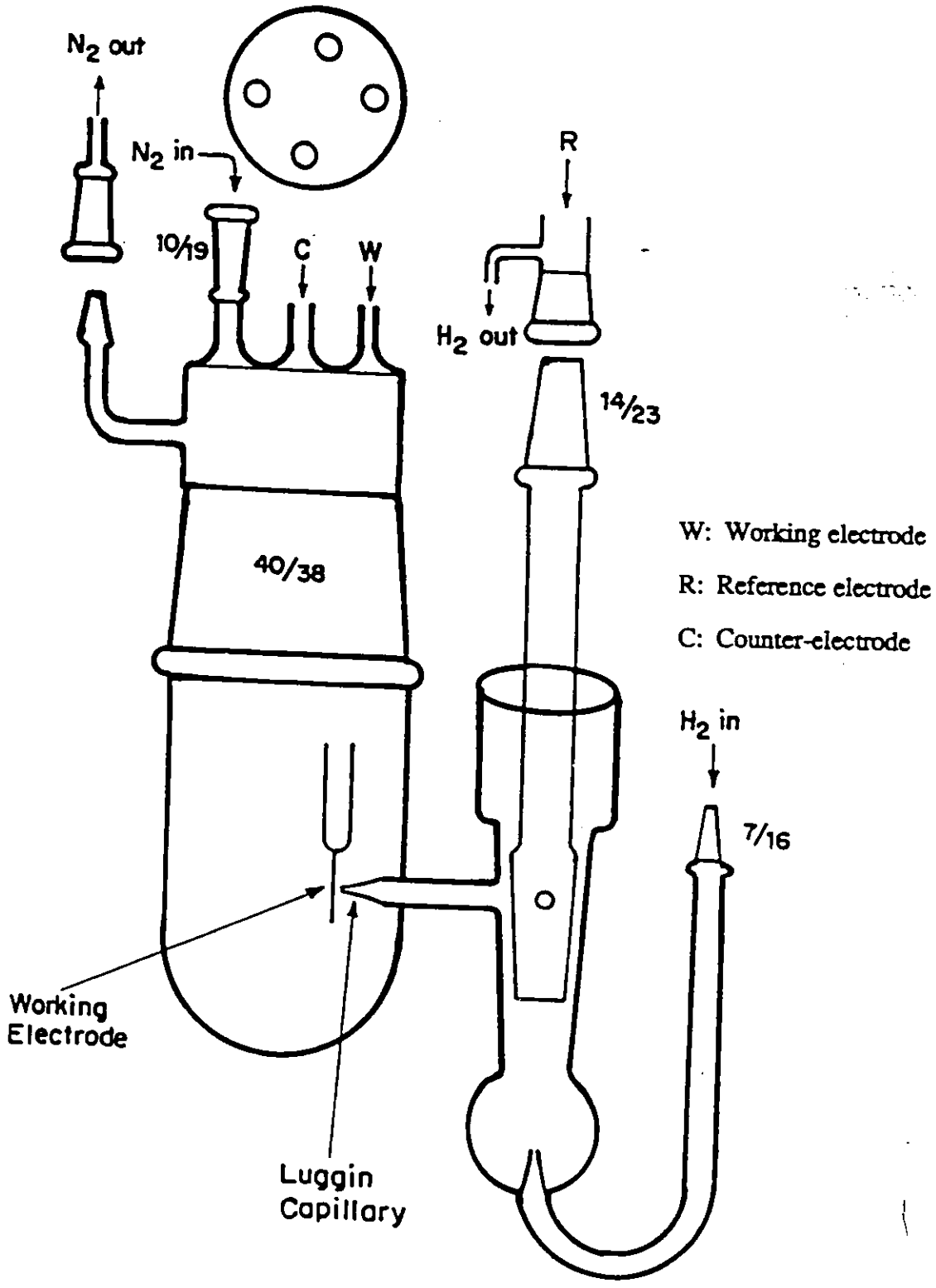

Fig. 2.3 (a) Schematic diagram of the two-compartment electrochemical cell employed for experiments conducted in aqueous medium.

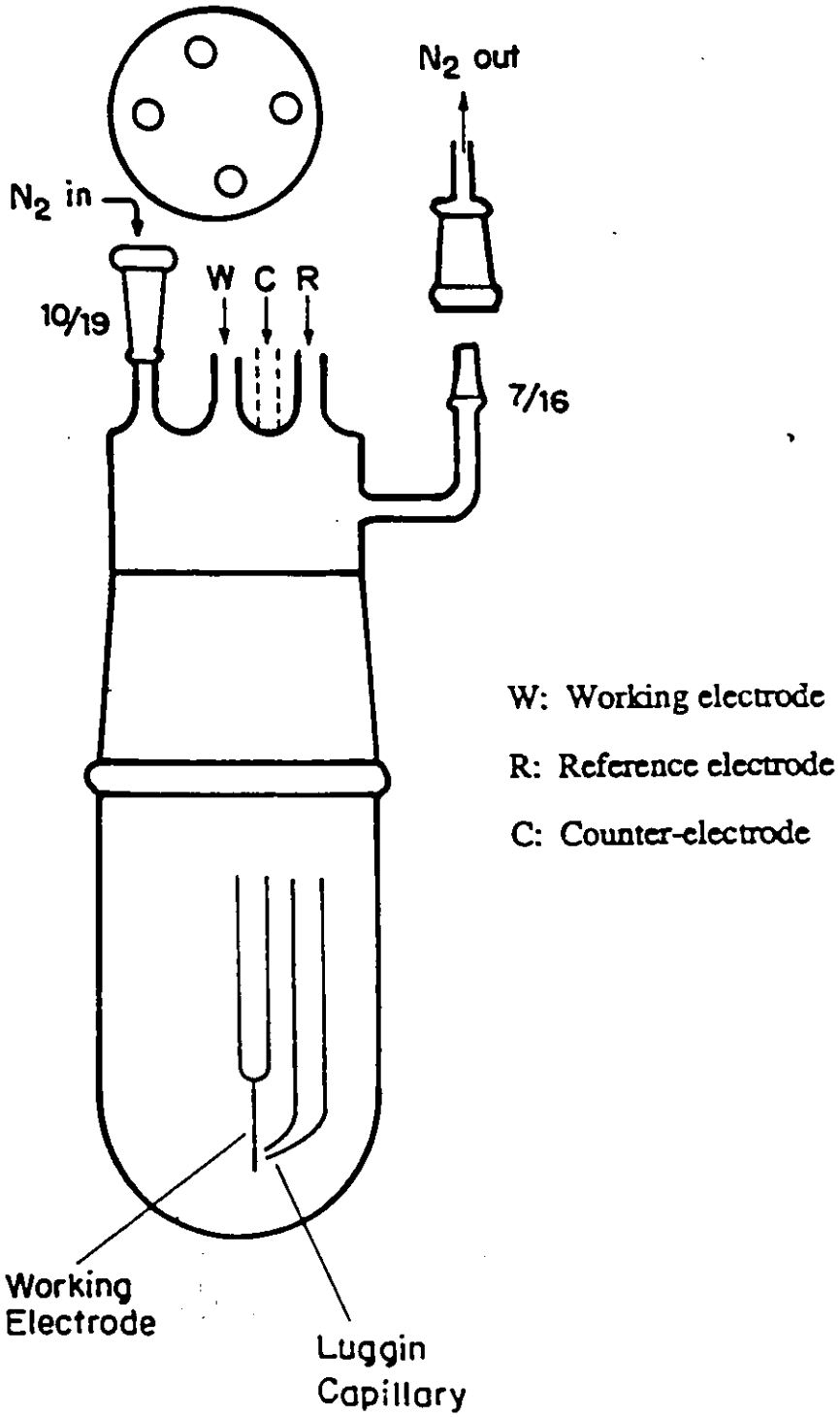

Fig. 2.3 (b) Schematic diagram of the one-compartment electrochemical cell employed for experiments conducted in non-aqueous media.

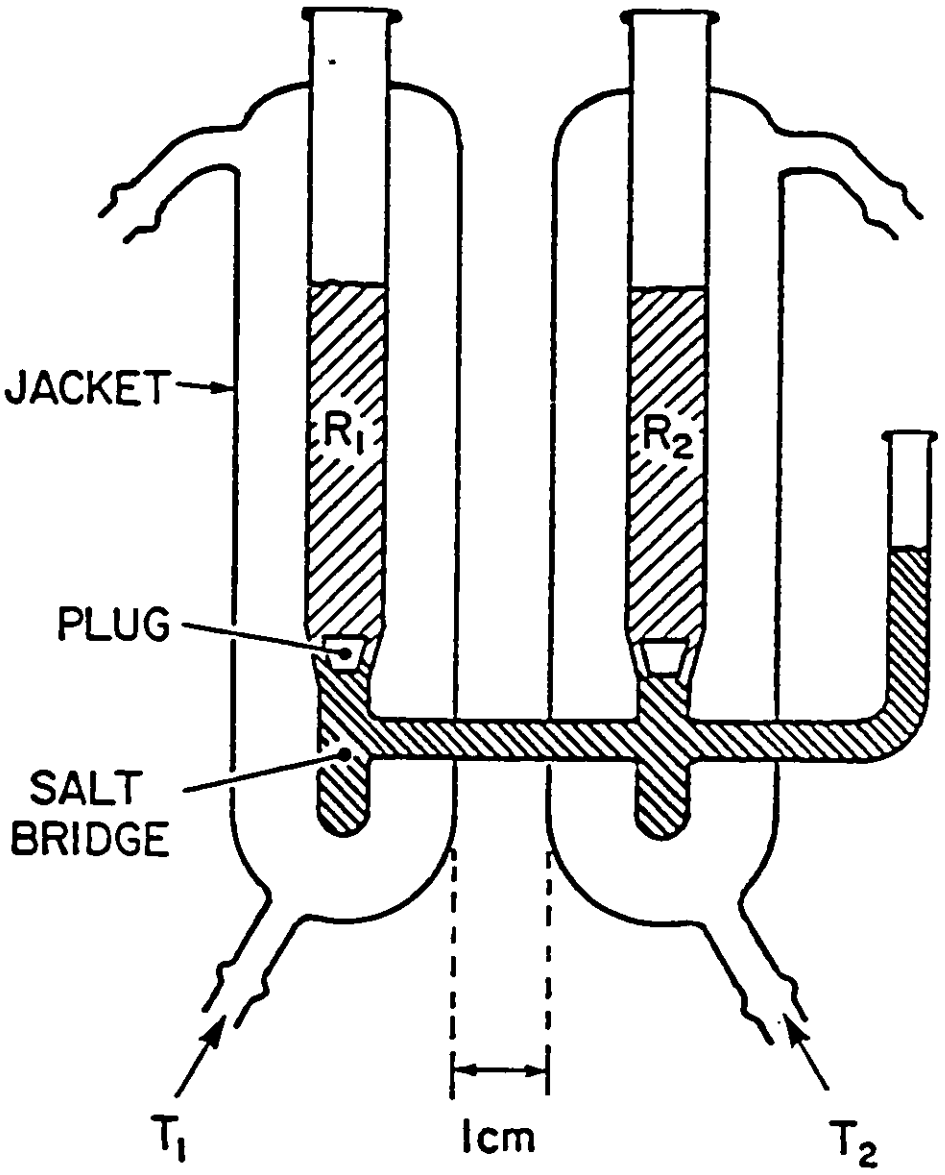

Fig. 2.4 Water jacketed, non-isothermal reference electrode cell with provision for a salt-bridge in the region of the thermal liquid-junction.

the jacket compartment without the side arm was kept at 298 K by circulating through it thermostated water using a Haake circulator. The temperature of the second jacketed compartment was varied by circulating pre-cooled, technical 95% ethanol (for low temperatures) or water (for higher temperatures) at different, thermostatically-controlled, temperatures. The salt bridge thermal junction section between the two electrode vessels (Fig. 2.4) was filled through the side arm with provision for volume expansion or contraction that occurs during variations of temperature. Consequently, a thermal liquid junction was established in the 10 mm by 8 mm internal diameter tube connecting the two jacketed compartments. Concentration polarization due to thermal diffusion (Soret effect) was minimized by the short distance (1 cm) between the jacketed compartments. The two plugs were removed by immersing the cell in water in an ultrasonic bath. The use of a salt-bridge thermal liquid junction was previously found [149] to minimize very satisfactorily the otherwise significant thermal junction potential, as shown by the example illustrated in Fig. 2.5.

2.10 Temperature Control

For experiments conducted above room temperature (298 K < T < 338 K), the electrochemical cell was placed in a bath of water contained in a large Dewar flask where the temperature was controlled to ± 0.5 K by a Haake E3 circulating water heater. For the low-temperature experiments, (213 K < T < 298 K), technical-grade 95% ethanol (f.p. 158.5 K) was employed as the fluid of the cooling bath. For moderately low temperatures (up to 233 K), a CC-100 Neslab Cryo Cool immersion cooler, with a flexible probe was used and could maintain the temperature to within ± 0.5 K. For temperatures below 233 K, the temperature of the cooling bath was maintained at low values by periodically adding small lumps of dry ice into ethanol in the Dewar flask. The level of the electrolyte in the electrochemical cell was always kept below that of the thermostated fluid, the reference electrode was, in this case, at the same temperature as the working electrode so that no thermal liquid-junction was involved. Temperature coefficient corrections for the true potential of the reference electrode were made using results obtained from the non-isothermal cell measurements.

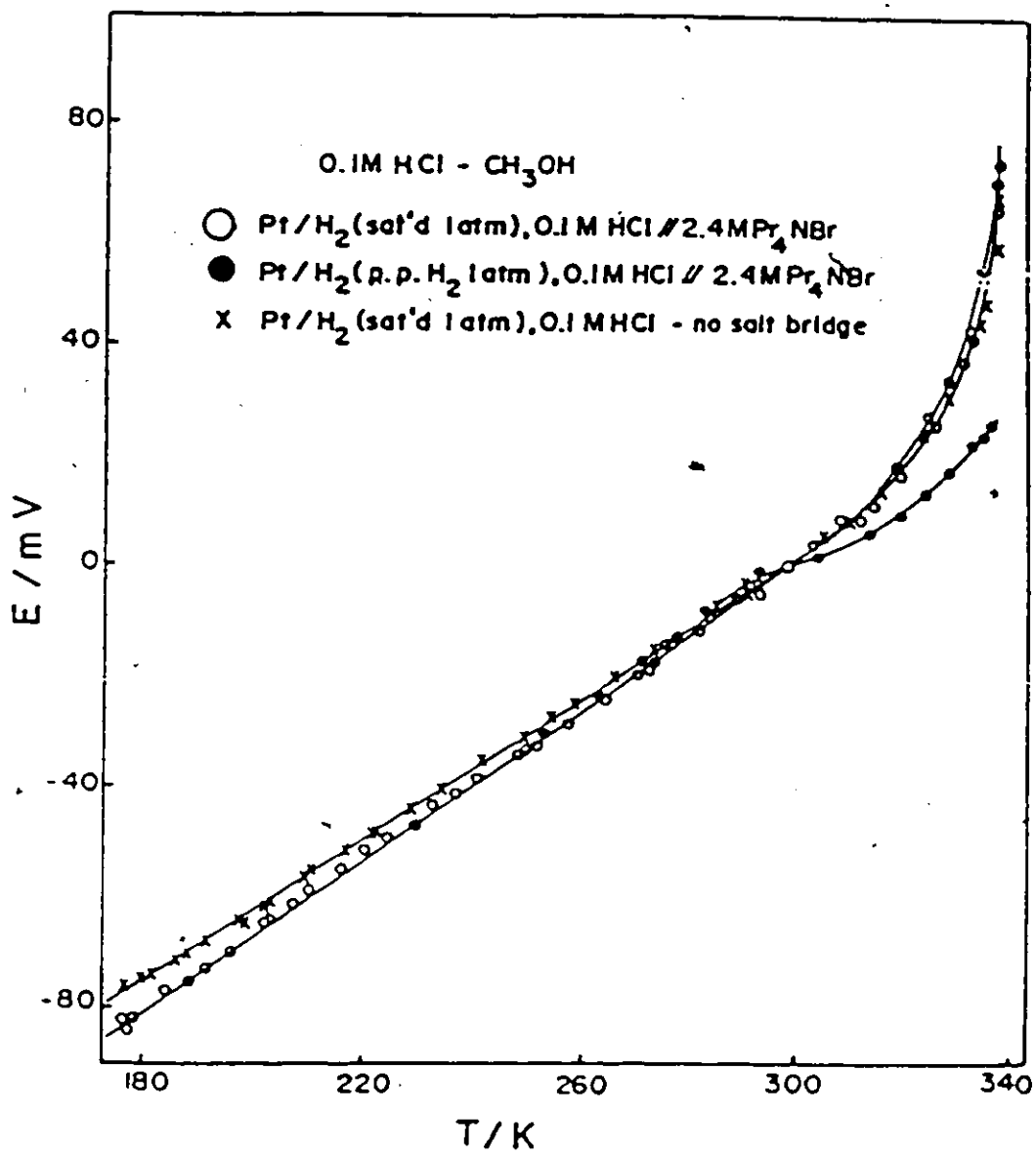

Fig. 2.5 Non-isothermal cell potentials for the H^+/H_2 reference electrode in 0.1M HCl in CH_3OH with and without a salt-bridge, referred to 298 K. (From ref. 149).

2.11 Determination of Real Surface Area of Au Electrodes

Unlike the situation with Au electrodes, real surface areas of Pt electrodes are easily determined from the measurable accommodation for electrodeposited H species [150,151] since the amount of charge required for electrodeposition of a monolayer of H is 210 μC per real cm^2. A similar method cannot be applied in the case of Au electrodes since there can be no "internal" standard for Au electrodes based on H accommodation.

The real areas of Au electrodes were therefore determined following the procedure of Mchri, Pshchenichnikov and Burshtein [152] who found that the charge required to electrodeposit O species in 0.5M H_2SO_4 below the potential of the well-defined current minimum ("Burshtein minimum"), immediately preceding O_2 evolution (see Fig. 2.6), was 400 μC per real cm^2, which was assumed to be the charge required to electrodeposit a monolayer of O species. These authors used B.E.T. measurements to obtain calibration data for the Au electrode areas, and their method based on this O-charge evaluation, was shown to be valid over a wide range of temperatures and sweep-rates.

Oxide coverages were therefore measured by this procedure and hence Au electrode real areas could be calculated by means of graphical integration of anodic linear sweep i vs E profiles to the "Burshtein minimum" potential by weighing cut-out i vs E profiles of fine graph paper (accuracy ± 1%) using the charge value for one monolayer of oxide, counted as a film of "2-electron" O species, as 400 μC real cm^2 [152]. The charge arising from currents associated with double-layer charging ($i_{dl} = C_{dl} \times s$) at a sweep-rate s, V s^{-1}, were subtracted on the basis that they would be approximately the same on the O-covered surface as on the bare Au at potentials lower than that for the onset of surface oxidation, preferably in the potential region negative to the potential of zero charge. The roughness factor of the Au electrodes used in the present work was about 1.3.

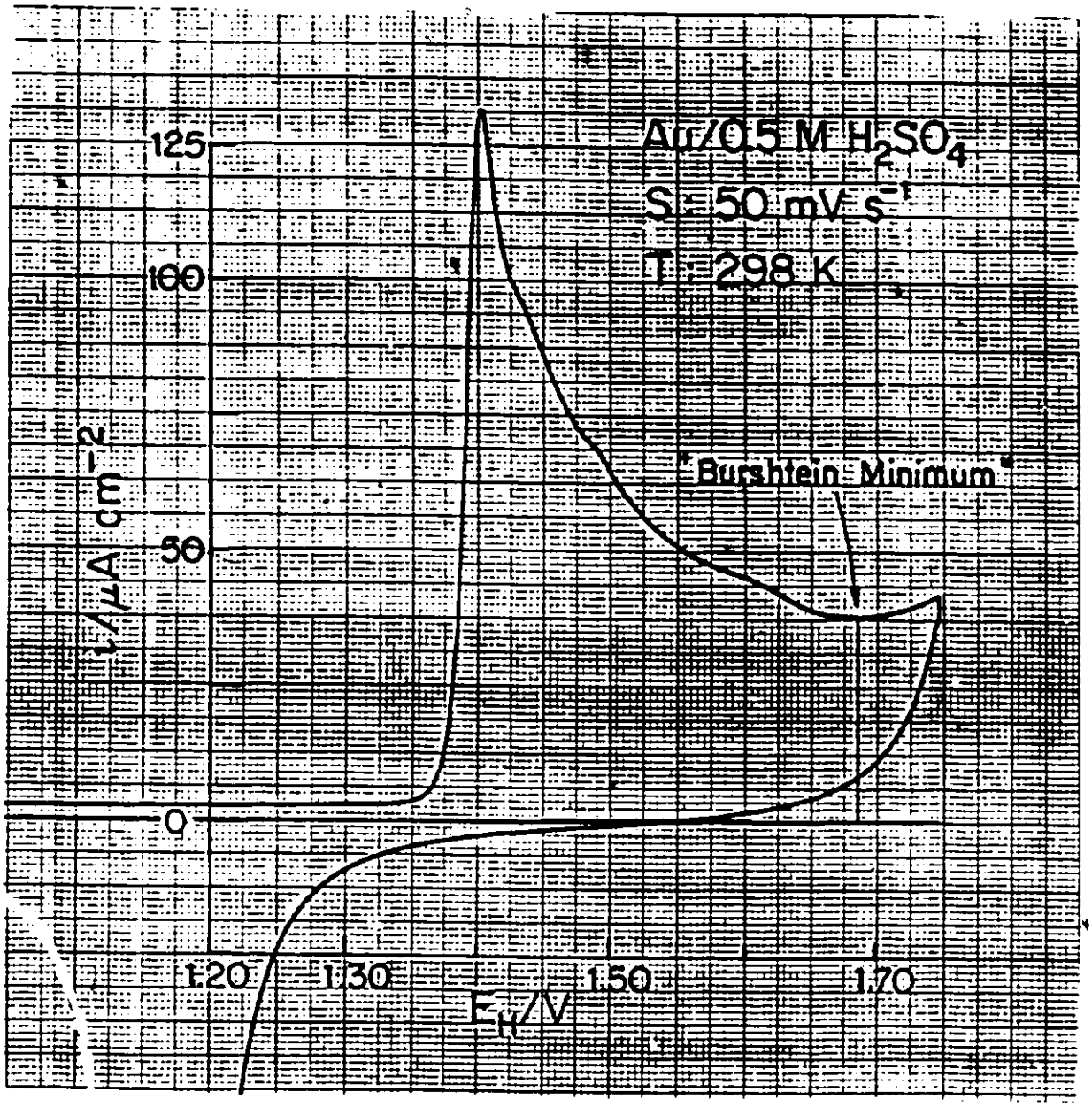

Fig. 2.6 The anodic i vs E profile for Au in 0.5M H_2SO_4 at 298 K used in the evaluation of the Au electrode real surface area. s = 50 mV s^{-1}.

CHAPTER 3

THE METHOD OF CYCLIC-VOLTAMMETRY AND ITS APPLICATIONS TO ELECTRODE SURFACE PROCESSES

3.1 Introduction

The cyclic-voltammetry technique, though relatively simple, has become increasingly useful in electrochemical studies, especially on electrode surface reactions; it can also be used to obtain a wealth of other information , e.g. the kinetic parameters of sequential steps of simple to fairly complicated electrode reactions. In cyclic-voltammetry, this information is gained from the profile of current response, in time, when the current is recorded as a function of potential, linearly varied in time, as shown qualitatively in Fig. 3.1.

3.2 Method

In cyclic-voltammetry, the potential, E, of the working electrode is changed linearly with time, t, at a constant sweep-rate s ($V\ s^{-1}$) according to the equation

$$E = E_i + st \qquad (3.1a)$$

or

$$dE/dt = s \qquad (3.1b)$$

where E_i is some initial potential that may or may not have been held constant for some time t before the start of the sweep.

The method may employ only a single sweep set between two potentials E_i and E_f (E_f is a final potential), hence the terms "potentiodynamic sweep" or "linear potential sweep" for this technique. The potential may be programmed to give a repetitive response of the electrode by varying the potential in a continuous back and forward manner between the E_i and E_f values; this procedure is hence referred to as "cyclic-voltammetry", usually abbreviated by the letters "CV".

Usually the potential is varied linearly with time at a sweep-rate s ($V\ s^{-1}$) while the current is

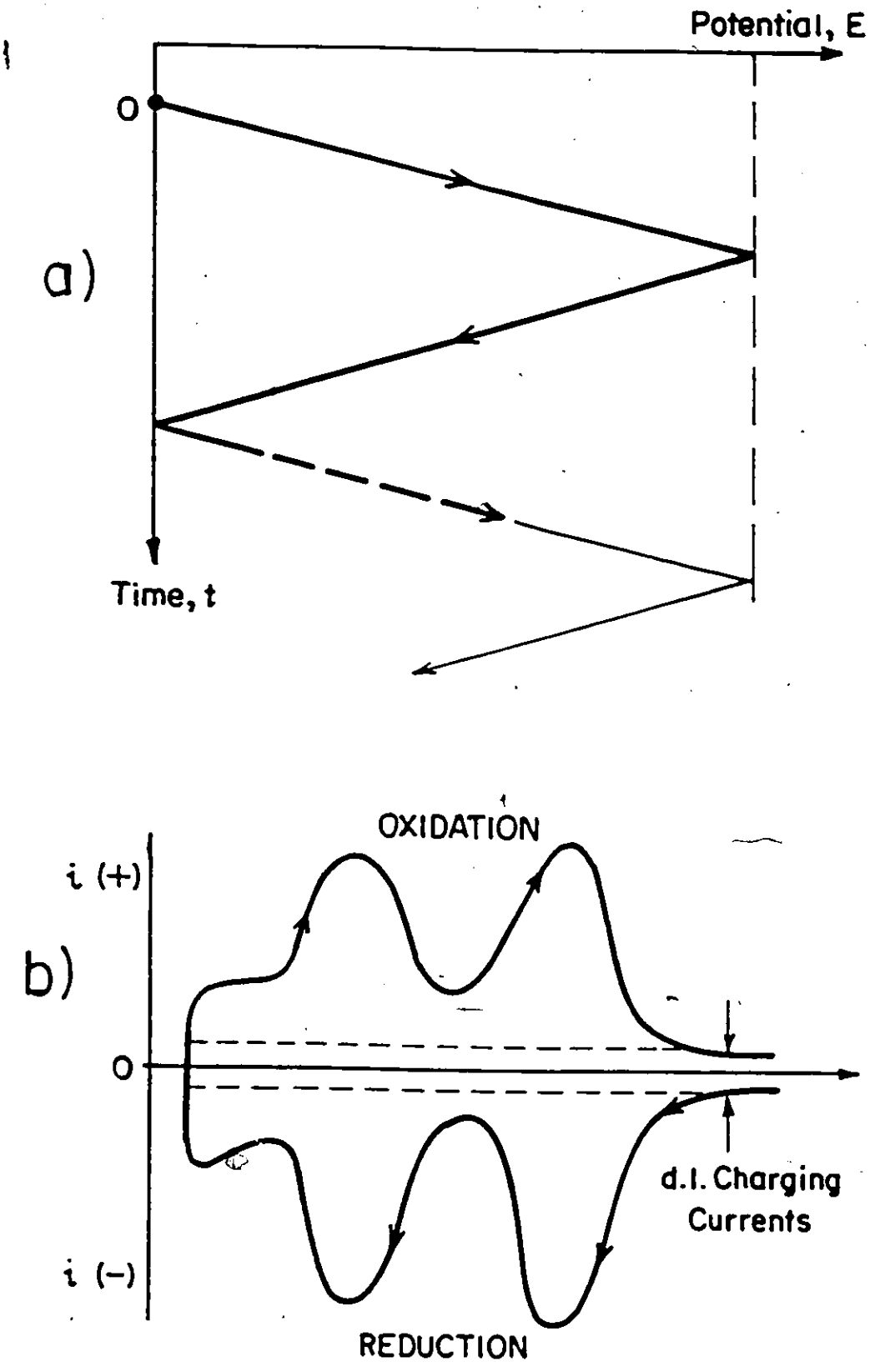

Fig. 3.1 a) Schematic diagram of the cyclic potential sweep; b) Resulting cyclic-voltammogram for a reversible surface process.

simultaneously recorded as a function of potential, as illustrated in Fig. 3.1. After traversing the potential region over which one or more electrode reactions take place (as exhibited by manifestation of peak currents), the direction of the linear sweep is usually reversed. Thus the potential is scanned beyond the current peak(s) and then reversed in a further linear sweep ("linear potential sweep") or in a continuous repetitive manner ("cyclic-voltammetry").

The information obtained from this technique includes the behaviour and characteristics of the electrochemical processes involved, indication of any complicating side reactions such as "pre-electrochemical" and "post-electrochemical" chemical reactions, and general kinetic behaviour such as slowness of charge-transfer steps or the development of limiting currents due to a pre-electrochemical chemical step such as molecular dissociation, chemisorption or ionization.

The electrical circuitry required for cyclic-voltammetry experiments is schematically illustrated in Fig. 2.2 Section 2.2.2.

3.3 Kinetic Conditions

From theoretical calculations and computer simulations of the kinetic behaviour for various types of chemical reactions under cyclic or linear variation of potential with time, as treated by various workers [153 - 155] two principal conditions and a possibility of a third condition may arise, as with any electrode process:

(i) The kinetic behaviour of the electrode reaction may be reversible or irreversible and usually an intermediate behaviour between these kinds of limiting conditions can arise depending on conditions such as temperature, sweep-rate, electrode potential limits, etc.;

(ii) The electrode reaction rate (or current-density) is either under activation (i.e. reaction kinetic) or diffusion control;

(iii) A third and important situation may arise where the electrode process involves only, or mainly a surface phase or adsorbed layer of the electrochemically reactive material. In such a situation, a characteristic CV behaviour arises that can be distinguished from that under conditions of bulk-diffusion control. As may be expected, both reversible and/or irreversible behaviour may be

observed in surface processes. This case of surface processes applies in the present work.

3.4 Sweep-rate Dependence of Current: Diffusion Control

For an electrochemical reaction having a sufficiently large rate constant and/or at sufficiently low reagent concentration, the process may be diffusion-controlled, with a concentration gradient developed normal to the electrode surface where the reagent is consumed. In a simple redox charge-transfer process,

$$O + ze \rightleftharpoons R, \tag{3.2}$$

which may behave either reversibly or irreversibly, the rate of electron transfer at the electrode surface in relation to the rate of diffusion along the concentration gradient determines if the reaction is diffusion-controlled or not. The activities (or concentrations) of oxidized, [O], and reduced, [R], species at the electrode surface are related to potential by the Nernst equation:

$$E = E^{\circ} + RT/zF \ln[O]/[R] \tag{3.3}$$

where E° is the standard reversible potential for process (3.2).

Various workers [156 - 159] have solved the Fick equations for linear potential sweep and cyclic-voltammetry experimental conditions where the observed kinetics are under diffusion control. For such conditions, the peak current I_p varies linearly with $s^{\frac{1}{2}}$, both for reversible and irreversible processes, according to the equations:

$$I_p = (2.69 \times 10^5) z^{3/2} D^{\frac{1}{2}} C_o A\, s^{\frac{1}{2}} \quad \text{(reversible)} \tag{3.4}$$

and

$$I_p = (2.99 \times 10^5)(z_a \alpha)^{\frac{1}{2}} z C_o A (Ds)^{\frac{1}{2}} \quad \text{(irreversible)} \tag{3.5}$$

for the electrode area A in cm^2, D the diffusion coefficient in $cm^2\ s^{-1}$, C_o in mol cm^3 and s in $V\ s^{-1}$; z_a is the number of electrons (usually 1) passed in the rate-controlling step and α is the transfer coefficient in the irreversible case.

Under diffusion-controlled conditions, the following quantitative characteristics of the i vs E profiles are also to be noted:

(i) The difference between anodic and cathodic peak potentials at 298 K:

$$\Delta E_p = E_{p,c} - E_{p,a} = 2 \times (0.028/z) \qquad (3.6)$$

(ii) Difference between peak potential E_p and the half-wave potential, $E_{\frac{1}{2}}$:

$$E_p - E_{\frac{1}{2}} = -1.1 \times (RT/zF) \qquad (3.7)$$

3.5 Peak Potential and Peak Current for Surface Process Control

As discussed in Section 1.5 above, a simple one-electron surface reaction, not influenced by diffusion, may be represented by the simple reaction scheme (c.f. also eqn. 1.13)

$$\underset{(1-\theta_A)}{M} + \underset{C_A\pm}{A^{\pm}} \underset{k_{-1}}{\overset{k_1}{\rightleftharpoons}} \underset{\theta_A}{MA_{ads}} + \underset{E}{e} \qquad (3.8)$$

where the parameters are as defined previously in Chapter 1, Section (1.7) above. The forward reaction (adsorption) rate is proportional to (1 - θ_A) and the reverse reaction (desorption rate is proportional to θ_A, where θ_A is the coverage of adsorbed A species expressed as a surface-site fraction. If the reaction is reversible and potential-dependent, the current can be written as

$$I = Q_M[k_1 C_A(1 - \theta_A)\exp \alpha\eta F/RT - k_{-1} C_A \theta_A \exp -(1 - \alpha)\eta F/RT] \qquad (3.9)$$

where Q_M is the charge required for formation or desorption of a monolayer of species A, k_1 and k_{-1} are the standard rate constants at the reversible potential and η is the overpotential. The Gibbs energy of activation is potential-dependent corresponding to the usual Butler-Volmer factor exp ($\alpha\eta F/RT$), i.e. the Tafel exponent in the rate-equation for the current density.

A process is said to be reversible if, at any potential, both forward and backward (i.e. for the anodic and cathodic processes or vice-versa) current components involving the factors exp ($\pm\alpha EF/RT$) and exp[$\pm(1 - \alpha)EF/RT$] determine to comparable extents the i vs E relation of the CV profile while the irreversible case arises when only one or other of these factors is involved, e.g. corresponding to the "back" reaction rate being negligible. For the irreversible case, the second term in eqn. (3.9) above would be negligible since $k_1 \gg k_{-1}$ or $\alpha\eta F/RT \gg 1$.

Srinivasan and Gileadi [160] have derived equations relating current to potential as a function of sweep-rate for cyclic-voltammetry of simple surface processes.

For an adsorption process which is reversible, I_p is given by the equation

$$I_p = (Q_M F/4RT)s \qquad (3.10)$$

and

$$E_p = -RT/F \ln K_1 \qquad (3.11)$$

For an irreversible process, i.e. $k_1 >> k_{-1}$,

$$I_p = 1/e(Q_M \alpha F/RT)s \qquad (3.12)$$

and

$$E_p = (RT/\alpha F)[\ln s + Q_M \alpha F/k_1 RT] \qquad (3.13)$$

Thus for an irreversible process (eqn. 3.13), the peak potential , E_p, is a function of s while, for a reversible process, E_p, is independent of s.

For a simple surface process, irreversible behaviour can be distinguished from reversible behaviour by means of the following criteria:

(i) I_p for an irreversible process is lower by about 27% than the corresponding I_p for a reversible process.

(ii) The corresponding anodic and cathodic peaks of the i vs E profiles are symmetrical for the reversible process while, for an irreversible one, they exhibit asymmetry even at low sweep-rates if they are $> s_o$ (see below).

(iii) The peak potential is not independent of s but is a function of log s, as with a Tafel relation. Also, for a surface reaction process, I_p varies linearly with s while for a diffusion-controlled process I_p varies linearly with $s^{\frac{1}{2}}$, Fig. 3.2. This forms the principal basis for distinguishing a surface reaction from a diffusion-controlled process. Sometimes, however, mixed conditions are encountered where both diffusion and surface reaction processes appear to take place in a consecutive and/or parallel relationship as was found by Conway and Kannangara [161] in the study of zinc dissolution/passivation which involves both ZnO film formation and dissolution of Zn as ZnO_2^{2-} ions.

(iv) The peak potential is progressively shifted from the reversible value with log s due to a polarization effect, as with an irreversible polarographic wave.

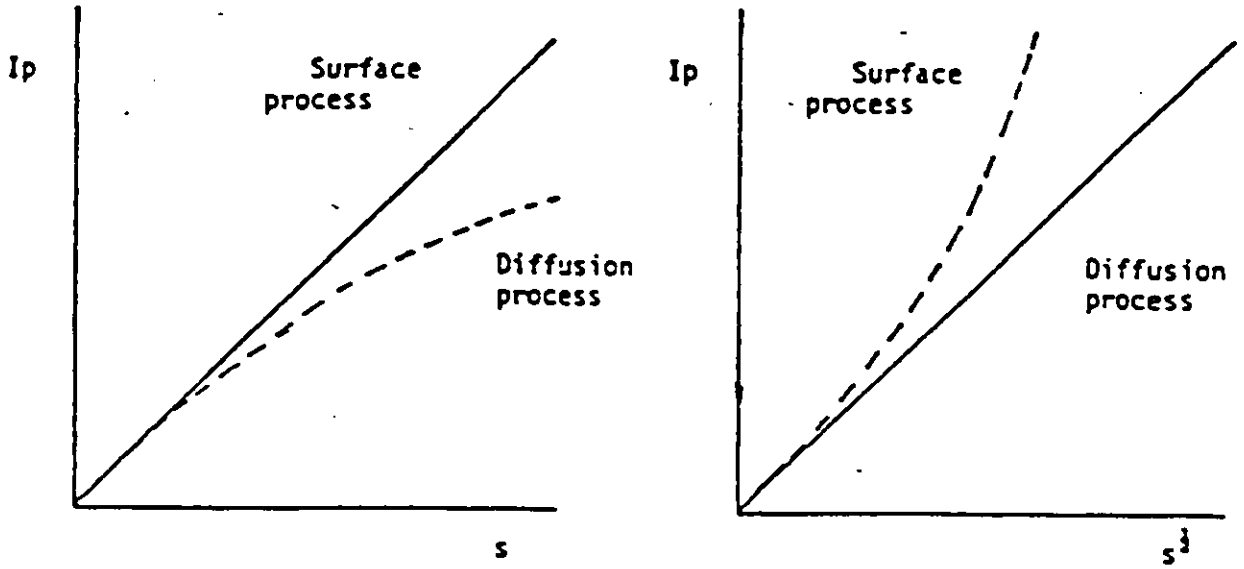

Fig. 3.2 Sweep-rate dependence of peak currents for a surface reaction and a diffusion-controlled electrochemical reaction.

In the present work, one of the important results was the determination of the so-called s_o value [127], the sweep-rate at which the underpotential deposition reaction Pb on Au, viz.,

$$Au + Pb^{2+} + 2e \rightleftharpoons Au.Pb, \qquad (3.14)$$

which is fast in aqueous medium, just becomes an irreversible process; i.e. when $s \geq s_o$ in various non-aqueous solvents causing E_p to become dependent on log s. The examination of this surface process (3.14) in its various kinetic and energetic aspects will be described in Section 6.7 below.

3.6 Determination of the s_o parameter

In linear potential-sweep amperometry or cyclic-voltammetry methods, the current response to a linear potential scan at a constant sweep-rate ($dE/dt = s$ V s^{-1}) is monitored at various values of s over a wide range, and over a sufficient potential range. The peak current I_p can be expressed as a pseudocapacitance $C_p = I_p/s$ over a wide range (several decades) of s, and plotted against the peak potential, E_p. Usually, for conditions of reversibility of the process, the peak potential is independent of s below a certain critical value of $s = s_o$, where s_o is the so-called reversibility parameter [127]. When $s > s_o$, however, E_p ceases to be independent of s and when $s >> s_o$ it becomes logarithmic in s. Hence s_o, the maximum sweep-rate for which the surface reaction process just remains reversible, is obtained by extrapolation of the logarithmic region of E_p vs log s plots to the reversible peak potential region, $E_p \cong E_{p,rev}$ for $s \leq s_o$.

It is easily seen that the reversibility parameter s_o corresponds to the exchange current-density i_o for the surface reaction process. The relation of E_p to log s for $s >> s_o$ may be compared to the Tafel equation for an electrode process:

$$\ln i = \ln i_o + \beta\eta F/RT \qquad (3.15)$$

and hence the slope of E_p vs ln s for $s >> s_o$ corresponds to the Tafel slope for the electrode surface process thus enabling the electron transfer barrier symmetry factor β for simple cases of atomic deposition or desorption to be evaluated or, for more complex cases, the reaction mechanism [155] of the surface reaction process to be elucidated.

Angerstein-Kozlowska and Conway [127] developed the equations relating peak potentials to sweep-rate, obtaining:

$$E_{p,irrev} = E_{p,rev} + RT/\beta F \ln F/k_o RT + RT/\beta F \ln s \qquad (3.16)$$

where $RT/\beta F$ (= b/2.3) is the Briggsian Tafel slope, k_o the standard rate constant [$k_o = k_1 \exp \beta E°F/RT = k_{-1} \exp -(1 - \beta)E°F/RT$] for the standard potential, E°, of the surface reaction defined as the peak potential (for $\theta_A = \frac{1}{2}$) when the process behaves reversibly. From eqn. (3.16) above, s_o can be defined by

$$s_o = \beta F/k_o RT \qquad (3.17)$$

Hence s_o characterizes the kinetics of a surface process like i_o does for a regular continuous Faradaic process. In contrast to i_o, however, s_o has an important advantage for kinetic evaluations in electrocatalysis in that the real area of the electrode in <u>not</u> a required parameter characterizing the kinetics. s_o is related to i_o through the pseudocapacitance (see Section 1.7.3) $C_{\phi,rev}$ for reversible behaviour, viz. $s_o = i_o/C_{\phi,rev}$. Since both i_o and $C_{\phi,rev}$ depend directly on electrode area, s_o is <u>independent</u> of it.

When lateral interactions between electrodeposited particles on the surface are significant, (i.e. $g \geq 0$ or $g \leq 0$), where g is an interaction parameter) the derived expression which gives a general relation for log s_o for a 1 e process is [127]:

$$\log s_o = \log s_o'' - \log[1 + g/s(1 - \theta_{p,irrev})] + g/4.6(\theta_{p,irrev} - \tfrac{1}{2})E°/2.3b \qquad (3.18)$$

where

$$\log s_o = \log s_o'' \text{ (experimentally evaluated by extrapolation)} + \text{(correction term due to interaction effects)} \qquad (3.19)$$

and $\theta_{p,irrev}$ is 0.63. Hence the s_o parameter can be determined since g can be derived [67] from the half-width of the i <u>vs</u> E profile. Therefore, since the parameter s_o as well as coverage and relative energy of the states can be measured, the electrochemical kinetics of the surface processes, including those for resolved submonolayer states, can hence be completely characterized.

An illustration of results obtainable by these procedures is shown schematically in Fig. 3.3

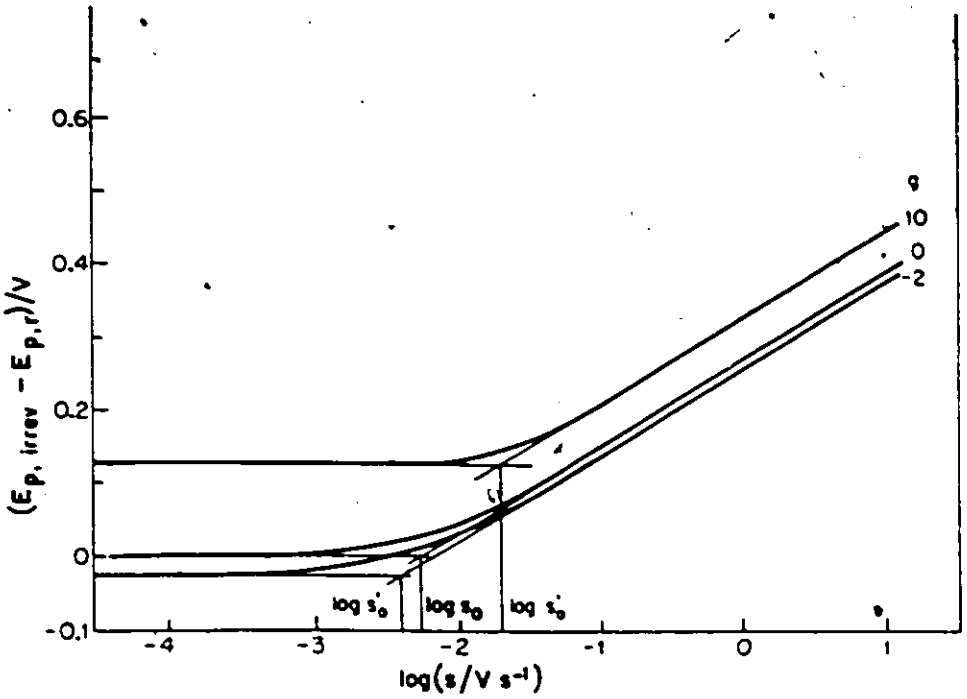

Fig. 3.3 Schematic plots of variation of peak potential with sweep-rate, s, for an ad-layer in which interactions are of various strengths determined by the g value. (From ref. 127).

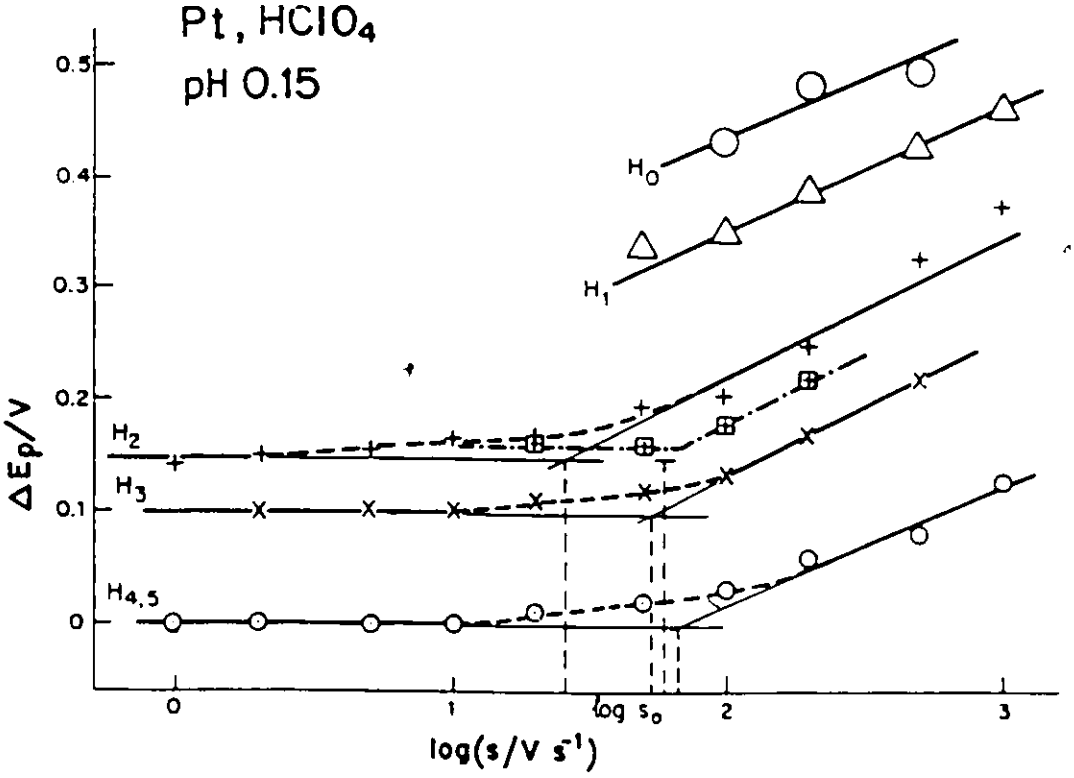

Fig. 3.4 Some peak potential vs log s plots for states of H electrosorption at Pt. (From ref. 127).

where the peak potential is plotted against log s for an ad-layer in which interactions are of various strengths as determined by the g value. Experimental results [127] for four of the states of H deposition at Pt are illustrated in Fig. 3.4.

Some of the critical parameters, useful for analysis of results of cyclic-voltammetry experiments on monolayers at electrode surfaces, are summarized in Table 3.1 below.

Table 3.1 Critical Parameters of Cyclic-Voltammetry Experiments on Monolayers at Electrodes

	Observation on i vs E Profile	Information/Interpretation
1.	Multiple-state adsorption in the monolayer	Surface is heterogeneous or succession of array structures arises.
2.	The dependence of peak potential on sweep-rate, s	Rate constants and charge-transfer coefficients for the surface process can be evaluated.
3.	Temperature dependence of peak potential, dE_p/dT	Entropy of distinguishable ad-states can be evaluated indicating if the ad-layer particles are 2-dimensionally mobile or not.
4.	Asymmetry of peaks	The process is kinetically irreversible or, if the process is reversible, the behaviour indicates the type of lateral interaction e.g., between dipoles or free charges.
5.	Half-widths of peaks, $\Delta E_{\frac{1}{2}}$	Measures the free-energy of lateral interaction of adsorbed species, A, as a function of coverage, θ_A.
6.	Peak potential, E_p, relative to E_r	Free energy of distinguishable 2-d ad-states, relative to that of bulk phase, is determinable.

7. Reversibility between anodic and cathodic peak current profiles	Kinetic reversibility or hysteresis between formation and desorption of monolayers is indicated.
8. Ion effects on i vs E profile	Interaction on ion field with surface dipoles of ad-species; competitive adsorption between ion and upd A species. Effects depend on potential range of upd relative to p.z.c.
9. Effects of reversal of direction of sweep at successively increasing or decreasing potentials in a range, ΔE, of potential	Distinction of various successive processes in the ΔE range and the relation between the states observed on the adsorption and the corresponding desorption sweep, in so far as reversibility and hysteresis are involved.

The s_o and other kinetic parameters that have been evaluated in the present study of upd of Pb at Au by means of cyclic-voltammetry in protic and aprotic non-aqueous solvents are given and discussed in Chapter 6.

3.7 General Form of i vs E Profiles

In general, the i vs E profiles for diffusion and surface-reaction-controlled currents are found to be somewhat similar in their peaked shape and overall form. The differences arise from the nature and involvement of concentration of the reactant species. In the diffusion-controlled case, reactant material is consumed from the diffusion layer, eventually depleting the solution completely at the electrode interface (limiting-current condition). However, during the sweep, depending on its duration measured by s^{-1}, reactant material continues to diffuse into the boundary region so that the charge under the i vs E(t) profile increases with diminishing s. In the case of a surface reaction, however, there is a finite quantity of material in the surface phase which is eventually consumed during passage of the sweep so that the current goes to zero apart from the residual double-layer charging current $C_{dl}(dE/dt)$ that passes at all potentials, as also in the diffusion-control case (Fig. 3.1).

In the surface-reaction case, since the consumable reactant is fixed, determined by geometry and thickness of the surface phase, the total charge, Q, under the cyclic-voltammogram ($Q = \int i dt = \int (i/s) dE$) measured is independent of sweep-rate, provided the reaction is 100% coulombically efficient, i.e. parasitic or impurity currents are insignificant.

In both cases, the rising side of the curve is associated with the exponential increase of current with E, while the descending current side is associated with continuing consumption of the reagent - either from the diffusion layer or from the surface phase, although, of course, the potential continues to increase in the given direction of the sweep.

In some easily recognizable cases, the potential of the electrode surface phase remains almost constant during its consumption while for a Langmuir-type adsorbed layer the potential varies as $\ln(\theta/1-\theta)$; in the first case, for a surface phase, the ascending current sides of the profiles at increasing sweep-rates are almost coincident but fall away to the descending side at various currents as the sweep-rate is varied. For the Langmuir ad-layer, however, the curves fall more symmerically above each other with increasing sweep-rate, especially in the reversible reaction case (Fig. 3.5).

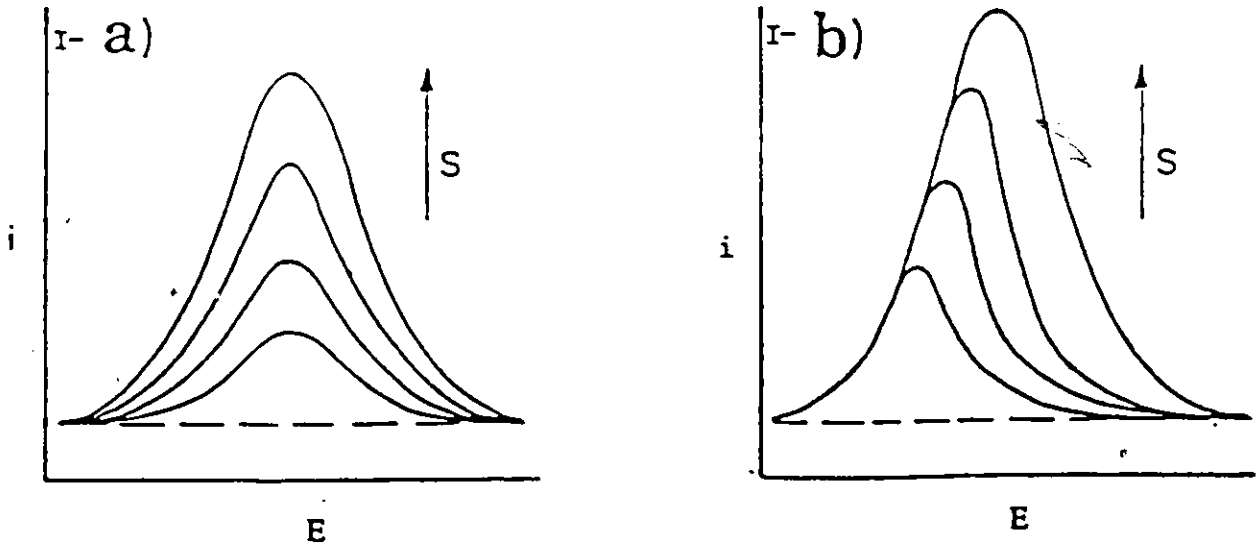

Fig. 3.5 Shapes of i vs E profile with increasing s for a surface process involving:
a) a 2-d array of adatoms on an electrode e.g. Pb on Au
b) consumption of a 2-d surface phase on an electrode.

Referring again to the first case where ascending current curves are almost coincident at various sweep-rates, this behaviour arises because a regular Faradaic current passes for essentially a bulk phase process where the thermodynamic potential does not change during its consumption (except at the very last stages). This situation applies to multilayers or thick films. In the Langmuir ad-layer case, however, only a monolayer or submonolayer is involved where the thermodynamic potential is $f(\theta)$ and hence changes continuously during the sweep. The resulting i vs E profiles are therefore characteristically different for these two cases and both are different from that for the diffusion case. Their differences provide diagnostic criteria for the types of processes and/or conditions involved.

CHAPTER 4

SOLVENT AND ANION EFFECTS ON THE i vs E UPD PROFILES FOR Pb AT Au

4.1 Introduction: Factors Characterizing i vs E Profiles for UPD of Pb on Au

The experimental results obtained in the present work will be presented and discussed in the light of the points indicated in the Section "Aims of the Present Work". In the present section, the results of the cyclic-voltammetry experiments that provided the upd i vs E profiles for Pb at Au in various non-aqueous solvents and comparatively in aqueous medium will be given, with the aqueous medium being treated as the reference solvent.

The upd i vs E profiles for Pb adatom deposition/desorption in various non-aqueous solvents will be examined and their features discussed in terms of the following factors:

(i) Multiplicity of the peaks in corresponding cathodic and anodic upd i vs E profiles. This, as noted earlier, demonstrates the heterogeneity of the electrode surface as adsorption/desorption takes place, as well as the succession of distinguishable array structures which arise as the sub-monolayer or monolayer is laid down over the upd range. (Note that a multiplicitity of submonolayer states of deposited Pb adatoms also arises at Au single-crystals [39]).

(ii) Potentials, E_p, of individual peaks, relative to the reversible potential for electrodeposition of the bulk adsorbate, Pb. This enables the Gibbs energies of distinguishable adstates to be directly determined relative to that of the bulk phase.

(iii) Half-widths of peaks, $\Delta E_{1/2}$, which enables the magnitude of the free energy of lateral interaction between the adsorbed species (adatoms) to be estimated as a function of coverage, θ_A. However, with the upd i vs E profile for Pb at Au, extensive overlap of peaks makes such an analysis unreliable.

(iv) Metal/solvent interactions in the various non-aqueous solvents in terms of the double-layer structure at the interface.

(v) Competitive effects of the ions.

4.2 Origin of Solvent Effects on UPD Profiles for Pb at Au

In the interpretation of the results of the present study of solvent effects on the upd behaviour of Pb at Au, the following factors will be considered:

a) The possible role of the solvent itself directly affecting the energetics of the adatom array formation as the monolayer of upd species is developed. This effect arises on account of the requirement that a solvent molecule adsorbed at the Au substrate must be displaced as a Pb adatom is deposited and the energy of this process may not be entirely compensated by the new Pb-adatom-solvent interaction that will arise after the adatom has been deposited. Also, in the course of development of adatom arrays, it is to be expected that solvent molecules which can develop their own array structure in their adsorbed state at the electrode [162], will interfere in metal adatom array formation process and possibly cause changes in the potentials of various peaks in the i vs E profile relative to the bulk Pb/Pb^{++} potential for the given solvent, since the geometries of solvent and Pb adatom arrays will hardly be expected to be similar.

b) Since both a lead salt and a supporting electrolyte are required for the conduct of the experiments, account must be taken of the different degrees of solvation of the ions, especially the anions, of the electrolytes from one solvent to the other. This can become manifested as an effect on the upd profiles on account of a solvent-dependence of the strength (Gibbs energy) of adsorption of ions of the electrolyte at the substrate metal (here Au). Thus, it is generally recognized that specific adsorption of anions involves partial desolvation of the ion and electronic interaction of the lone pairs of electrons with the electrode metal surface. Grahame [163] drew the distinction between anion adsorption involving partial or even complete desolvation (involving charge-transfer chemisorption) and cation adsorption, the energy of which was mainly electrostatic in origin, with little change in the ion's solvation shell. Hence solvent-dependence of ion adsorption can lead to an important indirect solvent effect on upd, when anion adsorption influences the upd on account of competition with the adatom deposition process, especially in its initial stages at low coverage by the adatoms.

c) Effect of the solvent on the potential of zero charge of the substrate and adatom layer. This effect can arise on account of the dependence of the electron work function, ϕ, on solvent orientation at the electrode interface and the p.z.c. known to vary in parallel way with changes of ϕ [164,165]. Adsorbed ions also affect the p.z.c. in well known ways.

We summarize these effects in the table below.

Table 4.1: Possible Origins of Solvent Effect on UPD Metal Adatom Profiles

1. Solvent-specific displacement energy as upd, competitive with solvent adsorption, progresses.
2. Solvent-specific anion adsorption, in competition with the upd process, arising from:
3. Solvent-dependent anion adsorption due to the dependence of anion solvation energy on solvent properties.
4. Dependence of p.z.c. of substrate metal on solvent and on presence of adsorbed ions.
5. Changes of work function and hence p.z.c., of the substrate as the upd metal adatom film is developed towards full coverage.
6. Due to change of p.z.c. with coverage of the adatoms, solvent orientation, at a given metal/solution potential difference, may change with coverage.
7. Dependence of the upd peak potentials on the solvation energy of the ion being electrodeposited on the solvent properties, but this effect will be cancelled out in the solvent-dependence of the bulk metal electrode potential if complete charge-transfer arises in all stages of the upd process as the monolayer is developed.

4.3 Comparison of UPD Profiles for Pb Adatom Deposition on Au in Five Solvents

The upd i vs E profiles for Pb at Au in solutions of $NaClO_4$ in acetonitrile (AN), methanol (MeOH), dimethylformamide (DMF) and propylene carbonate (PC) are shown comparatively in Figs. 4.1 to 4.4 and the corresponding i vs E profile for aqueous medium, given in Fig. 4.5, is to be used as reference for comparison. These profiles were all obtained in 0.1M $NaClO_4$ as electrolyte to

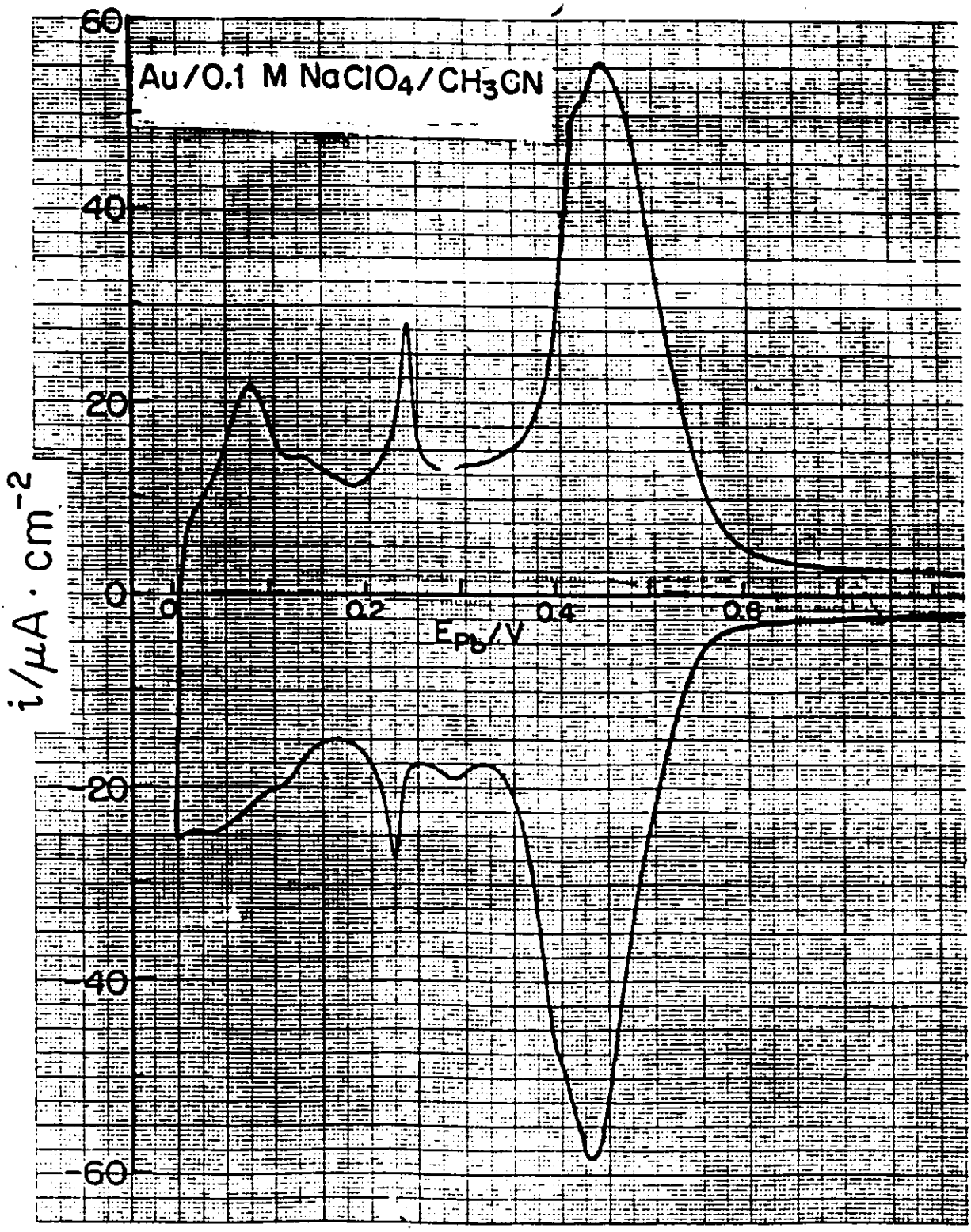

Fig. 4.1 Cyclic-voltammetry i vs E profile for Pb upd at Au from 0.1M $NaClO_4$ + 10^{-2}M $Pb(CF_3SO_3)_2$ solution in acetonitrile (AN) at 298 K. $s = 50$ mV s^{-1}.

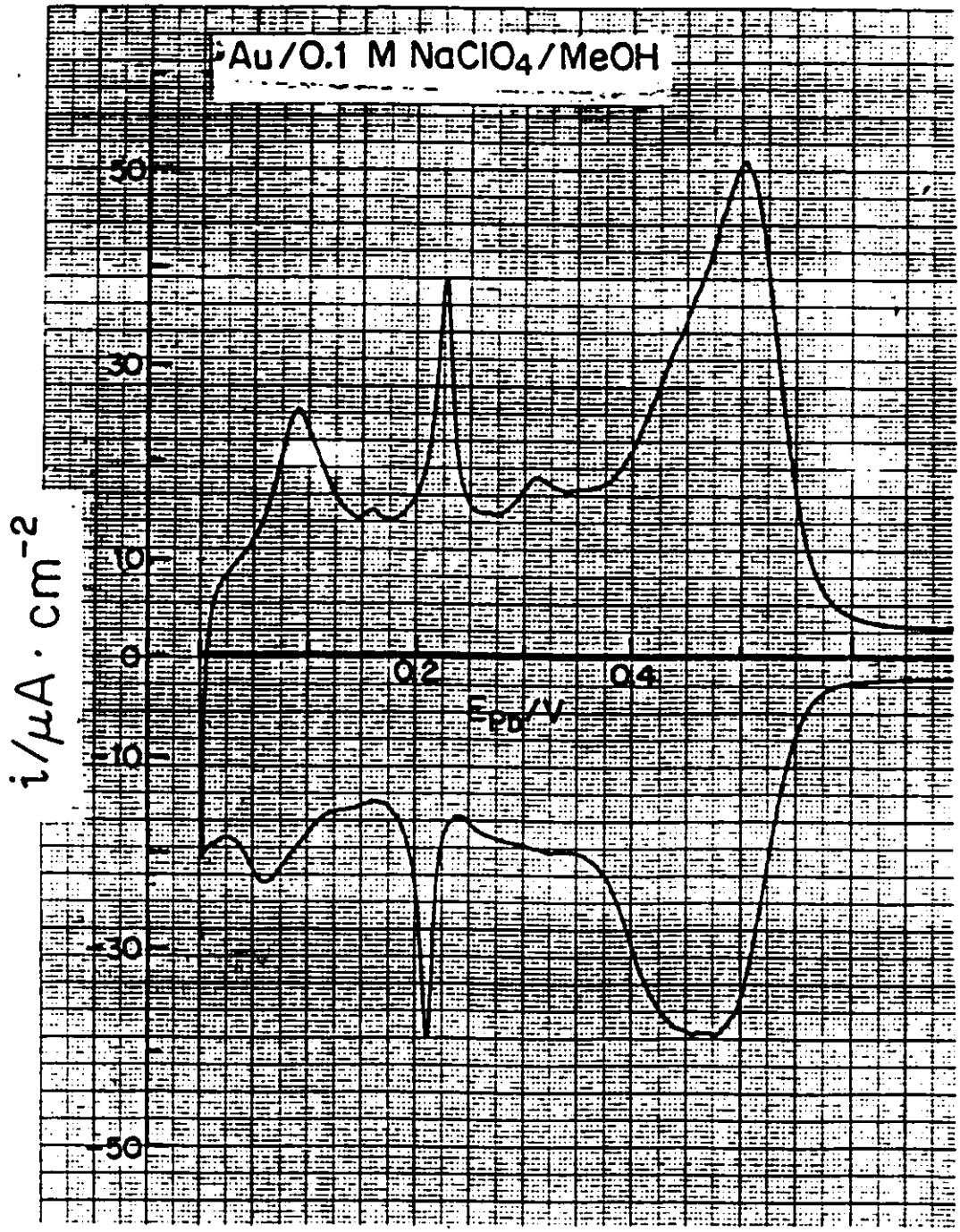

Fig. 4.2 Cyclic-voltammetry i vs E profile for Pb upd at Au from 0.1M $NaCLO_4$ + 10^{-2}M $Pb(CF_3SO_3)_2$ solution in methanol (MeOH) at 298 K. s = 50 mV s^{-1}.

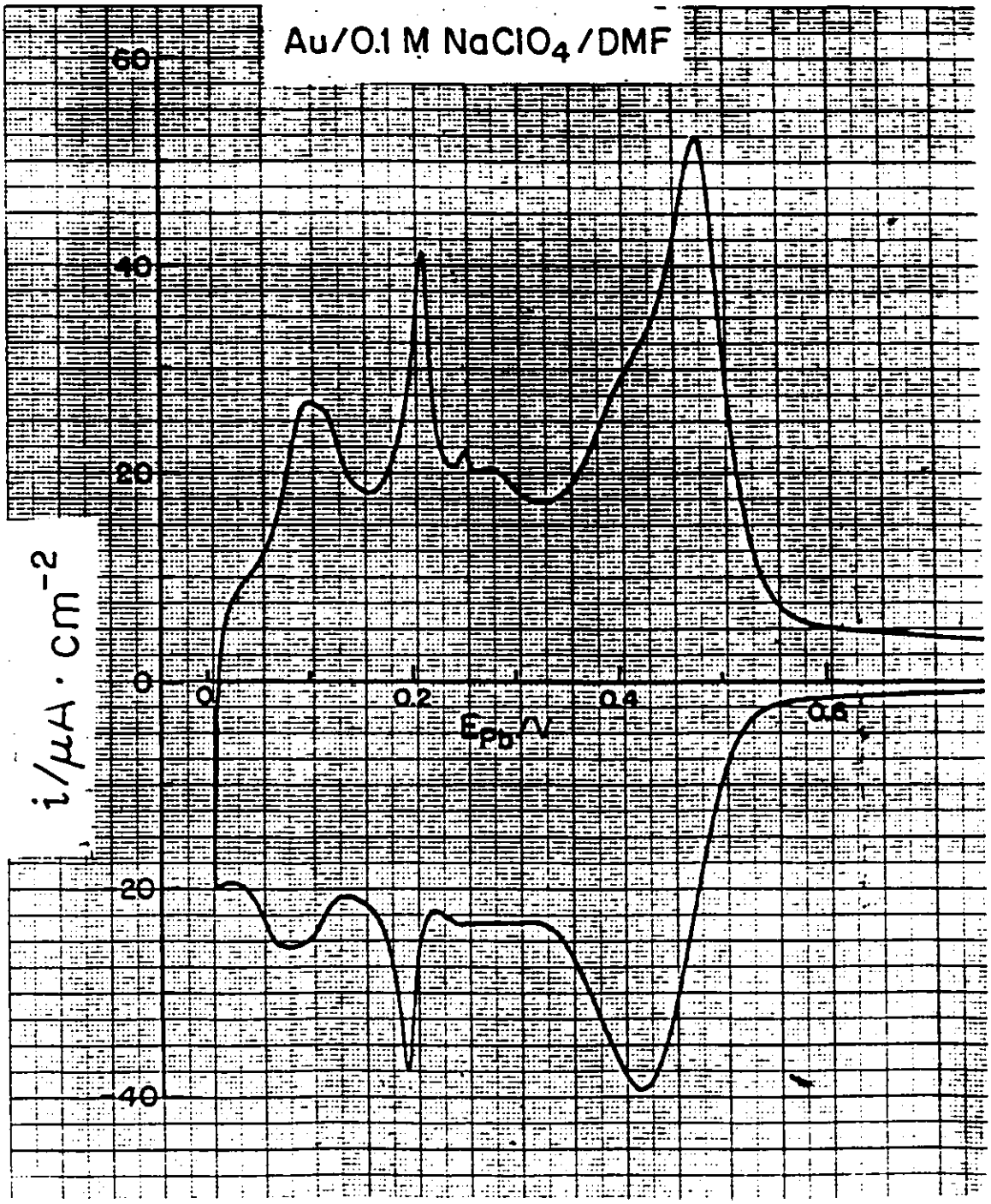

Fig. 4.3 Cyclic-voltammetry i vs E profile for Pb upd at Au from 0.1M $NaClO_4$ + 10^{-2}M $Pb(CF_3SO_3)_2$ solution in dimethylformamide (DMF) at 298 K. s = 50 mV s^{-1}.

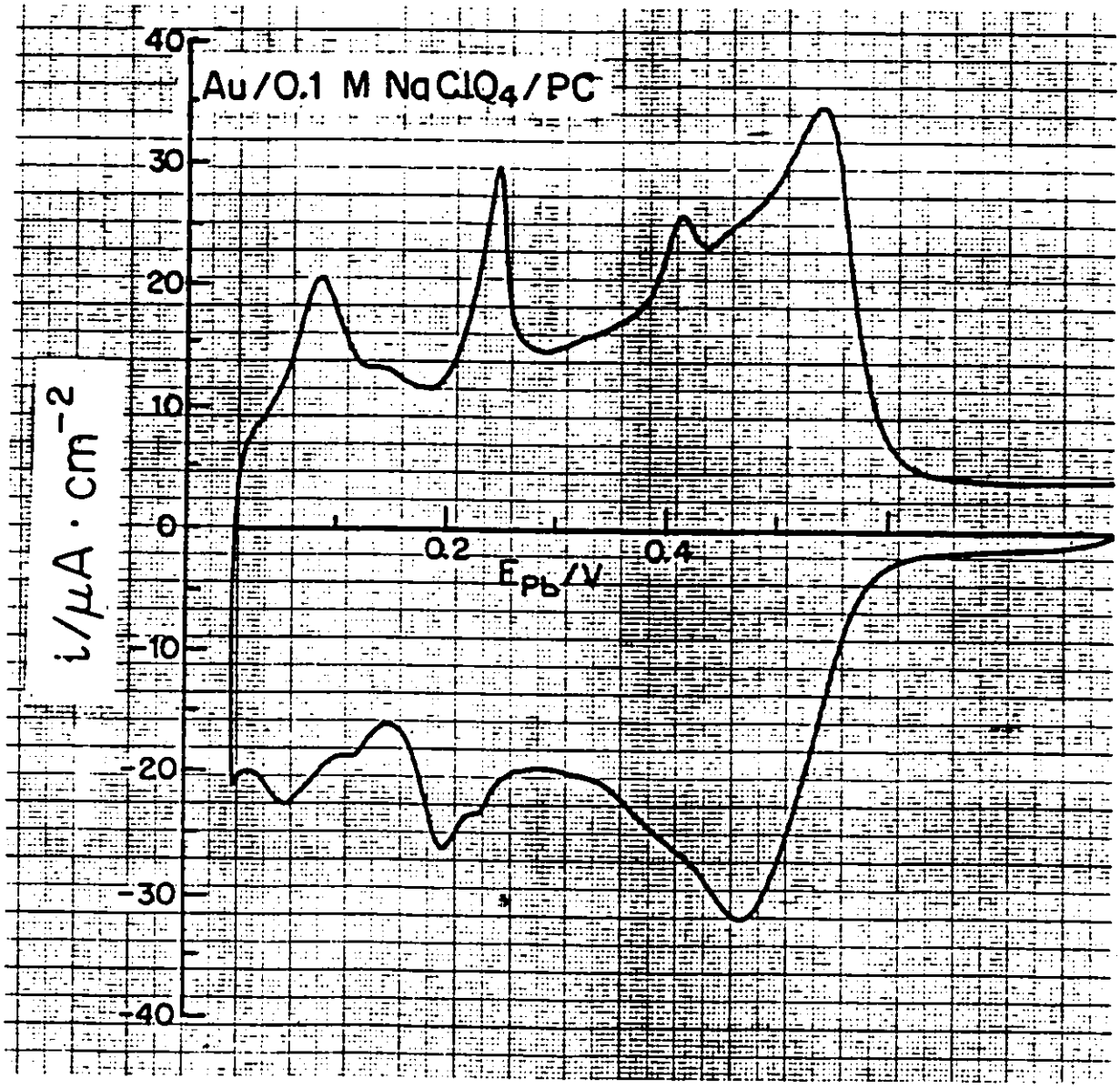

Fig. 4.4 Cyclic-voltammetry i vs E profile for Pb upd at Au from 0.1M $NaClO_4$ + 10^{-2}M $Pb(CF_3SO_3)_2$ solution in propylene carbonate (PC) at 298 K. s = 50 mV s^{-1}.

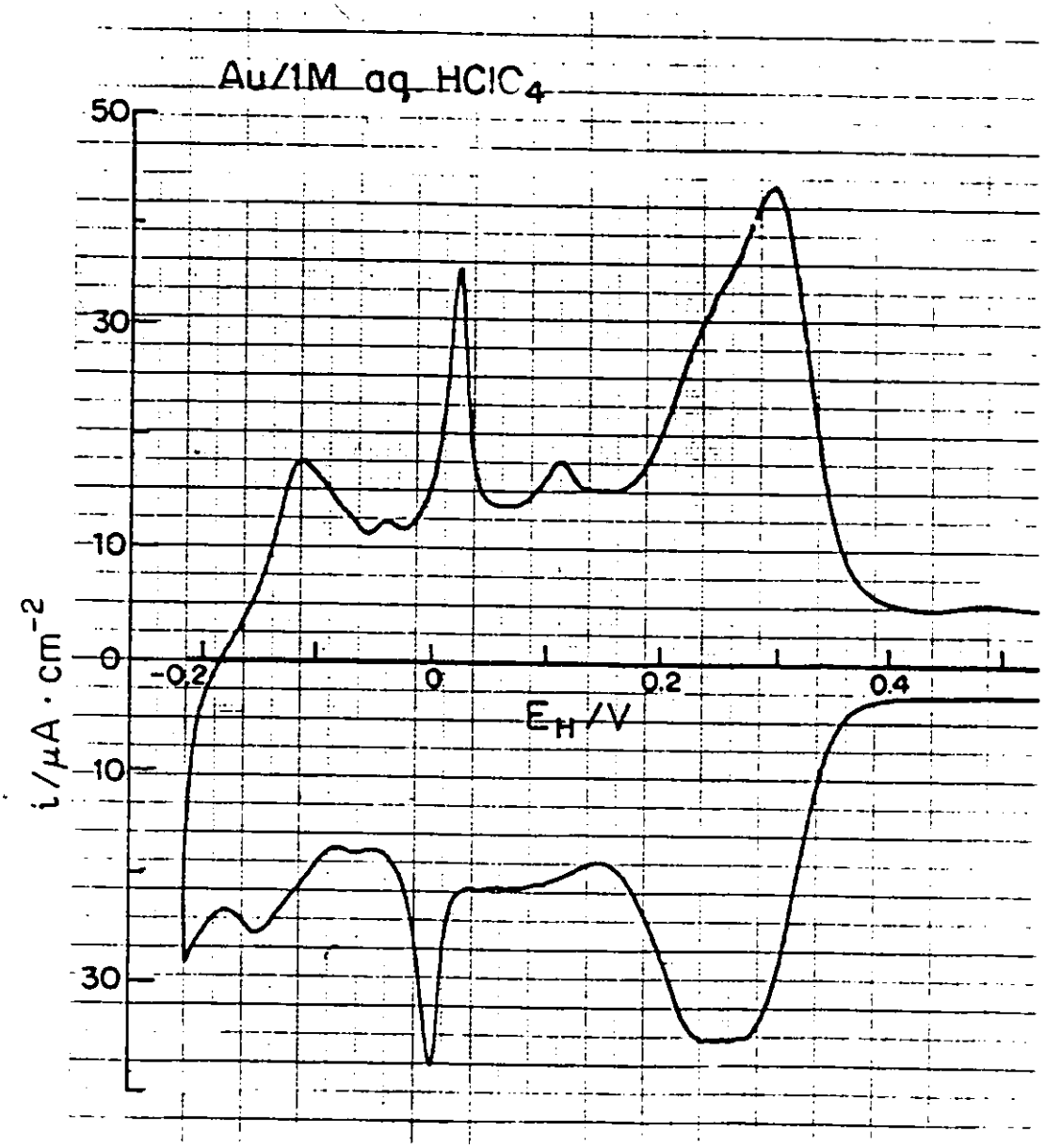

Fig. 4.5 Cyclic-voltammetry i vs E profile for Pb upd at Au in aq. 1M $HClO_4$ + 10^{-3}M $Pb(NO_3)_2$ solution at 298 K. s = 50 mV s^{-1}.

avoid or minimize anion adsorption effects which arise, e.g. with halide ions, as will be described later.

From examination of the i vs E profiles obtained in the various protic and aprotic solvents, it is evident that regardless of the solvent in which the upd experiment was carried out, the i vs E profiles have one general common feature: they are all characterized by five or six distinct cathodic and anodic peaks occuring at different potentials as the monolayer of underpotential-deposited Pb is laid down, as is also found in aqueous solution. This phenomenon, referred to as multiple-state adsorption, corresponds to distinguishable states of the electrodeposited Pb adatom film on Au as the upd occurs over a wide range (ca. 0.6 V) of potentials although this range is solvent-dependent.

An important and experimentally significant aspect of the results shown in Figs. 4.1 to 4.4 for several solvents is that good, i vs E profiles can be obtained which demonstrates, in most cases, good reversibility between anodic and cathodic processes except (see e.g. Fig. 4.13) when strong competitive adsorption of anions interfere (see later) with the upd process. Thus, no indications of impurity effects or skewing of the anodic/cathodic profiles is evident and background currents are also agreeable low. Thus, for the pure solvents, the background cyclic-voltammograms show that little or no electroactive impurities are present (Fig. 4.6).

4.4 Comparison of Potentials of Corresponding Peaks in Various Solvents

4.4.1 Basis for Comparisons

Electrode potentials cannot be compared in different solvents without introduction of undesirable experimental situations (e.g. liquid junction between two solvents) or extra-thermodynamic assumptions about individual ionic solvation energies.

However, with regard to upd profile peak potentials, E_p, they can be compared unambiguously in different solvents if, in each solvent, the E_p value for a given recognizable peak is referred to the bulk Pb/Pb^{++} potential set up at the bulk Pb electrode in that same solvent.

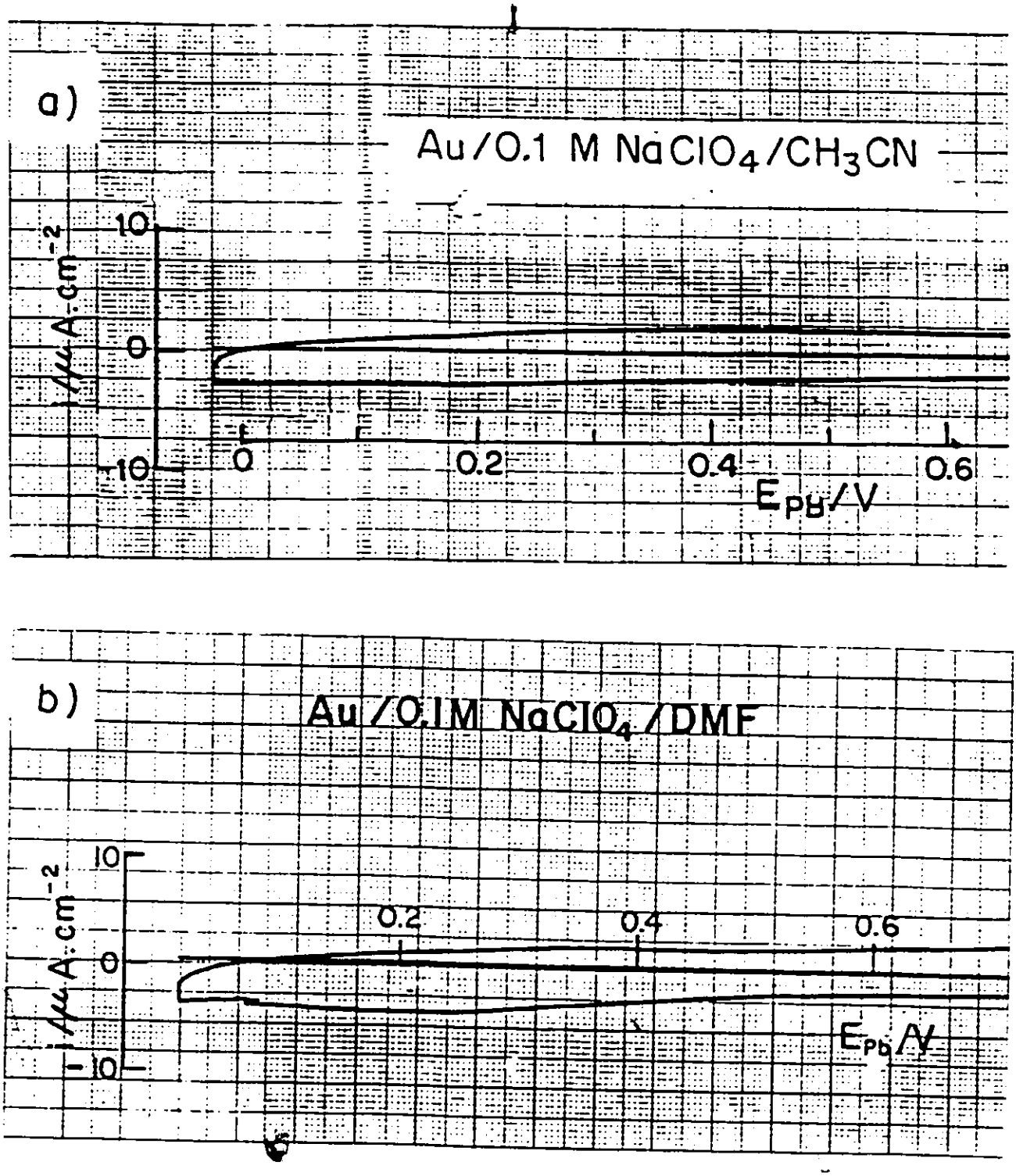

Fig. 4.6 Cyclic-voltammograms for Au in 0.1M $NaClO_4$ supporting electrolyte without a Pb salt being present: (a) acetonitrile and (b) dimethylformamide. $s = 50\ mV\ s^{-1}$.

Then, for example, in any solvent, S, the process

$$2e + Pb^{++}(S) + Au(lattice) \rightleftharpoons (Pb\ adatom,Au) \qquad (4.1)$$

can be compared with the process

$$2e + Pb^{++}(S) + Pb(bulk) \rightarrow Pb(bulk) \qquad (4.2)$$

so that the Gibbs energy of solvation of the Pb^{++} ions in <u>any</u> solvent, S, cancels out when E_p values are referred to the bulk E_{Pb} reversible potential for the same solvent. On this basis, values of upd peak potentials for Pb adatom states on Au are compared for the various solvents used in Figs. 4.7 and 4.8 and in Tables 4.2 and 4.3.

4.4.2 Values of Peak Potential Shift with Change of Solvent

In relation to the results of Figs. 4.1 - 4.5, it is useful to illustrate graphically how the peak potentials for the various resolvable and clearly recognizable peaks in the i <u>vs</u> E profiles depend on the solvent. This is shown in Figs. 4.7 and 4.8 for the anodic and cathodic peaks, respectively. It is clear from these plots, as also visually from the original i <u>vs</u> E profiles, that there is a substantial effect of the solvent on peak shapes, peak potentials and overall resolution of the profiles into sub-monolayer state components. There are also some systematic small but significant differences between the peak potentials for corresponding sub-monolayer states as revealed on the cathodic sweeps in comparison with the anodic sweeps. This is probably due (see Section 4.5) to some irreversibility in anion adsorption/desorption, even in the $NaClO_4$ supporting electrolyte.

Figs. 4.7 and 4.8 show that the solvent effect is most pronounced in the initial stages of Pb adatom electrodeposition. Generally, the solvent effects on the peak potentials cover a range of 50 to 100 mV (Figs. 4.7 and 4.8), which is well outside any uncertainities of peak-potential assignment, except for the most overlapping peaks. These diagrams show that the peaks in the i <u>vs</u> E profiles for the upd of Pb at Au from various electrolytes arise at different relative potentials, especially for low Pb atom coverages. This is to be expected, especially for the first cathodic peak, C_{Pb1}, because, before Pb electrodeposition commences, the electrode surface is fully covered by the solvent molecules, together with some anions, and the electrode/solvent interaction is, as was discussed in

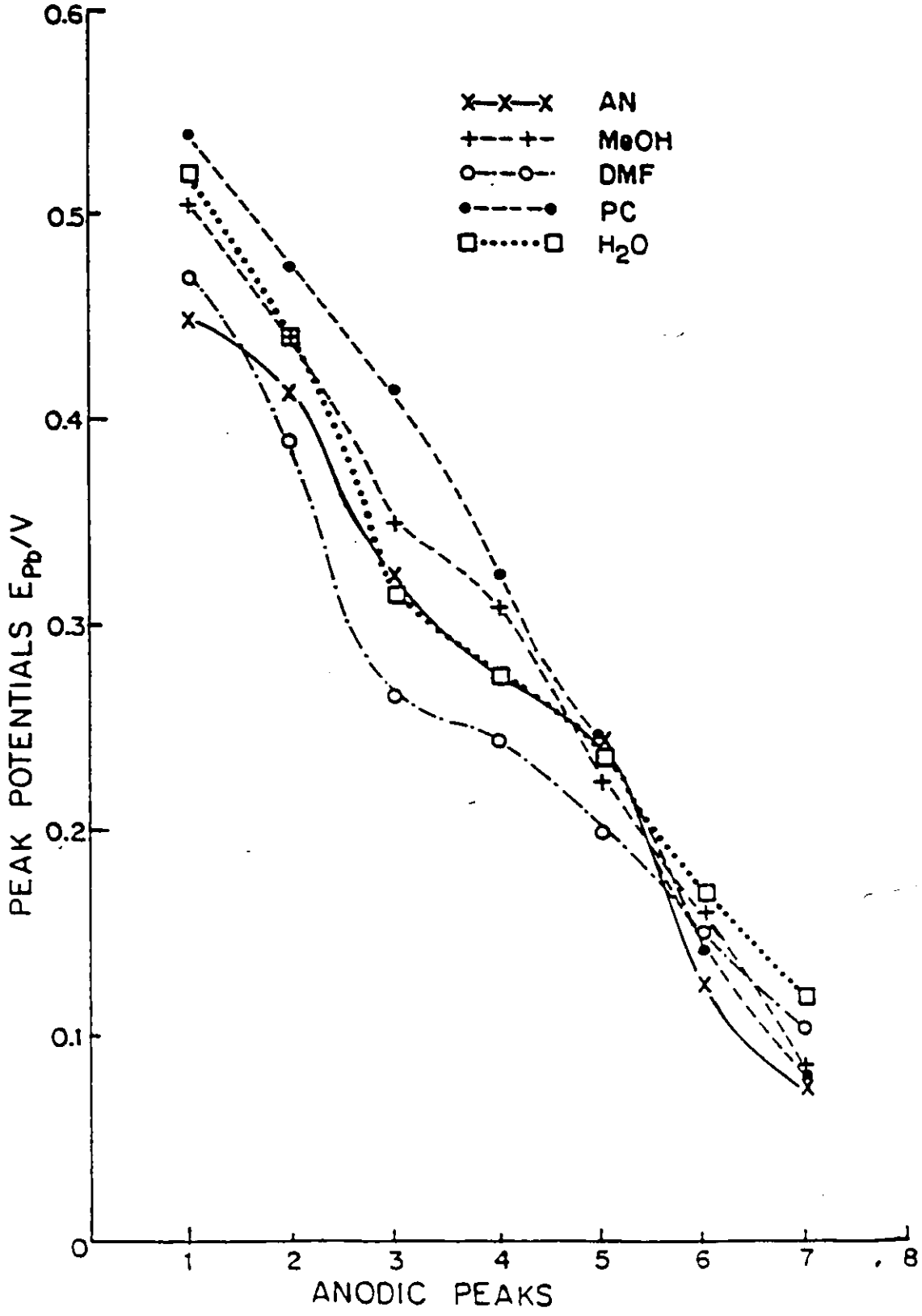

Fig. 4.7 Plots of variation of the individual anodic peak potentials versus Pb^{2+}/Pb in the i vs E upd profiles for Pb at Au in various solvents.

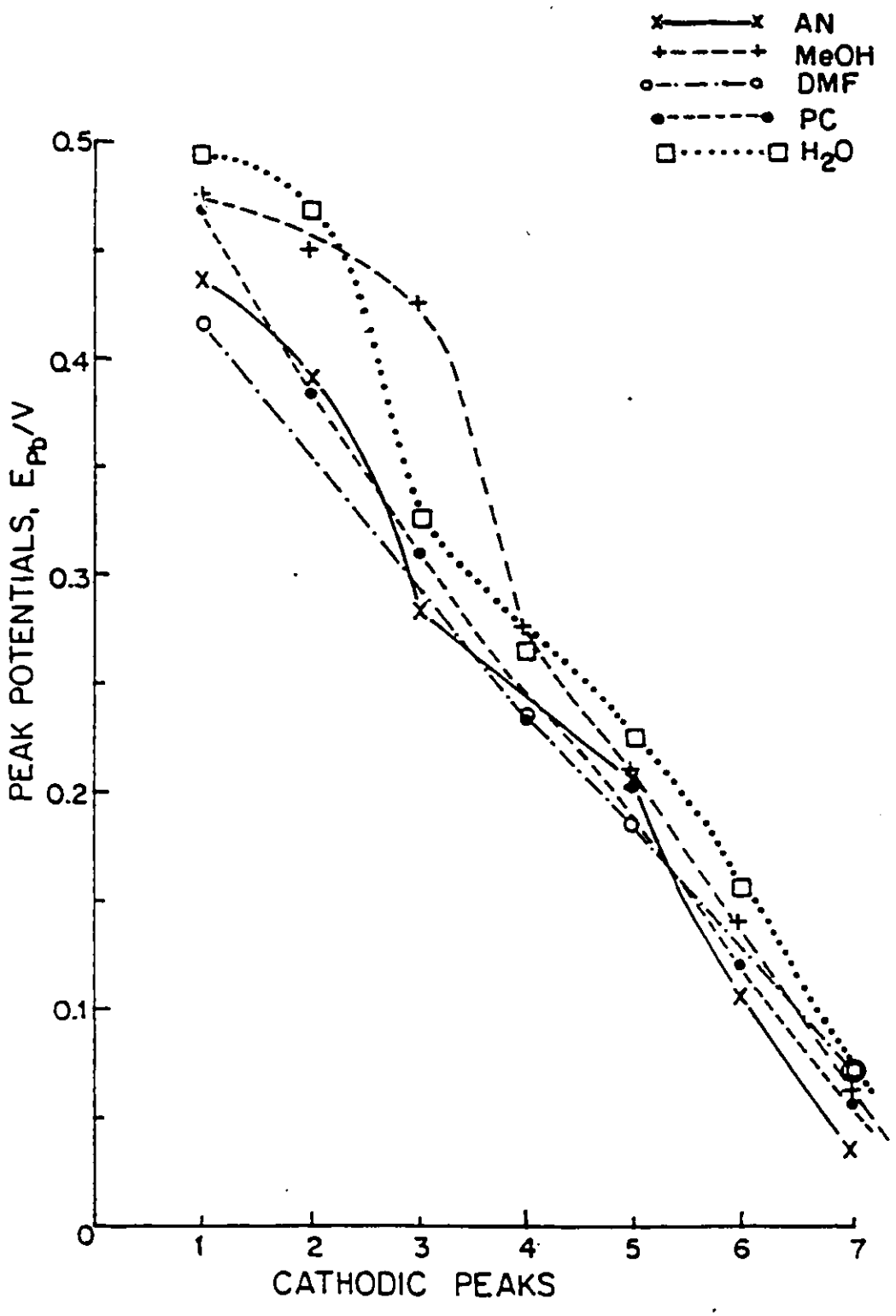

Fig. 4.8 Plots of variation of the individual cathodic peak potentials versus Pb^{2+}/Pb in the i vs E upd profiles for Pb at Au in various solvents.

Table 4.2 Peak Potentials of the Anodic Peaks Relative to Pb/Pb^{++} of the UPD i vs E Profiles of Pb at Au in Various Solvents

Solvent	Anodic Peaks and Peak Potentials						
	A_{Pb1}	A_{Pb2}	A_{Pb3}	A_{Pb4}	A_{Pb5}	A_{Pb6}	A_{Pb7}
	(1)	(2)	(3)	(4)	(5)	(6)	(7)
H_2O	0.50	0.440	0.315	0.275	0.235	0.170	0.120
MeOH	0.505	0.440	0.350	0.310	0.225	0.160	0.085
DMF	0.470	0.390	0.265	0.245	0.200		0.105
PC	0.540	0.475	0.415	0.325	0.245	0.140	0.085
AN	0.450	0.415	0.325		0.245	0.125	0.075

Table 4.3 Peak Potentials of the Cathodic Peaks Relative to Pb/Pb^{++} of the UPD i vs E Profiles of Pb at Au in Various Solvents

Solvent	Cathodic Peaks and Peak Potentials						
	C_{Pb1}	C_{Pb2}	C_{Pb3}	C_{Pb4}	C_{Pb5}	C_{Pb6}	C_{Pb7}
	(1)	(2)	(3)	(4)	(5)	(6)	(7)
H_2O	0.495	0.470	0.325	0.265	0.225	0.155	0.070
MeOH	0.475	0.450	0.425	0.275	0.210	0.140	0.060
DMF	0.415			0.235	0.185		0.070
PC	0.470	0.385	0.310	0.230	0.200	0.120	0.055
AN	0.435	0.390	0.285		0.230	0.105	0.035

Section 4.2, solvent dependent. For the non-aqueous solvents used in the present work, the C_{Pb1} peak potential in PC and MeOH is more positive (or less negative) relative to the bulk reversible potential of Pb^{++}/Pb, in DMF it is more negative.

The corresponding resolvable anodic peaks for the Pb desorption processes in the various solvents are also solvent-dependent, especially at low coverages. The first anodic peak, A_{Pb1}, of the i vs E profile obtained in PC arises at the most positive relative potential, while the corresponding peak of the i vs E profile obtained in AN occurs at the least positive potential (ca. 0.54 and 0.45 V vs Pb^{++}/Pb, respectively, see Fig. 4.8). In PC both cathodic deposition and anodic desorption of Pb adatoms takes place at more positive potentials than in the other solvents. This effect could arise if the PC solvent molecules are least strongly adsorbed at the Au electrode surface, compared with the other solvents, and hence are easily displaced by the electrodeposited Pb adatoms which thus are, comparatively, more strongly bound. In such a situation, the Pb adatoms would tend to become electrodeposited at less negative potentials (more positive potentials) which reflects an increased stability of the Au-Pb adatom bond. Another possibility is that the anions present are not, or are only weakly, specifically adsorbed on the Au electrode surface in PC, which would otherwise alter the i vs E profile, especially by shifting the first cathodic peak to more negative potentials.

The pronounced solvent effect on the i vs E profile for Pb at Au at low and intermediate Pb adatom coverages, say up to $\theta = 1/2$, may be attributed to mixed interactions because, for a Au electrode surface partially covered by Pb adatoms, the resulting mixed interactions are: Au-Pb interactions, Au-solvent interactions and Pb-solvent interactions (see Fig. 4.9). These mixed interactions will be different for different solvents.

At higher Pb adatom coverages, the solvent effect on the resolvable cathodic peaks and the corresponding anodic peak potentials is less pronounced. On examining both Figs. 4.7 and 4.8, the peak potentials of the cathodic "spike" (C_{Pb5}) for the different profiles are seen to arise at approximately 0.2 V vs Pb^{++}/Pb except for the behaviour in DMF and aqueous $HClO_4$ where the anodic "spikes" (A_{Pb5}) of the different profiles are observed at approximately 0.24 V vs Pb^{++}/Pb, except for DMF again. The "spike" has been interpreted as being due to a 2-dimensional phase

Fig. 4.9 Model for competitive adsorption between solvent molecules (S) and Pb metal adatoms on Au electrode surface.

a) Initial substrate; solvent-to-Au interactions.

b) Substrate partially covered by upd Pb adatom film; mixed interactions.

c) Substrate completely covered by Pb adatom film (p.z.c. changed): solvent-to-Pb adatom interactions.

a) $\theta_{Pb}=0$

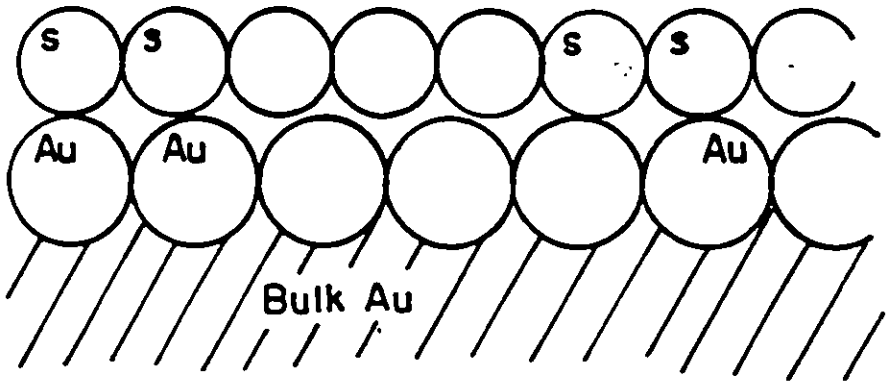

b) $0<\theta_{Pb}<1$

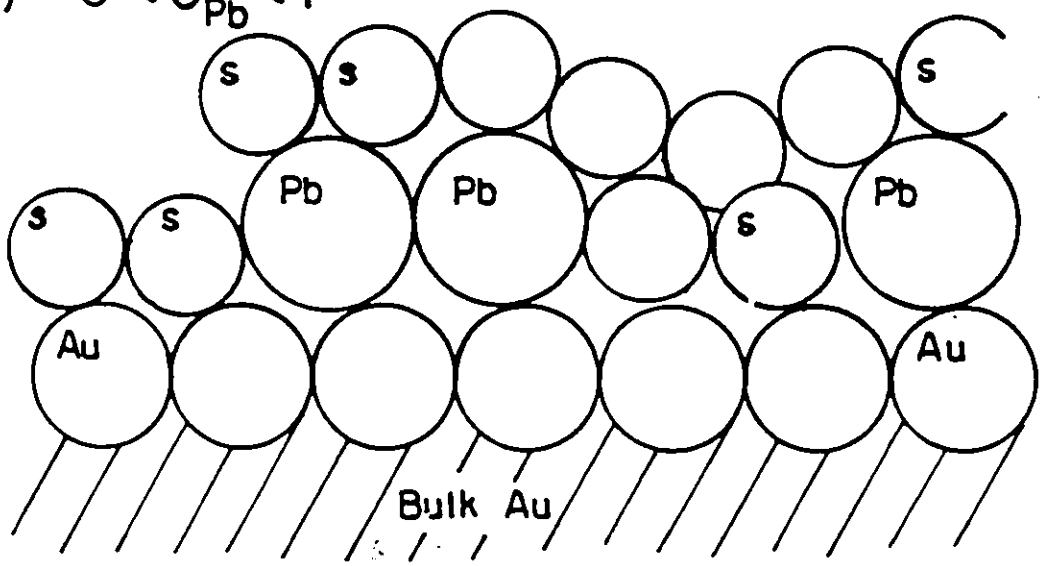

c) $\theta_{Pb} \longrightarrow 1$

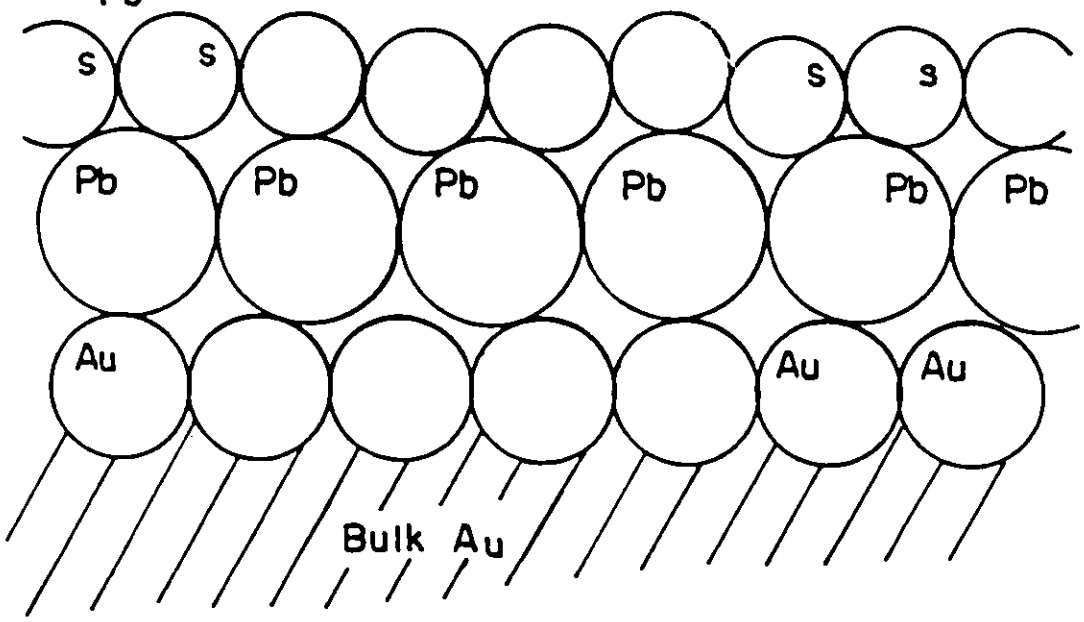

transition in the ad-layer and it represents a coverage $\theta_{Pb} \cong 68\%$. The remaining effect of solvent at higher coverages arises probably because, as $\theta_{Pb} \rightarrow 1$, most of the Au electrode surface is now covered by Pb adatoms and now the main interactions are between the Au lattice and Pb atoms together with Pb-solvent interactions at the interface of the double-layer.

4.5 Commentary on Behaviour in Individual Solvent Systems

The i vs E profiles recorded in experiments conducted in MeOH and DMF are (Figs. 4.2 and 4.3, respectively) in a general way, similar to that for aqueous medium in terms of peak multiplicity, shape and resolution of the peaks. This is not surprising in the case of H_2O and MeOH because both are polar, H-bonded protic solvents but with differing bulk dielectric constants (ε = 78 for H_2O and 33 for MeOH). Also the general electrochemical solvent behaviour of MeOH is similar to that of water. Hence, it is to be expected that the Au/H_2O and Au/MeOH interactions are rather similar and, since the upd profile for the initial stages of deposition (low θ_{Pb}) are not shifted to significantly more cathodic potentials, it seems that both the water and MeOH solvent molecules are only weakly adsorbed at the Au surface. Another factor determining the similar upd behaviour in the two solvents is that the electrolyte ions, especially ClO_4^-, are either adsorbed to similar extents in the two solvents or the ClO_4^- anions are not appreciably specifically adsorbed on Au from MeOH, as found in H_2O. Were co-adsorption of anions competitive with Pb adatom deposition, as with some other solvents (see below), the i vs E profile would be altered, especially in the initial stages of electrodeposition of the Pb adatom monolayer, a behaviour encountered with halides ions. Borkowska and Fawcett [94] found no specific adsorption of the anion at the Hg/MeOH interface in $NaClO_4$ solutions.

Some differences are noticeable, however, if the i vs E profile in DMF is compared with those in MeOH and aqueous medium. Firstly, the cathodic peak for deposition of the most strongly bound species in DMF (referred to by some authors in the literature inappropriately as the " monolayer" peak, e.g. in ref. 31) is slightly shifted to more negative potentials. Whereas in DMF and AN, this particular peak is sharp at its top but more drawn out overall, in MeOH and aqueous

media, it is broad and actually resolved into two peaks. (In DMF and AN the shape of this first peak is really determined by the extent of overlap of the two peaks which are resolved in MeOH and water).

The shift of the first cathodic upd peak to more negative potentials may be due to:

(i) Au/DMF interactions. If the DMF molecules are strongly adsorbed and/or interacting on the Au electrode surface, electrodeposition with displacement of the DMF molecules would require more negative potentials before the Pb adatom electrodeposition could commence. Studies of adsorption of DMF from aqueous solutions [100,101] have shown that the DMF molecule is predominantly adsorbed on Hg at and around the p.z.c. with its dipole parallel to the electrode surface. At other potentials where the electrode bears a net charge the DMF solvent molecules may assume other possible orientations (see Section 1.11).

(ii) Competitive co-adsorption of the anions with Pb adatoms. Since the effect is not at all as great as in the case of strongly adsorbing halide ions, specific adsorption, if any, must be weak. Electrocapillary measurements [101] at the Hg/DMF interface indicate that specific adsorption of anions at the p.z.c. increases in the order: SO_4^{2-}, ClO_4^-, NO_3^- < SCN^- < Cl^- < Br^- < I^-. Indications that the metal cations, especially K^+ and Cs^+, exhibit specific adsorption in DMF at more negative potentials have been noted [166]. In the light of these observations, it seems that Na^+ and/or ClO_4^- (more probably the ClO_4^- ion) influence the Pb adatom deposition by competitive adsorption, slightly modifying the first cathodic peak corresponding to the initial stage of Pb electrodeposition.

The i vs E profiles obtained in AN are characteristically different from the profiles in the other media, including water. The first cathodic peak (referred to as C_{Pb1} in the present work) due to Pb^{++} reduction and the corresponding anodic peak due to Pb adatom oxidation is sharp at its top but overall it is drawn out (i.e. it contains one or more other unresolved components) compared with the i vs E profiles in the other solvents investigated. The "spike" (on both the cathodic and anodic sweeps) is also less pronounced. Unlike the i vs E profile in DMF, where it is only the first cathodic peak that is shifted to more cathodic potentials (thus exhibiting some irreversibility between the

cathodic process and the corresponding anodic one), the cathodic and corresponding anodic peak are almost mirror images in shape, extent of charge and peak potential positions, thus corresponding to a rather reversible process.

The narrow peaks found for upd of Pb in AN (C_{Pb1} and A_{Pb1}) in contrast to the broader peaks observed in other solvents, especially water, MeOH and PC, could be attributed to enhanced adsorption of the ClO_4^- and/or Na^+ ions at the Au electrode in AN. Another possibility is the competitive adsorption between the Pb adatoms and the AN solvent molecules themselves. From inner-layer capacity measurements, Trasatti [167] found that the AN molecule is strongly adsorbed on Hg with the negative end of its dipole oriented towards the Hg. Also, at Hg/AN interface, the inner-layer capacity in solutions of alkali metal cations increases with increasing size of the cation [90]. In the absence of any specific adsorption, this order is attributed to a decrease in solvation of the cations as their radii increase. However, Crum [168] attributed the above order to cation specific adsorption at higher cathodic potentials, in contrast to the findings of Fawcett and Loufty [90] whose results indicated no specific adsorption of Li^+ and Na^+ ions.

In their investigation of electrochemisorption and reactivity of nitriles at Pt electrodes, Angerstein-Kozlowska et al. [169] found that in 0.5M aq. H_2SO_4, AN and H species were co-adsorbed over the potential range of H-region at Pt. The AN is adsorbed at Pt through the CN group rather than the $-CH_3$ group.

Another property, which AN exhibits that is not found with other non-aqueous solvents, is the high degree of association of $CF_3SO_3^-$ with divalent metal ions in that solvent although such electrolytes are completely dissociated, for example, in DMF. In AN the first association constant of $Pb(CF_3SO_3)_2$ is 2280 mol^{-1} dm^3 at 298 K compared to a maximum value of 21 mol^{-1} dm^3 for $NaClO_4$, also in AN at 298 K [170]. Such an high degree of association would be expected to reduce the effective concentration or activity of the Pb^{2+} ions in solution but since the reference electrode is in the same solution, this would lead to a parallel shift of the i vs E upd profile in the negative direction compared to the potentials over which it would be observed if $Pb(CF_3SO_3)_2$ was completely dissociated in AN. However, this effect is completely compensated by a corresponding

shift at the bulk Pb reference electrode.

In order to establish if this high degree of association had an effect on the upd profile, a similar experiment was conducted using $Pb(ClO_4)_2$, which is almost completely dissociated in AN, instead of $Pb(CF_3SO_3)_2$. It was found that the i vs E profiles for these two salts were identical in shape and in the relative positions of the peaks, i.e. there was no parallel shift when $Pb(ClO_4)_2$ was used, as is expected on the thermodynamic basis mentioned above.

In solutions with salts of $CF_3SO_3^-$ as supporting electrolytes, the half-wave potentials of lithium and divalent metal ions in AN [148,170] at Hg are slightly more negative by about 25 mV. These shifts were explained quantitatively in terms of ion-pair formation between the metal ion to be reduced and the anion of the supporting electrolyte. However, it should also be noted that $NaClO_4$ has the highest conductivity in AN compared with that in the other non-aqueous solvents used in the present work. In AN, $\Lambda_0 = 180.63\ \Omega^{-1}\ cm^2\ mol^{-1}$ but again it is slightly associated, with $K_A = 11\ mol^{-1}\ dm^3$.

Dissolved $LiClO_4$, $NaClO_4$ and $Mg(ClO_4)_2$ have been found to cause changes in the IR spectra of AN [171], although perchlorate ion was said to have no effect on the absorption bands. The blue shifts of the $-C \equiv N$ and C-C vibrations were attributed to binding of AN to cations. Also the IR stretching bands for C-C and $C \equiv N$ in AN were found to split into two components upon addition of Cu^{2+}, Ni^{2+}, Co^{2+} and Na^+. According to Kecki [172] one band corresponds to the frequency of the pure solvent and the second band, at higher frequencies, is attributed to AN solvating the cations.

The upd i vs E profile in PC (Fig. 4.4) has a significant feature which is characteristically different from that in the other solvents. The whole i vs E profile is somewhat more extended than is the case for the other solvents, so that the initial cathodic current for the upd process commences already at +0.63 V (vs Pb/Pb^{++}), i.e. some 0.05 to 0.09 V more positive than for the other solvent systems. The main difference is that the first two peaks are more separated, within the profile, than is the case with the other solvents, e.g. AN and DMF. There is also a significant negative shift of the initial cathodic peak relative to the potential of the corresponding first anodic peak (Fig. 4.4).

Since this effect arises again at the initial stages of Pb electrodeposition, it must be attributed to electrode/solvent interaction and/or anion co-adsorption effects referred to earlier. Perhaps the large PC molecules require a more negative potential before they can begin to be displaced by the onset of Pb adatom deposition.

Interfacial studies [102] at Hg/PC have shown that the maximum entropy of adsorption, at least at the p.z.c., is positive which indicates that the molecular arrangement of the solvent is more disordered in the adsorbed layer than in the bulk. Also ClO_4^- was found not to be specifically adsorbed on Hg from PC solutions. This suggests then that the above effect is to be attributed more to PC displacement than to ClO_4^- desorption.

In preliminary studies on the electrochemical behaviour of a polycrystalline Au electrode in PC, Nguyen van Huong [173] found a low interfacial capacity value at negative electrode surface charge. He suggested that this behaviour was due not only to an increase in the thickness of the inner-region solvent layer and a decrease in its dielectric constant but also to changes in the properties of the metal surface itself as indicated by the shift of the p.z.c. in PC with small additions of water. In experiments on the single-crystal Au/PC interface, he found only minor differences among the curves for the (111), (100) and (110) faces whereas, in aqueous medium, the corresponding curves showed significant crystallographic surface orientation dependence.

In the work of Xing et al. [37], the i vs E upd profiles of Cd on Ag(111) in PC are characteristically different from the corresponding profiles in aqueous medium while they found the i vs E profiles for Pb on Ag(111) to be similar in PC and aqueous medium, in agreement with the earlier work in this laboratory [36] where it was found that there were small but significant differences in the i vs E profiles for the upd of Pb on polycrystalline Au in aqueous medium, MeOH and AN.

4.6 Infuence of Ions of the Supporting Electrolyte on the i vs E Profiles for UPD of Pb on Au: Ion Adsorption Effects

Since ion adsorption is solvent-dependent, the effects of the nature of the ions of the supporting electrolyte and the anion of the Pb salt itself were investigated in several solvents in which the salt solubilities are appreciable and adequate.

4.6.1 Cation Effects

– Tetraethylammonium perchlorate (TEAP), a suitable and widely used supporting electrolyte in work in most non-aqueous solvents, was used as the supporting electrolyte in AN in order to examine the effects of a large organic cation. The resulting i vs E profile recorded for Pb deposition on polycrystalline Au from TEAP solution is given in Fig. 4.10. It should be compared with the one obtained in $NaClO_4$ solution in AN given earlier in Fig. 4.1.

There is evidently a large shift of the first cathodic peak to more negative potentials in TEAP solution, leading to marked irreversibility between the deposition and the corresponding desorption process. The whole i vs E profile is also less well resolved.

It seems clear that this large shift is due to adsorption of the TEA^+ cations rather than the ClO_4^- anions which are only weakly adsorbed. Thus, it is the TEA^+ cations that are strongly adsorbed on the Au electrode surface thus blocking the electrodeposition of Pb adatoms. These cations become desorbed at more negative potentials leading to a subsquent deposition of Pb adatoms, effectively at a cathodic overvoltage. This behaviour is not a temporary blocking effect because the upd proifile does not change with continuous cycling, a situation different from that found in upd of Pb at Au in PC when $LiClO_4$ is used as the supporting electrolyte [37]. Temporary blocking effects were observed in that work and explained as being due to the reaction of hydroxyl ions generated during the reduction of traces of water in the solution with Li^+ to form LiOH which initially forms a film on the electrode surface because it is less soluble in PC than in water. When $LiClO_4$ was used a supporting electrolyte in AN instead of $NaClO_4$, there was no difference in the upd i vs E profiles, indicating similar behaviour of Li^+ and Na^+ cations in AN.

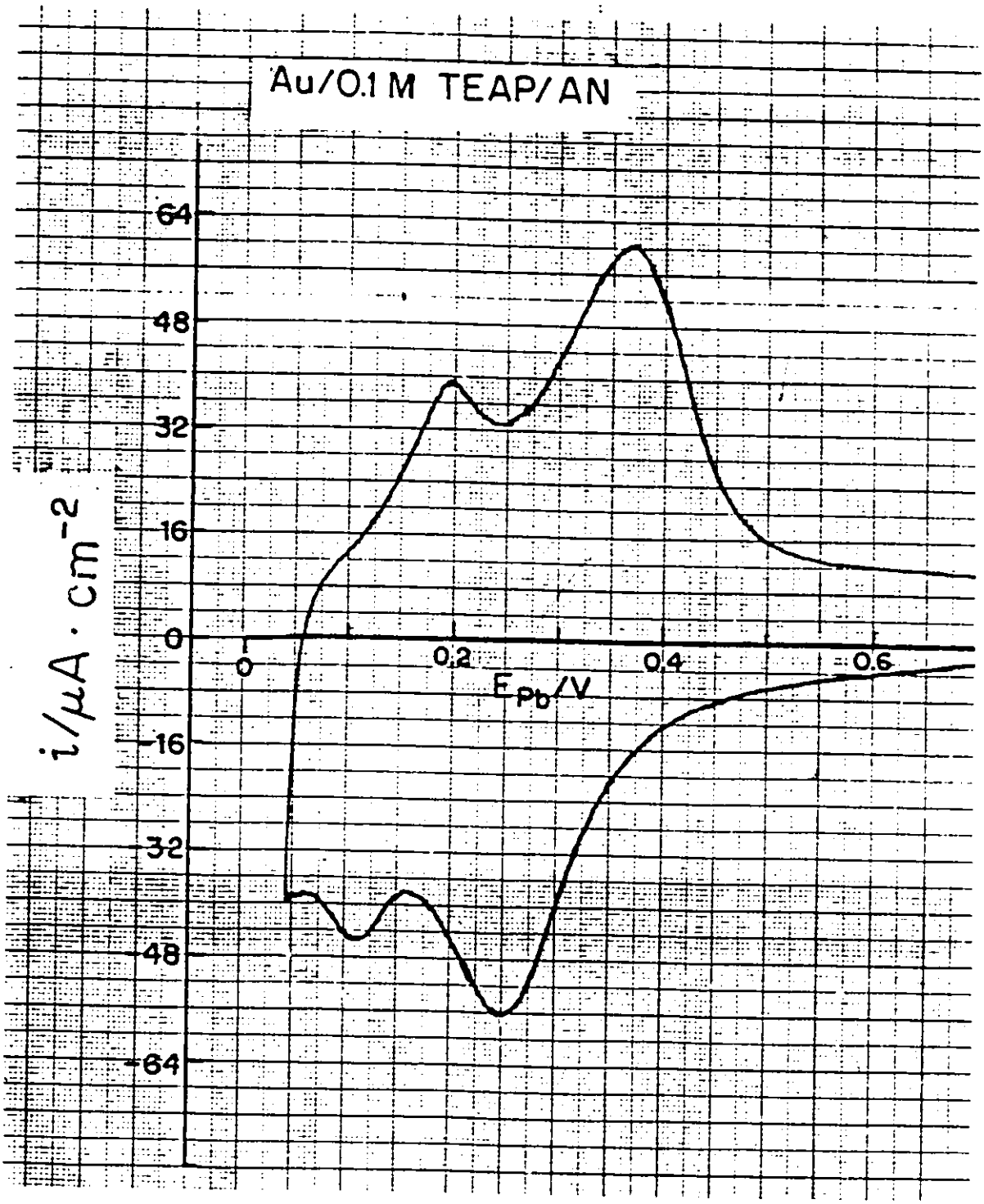

Fig. 4.10 Cyclic-voltammetry i vs E profile for Pb upd at Au in 0.1M TEAP + 10^{-2}M $Pb(CF_3SO_3)_2$ solution in acetonitrile at 298 K. s = 50 mV s^{-1}.

The effect of the ions of the supporting electrolyte on the upd profile has also been investigated by Xue-Kun Xing et al. [37] in their study of the upd of Cd on Ag(111) in aqueous solutions containing TEAP and $LiClO_4$ as supporting electrolytes. The resulting i vs E profiles are shown in Figs. 4.11 and 4.12. Clearly the cyclic-voltammograms for the above system in the two supporting electrolytes are different indicating that the nature of the cation can play an important role in controlling the energetics and dynamics of the upd process. The variations between the upd profiles were attributed to the differences in the extent to which the TEA^+ and Li^+ interact with the electrode surface. The specific adsorption of TAA ions on the Hg electrode increases in the order $TPA^+ > TEA^+ > TMA^+$ [81], and a similar sequence has been reported in the case of AN solutions of these ions on Hg [174].

It has been found that TAA cations are not solvated in AN [178 - 180], and ion-pair formation is negligible at low concentrations. At more negative potentials, because these ions are cations that are unsolvated, there is an indication of their adsorption at the Hg surface, the strength of adsorption increasing with chain length of the alkyl group due to lyophobic effects.

Based on the above information, it is to be concluded that the modification of the upd profiles in the presence of TEA^+ is due to the strong interaction of these cations with the Au electrode surface so that Pb adatom deposition can only take place when a sufficiently negative electrochemical driving (Gibbs) energy is provided that leads to favourable competitive adsorption of Pb adatoms vis a vis TEA^+ cations. The eventual preference for Pb adatom deposition with increasing negative potential arises because Pb is electrochemically deposited from Pb^{++} ions with passage of 2e per atom in an almost complete discharge event while TEA^+ is only electrostatically adsorbed at the Au electrode/solution double-layer without charge transfer.

4.6.2 Anion Effects

Because MeOH, like H_2O, is a polar solvent it provided a suitable medium in which to investigate the effect of some anions of salts which are sparingly or insoluble in most non-aqueous solvents. $NaNO_3$ was used as the supporting electrolyte so that the effect of NO_3^- anion could be

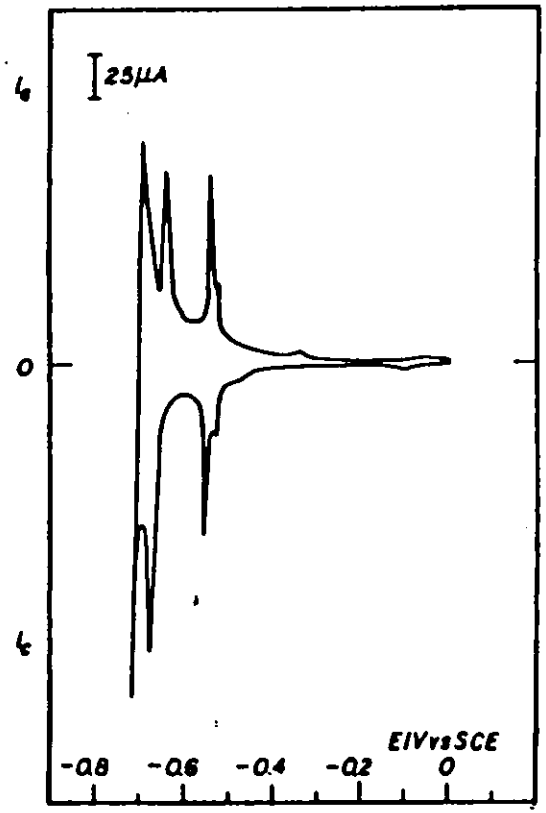

Fig. 4.11 Cyclic-voltammogram for the upd of Cd on Ag(111) in an aqueous solution containing 0.2M TEAP and 5 X 10^{-3}M $Cd(ClO_4)_2$. s = 10 mV s^{-1}. (From ref. 37).

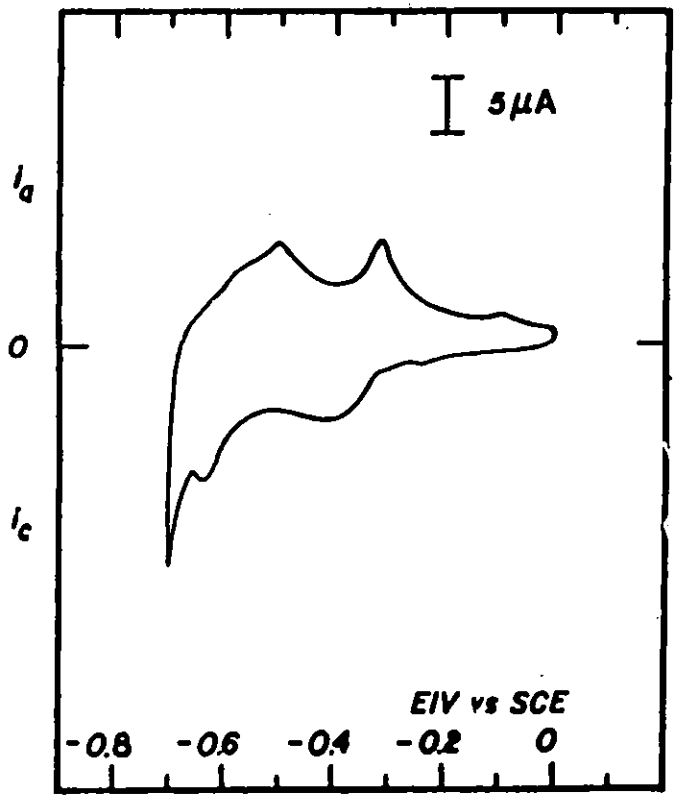

Fig. 4.12 Cyclic-voltammogram for the upd of Cd on Ag(111) in an aqueous solution containing 0.1M $LiClO_4$ and 5 X 10^{-3}M $Cd(ClO_4)_2$. s = 10 mV s^{-1}. (From ref. 37).

studied. In MeOH, $NaNO_3$ has a limiting molar conductivity of 106.2 $\Omega^{-1}cm^2$ mol^{-1}, slightly lower than the value of 116.2 Ω^{-1} cm^2 mol^{-1} for $NaClO_4$, also in MeOH. $NaClO_4$ is completely dissociated in MeOH whereas $NaNO_3$ is slightly associated, with an association constant of 19 mol^{-1} [178].

The cyclic-voltammogram for upd of Pb at Au from $NaNO_3$ solution in MeOH is shown in Fig. 4.13 and that from $NaClO_4$ was given earlier (see Fig. 4.2). The upd profile from $NaNO_3$ solution is significantly different from that in $NaClO_4$ solution. For the profile in $NaNO_3$ solution, the first cathodic peak is shifted to more cathodic potentials; the peaks are less well resolved and the "spike" is less pronounced, and appears as an ordinary peak.

The distortion of the upd profile, relative to that in $NaClO_4$, is clearly the result of adsorption of the NO_3^- anion. As pointed out earlier, this must be the result of NO_3^- being more strongly adsorbed on the Au electrode surface from MeOH than is ClO_4^-. Thus, it was explained earlier that the shift of the first cathodic peak to more negative potentials in the case of the change of electrolyte is to be attributed to competitive co-adsorption of the adatom being electrodeposited with the specifically adsorbing ion whose solvation state in solution is solvent-dependent.

Electrocapillary curves for NH_4NO_3, NaBr and NaI solutions in MeOH indicate that specific adsorption of anions at Hg increases in the order $NO_3^- < Br^- < I^-$ [84], and a similar order has been observed in aqueous solutions. However, the adsorption appeared to be somewhat weaker in MeOH than in aqueous solutions probably because of the lower activities of electrolytes in methanol. Contrasting results were later obtained by Grahame [85] who found from double-layer capacity measurements at Hg in ammonium salt solutions that the anion of the electrolyte does not affect the capacity at potentials sufficiently negative from the p.z.c.. This led him to conclude, rather generally, that specific adsorption of anions is usually absent in this potential region. This was supported in later measurements by Garnish and Parsons [179] who found no significant differences between the capacity behaviour in 1M solutions of KF and KI at more negative potentials.

It is quite surprising that NO_3^- has such an effect on the profile for upd of Pb at Au in MeOH and yet in aqueous medium it is the anion of the Pb salt used and has little or no effect on the upd profile relative to ClO_4^-. It should be pointed out, however, that the anion concentrations in the two

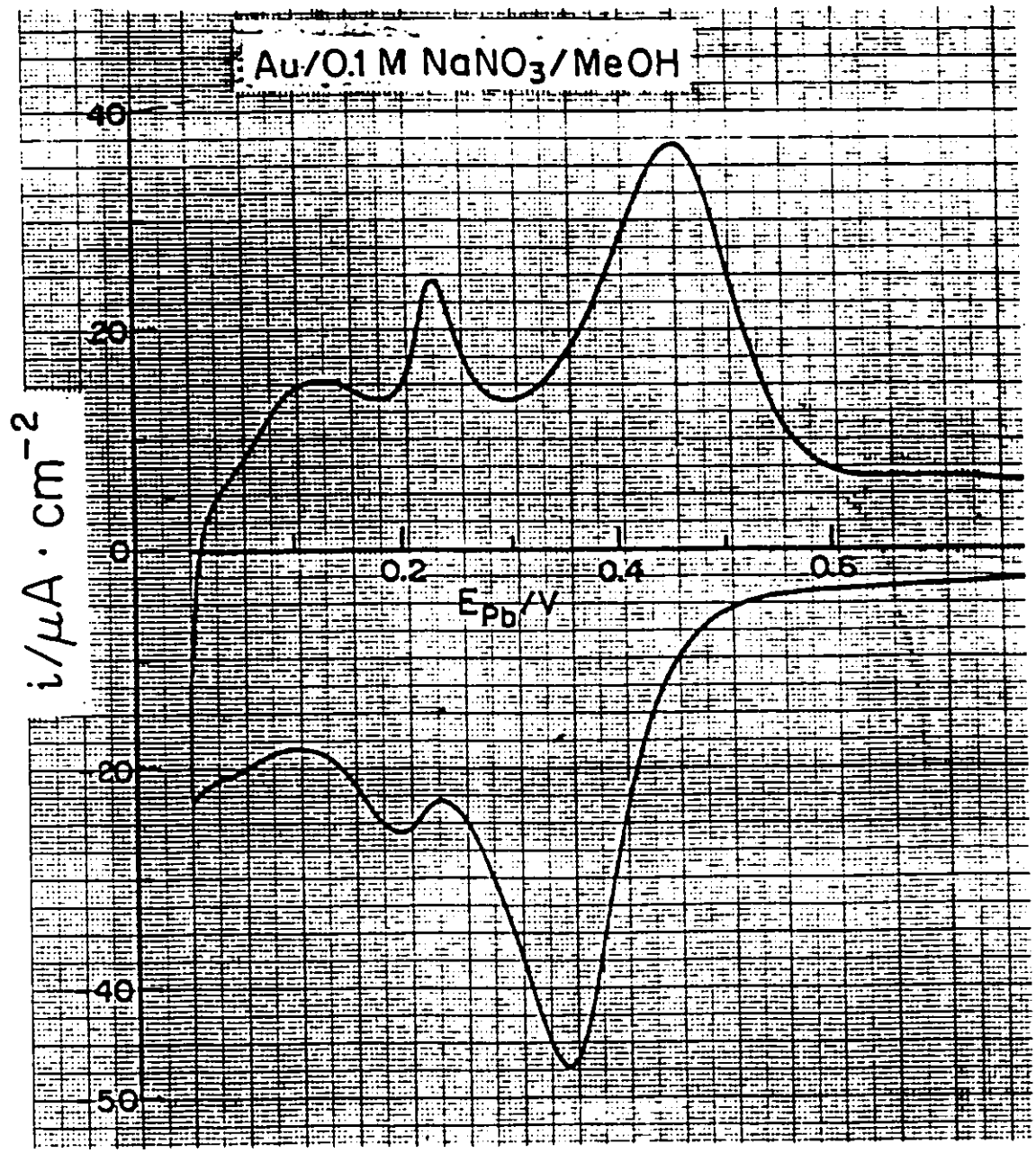

Fig. 4.13 Cyclic-voltammetry i vs E profile for Pb upd at Au from 0.1M $NaNO_3$ + 10^{-2}M $Pb(CF_3SO_3)_2$ solution in methanol at 298 K. s = 50 mV s^{-1}.

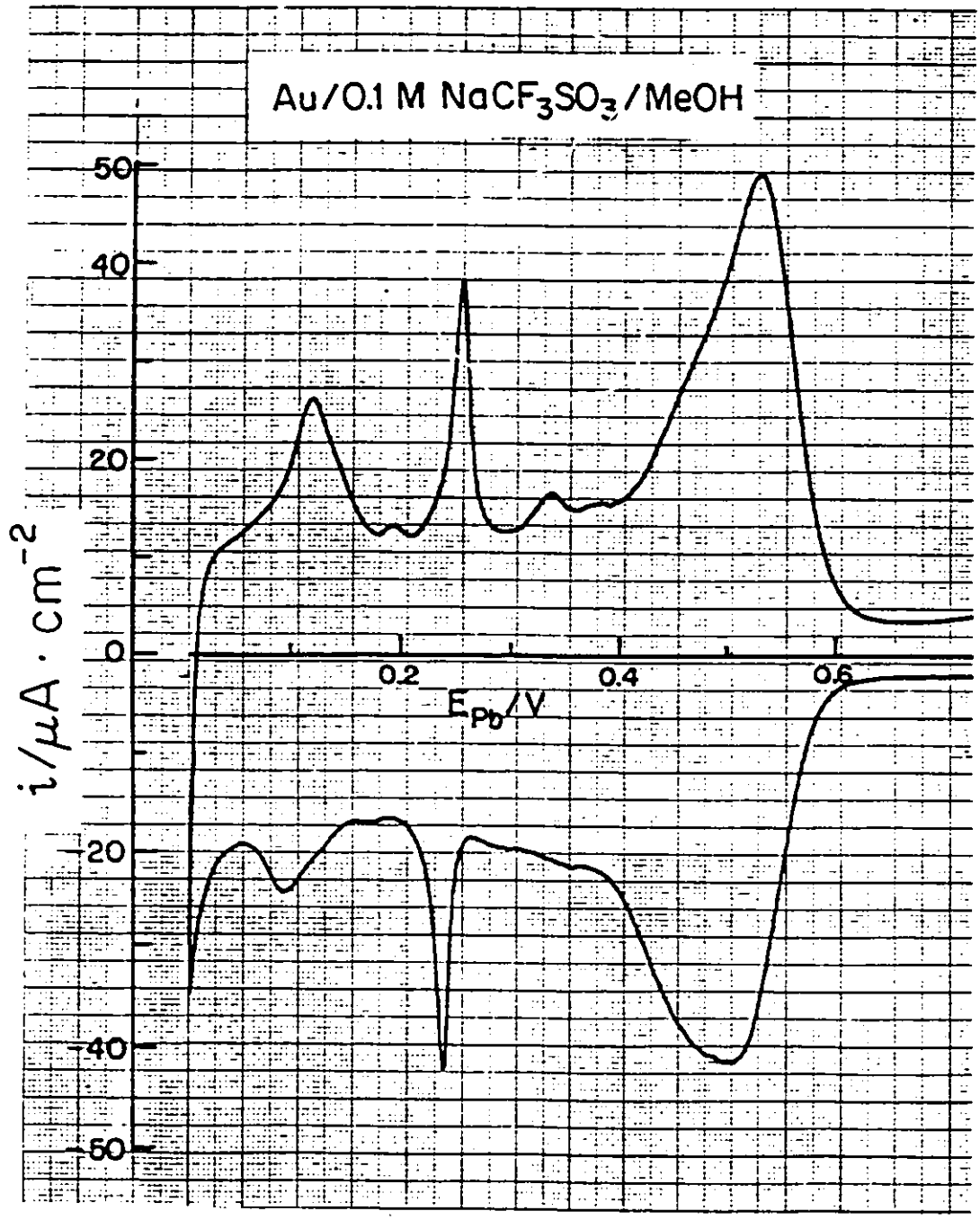

Fig. 4.14 Cyclic-voltammetry i vs E profile for Pb upd at Au from 0.1M $NaCF_3SO_3$ + 10^{-2}M $Pb(CF_3SO_3)_2$ solution in methanol at 298 K. s = 50 mV s^{-1}.

media differ by about two magnitudes (10^{-3}M in aq. $HClO_4$ and 10^{-1}M in MeOH).

In aqueous medium, the first cathodic peak for upd of Pb at Au is shifted to more cathodic potentials by adsorbing anions in the increasing order $ClO_4^- \leq NO_3^- < CH_3COO^- < Cl^- < Br^-$ [78] i.e. the NO_3^- ion has the least effect in aqueous solution.

Although the results from electrocapillary measurements at Hg are not conclusive about the state of NO_3^- at the Au/solution interface, in the present work the NO_3^- has been found to have a pronounced effect on the i vs E profile which must arise from a strong Au/NO_3^- interaction. Perhaps the difference from the behaviour of ClO_4^- ion is due to the different geometries of these ions: ClO_4^- is tetrahedral and NO_3^- is a flat, trigonal structure in which the N atom can approach a surface more closely than Cl in ClO_4^-. When $NaCF_3SO_3$ was used as the supporting electrolyte in MeOH, the upd i vs E profile obtained was similar to that from $NaClO_4$ solution, also in MeOH, as shown in Fig. 4.14.

In the case of $CF_3SO_3^-$ in MeOH, it is seen from Fig. 4.14 that the features of the upd profile are well resolved, in fact as clearly as for upd in water from ClO_4^- solutions (Fig. 4.5). There is very little displacement of the first cathodic peak relative to the end of the anodic one, so the $CF_3SO_3^-$ anion is, like ClO_4^-, evidently insignificantly adsorbed at Au in the MeOH solvent.

In comparing, the upd behaviour in ClO_4^- and $CF_3SO_3^-$ solution in MeOH it is relevant to note that the sodium salts of $CF_3SO_3^-$ and ClO_4^- are almost completely dissociated in MeOH and it has been stated that the anions are "not solvated" in MeOH.

Data for the Hg/MeOH interface in $CF_3SO_3^-$ solutions are not available in the literature so that conclusions cannot be drawn about their comparative behaviour in MeOH.

4.7 The Effect of the Anion of the Pb Salt

In order to study the effect of the nature of the anion of the Pb salt, $Pb(CF_3SO_3)_2$ was used instead of $Pb(NO_3)_2$ in experiments conducted in aqueous medium. The i vs E profile obtained using the $Pb(CF_3SO_3)_2$ is shown in Fig. 4.15 and is to be compared with that using $Pb(NO_3)_2$ shown in Fig. 4.16. The two upd profiles for the corresponding Pb salts in aq. $HClO_4$ are similar to one

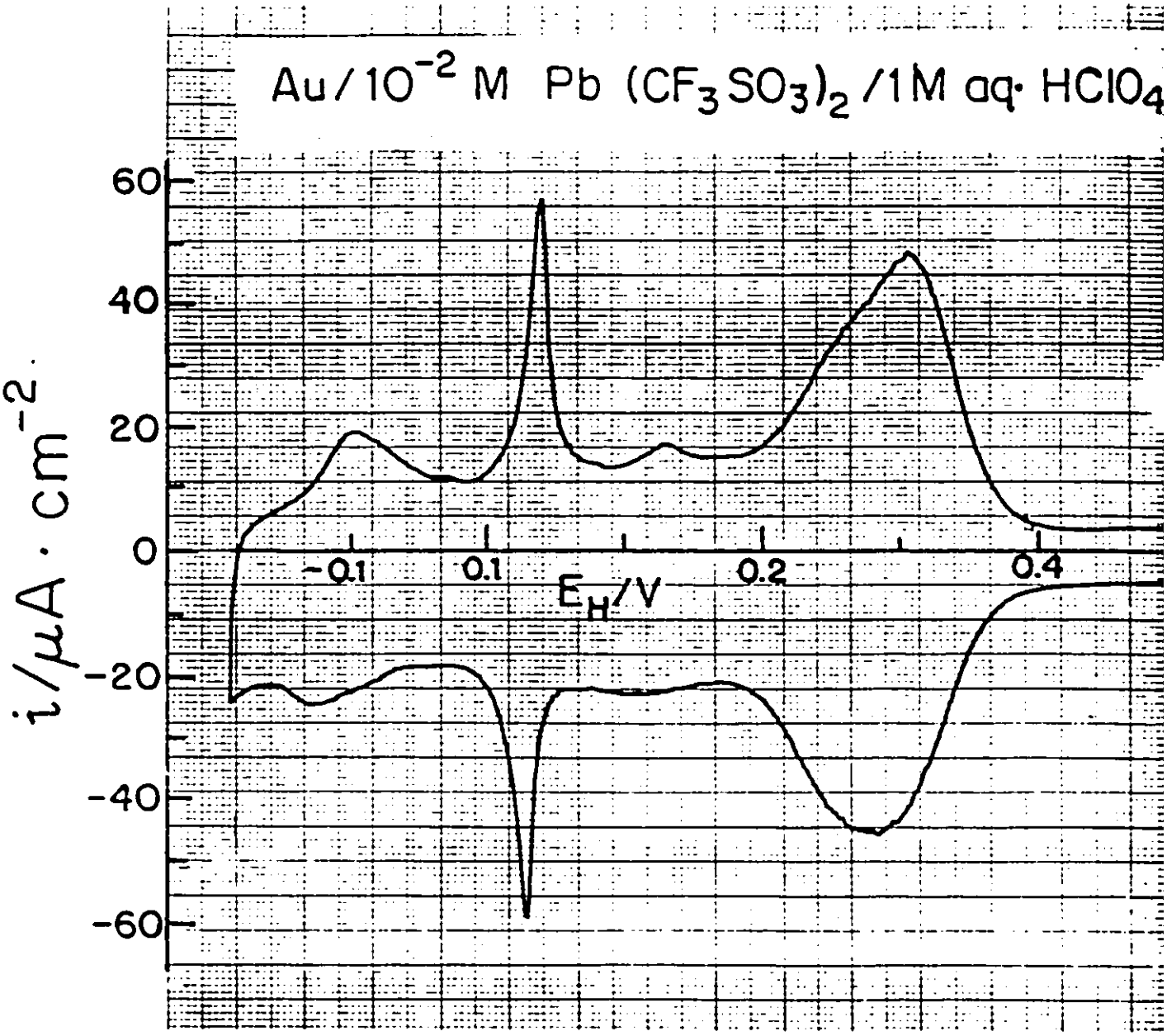

Fig. 4.15 Cyclic-voltammetry i vs E profile for Pb upd at Au in aq. 1M $HClO_4$ + 10^{-2}M $Pb(CF_3SO_3)_2$ solution at 298 K. s = 50 mV s^{-1}.

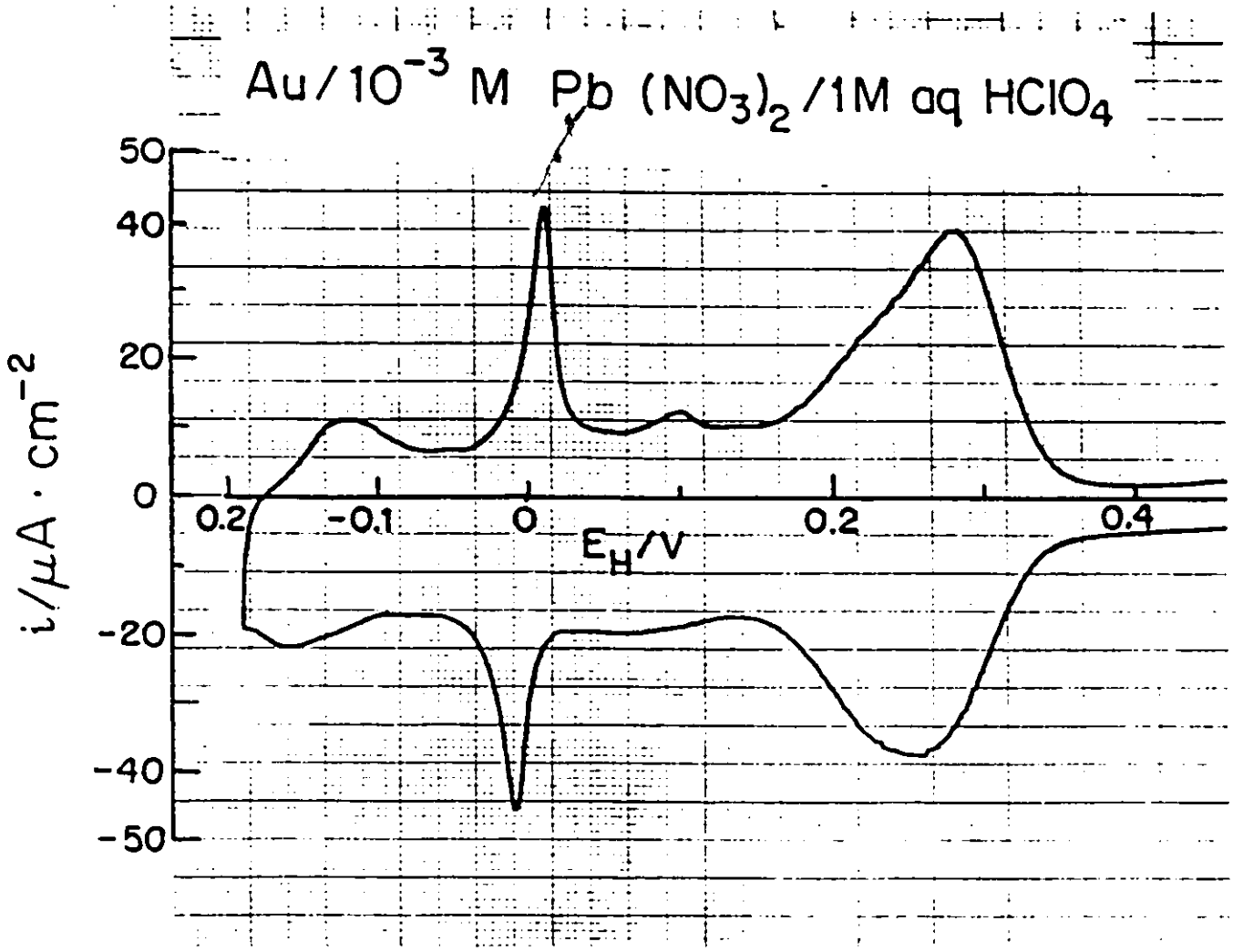

Fig. 4.16 Cyclic-voltammetry i vs E profile for Pb upd at Au in aq. 1M $HClO_4$ + 10^{-3}M $Pb(NO_3)_2$ solution at 298 K. s = 50 mV s^{-1}.

another in shape and peak resolution. This shows that the electrode/anion interaction of the two anions, NO_3^- and $CF_3SO_3^-$, in aqueous $HClO_4$ are similar. The two anions are evidently not specifically adsorbed, and hence have no effect on Pb adatom deposition. This result is not unexpected since the concentration of the anions of the Pb salts are some 100 x smaller than that of the perchlorate ion electrolyte.

Fig. 4.17 shows the i vs E upd profiles for the Pb adatom deposition on Au from MeOH solution of $Pb(ClO_4)_2$. This upd profile is similar to that obtained from MeOH solution of $Pb(CF_3SO_3)_2$ (see Fig. 4.2 given earlier). This indicates that the two anions (ClO_4^- and $CF_3SO_3^-$) exhibit similar behaviour in methanolic and aq. perchloric acid and therefore, interact with comparable strengths (or not at all) with the Au electrode surface in water and methanol. Also, in AN, the i vs E profiles obtained using $Pb(ClO_4)_2$ and $Pb(CF_3SO_3)_2$ are similar. The upd i vs E profile for Pb at Au obtained from MeOH solution of $Pb(NO_3)_2$ is given in Fig. 4.18. The cyclic-voltammogram is characteristically different from those given in Figs. 4.2 and 4.17, but resembles that given in Fig. 4.13 obtained from $NaNO_3$ solution in MeOH, in terms of peak resolution and shift of the first cathodic peak to more negative potentials. This again demonstrates the difference in behaviour of the NO_3^- anion in MeOH and aqueous solutions perhaps because of the reasons given earlier in Section 4.6.2. Because of the low solubility of lead nitrate in the other non-aqueous solvents used in the present work, it could not be used as the lead salt. This would have been an interesting experiment to do since, as was shown above, nitrate ion is found to have a strong effect on the upd profile when used as a supporting electrolyte and the anion of Pb salt in MeOH solutions. It was also found that $CF_3SO_3^-$ behaves similarly to perchlorate ion when they are used as supporting electrolytes in DMF during the reduction of divalent and alkali metal ions [148,170].

It can therefore be concluded from the present work that TEA^+ and NO_3^-, as ions of the supporting electrolyte, have marked effects on the upd profile in AN and MeOH, respectively, while ClO_4^- and $CF_3SO_3^-$ have virtually no effect in non-aqueous solvents. Also, $CF_3SO_3^-$ and ClO_4^- as the anion of the Pb salt have no effect in either aqueous or non-aqueous media.

For the ions which do have an effect on the upd profile, (in most cases manifested by the shift

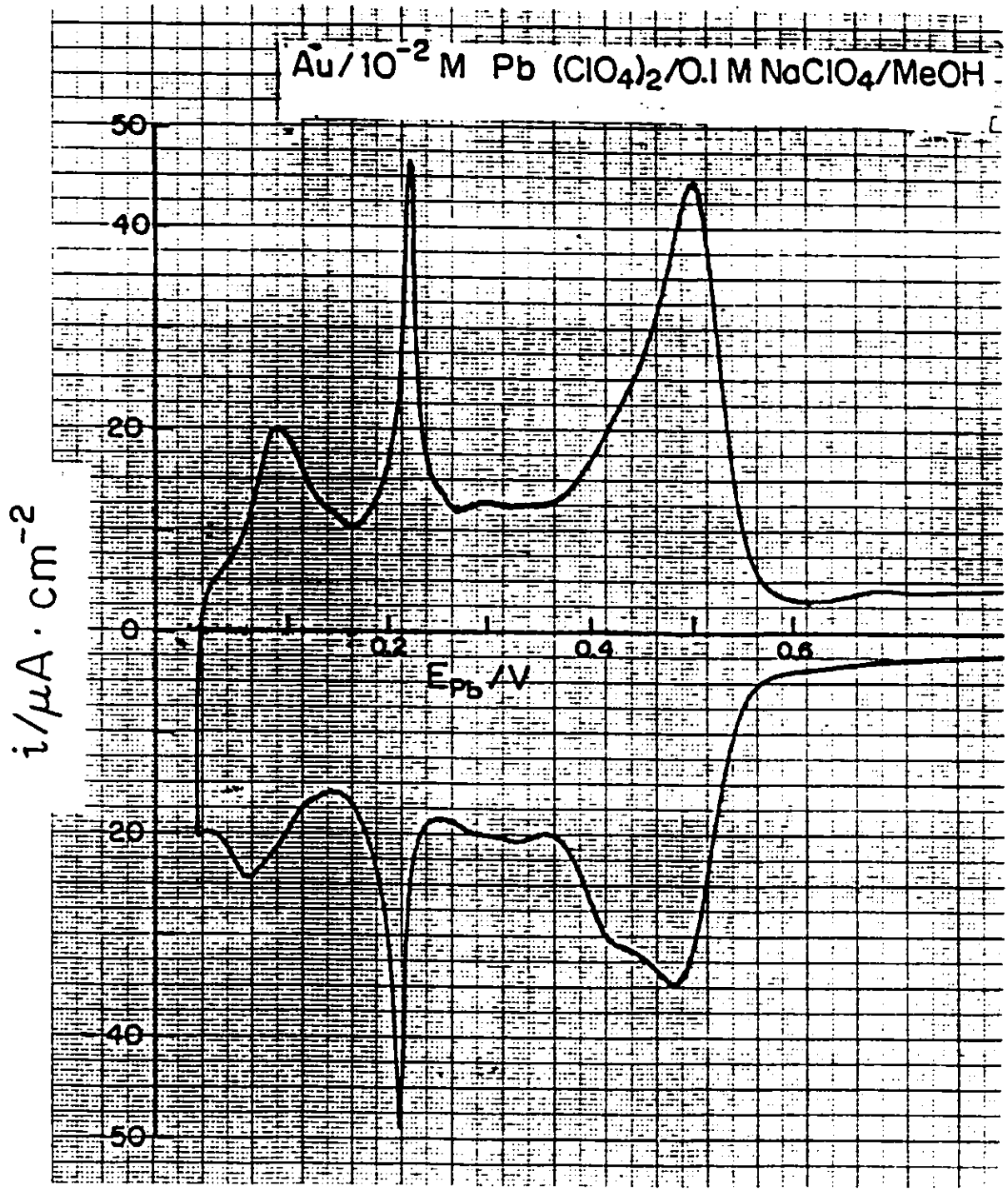

Fig. 4.17 Cyclic-voltammetry i vs E profile for Pb upd at Au from 0.1M $NaClO_4$ + 10^{-2}M $Pb(ClO_4)_2$ solution in methanol at 298 K. s = 50 mV s^{-1}.

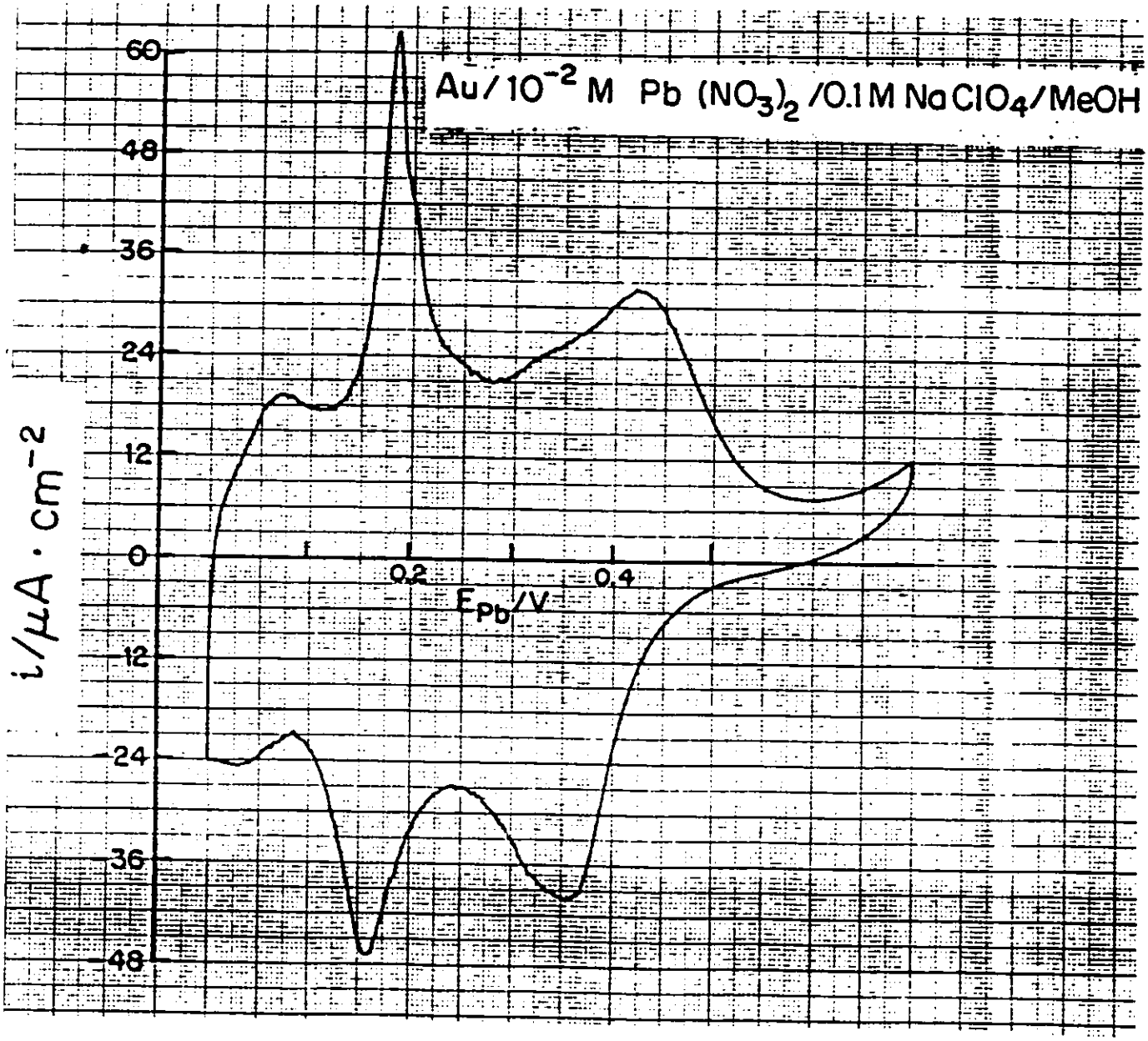

Fig. 4.18 Cyclic-voltammetry i vs E profile for Pb upd at Au from 0.1M $NaClO_4$ + 10^{-2}M $Pb(NO_3)_2$ solution in methanol at 298 K. s = 50 mV s^{-1}.

of the first cathodic peak to more negative potentials) this is due to specific adsorption of the ions on the electrode surface which is dependent on solvent and potential. This metal/ion interaction influences the thermodynamics and probably the kinetics of the upd process as manifested by the modification of the upd i vs E profile. For those ions which do not undergo specific adsorption, any changes in the upd profiles observed in different solvents must be due to the different strength of the metal/solvent interaction which is different for different solvents.

The results described above regarding the solvent effects on the upd i vs E profiles will be extended, in continuing work in this laboratory, using single-crystals, the technique for handling and characterizing them having been recently established in our laboratory.

4.8 Effects of added Water on the UPD i vs E Profiles for Pb at Au in the Four Non-aqueous Solvents Used

For most non-aqueous solvents employed in various electrochemical measurements, water is considered as the main impurity. It was, therefore, of interest to investigate its behaviour and effects on the upd i vs E profiles for Pb at Au in the various non-aqueous solvents used in the present study. Of the aprotic solvents used, there is special interest in PC because it is being used as a solvent medium in high energy-density batteries based on Li anodes since they cannot be used in aqueous medium because of the high reactivity of Li towards water.

For our starting high-purity solvents, DMF and PC had 0.01% H_2O and AN had 0.001% H_2O as determined by Karl-Fischer titration. MeOH had 0.02% H_20 but it was found necessary to distill it before use (see Section 2.3.2). The i vs E profiles of the 0.1M $NaClO_4$ background electrolyte in the various non-aqueous solvents obtained using the sensitive cyclic-voltammetry method showed no effects due to the presence of impurities within the usable potential range.

Since the exact amount of water in the made-up solutions was not determined, the original values given for the solvents were used in working out the estimated concentrations of the added water. To a known volume of working electrolyte solution, various aliquots of pyrodistilled water were added using an accurate micrometer titration syringe, starting with trace amounts. After each

addition, the solution was vigorously stirred by bubbling N_2 and the upd profile was recorded. The amount of water added varied from 0.005 to 5 ml (ca. 5.5×10^{-3} to 2 M in case of AN or 5.5×10^{-3} to 5 M in case of MeOH, DMF and PC).

Figs. 4.19 and 4.20 show the superimposed upd i vs E profiles for Pb at Au recorded corresponding to different aliquots of water added in AN and PC respectively, and are representative of the results obtained in the other non-aqueous solvents used in the present study. Examination of Fig. 4.19 shows that for the H_2O concentration of ca. $\leq 10^{-1}$ M, added water does not have significant effects on the upd i vs E profiles recorded in AN. However at higher concentrations, the first cathodic peak becomes broadened and its current somewhat decreases relative to values recorded at lower concentrations of added water. The cathodic "spike" also broadens, changing to a regular peak. Except for the first anodic peak, whose current decreases at higher concentrations of added water, there are no significant effects on the anodic profile with increasing concentration of added water.

As Fig. 4.20 shows, added water does not have any significant effects on the upd i vs E profiles recorded in PC at concentrations ca. $\leq 10^{-1}$ M. At higher concentrations of added water, important and significant effects are observed in the upd profiles. In the concentration range 1 to 5 M of added water, the first cathodic peak and the corresponding first anodic peak are both suddenly shifted to less positive potentials and their shifted peak potentials do not change with increasing concentration of added H_2O. Similar effects are also observed for the anodic "spike". The apparent shift may be due to changing Au/solvent molecule interactions as the PC/H_2O composition is changing at the electrode interface. Another possible explanation is the anion adsorption effects which are expected to change since the p.z.c. of the Au electrode will be changing with increasing concentration of added water.

The electrochemical behaviour of H_2O in PC solutions has been reported [173,180,181]. Nguyen [173] has investigated the electrochemical behaviour of polycrystalline Au electrodes in PC solutions to which various ammounts of water had been added. It was observed that the inner-layer capacity curves did not change in shape up to a concentration of 4×10^{-4}M of added water.

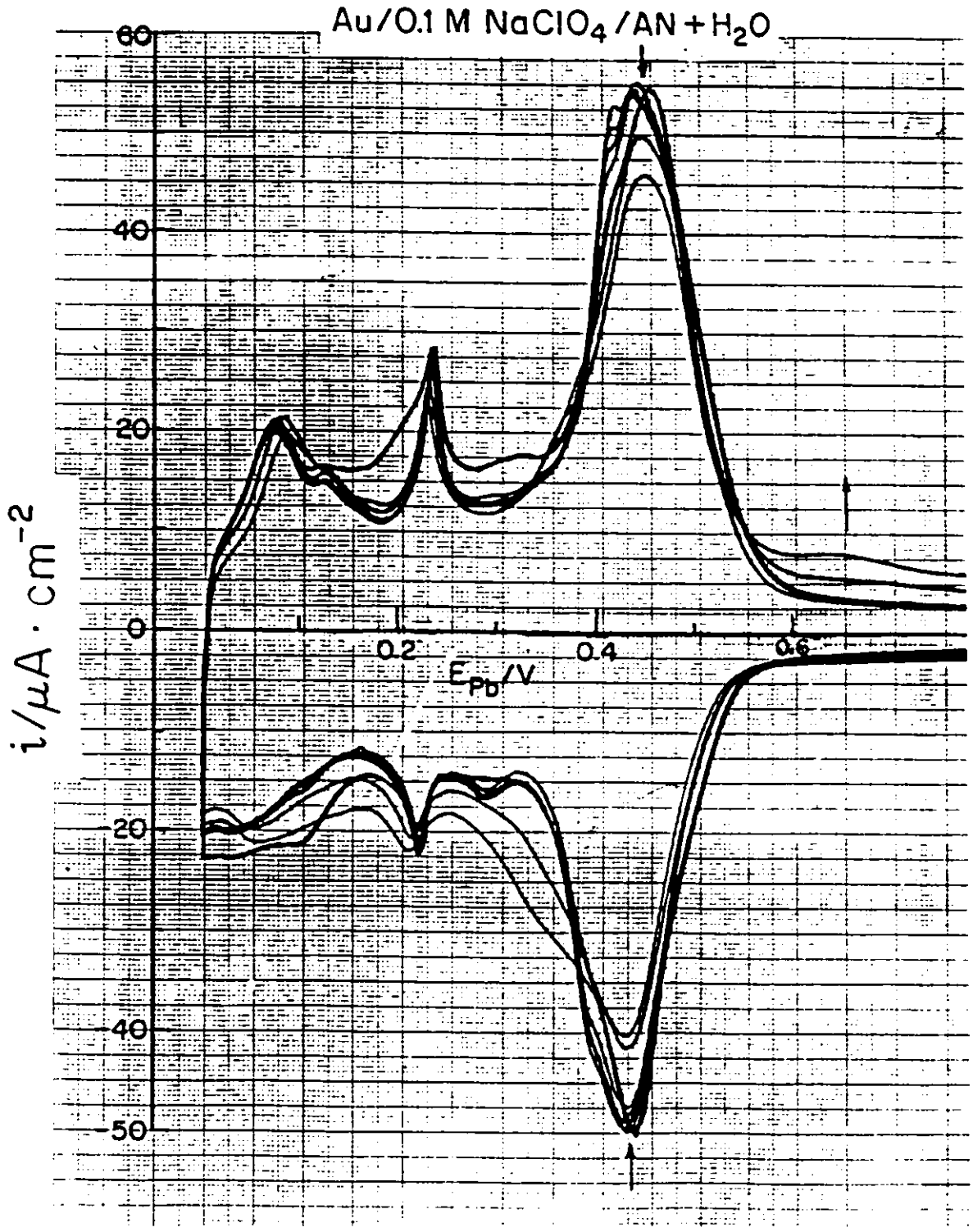

Fig. 4.19 Series of superimposed potentiodynamic i vs E profiles for Pb upd at Au from 0.1M $NaClO_4$ + 10^{-2}M $Pb(CF_3SO_3)_2$ solution in acetonitrile at 298 K with successive additions of water from ca. 5.5×10^{-5} to 2M. Arrows show directions of change of curves with increasing water content. s = 50 mV s^{-1}.

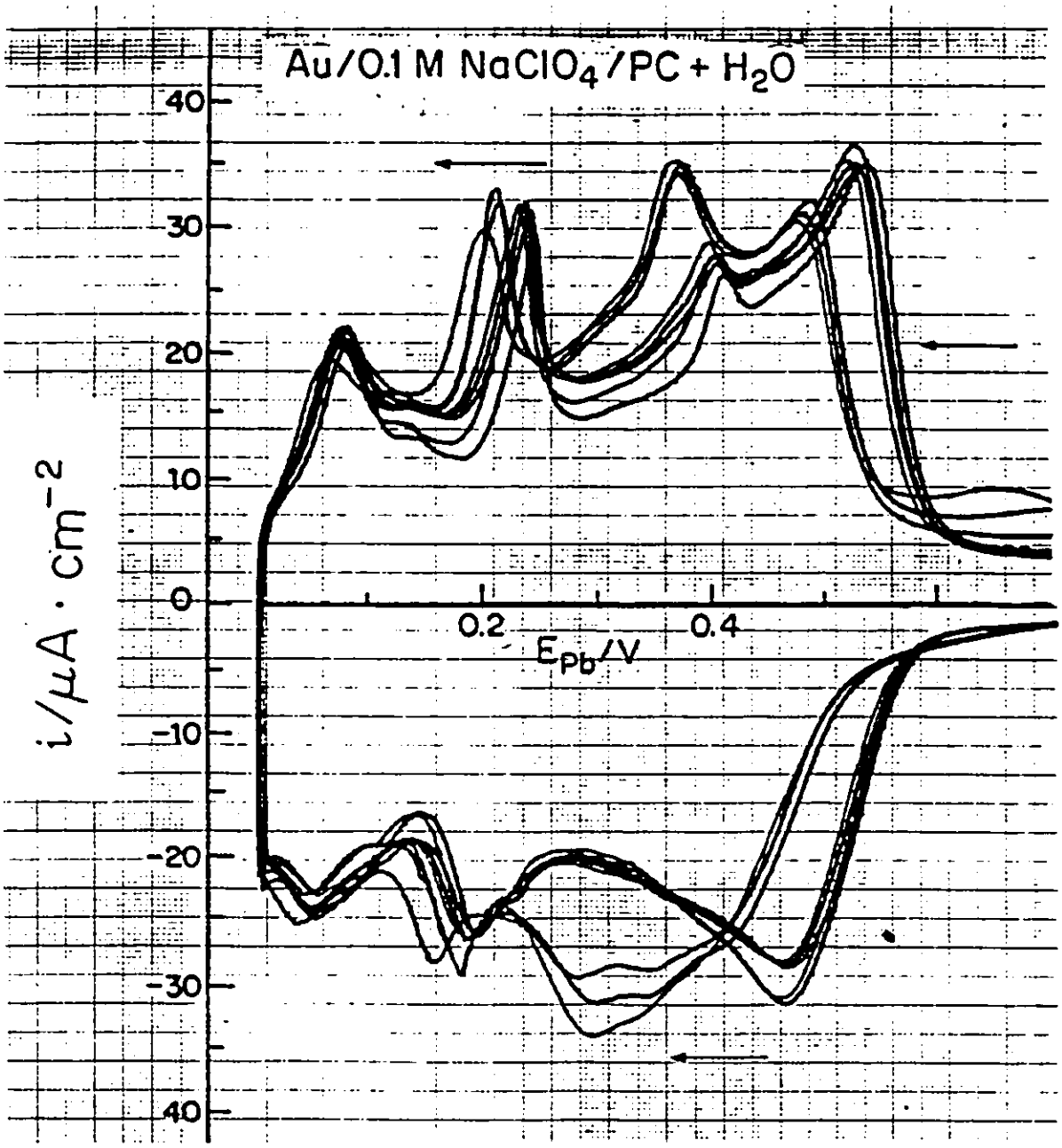

Fig. 4.20 Series of superimposed potentiodynamic i vs E profiles for Pb upd at Au from 0.1M $NaClO_4$ + 10^{-2}M $Pb(CF_3SO_3)_2$ solution in propylene carbonate at 298 K with successive additions of water from ca. 5.5×10^{-3} to 5M. Arrows show directions of change of curves with increasing water content. s = 50 mV s^{-1}.

However, the potential of the capacity maximum corresponding to the p.z.c. was shifted to more positive values with increasing concetration of added water.

As expected, added water had no effects on the upd i vs E profiles for Pb at Au in MeOH. This is not surprising because MeOH and H_2O are protic, polar solvents and their electrochemical behaviour is similar.

The unexpected result is that obtained in DMF. In the whole concentration range employed, added water had no effects on the upd i vs E profiles for Pb at Au. Like H_2O, DMF is a polar solvent but with a lower dielectric constant ($\epsilon = 37$) than that of water ($\epsilon = 78$).

CHAPTER 5

COMPETITIVE ADSORPTION EFFECTS OF HALIDE IONS (X^-) AND THIOUREA (TU) ON THE UPD OF Pb AT Au

5.1 Micrometer Titration Procedure

Although the effect of halide ions, especially Cl^-, on the upd of Pb at Au has been reported in the literature, e.g. in the refs [21,26,31], the experiments were done either at only one or over a narrow range of Cl^- concentrations. Therefore, in order to obtain more useful information on the progression of the competitive adsorption effects of added halide ions or thiourea on the upd profiles of Pb at Au from very low concentrations, a dilute solution of the X^- salt or thiourea was titrated in successive aliquots into the electrochemical cell by means of an accurate micrometer syringe through a 1 mm Teflon 'spaghetti' tube, terminating in a fine glass jet.

Depending on the species to be added, the measurements were commenced at very low concentrations, 10^{-8} to 10^{-6} mol dm^{-3}, since significant effects were already detectable at high dilutions, especially in the case of thiourea or I^-.

Before additions of any aliquots of X^- ion or TU were made an i vs E profile of the upd of Pb at Au was first obtained in the absence of added ion or TU; this curve was used as a reference against which i vs E profiles in the presence of various concentrations of halide ions or TU could be compared.

After each addition of the solution of the halide salt or TU into the electrochemical cell containing a known volume of working electrolyte solution, the solution was vigorously stirred by bubbling of N_2. Cyclic-voltammetry sweeps at 50 mV s^{-1} were recorded 60 - 300 s after addition of the halide ion or TU to allow time for adsorption equilibrium to be attained [183], especially at low concentrations. Two X-Y recorders were employed in parallel: one to record separately the i vs E profile for each halide or TU concentration for subsquent calculations, the other to build up a succession of superimposed i vs E profiles corresponding to each aliquot of the added solution, thus

displaying the progressive effects of the added halide ions or TU.

The micrometer titration procedure was also applied in order to record a series of individual and superimposed i vs E profiles for Au corresponding to different concentrations of the additions after successive additions of Cl^-, Br^-, I^- and TU had been made to the background electrolyte without a Pb salt being present. This gave a series of "control" or "background" curves.

The effects of Cl^-, Br^-, I^- and TU were determined in 1M aq. $HClO_4$, while in methanolic 0.1M $NaClO_4$ solution the effects of only Cl^- and Br^- were investigated because of the low solubility of some simple I^- salts in MeOH.

5.2 Effects of Adsorption of Halide Ions on the i vs E Profiles for UPD of Pb at Au

The effects of added halide ions on the i vs E profile for upd of Pb at Au in aq. $HClO_4$ or MeOH solutions can be detected at very low concentrations, around 10^{-5}, 10^{-6} and 10^{-7} mol dm^{-3} for Cl^-, Br^- and I^-, respectively, in aq. $HClO_4$. Similar effects are observed for Cl^- and Br^- in MeOH solution. A series of superimposed cyclic-voltammograms, corresponding to various additive concentrations, following successive additions of Cl^-, Br^- and I^- in aq. $HClO_4$, are shown in Figs. 5.1, 5.2 and 5.3, respectively. The concentration ranges are indicated in each case and the series of curves show the effects of progressive competitive adsorption of these halide ions on the upd profile for Pb monolayer formation on Au.

For MeOH solution, the superimposed i vs E profiles arising with additions of Cl^- and Br^- are shown in Figs. 5.4 and 5.5, respectively.

Significant and interesting differences are seen between the effects of these added species, even at very high dilutions, as will be discussed below for the individual effects of the three halide ions and TU.

5.2.1 The Effects of Cl^- Ion

The effects of Cl^- on the i vs E upd profile of Pb at Au in aq. $HClO_4$ or MeOH (Figs. 5.1 and 5.2) are rather similar. At very high dilutions, in the concentration range 10^{-7} to 10^{-6} mol dm^{-3}, the

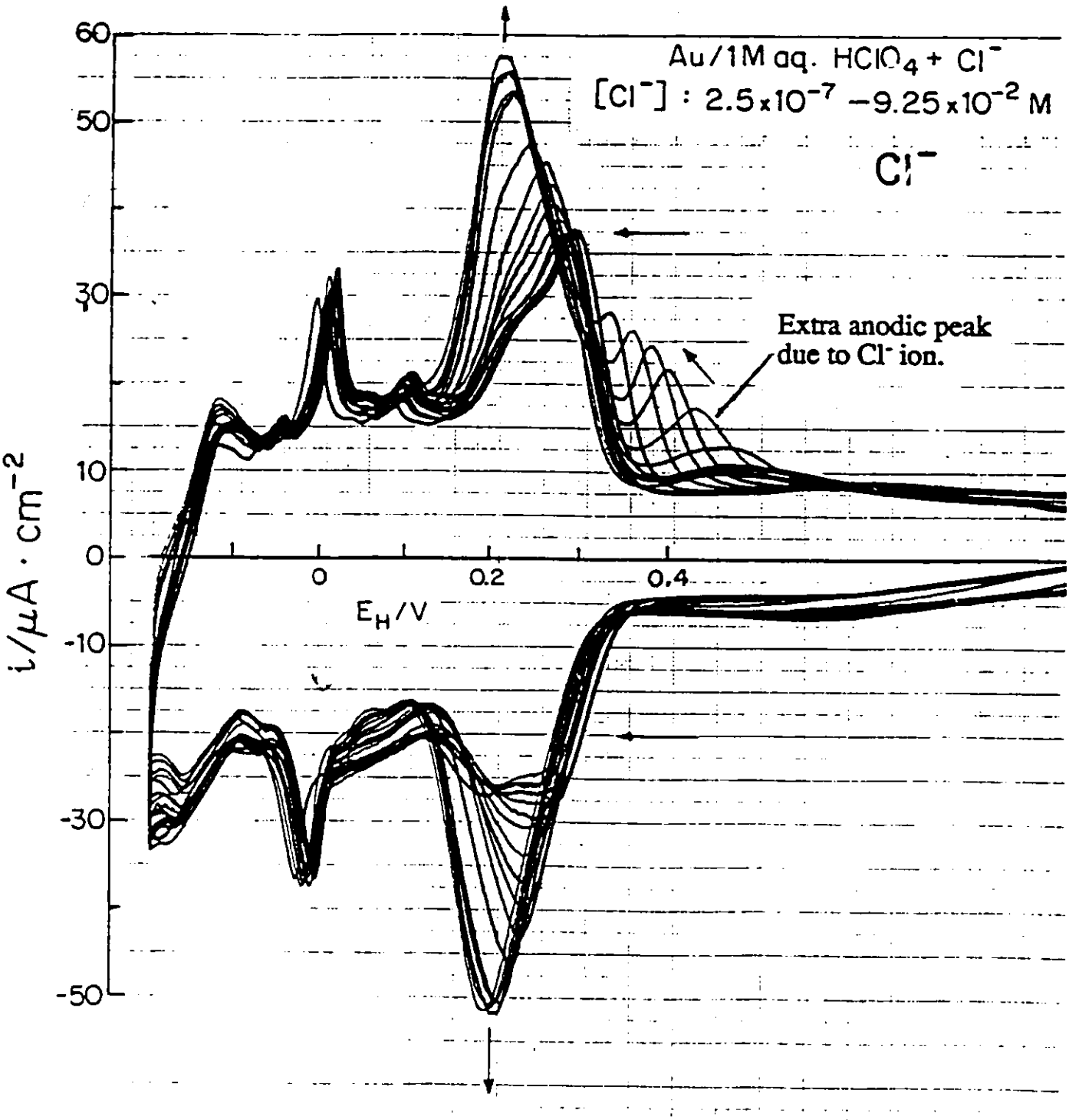

Fig. 5.1 Series of superimposed cyclic-voltammetry i vs E profiles for Pb upd at Au in aq. 1M $HClO_4$ + 10^{-3}M $Pb(NO_3)_2$ with successive additions of Cl^- ion from 2.5×10^{-7} to 9.25×10^{-2} mol dm^{-3}. Arrows show directions of change of curves with increasing $[Cl^-]$. s = 50 mV s^{-1}.

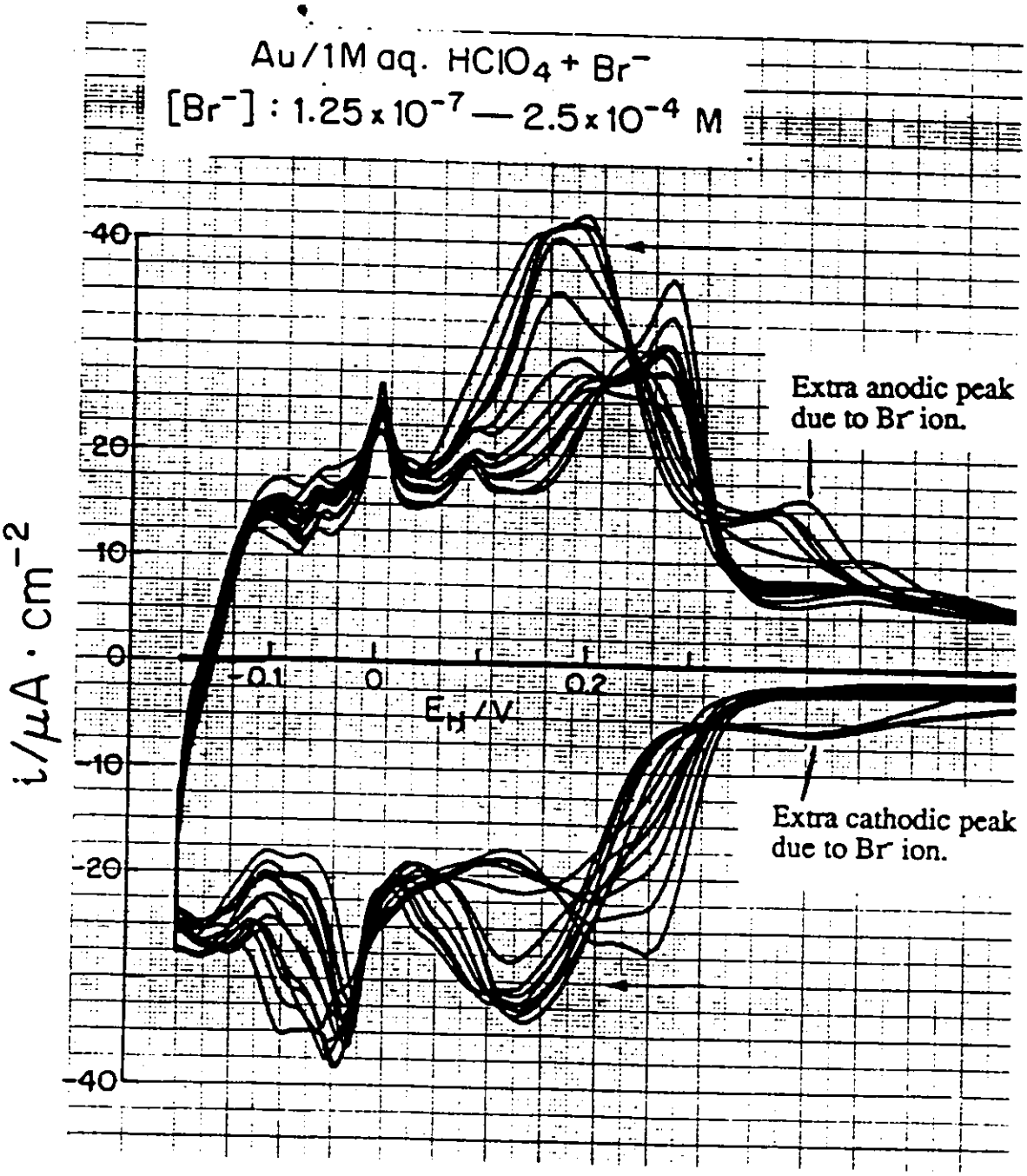

Fig. 5.2 Series of superimposed cyclic-voltammetry i vs E profiles for Pb upd at Au in aq. 1M $HClO_4$ + 10^{-3}M $Pb(NO_3)_2$ with successive additions of Br^- ion from 1.25×10^{-7} to 2.5×10^{-4} mol dm^{-3}. Arrows show directions of change of curves with increasing [Br^-]. s = 50 mV s^{-1}.

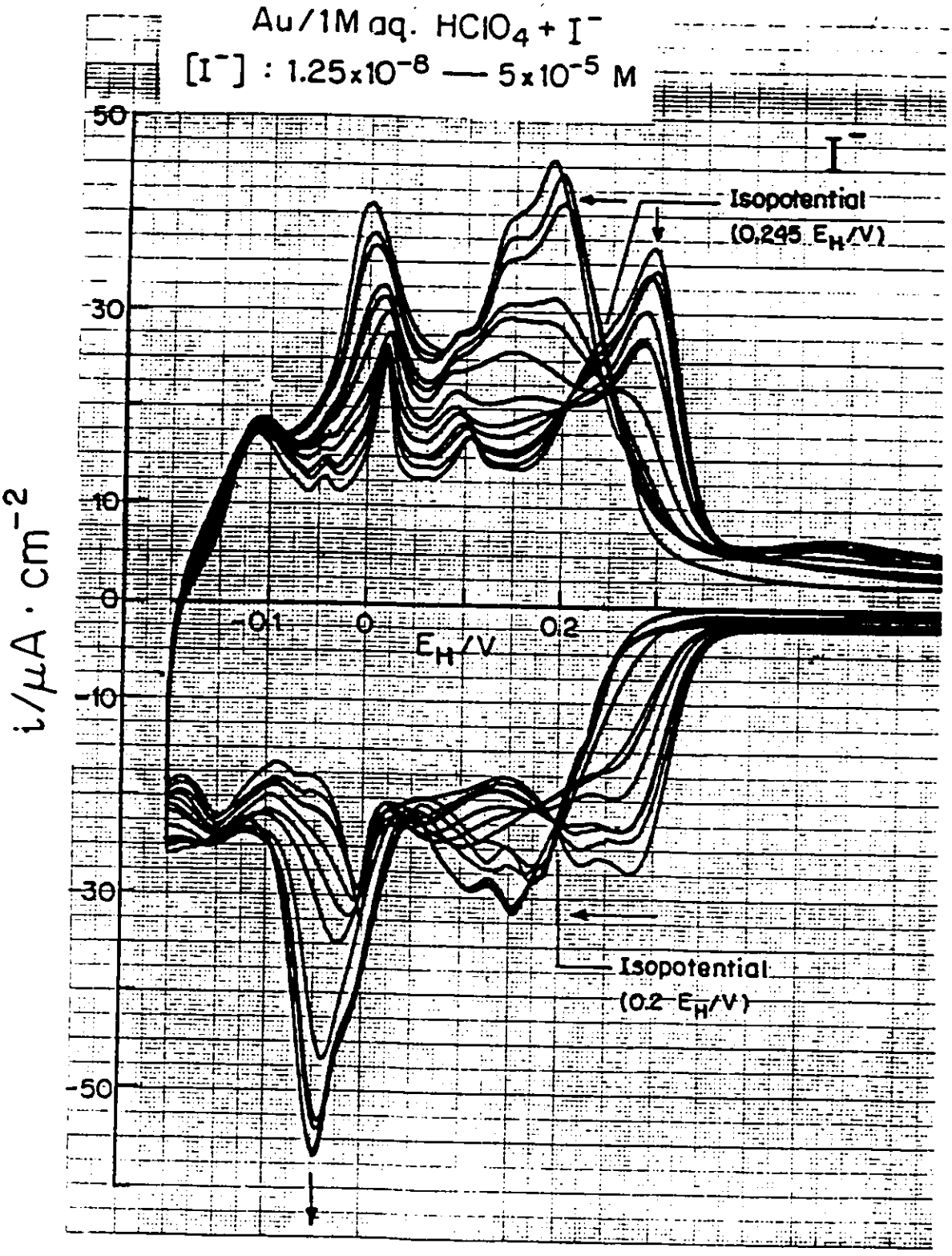

Fig. 5.3 Series of superimposed cyclic-voltammetry i vs E profiles for Pb upd at Au in aq. 1M $HClO_4$ + 10^{-3}M $Pb(NO_3)_2$ with successive additions of I^- ion from 1.25×10^{-8} to 5×10^{-5} mol dm^{-3}. Arrows show directions of change of curves with increasing $[I^-]$. s = 50 mV s^{-1}.

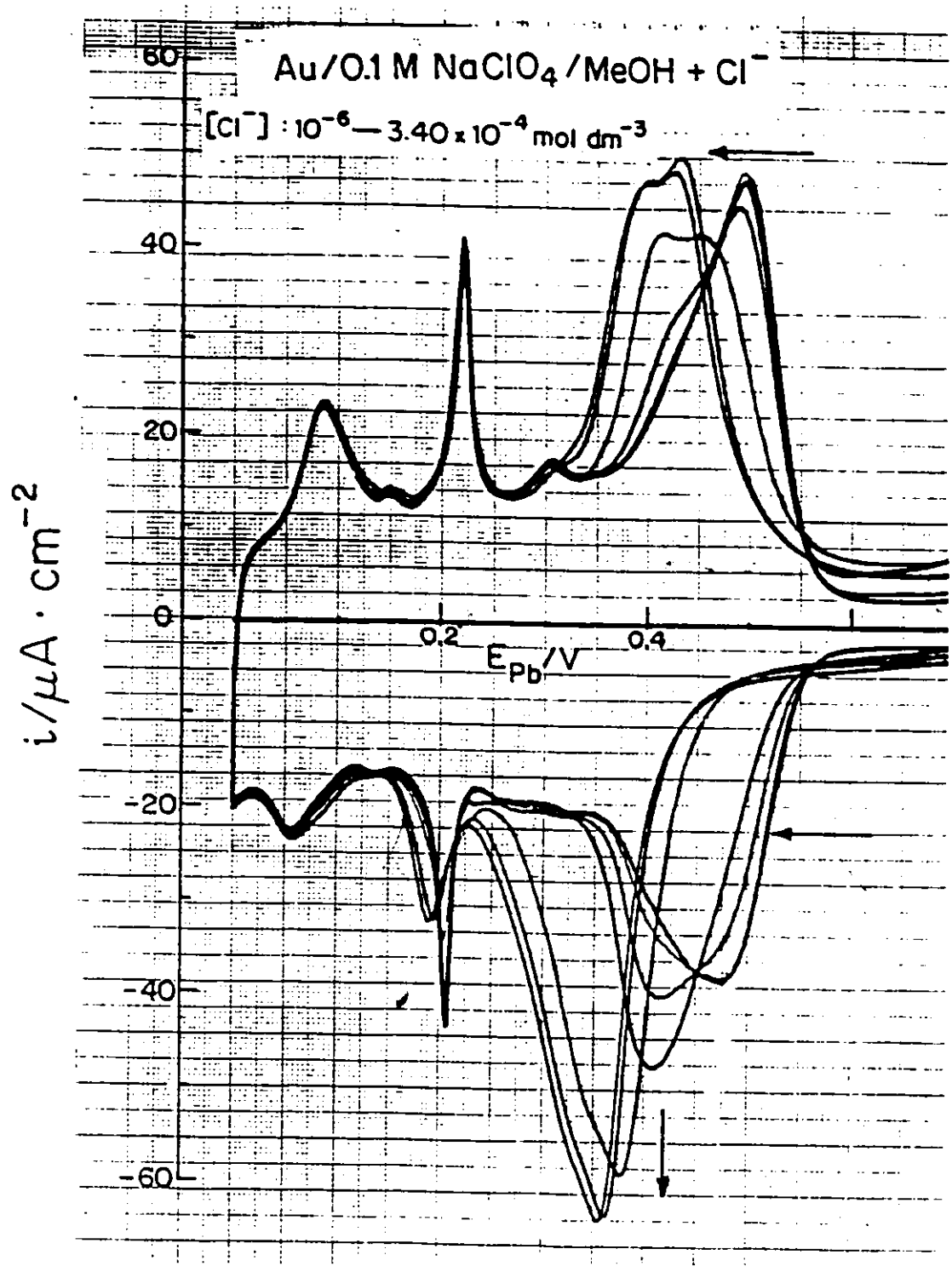

Fig. 5.4 Series of superimposed cyclic-voltammetry i vs E profiles for Pb upd at Au from 0.1M $NaClO_4$ + 10^{-2}M $Pb(CF_3SO_3)_2$ solution in MeOH with successive additions of Cl^- ion from 10^{-6} to 3.4×10^{-4} mol dm^{-3}. Arrows show directions of change of curves with increasing [Cl^-]. s = 50 mV s^{-1}.

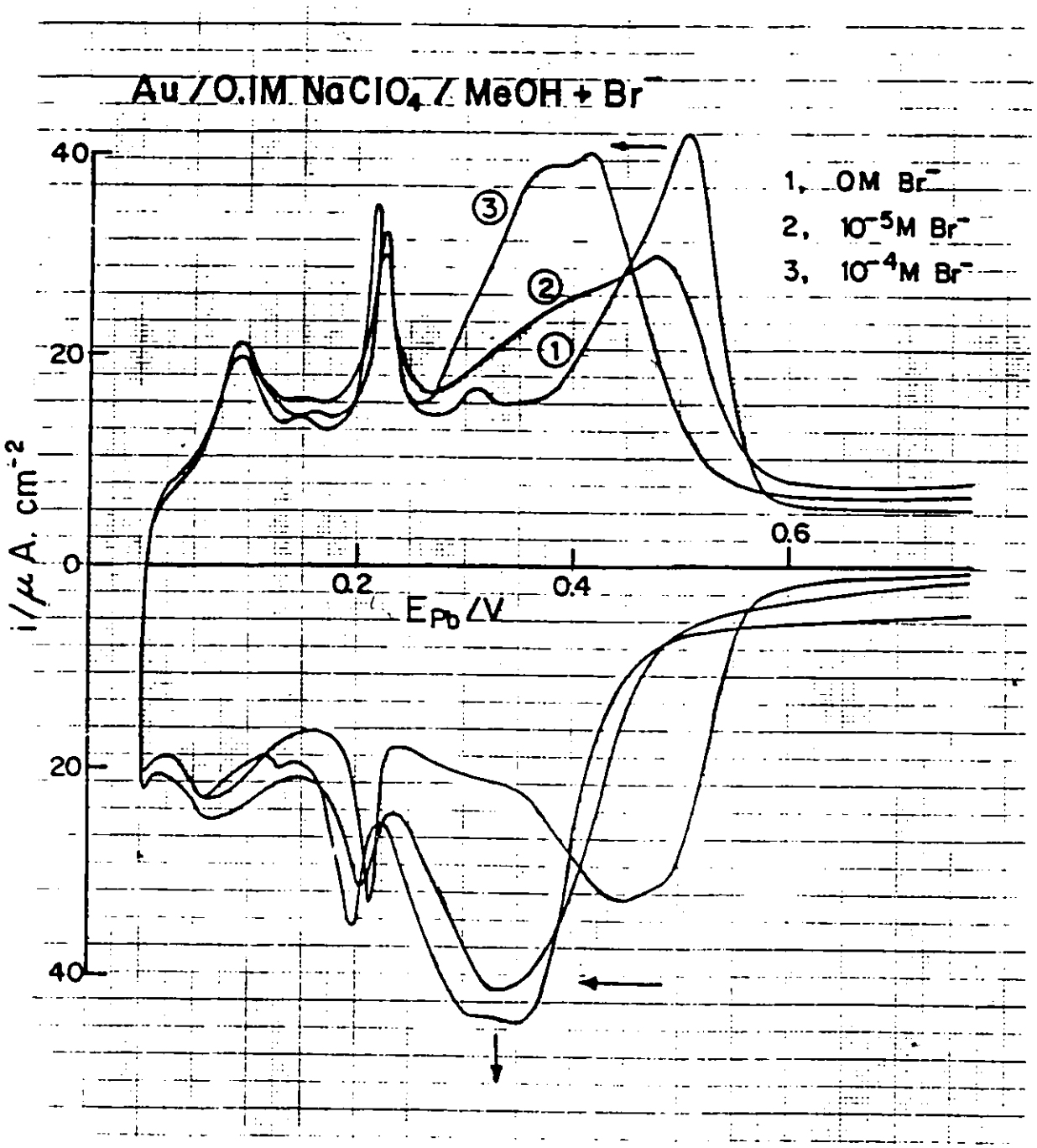

Fig. 5.5 Series of superimposed cyclic-voltammetry i vs E profiles for Pb upd at Au from 0.1M $NaClO_4$ + 10^{-2}M $Pb(CF_3SO_3)_2$ solution in MeOH with successive additions of Br^- ion from 10^{-5} to 10^{-4} mol dm^{-3}. Arrows show directions of change of curves with increasing [Br^-]. s = 50 mV s^{-1}.

initial effects are manifested as slight diminutions of the first cathodic peak. As the concentration of added Cl^- is increased, the first cathodic peak (C_{Pb1}) and the corresponding first anodic peak (A_{Pb1}) (Fig. 5.1) are progressively shifted to more cathodic, i.e. less positive, potentials at the same time becoming sharper than the corresponding peaks in the absence of added Cl^- ion. A saturation level of the effects of Cl^- are detected at a concentration of about 10^{-2} mol dm^{-3}. The added Cl^- has only small effects on the other resolvable peaks in the i vs E profile.

The most striking and interesting effect of Cl^-, not observed in the case of Br^- or I^- (see Fig. 5.1), is the appearence of an extra peak (shoulder) in the anodic sweeps at the most positive potentials of the sweeps. This effect arises in the potential range ca. 0.4 to 0.55 V/E_H, beyond the potential of the usual first anodic peak observed in "clean" solution. Important points to note about this peak are: it is observed only in the concentration range of approximately 10^{-5} to 10^{-3} mol dm^{-3} and its shape and size are concentration dependent; it shifts to less positive potentials with increasing Cl^- concentration until it becomes merged with the main anodic peak at higher concentrations; no corresponding peak arises on the cathodic side of the i vs E profile in the whole concentration range of Cl^- used in the present study; this peak is not observed in the case of experiments done in methanolic 0.1M $NaClO_4$ solution (see Fig. 5.2).

A series of progressively restricted range sweeps were performed on the upd i vs E profile for Pb at Au in aq. $HClO_4$ containing 4×10^{-4} mol dm^{-3} Cl^- (Fig. 5.6) in order to relate to which Pb ad-state on the cathodic sweep the extra anodic peak on the anodic sweep, due to Cl^-, corresponds. Examination of Fig. 5.6 shows that this extra anodic peak, at more positive potentials than the usual anodic peaks, is not associated with the ad-state C_{Pb1}. It starts to develop after the completion of C_{Pb1} and is fully developed or reaches saturation after the completion of the "spike" (ad-state C_{Pb5}). It was also found that this extra peak was independent of stirring, an indication that it is not due to some impurity from the electrolyte solution or from the electrode.

It is interesting to note that this extra peak which corresponds to some form of Pb which desorbs at potentials more positive than those of the other anodic peaks does not correspond, at least, to C_{Pb1} which is the peak for the most tightly bound Pb at the Au electrode surface.

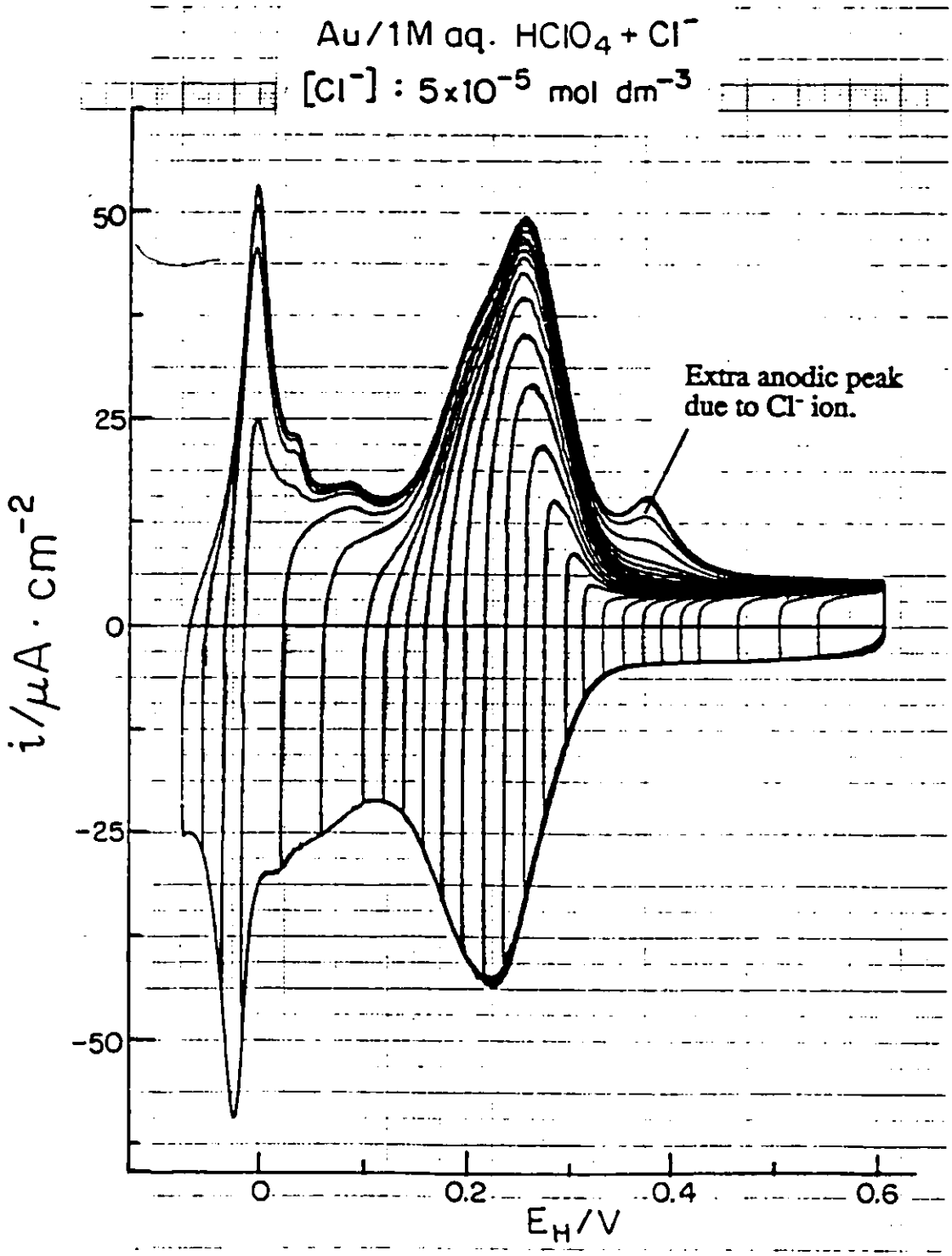

Fig. 5.6 Series of progressively restricted cyclic-voltammetry i vs E profiles for Pb upd at Au in aq. 1M $HClO_4$ + 10^{-3}M $Pb(NO_3)_2$ containing 5×10^{-5} mol dm^{-3} of Cl^- ion. s = 50 mV s^{-1}.

In the case of the series of the superimposed i vs E profiles obtained in aq. $HClO_4$ with successive additions of Cl^- (Fig. 5.7) but without a Pb salt being added, no anodic or cathodic peak is observed at the same potential or over the same concentration range for which the extra anodic peak was observed in the case of Pb upd at Au from aq. $HClO_4$ in the presence of added Cl^-. It is not therefore an artefact arising from the effect of Cl^- on the background curve.

The fact that this peak arises at more positive potentials, and is absent when the background electrolyte contains only Cl^-, leads us to propose that this peak is due to desorption of some kind of Pb adatoms, or possibly a Pb chloride complex, strongly interacting with the Au electrode substrate.

Vicente and Bruckenstein [21], in their studies of the upd of Pb at Au in solutions containing various concentrations of Cl^- using a rotating disk electrode, found that the first cathodic peak arose at slightly more positive potentials in contrast to what is observed in the present work. Although the first cathodic peak in their [21] investigation became sharper, similar to what was observed in the present work, they found that the cathodic charge increased with increasing Cl^- concentration, while in the present work the cathodic charge remained almost constant with increasing Cl^- concentration. They [21] also concluded that the Cl^- ion enhanced the Pb(II) (ion) adsorption and the adsorbed species in the upd layer was probably a chloride complex of Pb, such as $PbCl^+$.

Girgis et al. [183] have reported results on Pb electrodeposition on Au from aq. solutions of 0.2M ammonium acetate and 0.11M $PbCl_2$. They found that the presence of Cl^- had an appreciable effect on the i vs E upd profile for Pb at Au. The first cathodic peak was shifted to more negative potentials, although the shift was smaller in acetate solution than that reported in Cl^- in supporting electrolytes of perchlorate or sulphate [31,184]. They explained these observations in terms of involvent of co-adsorption of acetate in the upd phenomenon with Pb. Although Auger electron spectroscopy indicated the presence of small quantities of Cl in the first layers of Pb in the upd film, no lead chloride reflections, i.e. due to bulk $PbCl_2$, could be detected by X-ray diffraction.

Vilche and Jüttner [185] have studied the effect of CH_3COO^- and Cl^- anions on the upd of Pb at Cu(111) single-crystal in aq. 0.5M $NaClO_4$ solutions at various pH values. Their [185] results showed that in the presence of 0.01M CH_3COO^- anion the first cathodic peak was shifted to more

cathodic potentials. Addition of Cl^-, even at high dilutions, caused the first cathodic peak and the corresponding first anodic peak to shift to more negative potentials. These peaks also became sharper and increased in height, similar to what was observed in the present work.

Hubbard et al. [186] showed that adsorption of HCl from aq. solution onto Pt(111) gives rise to a stable (3x3) adlattice. The LEED pattern of the electrodeposited layer was ordered and underwent a series of changes with increasing θ_{Pb}. Auger electron spectroscopy also indicated the presence of Cl in the topmost layer of the surface at all Pb coverages.

Since the polycrystalline Au surface is assumed to consist principally of (100), (110) and (111) faced regions [31], and with some populations of higher-index stepped terraces, and also from the results of Hubbard et al. [186], it seems likely that, at low coverages, Cl^- adsorbs onto one of these single-crystal facets, probably (111), to form a stable overlay lattice. Electrodeposition of Pb onto such a surface might be influenced by the preadsorbed, ordered Cl^- adlattice to form an ordered layer of co-adsorbed Pb adatoms. Such a stable Pb adlayer would then tend to become desorbed only at more positive potentials. At very low or high Cl^- coverages, the favourable ordered adlattice may not be able to be formed and hence not influence the ordering of the electrodeposited Pb adatoms. This is, perhaps, why we do not observe the extra peak at low and high chloride concentrations.

The shifts in peak potentials of the first anodic peak (A_{Pb1}) due to Cl^-, observed by various workers using diffrent electrolyte compositions, are summarized in Table 5.1 below.

Table 5.1 Shifts in Potential of the Peak A_{Pb1} in the Presence of added Cl^-

$[Cl^-]$	ΔE_p(mV)
1. 0.11M (in aq. acetate solution)	- 45 [183]
2. 0.5M (in acidified aq. 0.1M $NaClO_4$)	- 75 [31]
3. 10^{-2}M (in 1M aq. $HClO_4$)	- 90*
4. 10^{-4}M (in 0.1M $NaClO_4$ MeOH solution)	- 65*

*Results of the present work

5.2.2 The Effect of Cl^- on the Double-Layer i vs E Profile for Au in 1M aq. $HClO_4$

The superimposed i vs E profiles corresponding to successive additions of aliquots of the Cl^- salt solution to 1M aq. $HClO_4$, without a Pb salt being added, are illustrated in Fig. 5.7. The observed general effect is that, as the concentration of added Cl^- increases, the double-layer charging currents increase progressively on both the anodic and the cathodic sides of the i vs E profiles. The effects can be detected already at very low Cl^- concentrations, e.g. $2x10^{-7}$ mol dm^{-3}, the same concentration for which the first effect on the i vs E profile for the upd of Pb at Au would be detected.

On the cathodic sweep the double-layer capacity increase extends to more positive potentials as the concentration of Cl^- increases, whereas the progressive increase on the anodic side of the sweep profile is rather uniform over almost the whole of the potential range. The increase of the double-layer capacity may be interpreted as an increase of the charge in the inner region of the double-layer. This could arise if the specifically adsorbing Cl^- ion looses some of its charge, i.e. γ is small but significant, in forming the adsorbed state of Cl^-. The form of the i vs E profile in the presence of Cl^- but in the absence of Pb^{++}, shows that the processes of Cl^- adsorption and desorption remain essentially reversible over the whole potential range.

5.2.3 The Effect of Br^- Ion

Unlike the considerably different effects of Br^- and Cl^- on the initial stages of surface oxidation of Pt [75], the effect of Br^- on the i vs E profile for Pb at Au from aq. 1M $HClO_4$ or 0.1M $NaClO_4$ methanolic solutions is rather similar to that of chloride. At low concentrations of added Br^- (approximately in the concentration range 10^{-7} to 10^{-6} mol dm^{-3}), it is observed that there is a progressive diminution of the first cathodic peak (C_{Pb1}) and the corresponding anodic peak (A_{Pb1}); at the same time, the two peaks shift to less positive potentials. It is also found that the efffectiveness of competitive adsorption of Br^- is greater than that of Cl^- because the first cathodic peak is shifted to less positive potentials at lower concentrations than with Cl^- and reaches a saturation limit suddenly, i.e. at a critical concentration. Thus saturation effects are observed at

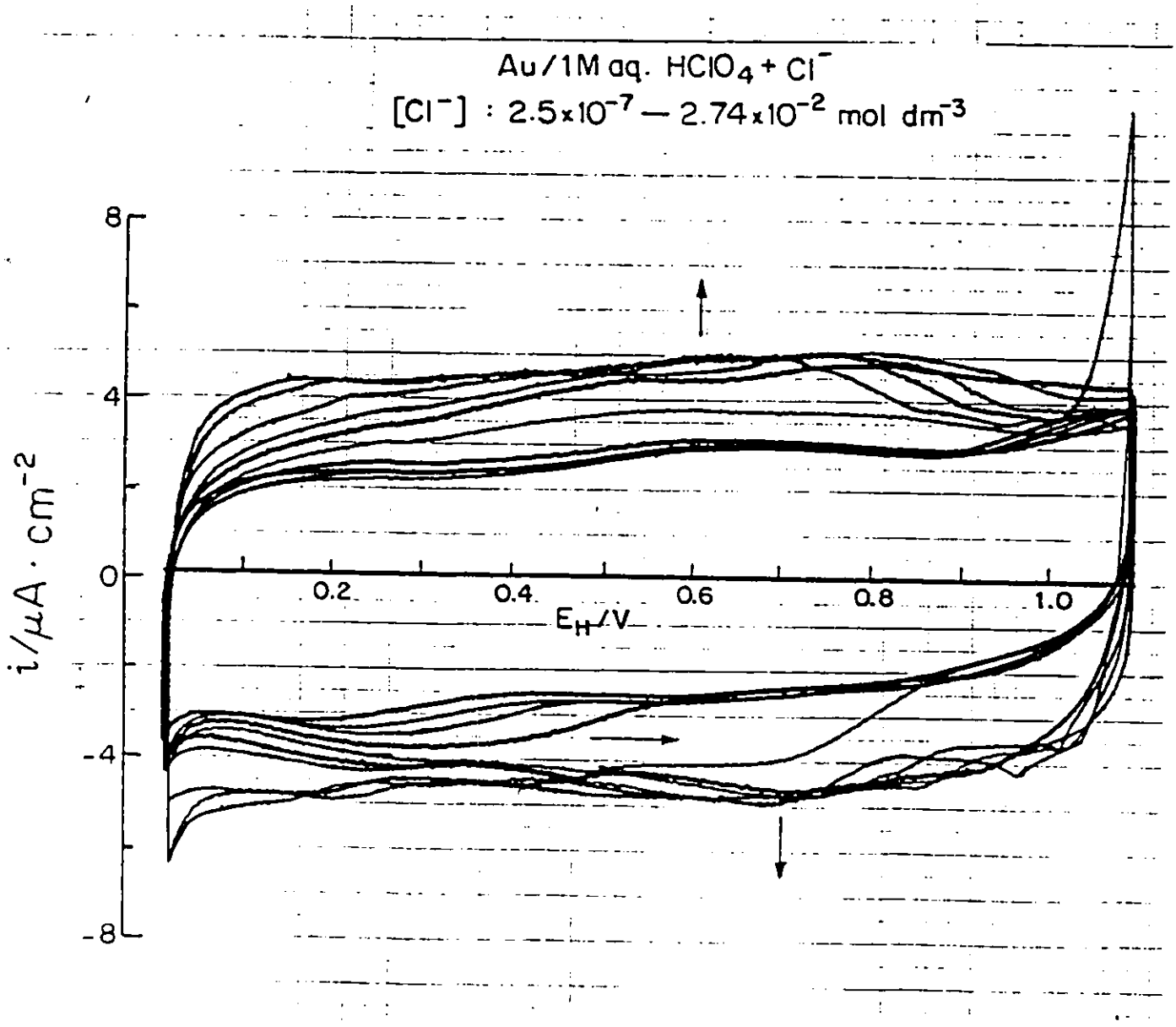

Fig. 5.7 Series of superimposed cyclic-voltammetry i vs E profiles for Pb upd at Au in aq. 1M $HClO_4$ with successive additions of Cl^- ion from 2.5×10^{-7} to 2.74×10^{-2} mol dm^{-3}, without a Pb salt being present. Arrows show directions of change of curves with increasing $[Cl^-]$. s = 50 mV s^{-1}.

a lower concentration in the presence of Br^- than that of Cl^-.

As the Br^- concentration is increased in aq. $HClO_4$ (Fig. 5.2) an extra peak develops at more positive potentials (ca. 0.4 V/E_{Pb}) both on the anodic and the cathodic sweeps of the i vs E profile. These peaks could be attributed to adsorption and desorption processes of Br^- at these more positive potentials where no coadsorption of Pb yet arises, noting that it occurs at potentials more positive than the potential of zero charge of the Au electrode and ion adsorption is, of course, potential dependent. Like the effect of Cl^-, the upd i vs E profiles for deposition and ionization of Pb remain in an overall way more or less symmetrical in the presence of Br^-, so that both Br^- adsorption and Pb deposition remain essentially reversible.

5.2.4 Effects of Br^- on the i vs E Profile in the Double-Layer Charging Region at Au in 1M aq. $HClO_4$

Fig. 5.8 shows a series of superimposed i vs E profiles corresponding to successive additions of aliquots of the Br^- salt solution to 1M aq. $HClO_4$ in the concentration range $2x10^{-7}$ to 10^{-4} mol dm^{-3}. The first effects of Br^- are detected at the lowest concentration of added Br^-, viz. $2x10^{-7}$ mol dm^{-3}. It is to be observed that up to a potential of about 630 mV/E_H the effect of Br^- is similar to that of Cl^-. In this region, both the anodic and cathodic charging current profiles for the double-layer capacity increase with increase of concentration of added Br^- ion. However, for a given concentration, the increase in the presence of Br^- is somewhat greater than that for the same concentration of Cl^-.

As suggested in the case of Cl^- effects, the increase of the double-layer charge is due to the increase of charge in the inner-layer corresponding to an increase of the surface concentration of Br^- ions in the double-layer at the Au interface. This behaviour also implies that the adsorbed Br^- ions lose much of their charge like the situation at Pt [75].

In the region of more positive potentials (ca. 0.63 to 1.0 V/E_H), the effect of Br^- is less pronounced as the increase or decrease of the double-layer capacitance with increasing concentration of added Br^- is generally small compared to the charging currents in the absence of added Br^-. It is

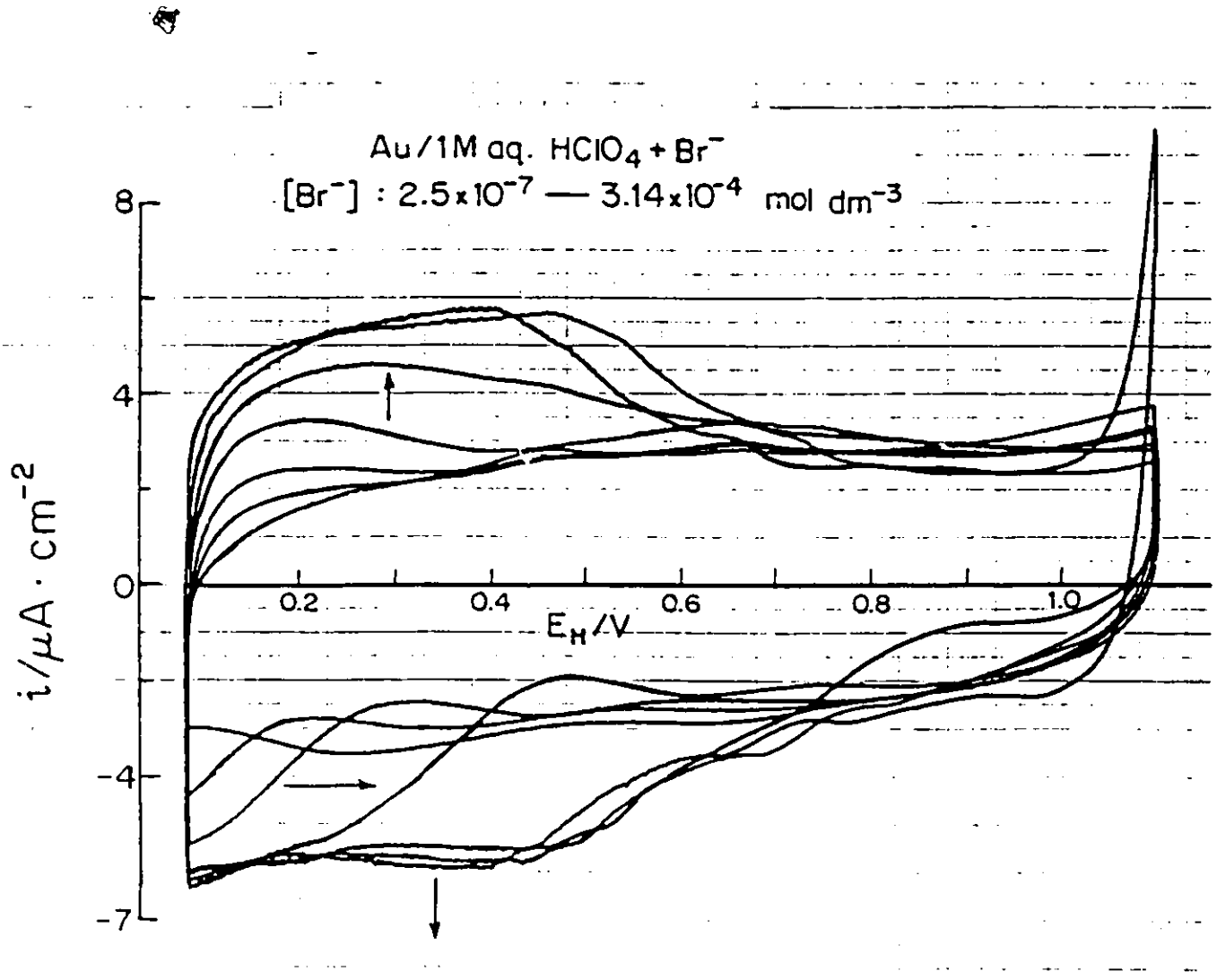

Fig. 5.8 Series of superimposed cyclic-voltammetry i vs E profiles for Pb upd at Au in aq. 1M $HClO_4$ with successive additions of Br^- ion from 2.5×10^{-7} to 3.14×10^{-4} mol dm^{-3}, without a Pb salt being present. Arrows show directions of change of curves with increasing $[Br^-]$. s = 50 mV s^{-1}.

likely that when this potential region has been reached, Br^- has undergone adsorption with almost complete charge transfer, i.e. $\gamma \rightarrow 1$.

5.2.5 The Effects of I^-

As Fig. 5.3 shows, the effects of I^- on the i vs E upd profile of Pb at Au are rather similar to those of Br^- at high dilutions. At low concentrations, the adsorption of I^- causes initially a lowering of the first cathodic peak with a small shift to more negative potentials. At the same time, the "spike" on the cathodic sweep broadens into a normal peak, and its height increases with added I^- concentration. This effect is different from that of Cl^- or Br^- (Figs. 5.1 and 5.2). Unlike the effects of Cl^- or Br^-, the presence of I^- does not result in the formation of the extra peak (Fig. 5.3) at the positive end of the anodic sweep.

In the case of coadsorbed I^-, there is sudden increase in the effectiveness of competitive adsorption vs Pb deposition at a critical I^- concentration in solution which results in a sudden transition to saturation at a lower concentration (ca. 10^{-7} mol dm^{-3}) than that for either Cl^- or Br^- required to reach corresponding saturation limits (in the case of Cl^-, the approach to saturation limit is not discontinuous; Fig. 5.14).

Unlike the effects of Cl^- or Br^-, co-adsorbed I^- does not cause the first cathodic peak and the corresponding first anodic peak to be sharper. In fact the shifted first cathodic peak is evidently made up of two peaks (Fig. 5.3); a similar situation is observed in the absence of I^- (Fig. 4.5), as will be discussed in Section 5.5. The increase in the effectiveness of the competitive adsorption of I^-, vis a vis Cl^- and Br^-, is manifested by the blocking of Pb deposition at more positive potentials in the sweep which leads to relatively more extensive deposition at more positive potentials, i.e. the first stages of Pb monolayer deposition are shifted to substantially more negative potentials, a kind of ''overpotential effect''. This is indicated by the increase in the "spike" peak which is normally associated with continued Pb deposition beyond the nominal level of monolayer coverage.

5.2.6 Effects of I^- on the i vs E Profile in the Double-Layer Charging Region at Au in 1M aq. $HClO_4$

The superimposed i vs E profiles corresponding to successive additions of aliquots of the I^- salt solution to 1M aq. $HClO_4$ solution without a Pb salt being added are shown in Fig. 5.9 (compare Figs. 5.7 and 5.8). The effects of I^- are detectable at a very low concentration (2×10^{-7} mol dm^{-3}) and are more pronounced and different from the effects of either Cl^- or Br^-. It is seen (Fig. 5.9) that addition of I^- causes a decrease of the double-layer charging currents on both the anodic and cathodic sweeps in the concentration range 2×10^{-7} to 3.75×10^{-6} mol dm^{-3}.

Decrease of the double-layer capacitance in the presence of I^- is an indication of neutral species in the double-layer. I^-, therefore, strongly adsorbs at Au with almost complete charge transfer, i.e. $\gamma \rightarrow 1$.

As the concentration of I^- is increased (ca. 10^{-5} - 4×10^{-5} mol dm^{-3}), a peak develops on the anodic sweep with a corresponding one on the cathodic sweep. These peaks increase with increasing concentration of added I^-. They correspond to the process of regular oxidation of I^- and reduction of discharged I_2 at potentials ca. 750 and 850 mV/E_H, respectively. The process is clearly diffusion-controlled as can be seen from the shape of the curve, and corresponds to the electrodeposition of I_2.

5.2.7 Effect of Temperature on the Co-adsorption of Anions

The effect of temperature on the upd i vs E profiles in the presence of co-adsorbed anions (Cl^- and Br^-) in aqueous $HClO_4$ was investigated at three temperatures, 278.5 , 295 and 318 K. The absolute shifts in peak potential (in mV) of the first cathodic peak (C_{Pb1}) against log concentration of Cl^- and Br^- are shown in Figs. 5.10 and 5.11 respectvely, at these three temperatures. Examination of Fig. 5.10 shows that for a given concentration of Cl^-, the shift in peak potential, to more negative potentials, at 295 and 318 K is approximately the same and that at 278.5 K is correspondingly lower at all Cl^- concentrations used in the present study.

For Br^-, except at the lowest concentration (10^{-6} mol dm^{-3}), the shift in peak potential, to

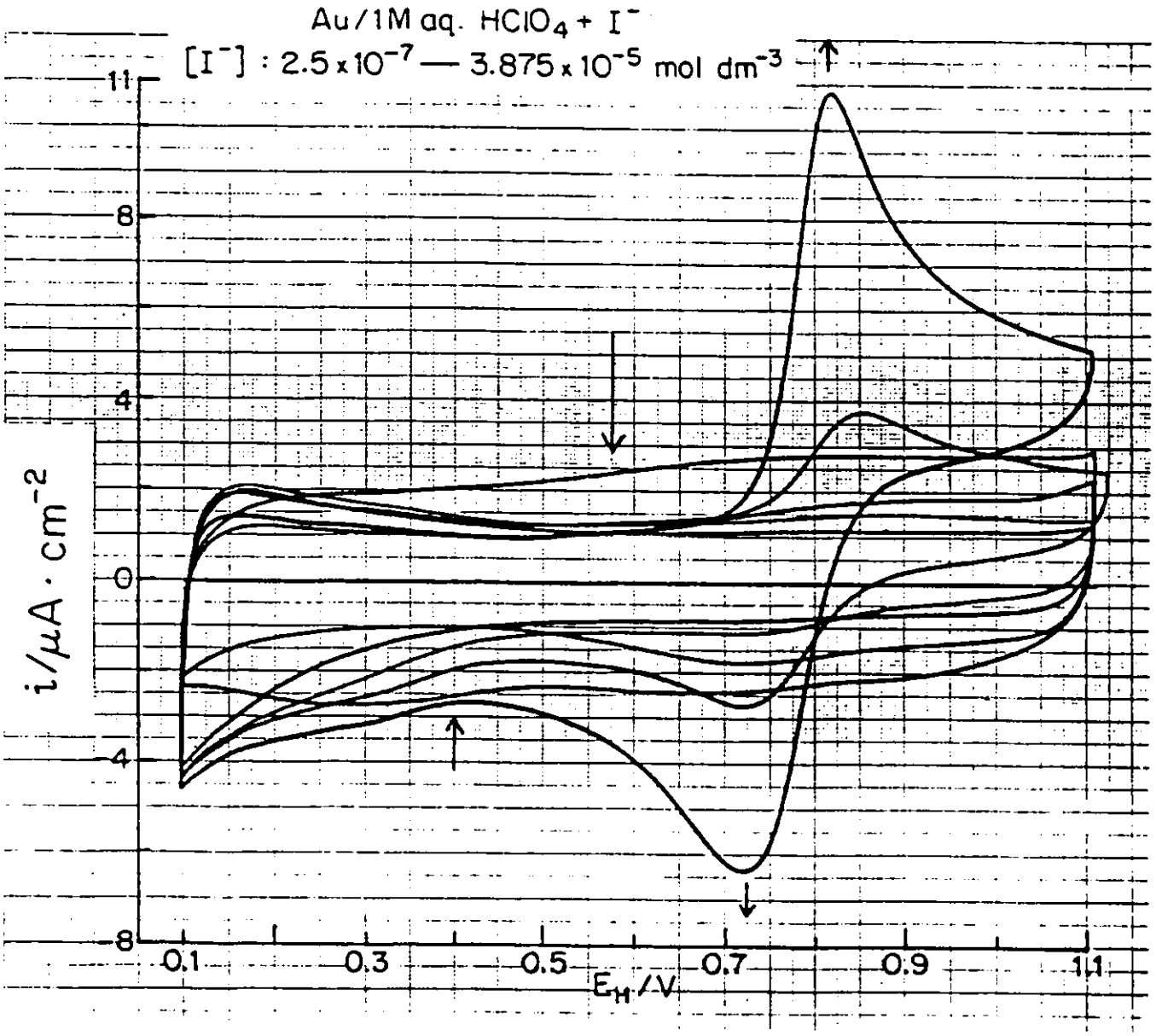

Fig. 5.9 Series of superimposed cyclic-voltammetry i vs E profiles for Pb upd at Au in aq. 1M $HClO_4$ with successive additions of I^- ion from 2.5×10^{-7} to 3.875×10^{-5} mol dm^{-3}, without a Pb salt being added. Arrows show directions of change of curves with increasing $[I^-]$. s = 50 mV s^{-1}.

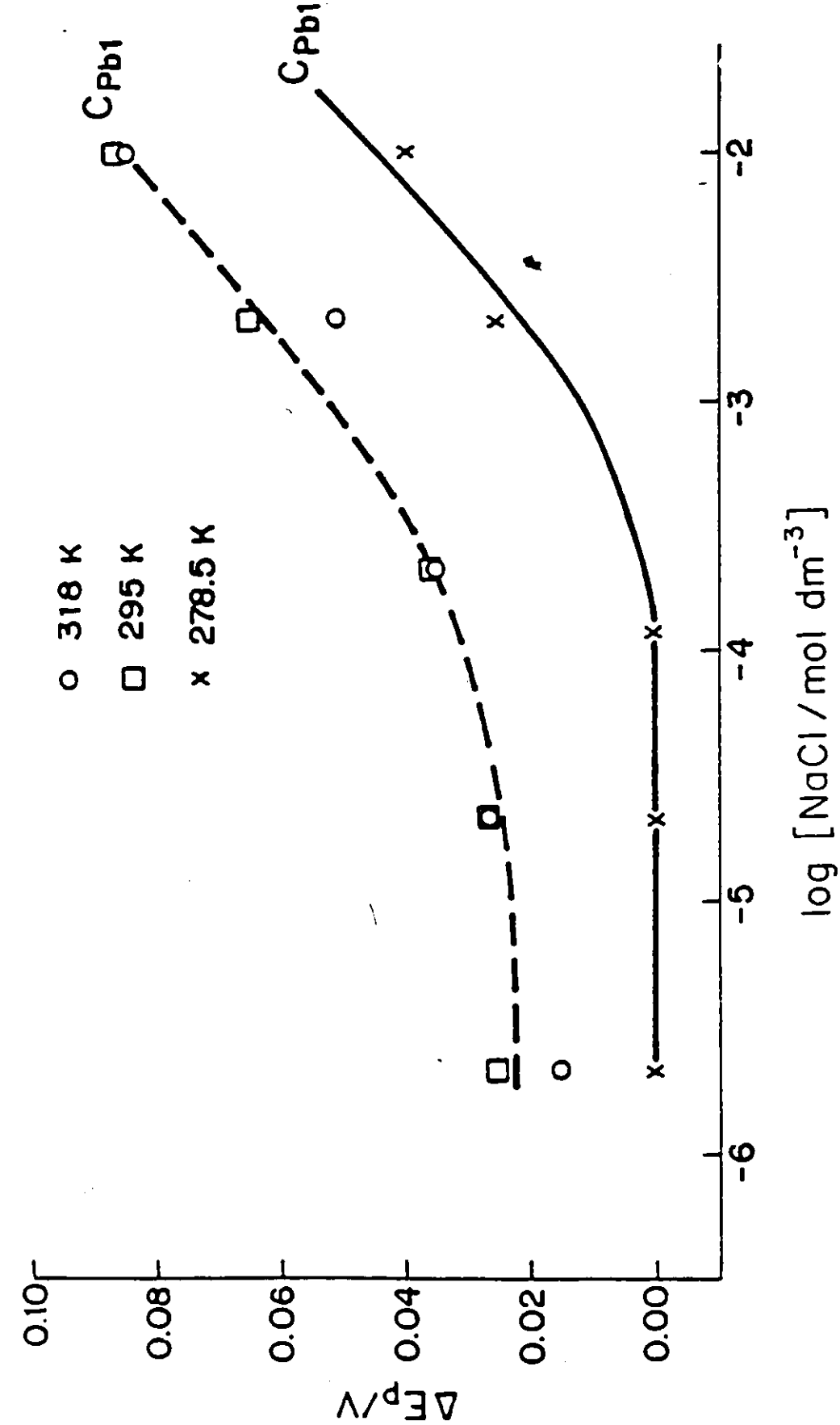

Fig. 5.10 Shift in peak potential of the first cathodic peak (C_{Pb1}) in the I vs E profile for Pb upd at Au in aq. 1M $HClO_4$ + 10^{-3}M $Pb(NO_3)_2$ as a function of log [NaCl] at three temperatures: 278.5, 295 and 318 K

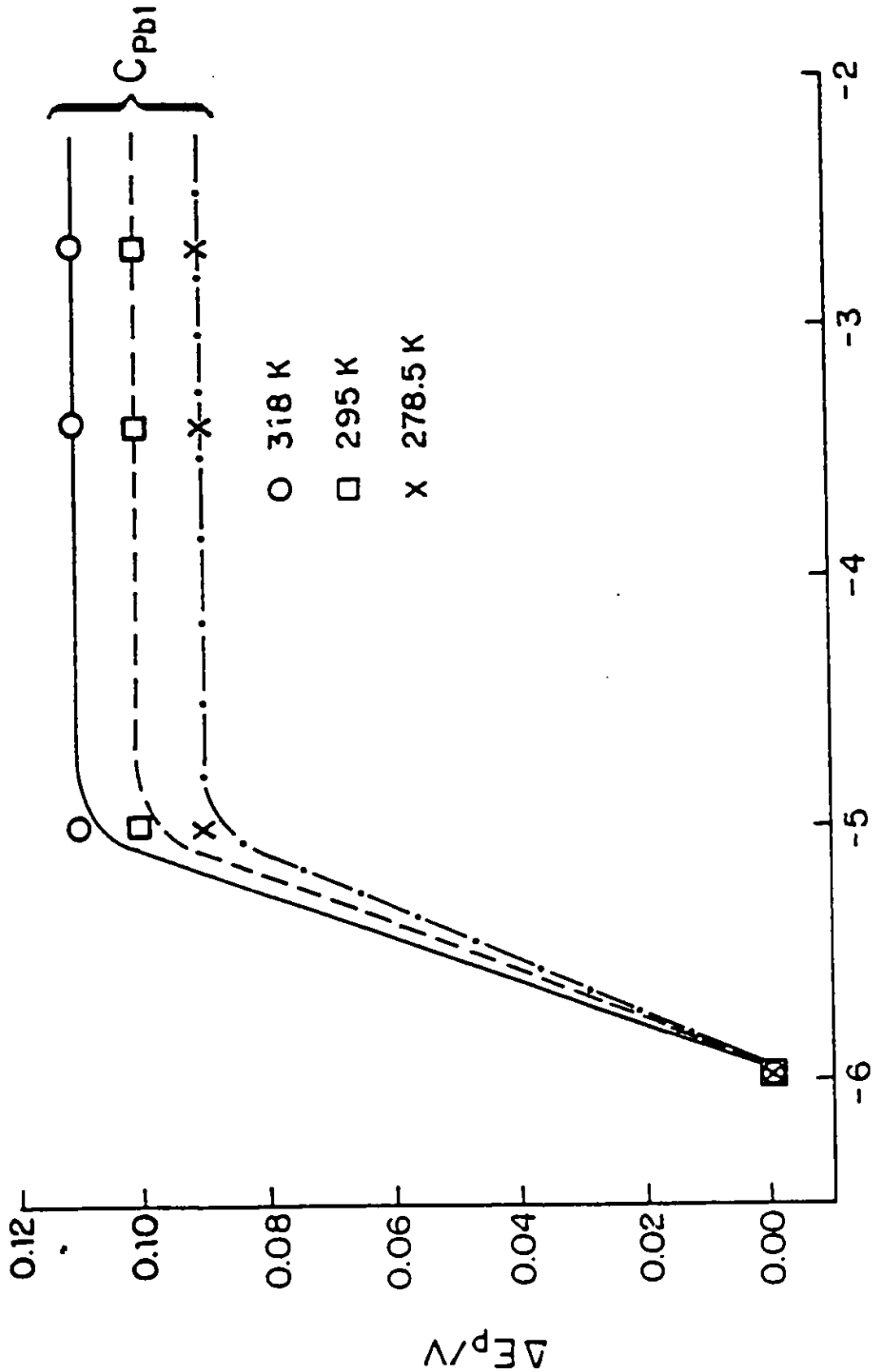

Fig. 5.11 Shift in peak potential of the first cathodic peak (C_{Pb1}) in the i vs E profile for Pb upd at Au in aq. 1M $HClO_4$ + 10^{-3}M $Pb(NO_3)_2$ as a function of log [NaBr] at three temperatures: 278.5, 295 and 318 K.

more negative potentials, increases with temperature rise at all concentrations of Br^-. A shift of the peak potential of the first cathodic peak to more negative potentials in the presence of added anions, which are known to cause such a shift, would imply that the adsorbability of these anions increases with temperature rise, an unexpected situation.

It has been found in the present work (see Chapter 7, Section 7.3 and Table 7.2) that the peak potentials of the upd i vs E profiles for Pb at Au in aqueous $HClO_4$ are shifted to more negative potentials with temperature rise in the absence of strongly adsorbing anions such as Cl^-, Br^- or I^-. Since the experiment was conducted with the reference electrode at the same temperature as the working electrode, it was concluded that such a shift was due to the negative temperature coefficient of the H_2 reference electrode. It is, therefore, likely that the observed shift in peak potentials in the presence of Cl^- or Br^- with temperature rise is not due to these anions. When the effect of Br^- was investigated in MeOH at different temperatures, it was found that temperature rise had no significant effects in the shift of the peak potentials of the first cathodic peak to more negative potentials. We, therefore, conclude that temperature, at least in the present range studied, has no noticeable significant effect on the upd i vs E profiles of Pb at Au.

5.3 Adsorption of Thiourea (TU)

5.3.1 Introduction and Previous Studies of TU Adsorption

A substantial amount of work has previously been carried out on TU adsorption, but mainly at Hg [187-189]. At this metal, the adsorption is very strong, with a substantial degree of charge-transfer with γ = ca. - 0.25 [190], corresponding to the well known affinity of S in low oxidation states for Hg. Some other work has been done at Sn [191] and Pb [192] but this will not be reviewed here.

TU adsorption at electrodes has attracted attention because its behaviour resembles that of anions, due to similar electron donicity.

The only study of TU adsorption from aq. solution on Au as a function of potential and concentration was that of Wroblowa and Green [193] using the radiotracer method.

In 5.3.2 below, we summarise the principal conclusions regarding TU adsorption and electrochemical behaviour.

5.3.2 Summary about Thiourea (TU) Adsorption

1. TU is a neutral molecule which behaves like an anion because of its tendency to act as an electron donor and it has a large dipole moment (4.9 D).
2. The strong interaction (adsorption) of TU with Hg and other metal electrode surfaces is due to specific interactions of its functional group (the 3s and 3p electrons) with the metal surface which leads to the formation of a covalent bond with the metal surface via the S atom.
3. The catalytic influence of TU on the rates of electroreduction of certain metal cations, e.g. Zn^{++}, Sn^{++} etc., is believed to be due to the formation of transition complexes with these metal cations in the double-layer where TU acts as a bridging ligand providing the most efficient path for electron transfer from the cathodes to the ions being discharged in the electrodeposition process.

5.3.3 Effects of Adsorbed Thiourea on the i vs E UPD Profile for Pb at Au

Fig. 5.12 shows the superimposed i vs E profiles, corresponding to incrementally increased concentrations, following successive additions of TU to aq. $HClO_4$; the behaviour observed arises from the progressive competitive adsorption of TU in relation to the formation of the Pb upd monolayer at Au. The effects are already detectable at a very low concentration of added thiourea, 10^{-6} mol dm^{-3}. Although there is an initial lowering of the first cathodic peak and a subsquent shift to more negative potentials as in the case with Br^- and I^-, the competitive adsorption of TU is stronger than that of the halide ions. For example, the shift of the first cathodic peak (C_{Pb1}) to more negative potentials, due to added TU, is greater than that due to halide ions at a given concentration before the saturation limit is reached.

This strong adsorbability of TU on Au causes the saturation effect to be attained very suddenly at a concentration substantially lower than that for any of the halide ions, X^-.

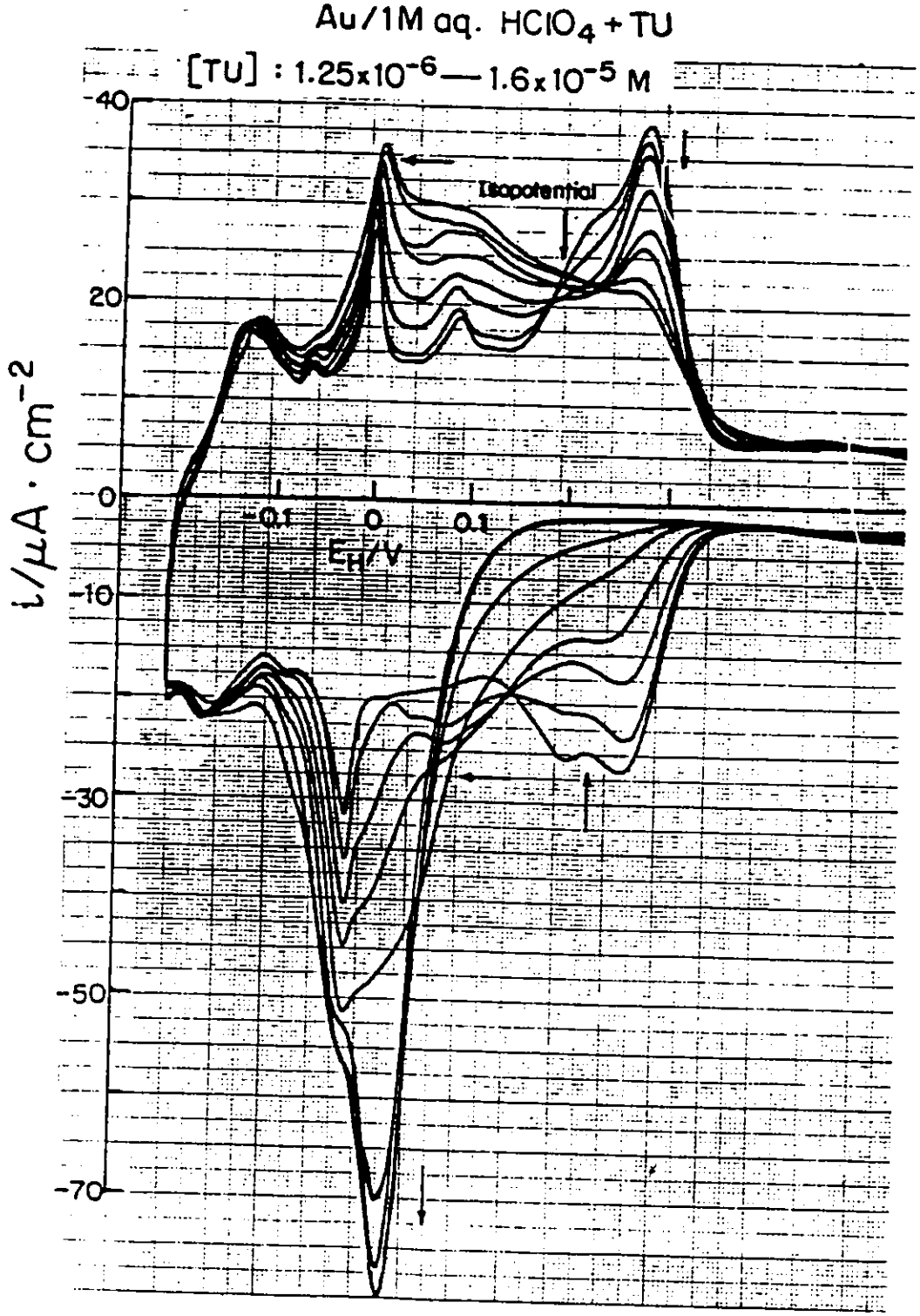

Fig. 5.12 Series of superimposed cyclic-voltammetry i vs E profiles for Pb upd at Au in aq. 1M $HClO_4$ + 10^{-3}M $Pb(NO_3)_2$ with successive additions of TU from 1.25 x 10^{-6} to 1.6 x 10^{-5} mol dm^{-3}. Arrows show directions of change of curves with increasing [TU]. s = 50 mV s^{-1}.

Another striking effect due to TU, not observed with any halide ion X^-, is the greatest shift of the first cathodic peak to more negative potentials; this results in the completion of the upd monolayer over a narrowed potential range. Thus, the first cathodic peak becomes merged with the "spike" to form a single peak. This shows that the strongly adsorbed TU does not become desorbed from the Au electrode surface until more negative potentials are reached but before bulk Pb deposition starts.

As with the effects of I^-, no extra peak arises at more anodic potentials, as was observed in the presence of Cl^- and Br^- (cf. Figs. 5.1 and 5.2). Also the upd profiles for deposition and ionization of Pb at Au in the presence of TU do not remain reversible, as they do (more or less) in the case of co-adsorbed anions (Figs. 5.1, 5.2 and 5.3).

5.3.4 Effects of TU on Double-Layer Charging Behaviour at Au in aq. $HClO_4$

As Fig. 5.13 shows, the effect of addition of TU to 1M aq. $HClO_4$, without a Pb salt being present, is less pronounced than with Br^- or I^-, especially at low concentrations. However, with increasing concentration of added TU, there is a slight decrease of the double-layer capacitance similar to that observed with I^- (see Fig. 5.9). This is consistent with increasing concentration of strongly adsorbed neutral molecules in the double-layer that replace water molecules.

Table 5.2 Maximum Shift of the Peak Potentials of the First Cathodic Peak (C_{Pb1}) in the Presence of Added Anions or Thiourea (TU).

Added Species	Shift in Peak Potentials (mV)
Cl^-	-110
Br^-	-115
I^-	-120
TU	-240

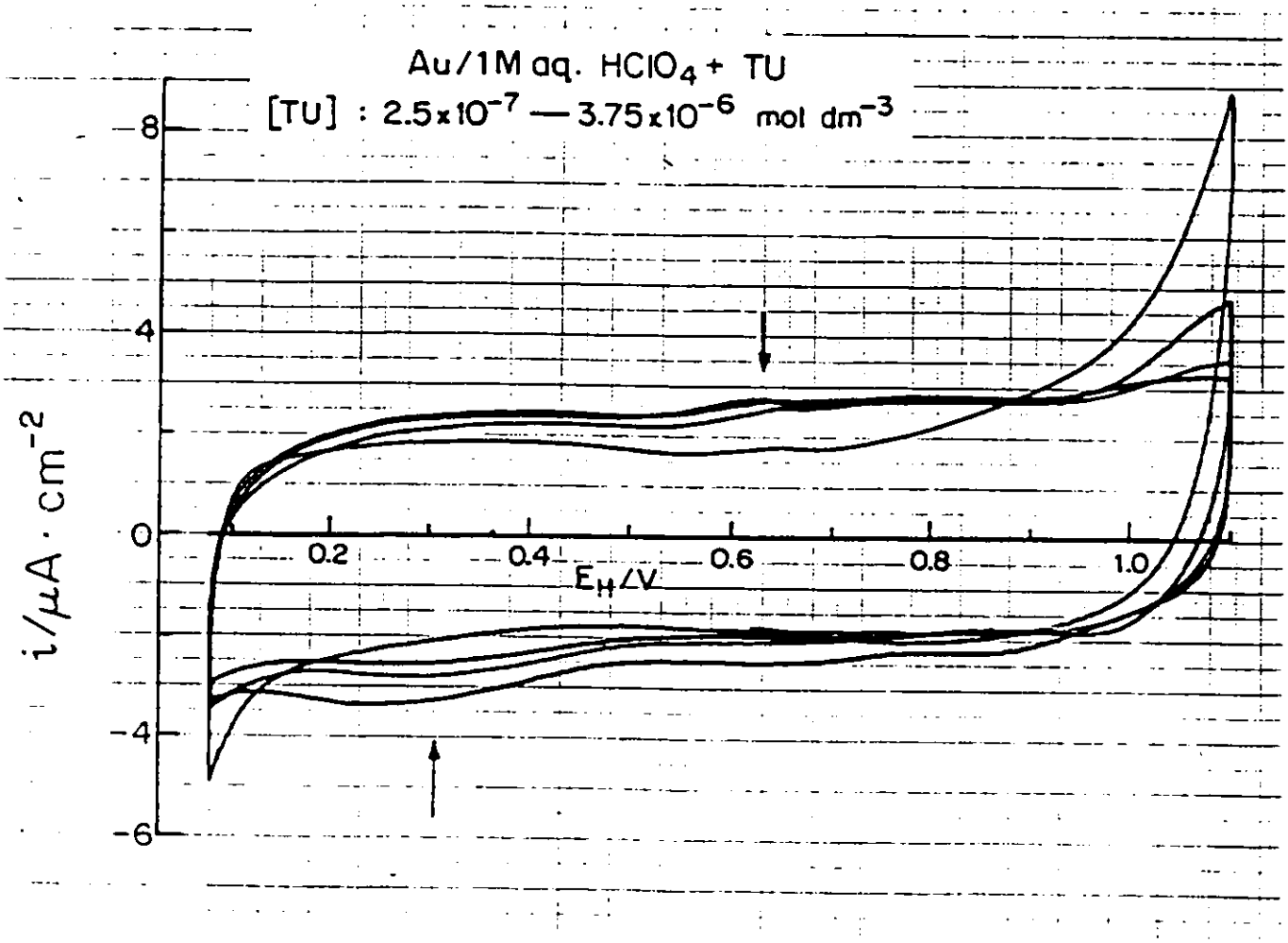

Fig. 5.13 Series of superimposed cyclic-voltammetry i vs E profiles for Pb upd at Au in aq. 1M $HClO_4$ with successive additions of TU from 2.5×10^{-7} to 3.75×10^{-6} mol dm^{-3}, without a Pb salt being added. Arrows show directions of change of curves with increasing [TU]. s = 50 mV s^{-1}.

5.4 Competitive Adsorption Isotherms for Co-adsorption of Halide Ion (X^-) or Thiourea (TU) with Electrosorbed Pb Adatoms

From the individual i vs E profiles corresponding to those of the sets shown in Figs. 5.1 to 5.3, and 5.12 the absolute shifts in peak potential of the first cathodic peak, C_{Pb1}, can be plotted as a function of the log of the concentration of the halide ion or thiourea. The resulting relations are shown in Figs. 5.14 to 5.17. The effects can also be represented in terms of the % surface blocked by the halide ion X^- or TU. The % blocking is calculated by fixing an arbitrary reference point, say $E_H = 0.2$, and then comparing the reduced charge for Pb deposition (due to competitive adsorption of the halide ion or TU) to that corresponding to the upd charge in the absence of added halide ion or TU at the beginning of the experiment.

Figs. 5.18 to 5.20 show such competitive adsorption isotherms for % blocking of Pb upd by the halide ion X^-, as a function of log [X^-] from measurements in aq. 1M $HClO_4$. Fig. 5.21 shows a comparison of the corresponding data for TU adsorption effects also from measurements in aqueous 1M $HClO_4$.

The competitive adsorption isotherms of Fig. 5.18 to 5.20, representing the effects of the halide ions, X^-, and Fig. 5.21, representing those of TU, show that the behaviour of Cl^- is different from that of either Br^- or I^-. The effect of chloride on the peak potential shift does not become significant until about 3 decades of Cl^- concentration are covered and the effect really stretches over a wide concentration change, about 5 decades, before it reaches a saturation limit. Unlike the behaviour of Br^- and I^-, the transition towards saturation is not sudden but continuous, and the saturation effect is reached at a Cl^- concentration of 10^{-2} mol dm^{-3}, substantially higher than that for either Br^- or I^-. The effects of Cl^- on upd Pb deposition observed here are, however, rather different from those of Cl^- at oxidized Pt reported by Conway and Novak [75]. For Pt surface oxide formation, the chloride blocking effect in aq. H_2SO_4 gave an excellent linear relation with log [Cl^-] over four and a half decades of concentration change, actually somewhat similar to what is observed in the effect of Cl^- on Pb adatom deposition.

With Br^- and I^-, the plots are rather similar, although the concentration at which the effects

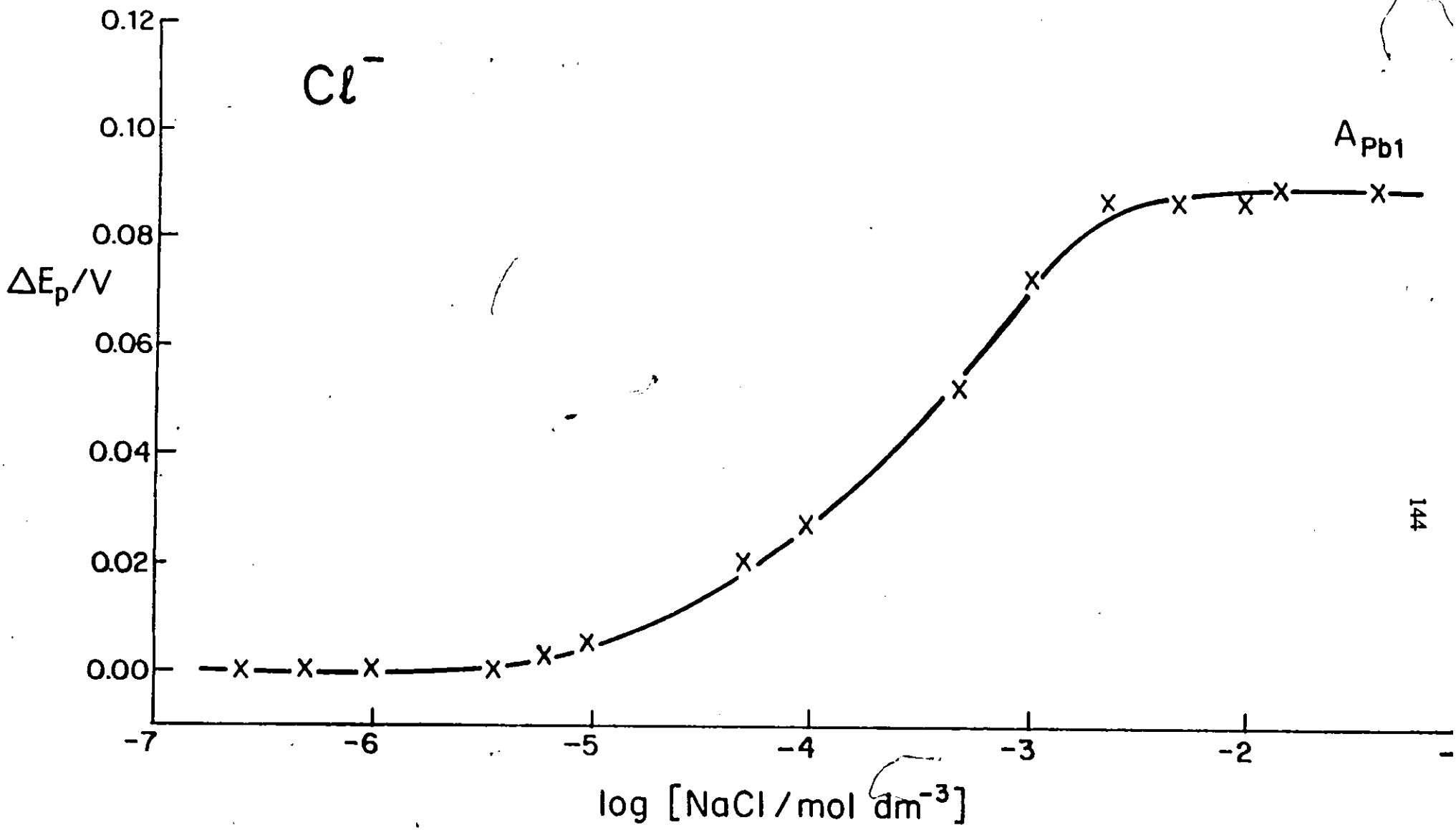

Fig. 5.14 Shift in peak potential of the first cathodic peak (C_{Pb1}) in the i vs E profile for Pb upd at Au in aq. 1M $HClO_4$ + 10^{-3}M $Pb(NO_3)_2$ as a function of log [Cl^-]. (Data from curves shown in Fig. 5.1).

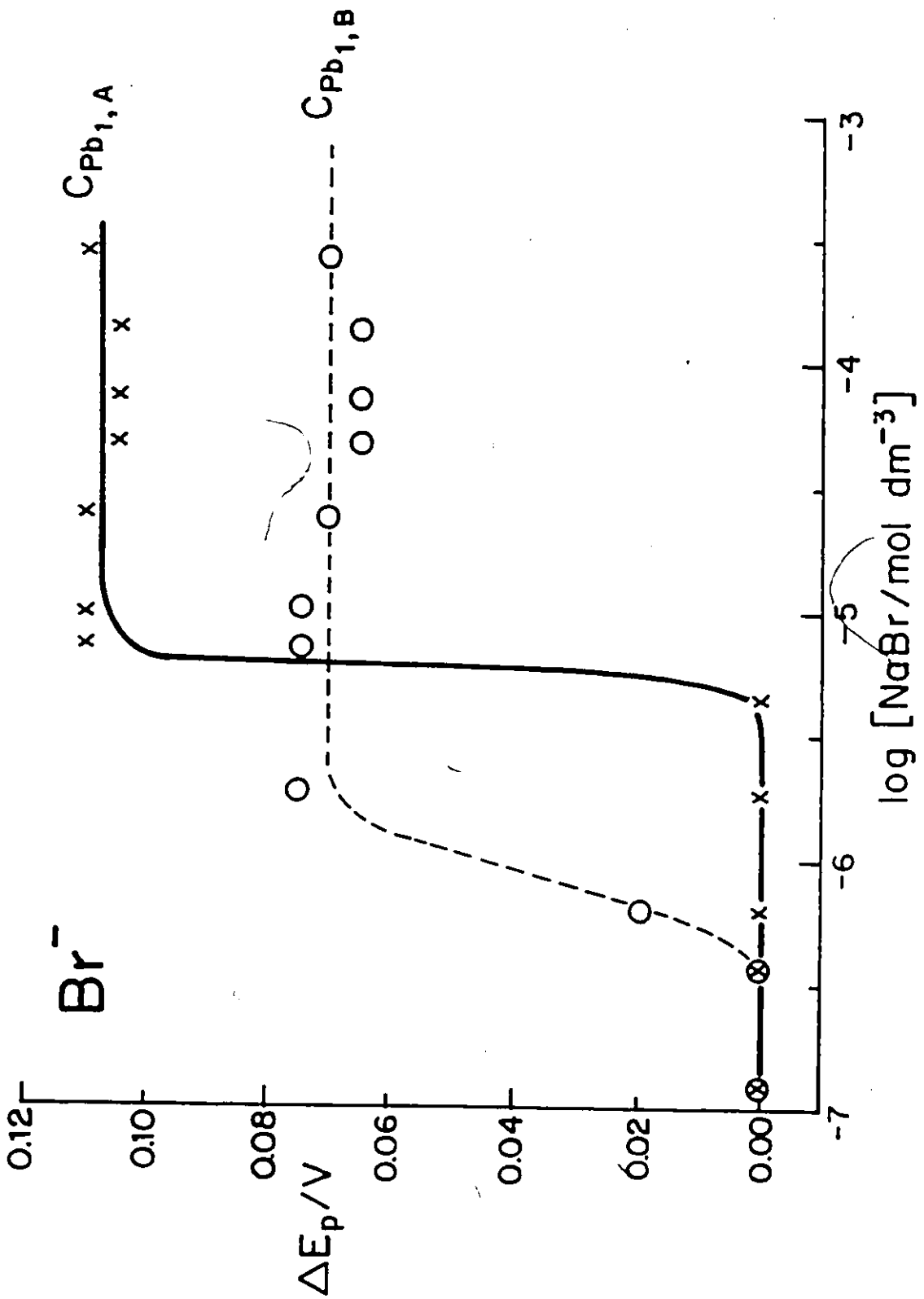

Fig. 5.15 Shift in peak potential of the first cathodic peak (C_{Pb1}) in the i vs E profile for Pb upd at Au in aq. 1M $HClO_4$ + 10^{-3}M $Pb(NC_5)_2$ as a function of log [Br⁻]. (Data from curves shown in Fig. 5.2).

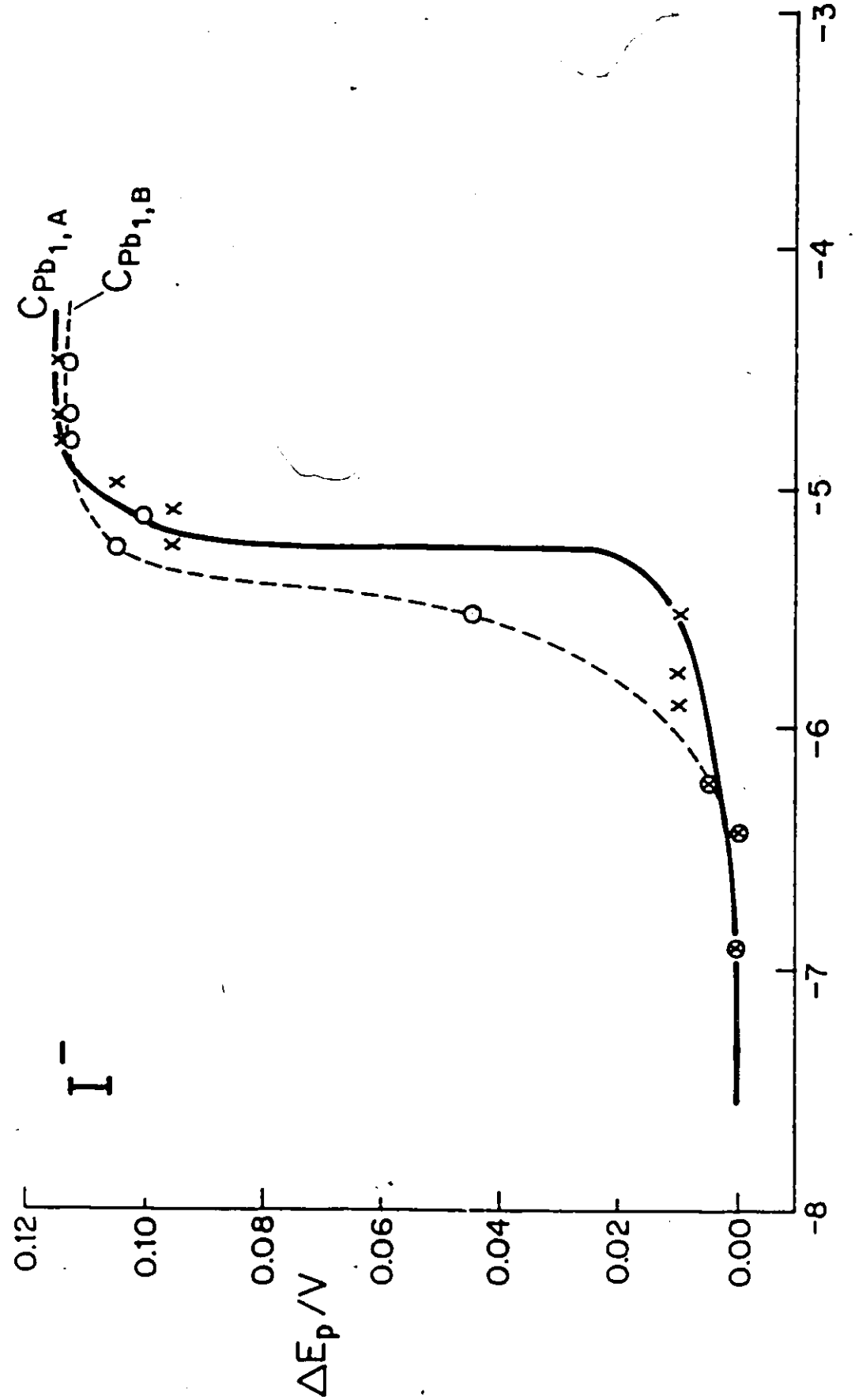

Fig. 5.16 Shift in peak potential of the first cathodic peak (C_{Pb1}) in the i vs E profile for Pb upd at Au in aq. 1M $HClO_4$ + 10^{-3}M $Pb(NO_3)_2$ as a function of log [I^-]. (Data from curves shown in Fig. 5.3).

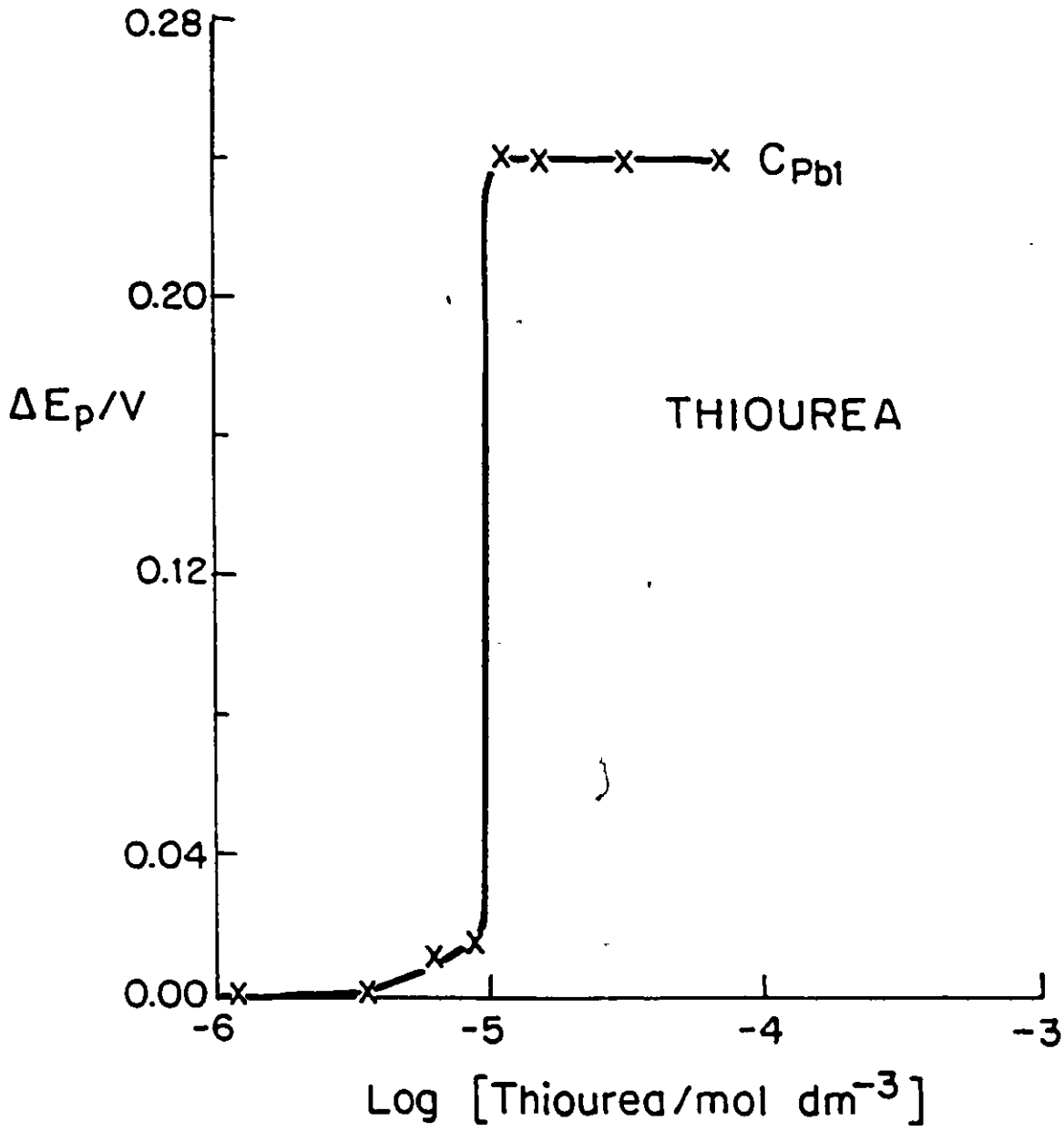

Fig. 5.17 Shift in peak potential of the first cathodic peak (C_{Pb1}) in the i vs E profile for Pb upd at Au in aq. 1M $HClO_4$ + 10^{-3}M $Pb(NO_3)_2$ as a function of log [TU]. (Data from curves shown in Fig. 5.12).

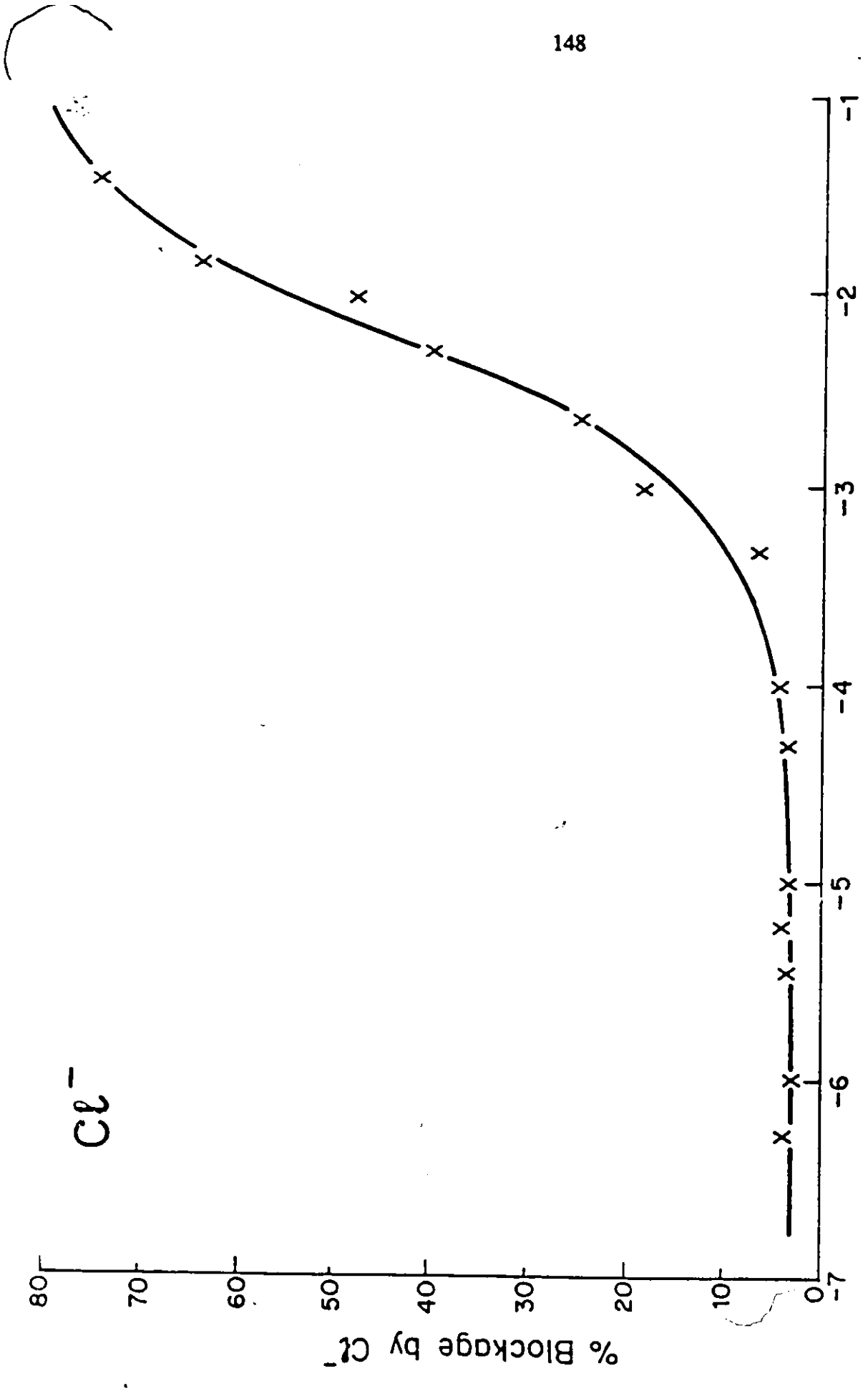

Fig. 5.18 Percentage blocking of Pb upd on Au in aq. 1M $HClO_4$ + 10^{-3}M $Pb(NO_3)_2$, measured as its charge reduction by Cl^- ion as a function of log [Cl^-]. (Data from curves shown in Fig. 5.1).

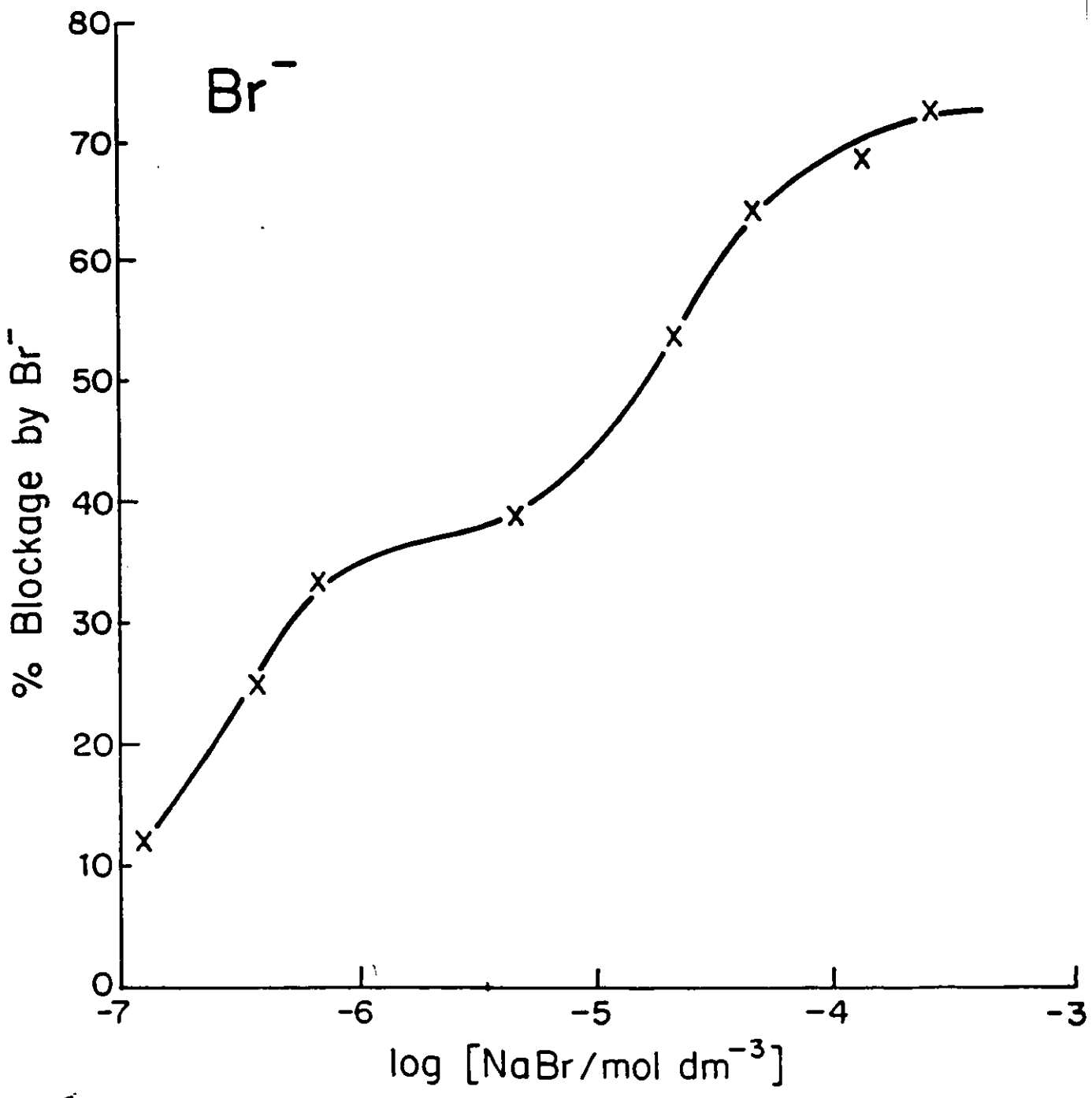

Fig. 5.19 Percentage blocking of Pb upd on Au in aq. 1M $HClO_4$ + 10^3M $Pb(NO_3)_2$, measured as its charge reduction by Br^- ion as a function of log [Br^-]. (Data from curves shown in Fig. 5.2).

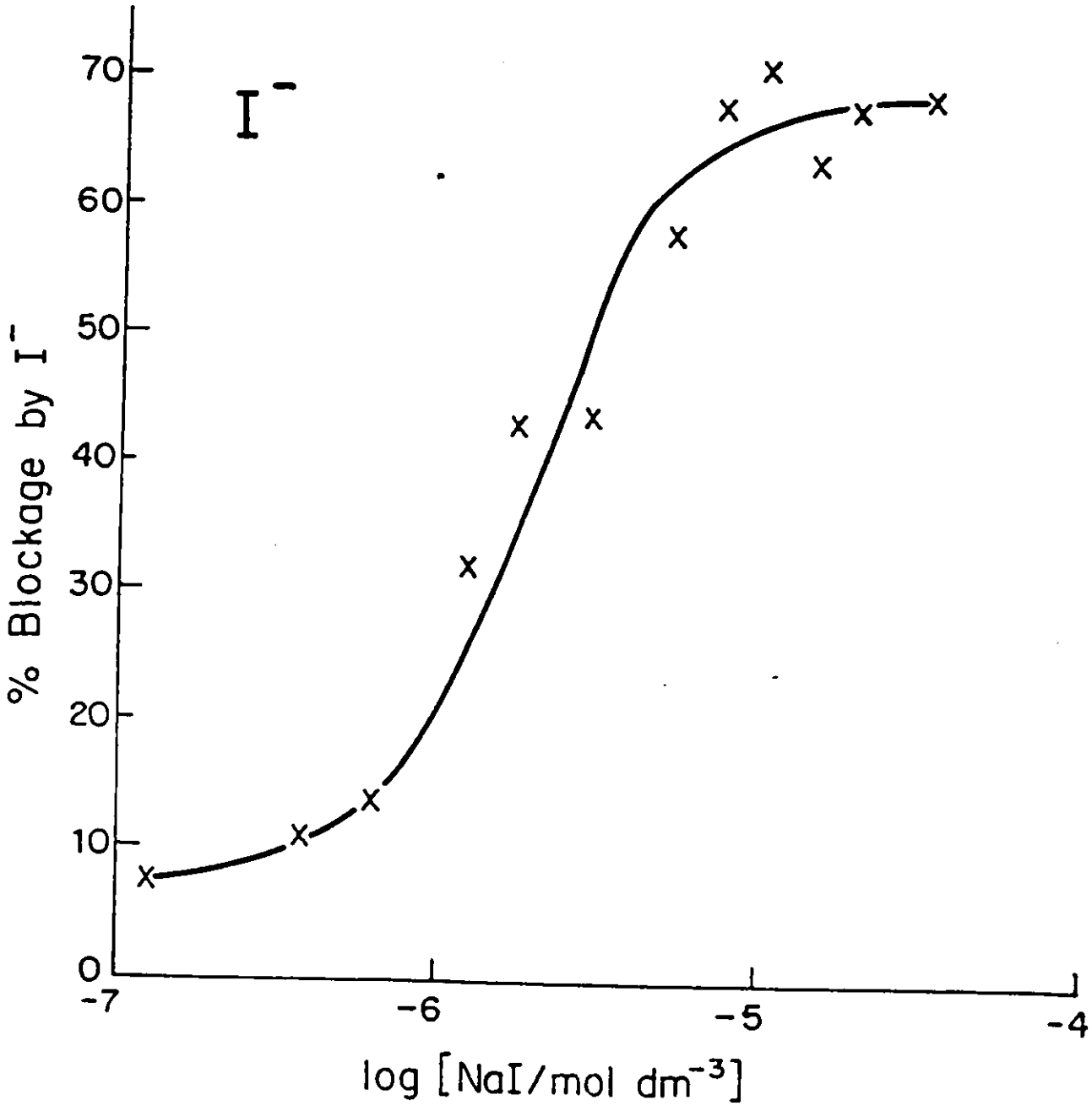

Fig. 5.20 Percentage blocking of Pb upd on Au in aq. 1M $HClO_4$ + 10^{-3}M $Pb(NO_3)_2$, measured as its charge reduction by I^- ion as a function of log [I^-]. (Data from curves shown in Fig. 5.3).

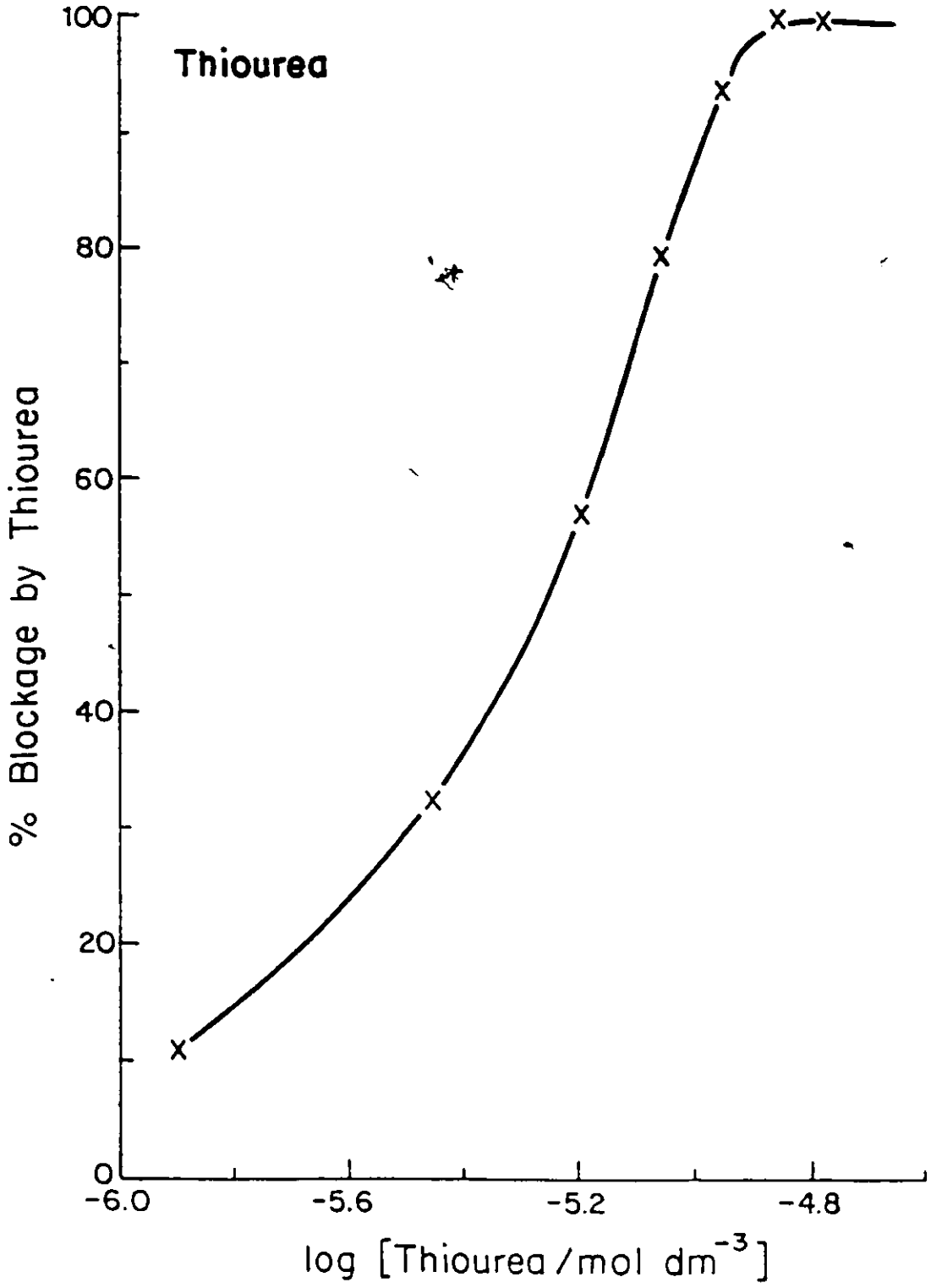

Fig. 5.21 Percentage blocking of Pb upd on Au in aq. 1M $HClO_4$ + 10^3M $Pb(NO_3)_2$, measured as its charge reduction by TU as a function of log [TU]. (Data from curves shown in Fig. 5.12)

become significant depends on the halide ion. The competitive adsorption isotherms of Figs. 5.15 and 5.16 show that the effect become significant at concentrations of approximately 5×10^{-6} and 5×10^{-7} mol dm^{-3} for Br^- and I^-, respectively. The striking similarity between the behaviour of Br^- and I^- is manifested in the shape of the log plot: they both give more normal (i.e. Langmuir-type) adsorption behaviour in an expected S-shaped curve on the log plot, unlike the wide stretch in the plot for the Cl^- effect. With Br^- and I^- there is , however, a sudden transition to a saturation effect, a feature not observed in the effects of Cl^- ion. This discontinuous transition could be due to a sudden rearrangement of the adsorbed Br^- or I^- and the electrodeposited Pb adatoms in the upd layer possibly with change of electron distribution. The difference of shapes of the curves for the log plots is also probably associated with interactions in the upd layer between the electrodeposited Pb adatoms and the co-adsorbed halide ions, X^-, depending on their partial charges in the adsorbed state, a point to be discussed later in Section 5.5.

The maximum shifts of the first cathodic peak due to competitive adsorption by Br^- and I^- are -115 and -120 mV, respectively, (see Table 5.2).

In the case of TU (Fig. 5.17), the effect is similar to that of Br^- and I^-, although there is a sudden increase in the effectiveness of competitive adsorption leading to saturation behaviour and a greater shift in the peak potential of the first cathodic peak compared to that observed with the halide ions, X^-.

With TU, the maximum shift in peak potential is -240 mV, although the effects are already significant and observable at a concentration of ca. 3×10^{-6} mol dm^{-3}, which is close to that for the limit of detectability of the influence of Br^-.

5.5 Discussion and Conclusions on the Effects of Anions

The sharpening of the peaks due to co-adsorbed Cl^- (Fig. 5.1) and the shape of the adsorption isotherm (Fig. 5.14) for competitive adsorption of Cl^- with Pb at Au, suggests that there are strong repulsive lateral interaction effects in the upd Pb layer when co-adsorbed Cl^- is present, leading to the rather extended shift in peak potential or % blocking with increasing log $[Cl^-]$. However Br^-

and I^- give a more normal (i.e. "Langmuir"-like) adsorption behaviour, i.e. in an "S - shaped" curve on the log plot. The plot of the adsorption behaviour of TU is similar to that for Br^- and I^-, although effects are stronger and more sudden. Therefore with co-adsorbed Br^-, I^- or TU, the interaction effects in the upd Pb layer are probably attractive (contrary to the situation with Cl^-) and lead to 2-d phase formation in a co-operative phenomenon.

It is well known that I^- is adsorbed (at Au) as neutral I atoms [74,75,194] and this is also indicated indirectly from its effects on the upd i vs E profiles for Pb at Au. Thus, the shifted cathodic peak (C_{Pb1}) still resembles the peak in the absence of I^- in shape and size. We therefore conclude that the more extended logarithmic effect of $[Cl^-]$ is due to strong lateral interaction effects: repulsion between the adsorbed Cl^- ions themselves and other interactions between adsorbed Cl^- and the electrodeposited Pb adatoms that form a polar bond with surface Au atoms. Since Br^- and I^- differ only from Cl^- in their size, donicity, polarizability and interactions with the solvent, it is suggested that the striking difference in their behaviour vis a vis that of Cl^- is due to the difference in the degree of charge-transfer when chemisorption takes place at the Au electrode. This chemisorption process may be represented as

$$X^- + Au \rightarrow AuX^{-(1-\gamma)e} + \gamma e_{Au} \qquad (5.1)$$

where γ is the electrosorption valency factor [22].

With adsorbed Cl^-, it is evident that $\gamma << 1$ and thus strong electrostatic interactions arise in the Pb upd layer due to the retained fractional charge. For Pb chemisorbed at Au in aq. $HClO_4$, $\gamma = 1.95$ [22]. For Br^- and I^- adsorbed at Au, $\gamma \rightarrow 1$ and hence they are adsorbed as almost neutral adatoms. Therefore Br^- and I^-, adsorbed at Au among electrodeposited Pb adatoms, will have much reduced electrostatic interactions with themselves and with neighbouring Pb adatoms in the upd layer.

The adsorption behaviour observed is competitive rather than simple, so that interactions are between X^- ions themselves and between X^- and Pb_{ads}, as well as involving pre-adsorbed solvent molecules. As with H at Pt [75], the same quantity of Pb is eventually electrodeposited as in the absence of co-adsorbed ions or TU but over a different range of potentials and in different sub-states.

It was noted earlier that the upd i vs E profiles for the Pb deposition and ionization at Au remain more or less reversible in the presence of co-adsorbed anions so that both anion adsorption and Pb deposition remain essentially reversible. Evidently with Pb at Au, readsorption of Cl^- ions occurs rapidly, following ionization desorption of Pb, as indicated by the cathodic shift of the C_{Pb1} peak on an immediately following anodic sweep.

It is also observed, as noted earlier, that the upd profiles for Pb at Au are most affected over the low Pb coverage region, as may be expected, since it is for such conditions that more surface is available for competing adsorption between the added anions or TU, and the upd adatom species.

CHAPTER 6

KINETICS OF Pb UPD PROCESSES AT Au IN VARIOUS NON-AQUEOUS SOLVENTS

6.1 Methods used in the Investigation of Kinetics of Electrochemical Surface Processes

Three experimental methods have been widely used in the study of the kinetics of electrode surface processes or reactions; they are a.c. impedance, galvanostatic and linear potential-sweep amperometry or cyclic-voltammetry [48].

The a.c. impedance of an electrochemical surface process is represented by a Faradaic reaction resistance R_F in series with the adsorption pseudocapacitance C_ϕ of the surface reaction in such an arrangement that both these elements are in parallel with the double-layer capacitance. The impedance behaviour of the surface process is conveniently described by a complex-plane plot of the real vs the imaginary component of the impedance or admittance over a range of frequencies. Determination of R_F enables the exchange current-density, i_o, to be evaluated which characterizes the dynamic reversibility of the reaction. In the region of linear response of the electrode reaction rate to changing potential, i_o is found directly from

$$R_F = RT/i_o F \qquad (6.1)$$

The galvanostatic technique involves recording charging curves for the surface process, giving rise to potential-time curves at constant current-densities. At sufficiently large current densities, i.e. for $i >> i_o$ for a surface reaction, the formation or desorption of the monolayer proceeds in a kinetically irreversible manner and the potentials required for attaining a given coverage are then logarithmically related to the density of the current pulse , i. The charging curves are hence displaced along the potential axis corresponding to various overpotentials arising at the various current-densities, i. The potential, E, corresponding to a given coverage can then be plotted as a function of log i so that the electrochemical kinetic parameter i_o and the Tafel slope ($b = RT/\beta F$) can be obtained for the surface process, as for a regular Faradaic reaction. Vetter and

co-workers [195,196] have used this method to study the kinetics of surface-oxide formation and reduction processes at noble metals.

The galvanostatic charging method gives rise to an inflected rather than a peaked curve. With regard to accuracy, the a.c. impedance and the potentiodynamic sweep methods are preferred.

Cyclic-voltammetry, discussed fully in Chapter 3, was the technique employed in the present work in the characterization of the kinetics of the upd processes of Pb at Au from various non-aqueous solvents. In this approach, measurements of the peak potentials, E_p, are made at various sweep-rates, s, and E_p is then plotted vs log s, from which the required kinetic parameter s_o [127] (anologous to i_o), the sweep-rate at which the process just ceases to be reversible, can be determined. The advantage of s_o over the anologous kinetic parameter, i_o, is that the real surface area of the electrode is **not** a parameter required for its evaluation.

In aqueous solutions, each stage of the formation of the upd film of Pb is a fast reaction, with s_o values of about 100 - 200 V s^{-1}. In non-aqueous solvent media, s_o is more difficult to evaluate owing to "iR" drop effects. A.C. impedance measurements have to be employed at potentiostatically held values of potential individually at the upd peaks, so that kinetic measurements can be made with complete separation of the ohmic impedance of the solution. However, in upd processes, the maximum currents are usually small or the "iR" drop effects can be internally compensated. The maximum currents are typically 1 mA which lead to "iR" drops of low values and hence the effect of uncompensated resistance can be neglected in most of the present results. For example, a maximum current on the order of $\leq$ 0.2 mA and a solution resistance of 8.2 Ω gives rise to an "iR" drop of less than 6.2 mV for an electrode of radius ca. 0.05 cm [161].

The kinetic techniques described above should be used in a complementary manner, rather than independently, for better understanding or characterization of the kinetics of the surface processes or reactions at the electrode.

6.2 Distinguishable States of the UPD of Pb at Au in the Monolayer Region

As shown earlier in Chapter 4, Section 4.3 (e.g. in Figs. 4.1 to 4.4), the i vs E profiles for Pb at Au indicate that surface processes involve multiple-state adsorption. Several distinct states of sub-monolayer quantities of Pb on Au can be resolved in the electrodeposition and ionization i vs E profiles before a upd monolayer of Pb is completed. It is to be noted that the number of resolvable peaks (corresponding to distinct states) and the degree of resolution is found, in the present work, to be solvent-dependent; for example, on the i vs E for the upd of Pb at Au in aq. $HClO_4$, up to seven distinct states can be resolved. On the other hand, in AN as a solvent (Fig. 4.1), the upd profile is least resolved.

6.3 Sweep-rate Dependence of the Anodic and Cathodic Peak Potentials in UPD of Pb at Au

The results to be presented below arise from investigations of the variation of peak potentials, E_p, corresponding to distinct sub-monolayer states in the anodic and cathodic directions of the i vs E profiles as a function of sweep-rates, s, using cyclic-voltammetry. For slow potential sweeps (≤ 150 mV s^{-1}), the i vs E profiles were acquired using an X-Y recorder while for higher sweep-rates (> 150 mV s^{-1}) they were recorded on a Nicolet oscilloscope, as described in the Experimental Section.

Since not all peaks remained resolvable over a reasonably wide range of sweep-rates, especially at sweep-rates greater than 1 V s^{-1} due to peak overlap problems, the sweep-rate dependence of peak potentials could only be reliably investigated for the two main peaks on each side of the upd profile: the first cathodic peak (C_{Pb1}) and the "spike" (C_{Pb5}), together with the corresponding peaks on the anodic side, i.e. A_{Pb1} and A_{Pb5}. The degree of resolution depends on the solvent and the conditions under which the experiment is carried out, e.g. the sweep-rate, temperature, etc.. These peaks (C_{Pb1} and A_{Pb1}) correspond to the formation and desorption, respectively, of the most tightly bound sub-monolayer of Pb at Au. The "spike" (C_{Pb5} and A_{Pb5}) is believed to correspond to a 2-dimensional phase transition of the Pb ad-layer on Au, and arises at ca. 68% coverage in all the solvent systems used.

6.4 Effect of Sweep-rate on the Anodic Peaks

It was found in this laboratory [52] that the electrodeposition/dissolution process in the upd of Pb at Au in aq. $HClO_4$, which may be represented by the equation

$$2e + Pb^{++}(S) + Au_{lattice} \rightleftharpoons Pb_{adatom}(Au) \qquad (6.2)$$

is a very reversible reaction, more so than most other upd systems. It was, therefore, of interest for us to investigate the kinetics of this process in non-aqueous media and compare the results with those obtained in aqueous medium. The series of superimposed cyclic-voltammograms obtained, corresponding to various sweep-rates recorded on the X-Y recorder for the indicated non-aqueous solvents, are shown in Figs. 6.1 and 6.2 and are representative of the results found it the study of the upd behaviour in the other non-aqueous solvents.

From the lowest sweep-rate employed in the present study (5 or 10 mV s^{-1}), increase in the sweep-rate does not seem to have any marked effects on the resolvable anodic peaks of the i vs E profile obtained in aqueous or non-aqueous media, at least for sweep-rates up to 1 V s^{-1}. The general observation is that the anodic peak currents increase progressively as the sweep-rate is raised (as is expected for a surface process for which $i = C_\phi s$) and the general resolution (peak multiplicity) is retained up to a sweep-rate of about 1 V s^{-1}. Overall, the shapes of the anodic peaks of the upd profiles obtained in aqueous or non-aqueous media are more or less independent of sweep-rate at these low sweep-rates.

At low sweep-rates (up to ca. 1 V s^{-1}), the anodic peak potentials are independent of s, although it is to be noted that this approximate constancy of the anodic peak potentials with s, especially in the non-aqueous media, is only over a relatively small range of sweep-rate. The constancy of the anodic peak potentials with s is an indication that the Pb dissolution process, which gives rise to these peaks, is a reversible process, at least at these low sweep-rates.

It is of interest that while the anodic peaks due to Pb oxidation from the Au electrode surface are evidently not sensitive to s at low sweep-rates, this is not always the case for the cathodic peaks, as will be discussed below. In general, as the sweep-rate is raised, the anodic peak potentials shift to more positive potentials, an indication of transition from kinetic reversibility to kinetic

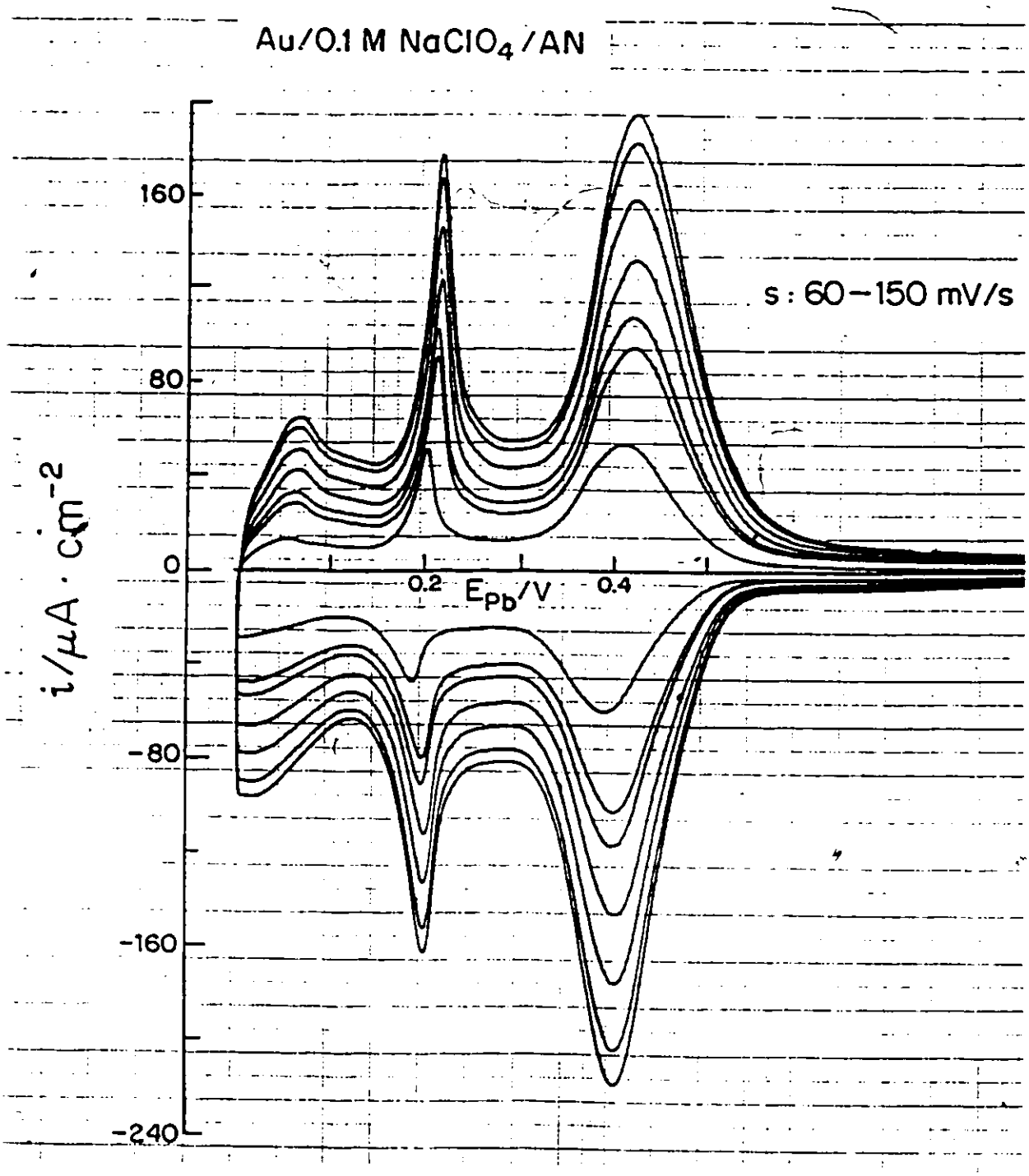

Fig. 6.1 Series of superimposed cyclic-voltammetry i vs E profiles for Pb upd at Au from 0.1M $NaClO_4$ + 10^{-2}M $Pb(CF_3SO_3)_2$ solution in AN for variable low sweep-rates. Sweep-rate varied from 60 to 150 mV s^{-1}.

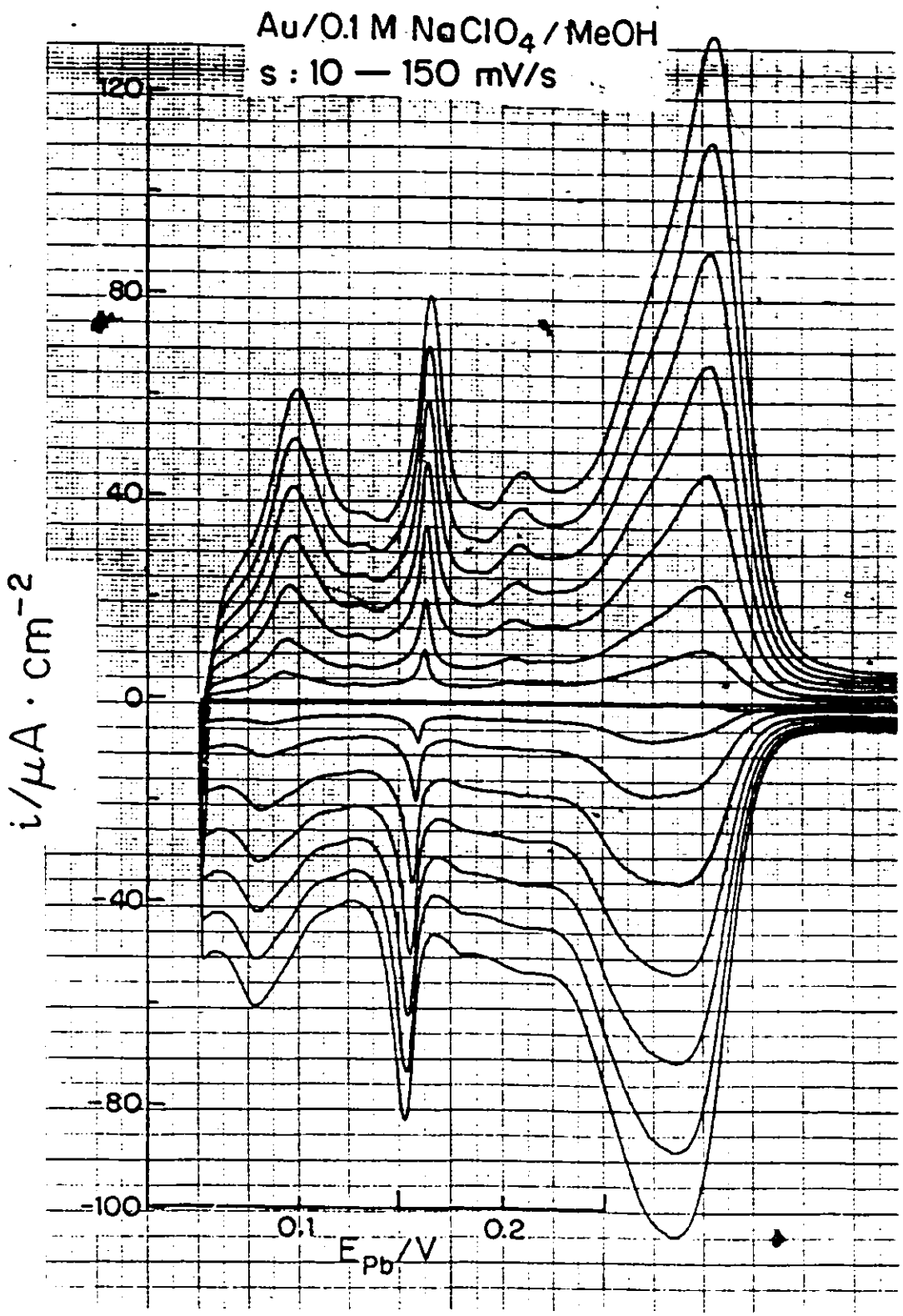

Fig. 6.2 Series of superimposed cyclic-voltammetry i vs E profiles for Pb upd at Au from 0.1M $NaClO_4$ + 10^{-2}M $Pb(CF_3SO_3)_2$ solution in MeOH for variable low sweep-rates. Sweep-rate varied from 10 to 150 mV s^{-1}.

irreversibility, especially at higher sweep-rates. Figs. 6.3(a)–(d) and 6.4(a)–(d) show a series of upd i vs E profiles for Pb at Au obtained in DMF solution of 0.1M $NaClO_4$ at various sweep-rates at 298 and 318 K, and serve as representative behaviour of the profiles obtained in the other non-aqueous solvents used in the present work. As the sweep-rate is increased, the i vs E profile becomes distorted: peak overlap occurs, resulting in less resolution of the upd profiles and hysteresis between the anodic and cathodic peaks becomes significant since the anodic peaks shift to more positive potentials while the cathodic ones shift to more negative potentials with increasing s, as expected for onset of kinetic irreversibility. Peak overlap on the cathodic side of the profile is more marked than on the anodic profile. For example, at $s = 20\ V\ s^{-1}$ (Fig. 6.3(d)), the cathodic side exhibits only one unresolved peak whereas the anodic side shows two peaks.

6.5 Effect of Sweep-rate on the Processes Associated with the Cathodic Peaks

The cathodic peaks of the i vs E should be expected to show more sweep-rate dependence than that for the anodic peaks because the cathodic process may be diffusion-controlled and also influenced by anion adsorption; thus there can be competitive adsorption between the Pb adatoms and the adsorbing ions and solvent molecules, as discussed in Chapter 4.

Examination of the cathodic sides of the upd i vs E profiles shows that, in some solvents, marked effects on the cathodic peaks already arise at low sweep-rates for which any influence of "iR" effects is out of question. For example, for $s = 10\ mV\ s^{-1}$, some interesting observations can be made on the cathodic side of the i vs E profile for Pb upd at Au in the experiment conducted in aqueous $HClO_4$ (see Fig. 6.5). Firstly, as s is diminished, bulk Pb deposition commences at less negative potentials (a phenomenon not observed at higher sweep-rates in the same potential range); secondly, the "spike", C_{Pb5}, is more pronounced at low sweep-rates, i.e. it increases in height (current-density) as the sweep-rate is lowered; thirdly, the first cathodic peak becomes sharper, probably due to anion adsorption effects and, overall, the processes seem to become more reversible. Since the "spike", as remarked earlier, is believed to due to a 2-dimensional phase transtion in the Pb adlayer on the Au electrode surface, then it is understandable that low sweep-rates provide enough

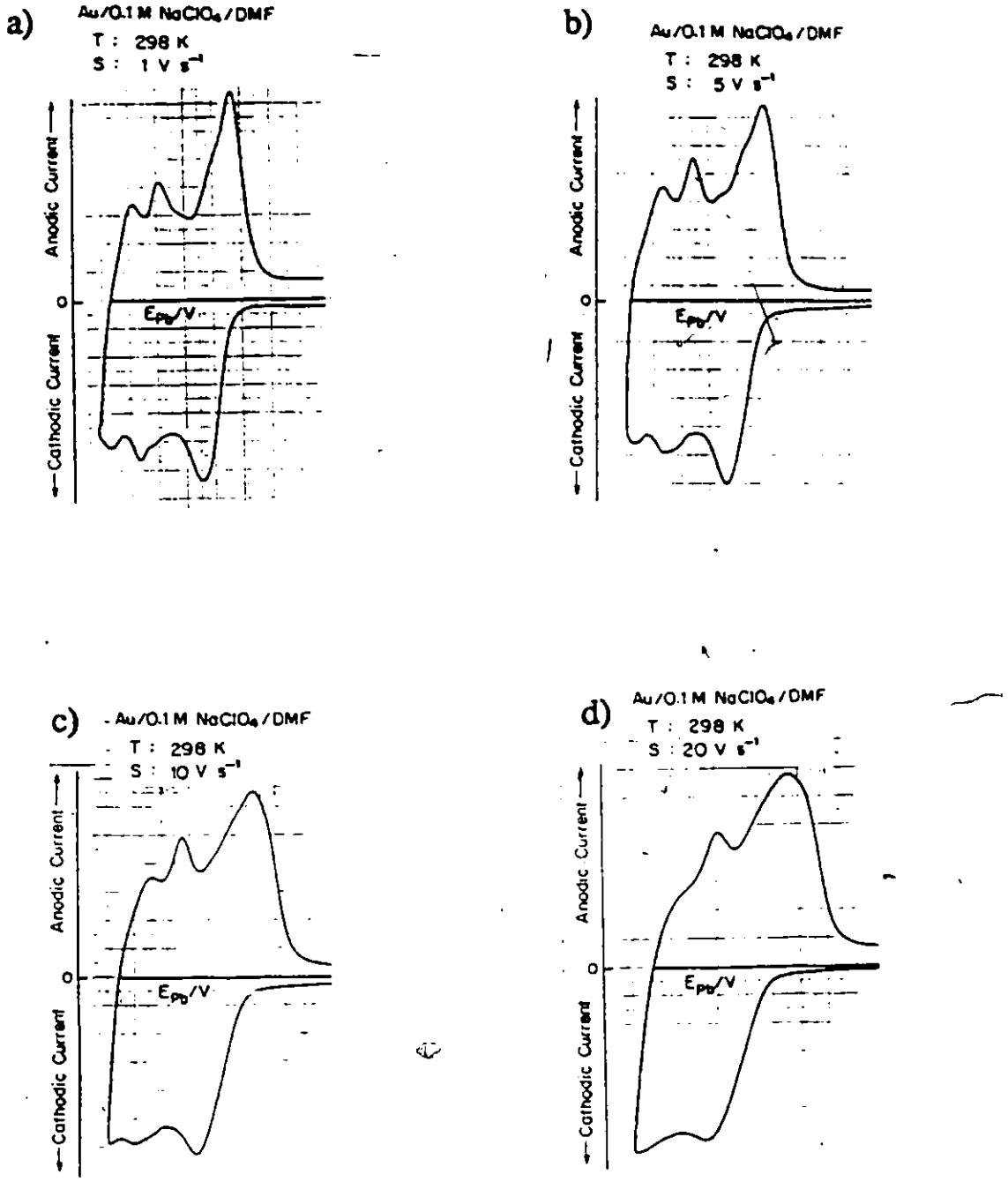

Fig. 6.3 Series of cyclic-voltammetry i vs E profiles for Pb upd at Au from 0.1M $NaClO_4$ + 10^{-2}M $Pb(CF_3SO_3)_2$ solution in DMF at various higher sweep-rates at 298 K: a) 1 V s^{-1} b) 5 V s^{-1} c) 10 V s^{-1} and d) 20 V s^{-1}.

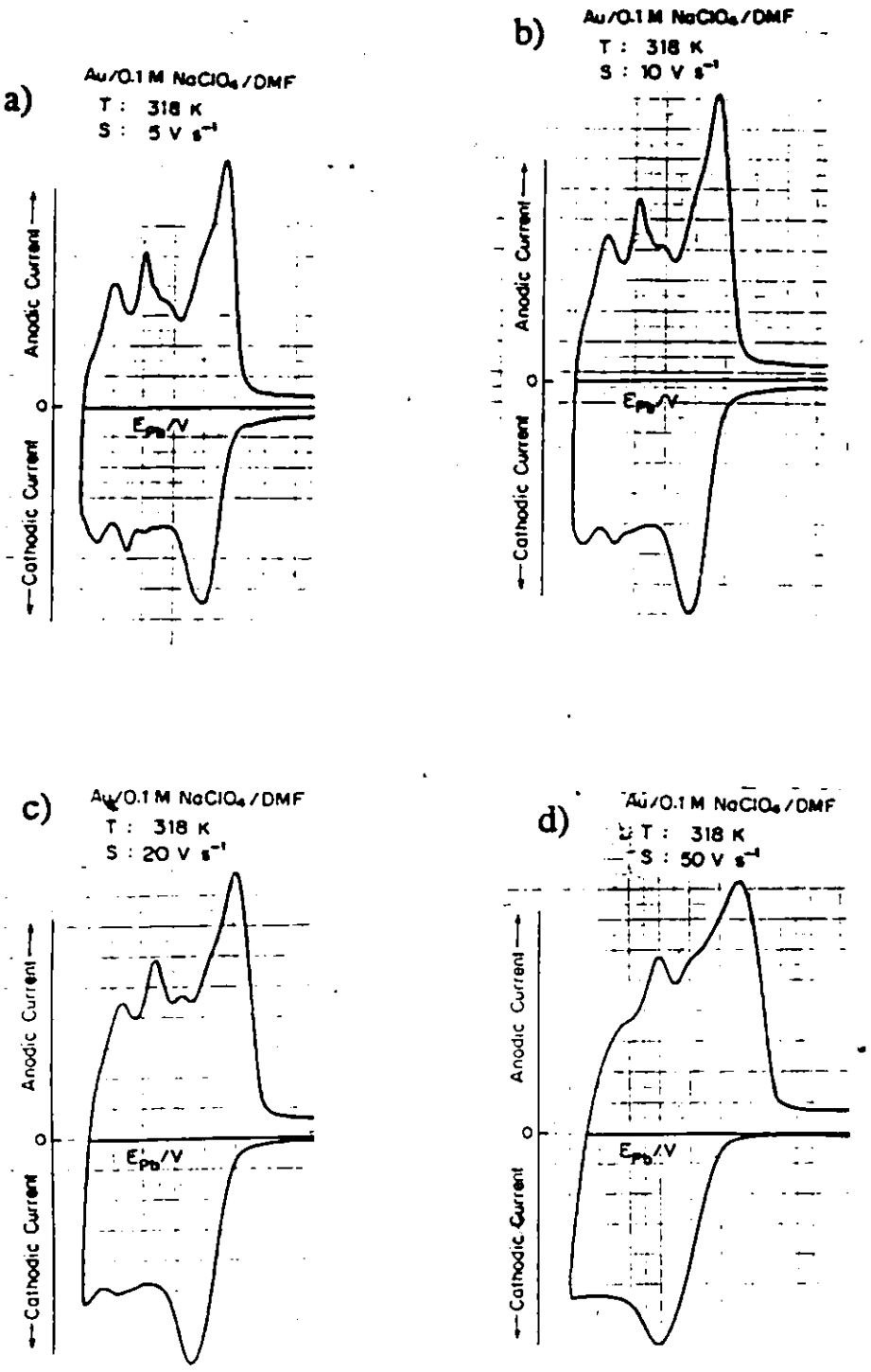

Fig. 6.4 Series of cyclic-voltammetry i vs E profiles for Pb upd at Au from 0.1M $NaClO_4$ + 10^{-2}M $Pb(CF_3SO_3)_2$ solution in DMF at various higher sweep-rates at 318 K: a) 5 V s^{-1} b) 10 V s^{-1} c) 20 V s^{-1} and d) 50 V s^{-1}.

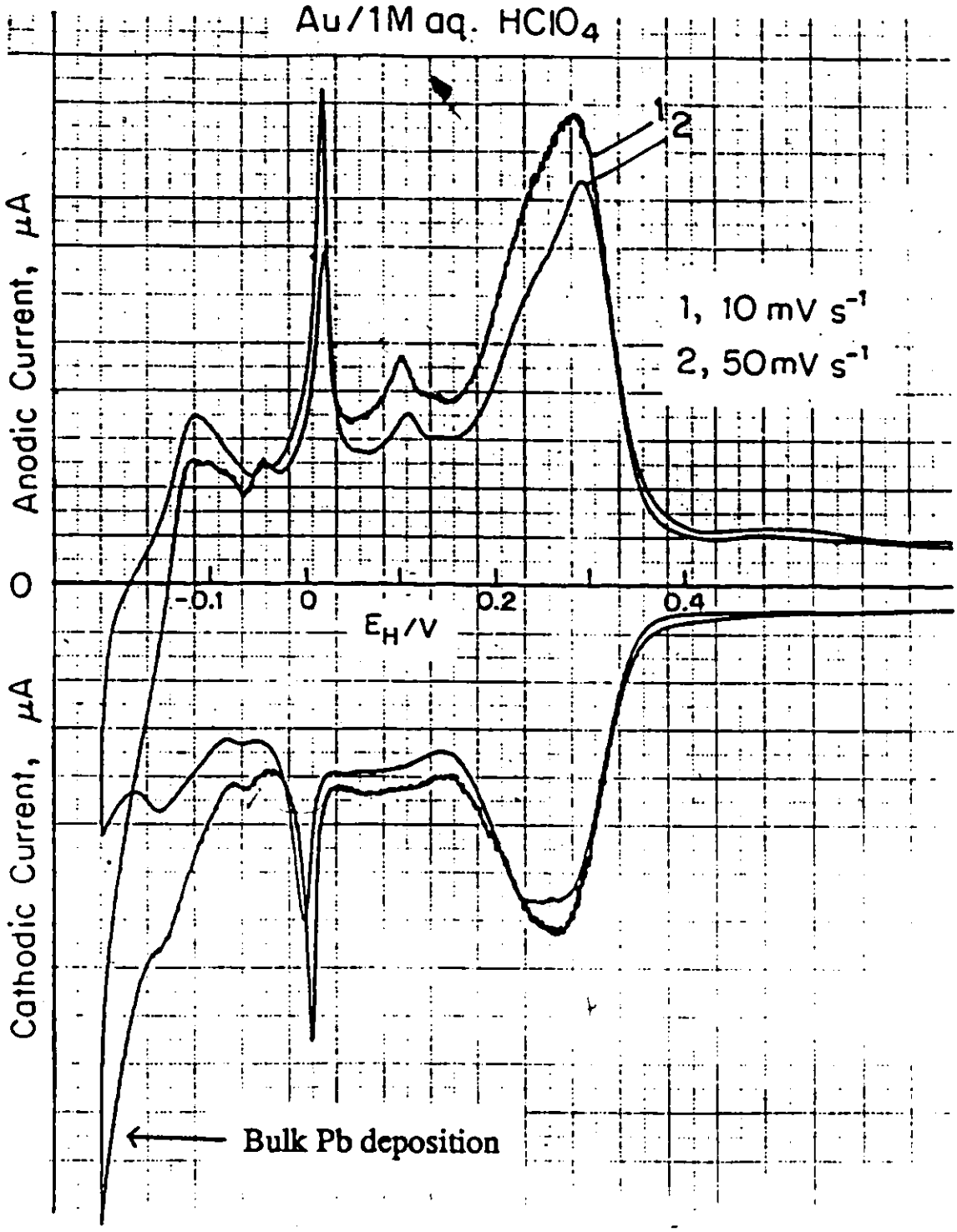

Fig. 6.5 Cylic-voltammetry i vs E profiles for Pb upd at Au in aq. 1M $HClO_4$ + 10^{-3}M $Pb(NO_3)_2$ solution at two low sweep-rates: 1. 10 mV s^{-1} and 2. 50 mV s^{-1}. T: 298 K.

time for this rearrangement to take place. For the non-aqueous solvents at low sweeps, the "spike" is not so pronounced and, in general, the shapes of the cathodic peaks are not affected by the sweep-rate. These pronounced differences observed between the cathodic peak behaviour in experiments conducted in aq. $HClO_4$ and non-aqueous media are evidently solvent dependent. Anion adsorption processes, which are expected to be solvent-dependent, could be responsible for these differences.

As observed with the anodic peaks, the cathodic peak currents also increase progressively with increasing s, as expected, with the peaks retaining their usual shapes. At low sweep-rates, the first cathodic peak, C_{Pb1}, corresponding to the most tightly bound states of Pb on Au, is generally broad but becomes sharpened with increasing s.

Angerstein-Kozlowska and Conway [127] have discussed the effects of adsorbed anions on H and O adsorption on Pt. Anions usually block various states of H and of O adsorption, and, in some cases, this results in a shift of the most positive H peak to more negative potentials. Surprisingly, they found [127] that anion co-adsorption increased the standard rate constant for the H adsorption process, presumably due to anion interaction with the transition state [197] . In slow sweep-rates, anions adsorbed in these surface states compete with the deposition of H and shift the H(2) peak to somewhat more negative potentials.

In the present work we have found that at the lowest sweep-rates used (5 or 10 mV s^{-1}) there was a small shift of the first cathodic peak (C_{Pb1}) to somewhat more negative potentials in DMF (see Fig. 6.6) and MeOH (Fig. 6.2) while, in AN and PC, no shift was observed. As is the case with H deposition, at low sweep-rates, anion adsorption, which is solvent-dependent, competes with the electrodeposition of Pb adatoms and shifts the first cathodic peak for Pb deposition to somewhat more negative potentials. For the non-aqueous solvents, no shift of the cathodic peaks is observed, which is an indication that only weak or neglible adsorption of either ClO_4^- (as the supporting electrolyte anion) or $CF_3SO_3^-$ (as the anion of the Pb salt) arises. It should be noted, however, that the concentration of ClO_4^- in aqueous $HClO_4$ is 10 times that in non-aqueous media.

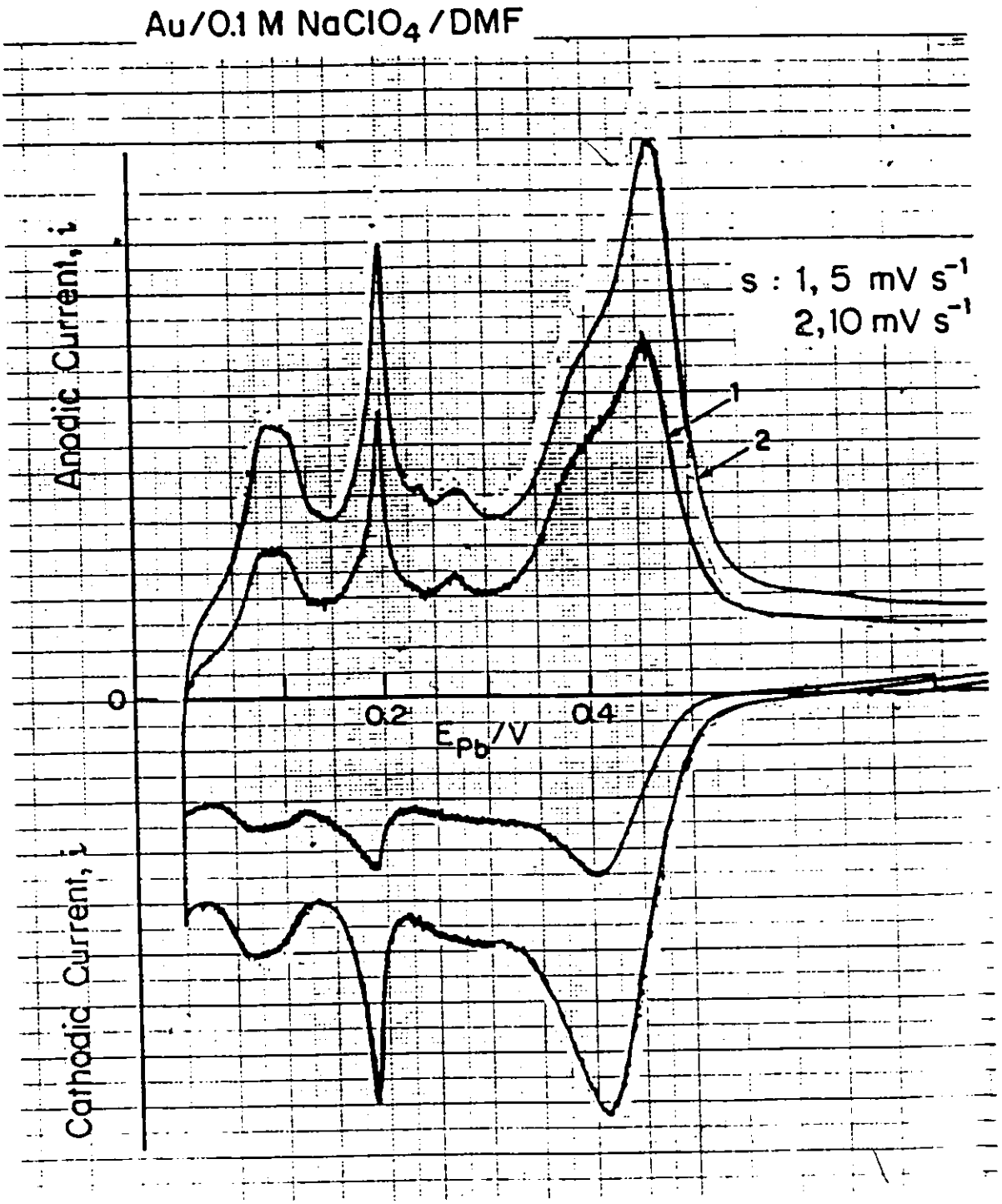

Fig. 6.6 Series of cyclic-voltammetry i vs E profiles for Pb upd at Au from 0.1M $NaClO_4$ + 10^{-2}M $Pb(CF_3SO_3)_2$ solution in DMF at low sweep-rates at 298 K: 1) 5 mV s^{-1} and 2) 10 mV s^{-1}.

6.6 Effect of Temperature

As the temeperature is raised, the upd process remains reversible up to higher sweep-rates as the upd profiles obtained at 318 K show (Fig. 6.4). The distortion of the upd profile becomes significant for $s \geq 50$ V s^{-1}, compared to $s = 20$ V s^{-1} at 298 K. At higher temperatures, the solution resistance, of course, becomes diminished and the diffusion-controlled process of transport of Pb^{++} ion is also minimized.

6.7 Tafel-type Plots: Evaluation of the s_o Parameter

The anodic and cathodic peak potentials ($E_{p,a}$ and $E_{p,c}$ of the cyclic-voltammetry i vs E profiles obtained in some of the experiments conducted in non-aqueous media are plotted vs log s in Figs. 6.7 to 6.9 and 6.11 to 6.13

These Tafel-type plots exhibit three regions, viz: a region where $E_{p,a}$ or $E_{p,c}$ is independent of log s (characteristic of kinetically reversible behaviour); a transition region (changing from reversible to irreversible kinetic behaviour) and a region where $E_{p,a}$ or $E_{p,c}$ is logarithmic in s (characteristic of kinetically irreversible behaviour) as the sweep-rate is increased from low to higher values in the range over which the peak potentials can be followed, i.e. peak resolution is maintained.

Extrapolation of the Tafel-type region for which $E_{p,a}$ or $E_{p,c}$ is logarithmic in s to the line where $E_{p,a}$ or $E_{p,c}$ is virtually independent of log s, gives the so called s_o parameter [128] which characterizes the kinetics of Pb desorption or adsorption on the Au electrode surface in the various non-aqueous solvents used in the present study. In the region where $E_{p,a}$ or $E_{p,c}$ is logarithmic in s, there is some deviation from linearity in log s at substantially higher sweep-rates (ca. $s \geq 30 - 50$ V s^{-1}) which is probably due to "iR" drop effects that begin to become significant at these higher sweep-rates.

Stonehart, Angerstein-Kozlowska and Conway [198] made the first calculations on the effect of "iR" drop on i vs E profiles for an electrode surface process in LPS experiments. These authors showed that, depending on the magnitude of R, significant distortions of the i vs E profiles can arise.

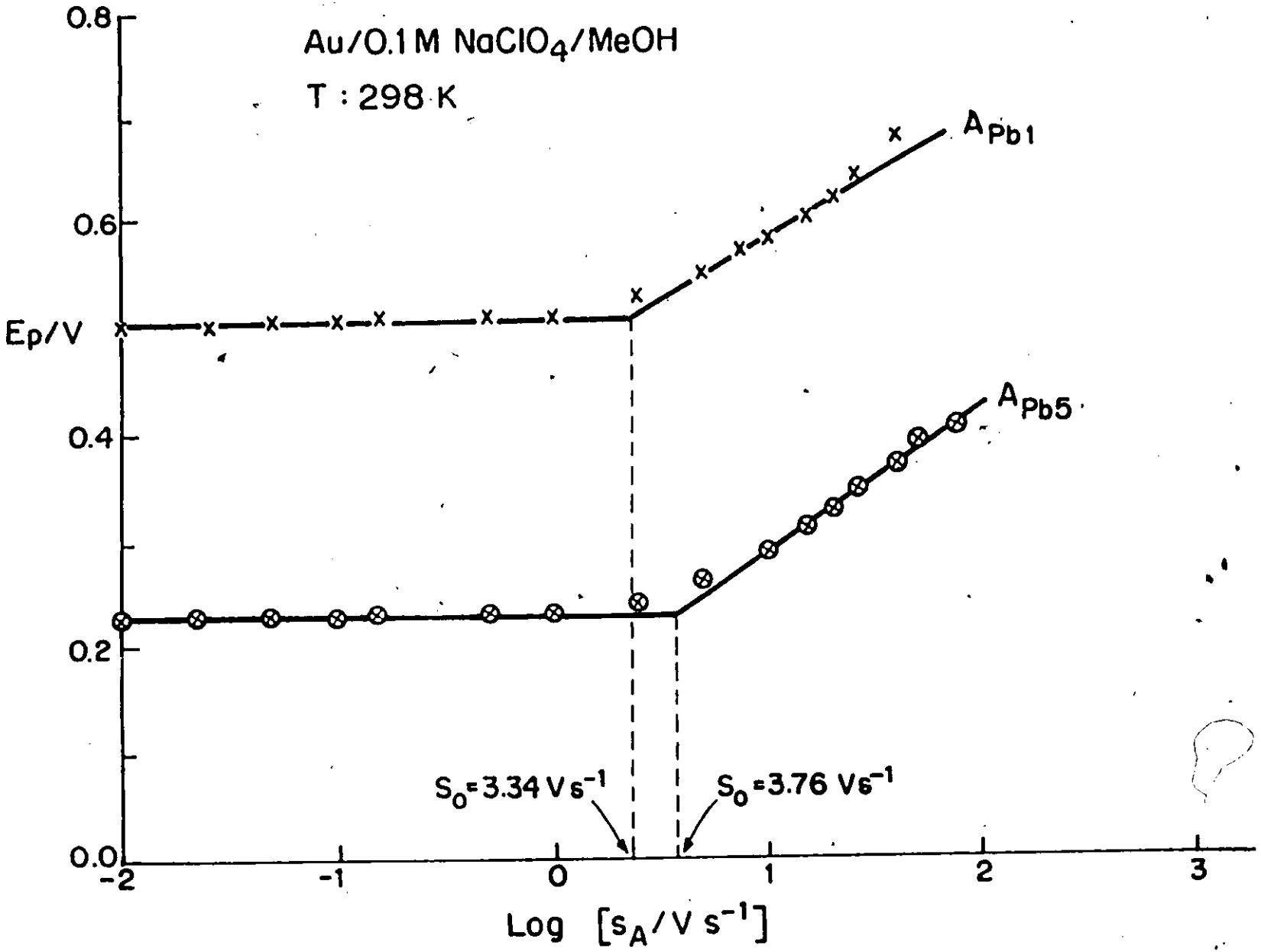

Fig. 6.7 Variations of peak potentials vs log s for desorption of Pb ad-states at Au in 0.1M $NaClO_4$ + 10^{-2}M $Pb(CF_3SO_3)_2$ solution in MeOH at 298 K.

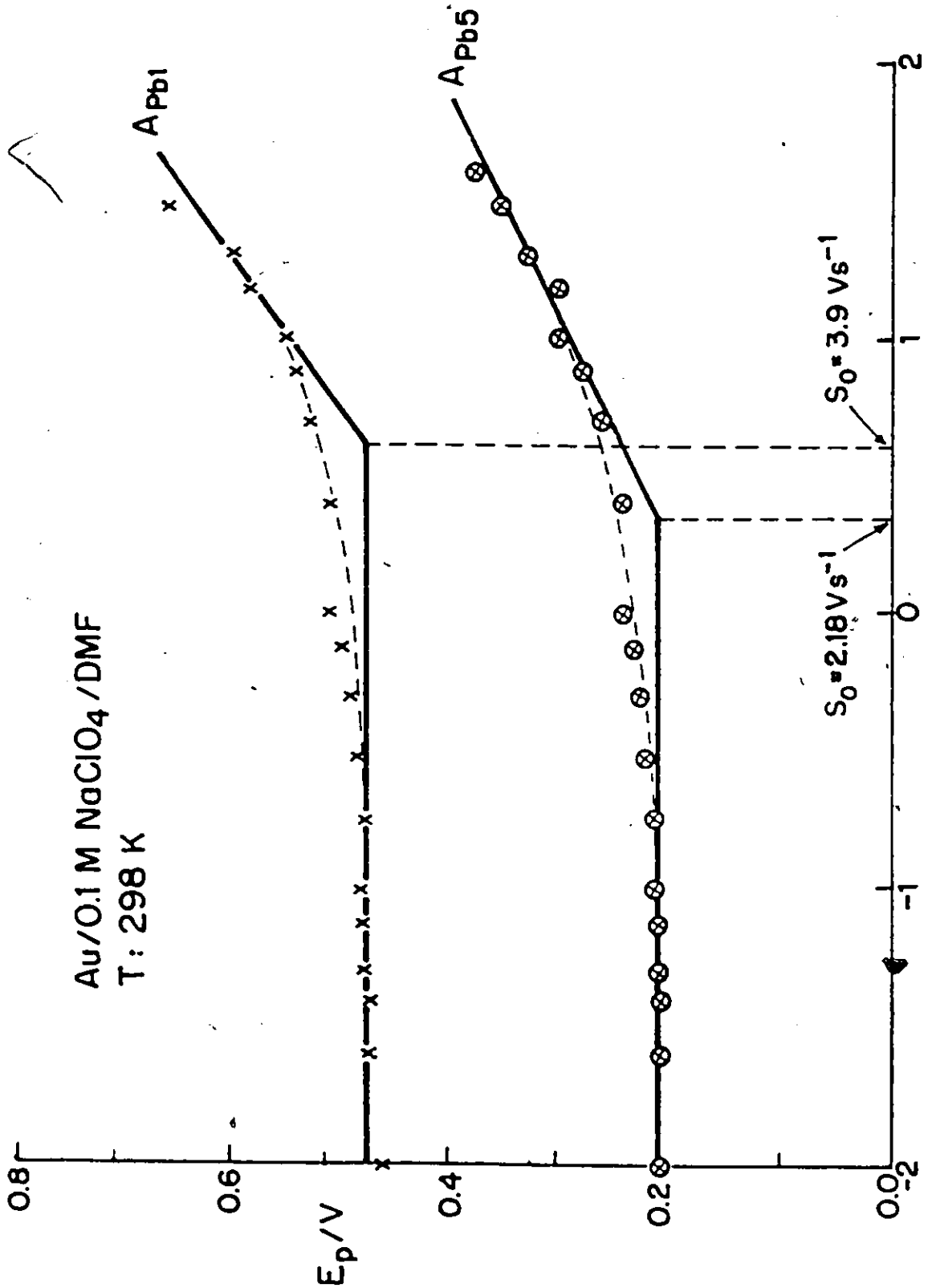

Fig. 6.8 Variations of peak potentials vs log s for desorption of Pb ad-states at Au in 0.1M $NaClO_4$ + 10^{-2}M $Pb(CF_3SO_3)_2$ solution in DMF at 298 K.

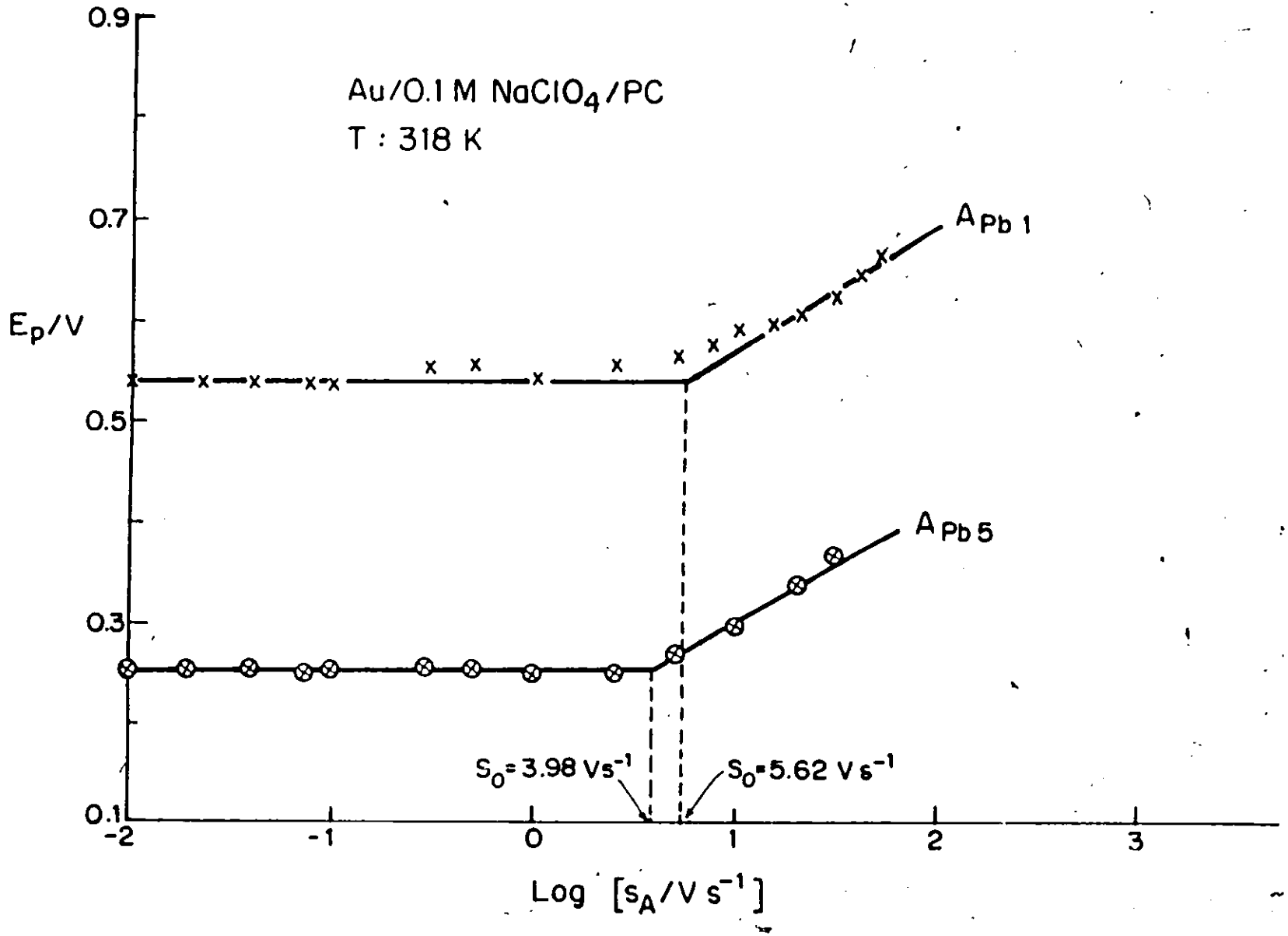

Fig. 6.9 Variations of peak potentials vs log s for desorption of Pb ad-states at Au in 0.1M $NaClO_4$ + 10^{-2}M $Pb(CF_3SO_3)_2$ solution in PC at 298 K.

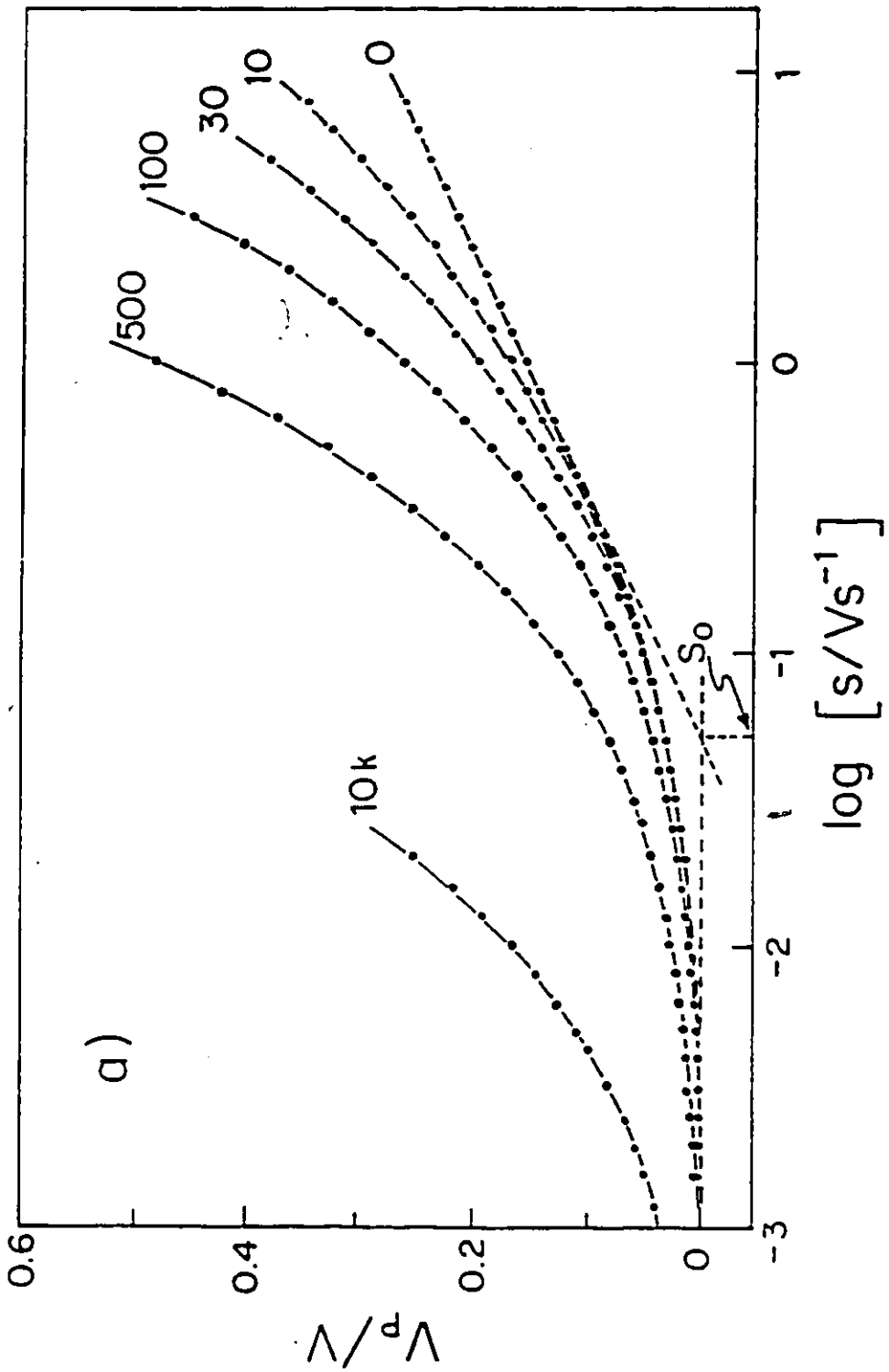

Fig. 6.10 Dependence of apparent peak potential on log s for various values of R_u. (From ref. 200).

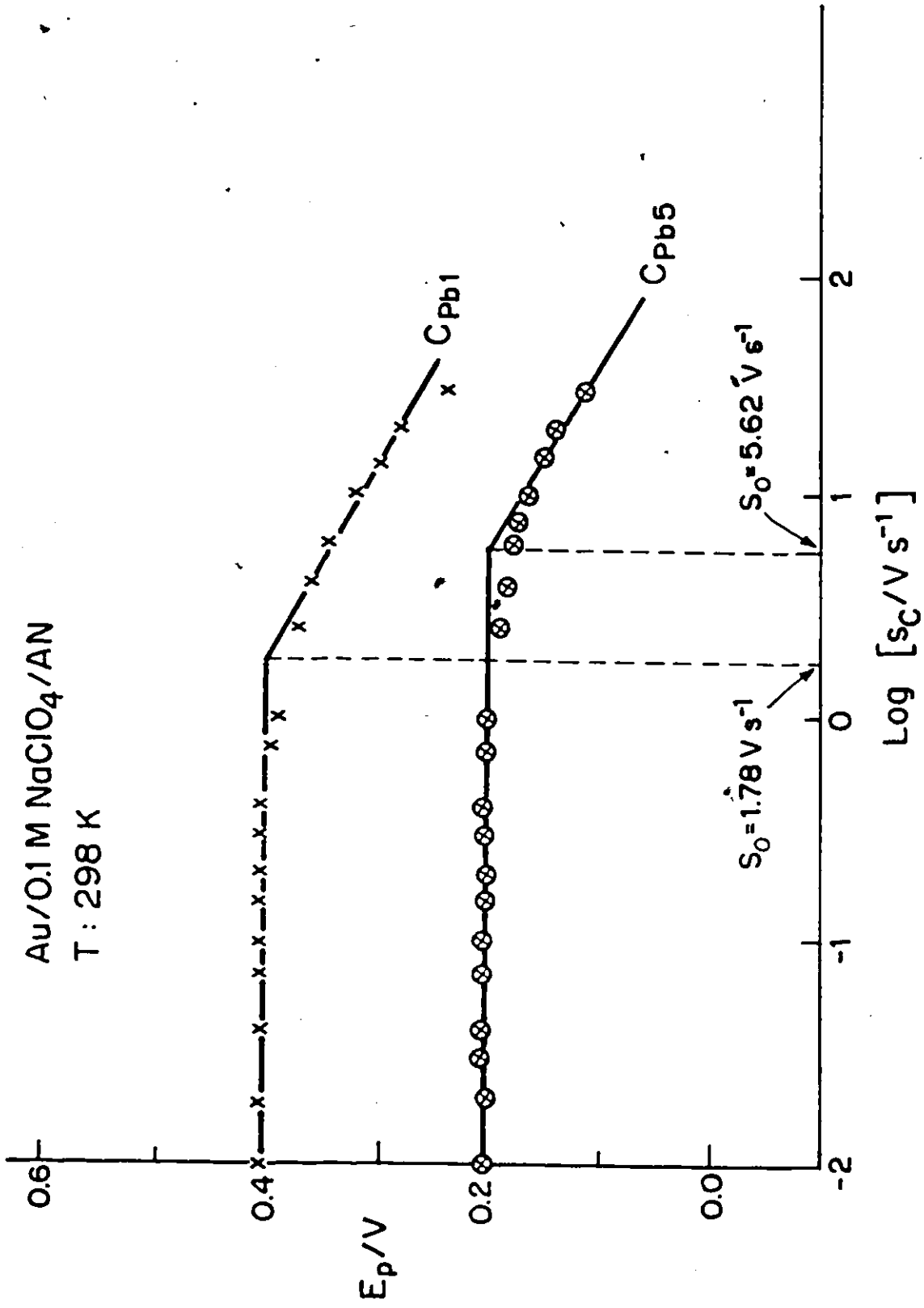

Fig. 6.11 Variations of peak potentials vs log s for deposition of Pb ad-states at Au in 0.1M $NaClO_4$ + 10^{-2}M $Pb(CF_3SO_3)_2$ solution in AN at 298 K.

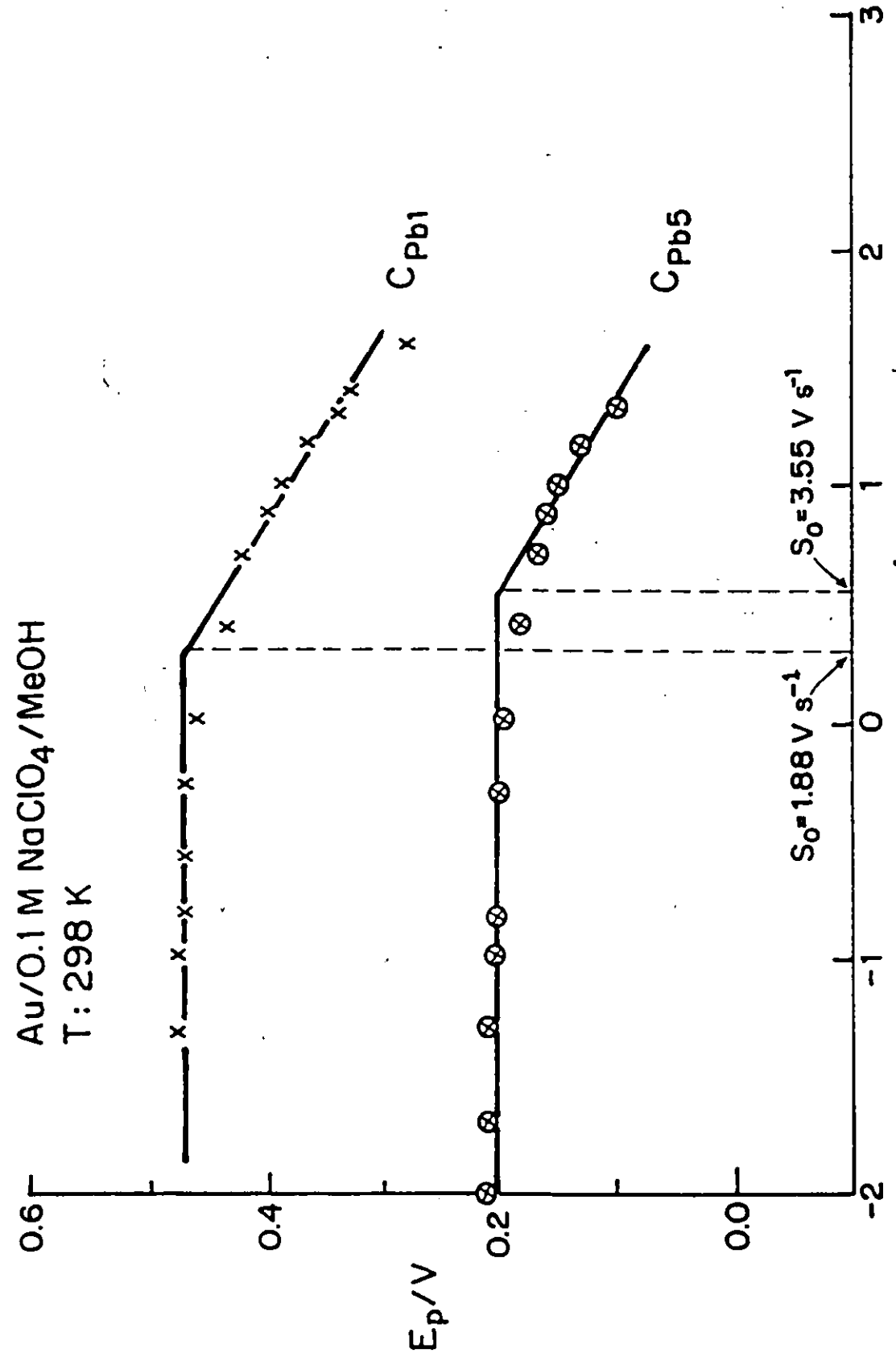

Fig. 6.12 Variations of peak potentials vs log s for deposition of Pb ad-states at Au in 0.1M $NaClO_4$ + 10^{-2}M $Pb(CF_3SO_3)_2$ solution in MeOH at 298 K.

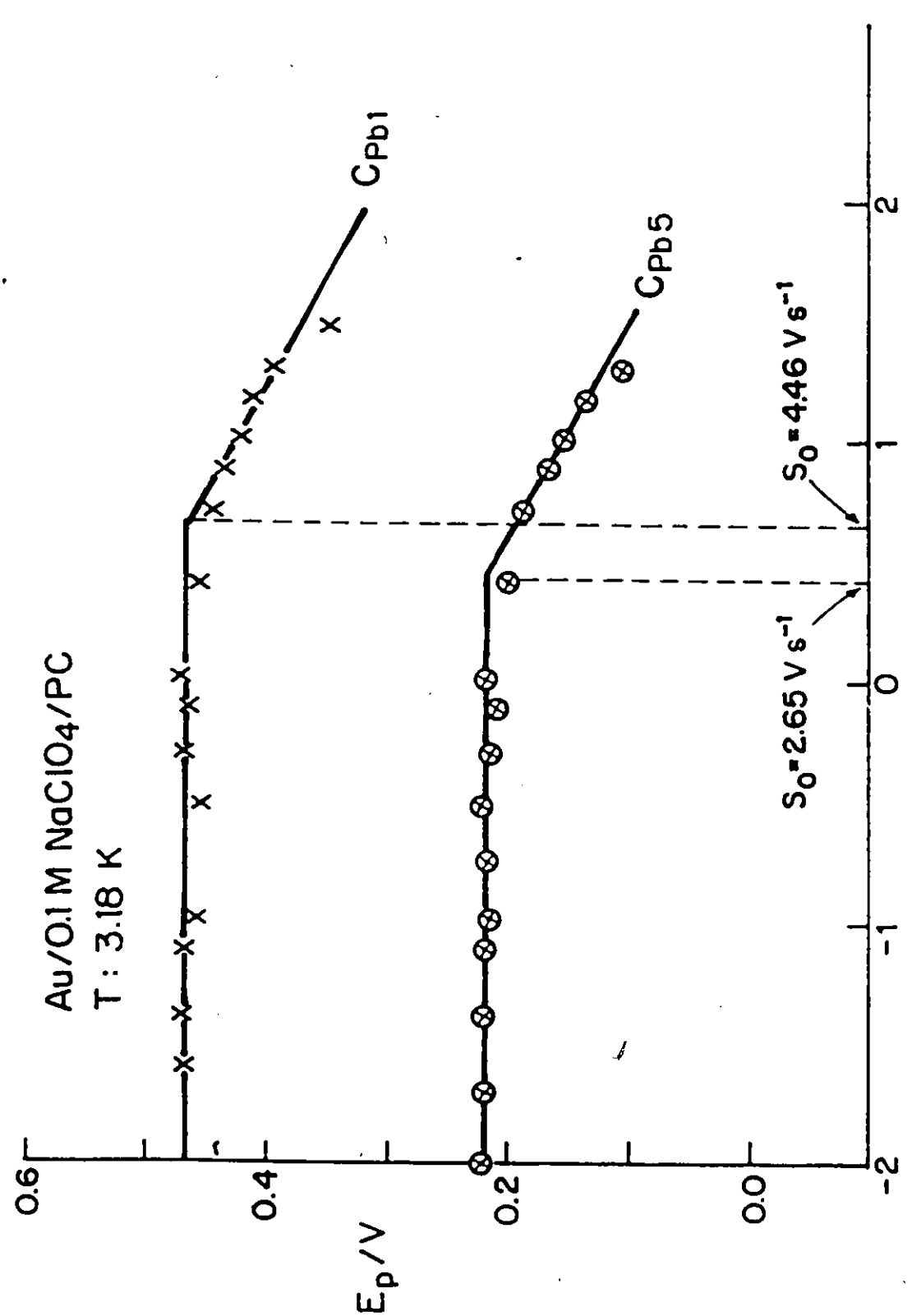

Fig. 6.13 Variations of peak potentials vs log s for deposition of Pb ad-states at Au in 0.1M $NaClO_4$ + 10^{-2}M $Pb(CF_3SO_3)_2$ solution in PC at 298 K.

Uncompensated "iR" drop effects have also been discussed by Roullier and Laviron [199] in the case of quasi-reversible surface process. They showed theoretically that "iR"- drop effects can induce changes in i vs E profiles over a small range of s similar to those due to kinetic irreversibility. This implies that transition of E_p behaviour to log s dependence can also apparently arise from "iR" drop effects as well as from change from kinetic reversibility to irreversibility. More recently Tessier and Conway [200] have discussed, in a more fundamental way, the nature of the "iR" drop effects on i vs E profiles and the anticipated extent of the "iR" effect in the evaluation of the kinetic parameter, s_o, at various arbitrary values of R (see Fig. 6.10). They showed that when "iR" drop effects are significant, the corresponding transition in the value of the pseudocapacitance, C_ϕ, with increasing log s can usually allow spurious "iR" and significant irreversibility effects to be distinguished. In the present work, we believe that the transition from log s independence to log s dependence, especially at sweep-rates where $E_{p,a}$ or $E_{p,c}$ is linear in log s, is due to change from kinetic reversibility to kinetic irreversibility of the surface process since "iR" drop effects could not be very significant because of low currents associated with upd processes. Examination of the upd i vs E profiles also indicate the absence of any significant "iR" drop effects at these sweep-rates.

The evaluated s_o values for the two anodic peaks, A_{Pb1} and A_{Pb5}, in the experiments conducted in the various non-aqueous solvents at indicated temperatures are given in Table 6.1. The s_o values obtained from the Tafel-type plots of the anodic peaks are expected to more reliable than those obtained from the plots using the cathodic peak potential values since the kinetics of the processes associated with cathodic peaks can sometimes be complicated by the anion adsorption/desorption effects which the present work has demonstrated (see Chapter 4, Section 4.5) are solvent-dependent. Also as s is raised, diffusion effects can become significant and affect the kinetics of Pb deposition. The s_o values obtained (Table 6.1) for experiments conducted in non-aqueous solvents are generally lower than those found for the aqueous medium. At 298 K, with AN as solvent, gives the highest s_o values for the anodic peaks (6.7 V s^{-1} for A_{Pb1} and 6.3 V s^{-1} for A_{Pb5}). Except for MeOH as solvent, it is to be observed that the s_o value for the process associated

Table 6.1 **Estimated s_o Parameters for the Deposition and Desorption of Pb at Au in Various Non-aqueous Solvents and at Different Temperatures**

Solvent	T/K	s_o(V s^{-1})			
		(A_{Pb1})	(A_{Pb5})	(C_{Pb1})	(C_{Pb5})
AN	273	4.2	3.0	1.0	1.8
	298	4.7	6.3	1.8	5.6
MeOH	268	2.5	1.6	0.9	
	298	2.3	3.8	1.9	3.6
DMF	278	4.0	2.1	3.2	
	298	4.0	2.2	3.5	2.6
	318	7.1	6.3	7.2	6.3
PC	298	2.8	2.4	2.6	1.2
	318	5.6	4.0	4.5	2.7

with peak A_{Pb1} (due to desorption of Pb adatoms most tightly bound to Au) is higher than that for the process A_{Pb5} (the "spike" which corresponds to a 2-dimensional phase transition). Thus, the process associated with A_{Pb1} remains reversible up to higher sweep-rates than for A_{Pb5}.

As would be expected, the s_o value for either of the A_{Pb1} or A_{Pb5} peaks in any given solvent is temperature-dependent. In general, except for a few discrepancies, the s_o value for any particular peak increases with temperature, although for one solvent, DMF, the s_o values at 278 K and 298 K are close for the two anodic peaks. Increease in s_o value with rise in temperature is expected as the solution resistance and diffusion-influence is decreased with increase in temperature.

At higher sweep-rates where $E_{p,a}$ becomes dependent on log s, it is observed that $E_{p,a}$ for process A_{Pb5} is more linearly dependent on log s than for A_{Pb1} in the sweep-rate range over which the two peaks can be followed (Figs. 6.7 to 6.9). However, for the range in log s over which A_{Pb1} can be followed, E_p vs log s deviates from linearity at higher sweep-rates probably because of "iR" drop effects which, as we have mentioned, can lead to difficulties in the correct evaluation of the s_o value. Transition from independence of $E_{p,a}$ on log s to dependence on log s is solvent-dependent: in some solvents, e.g. MeOH, the transition is sudden whereas in DMF it is smooth, occurring almost over 1 decade of log s (Figs. 6.8 and 6.9).

The s_o values obtained for the cathodic peaks, C_{Pb1} and C_{Pb5}, from the experiments conducted in non-aqueous media, are summarized in Table 6.1 together with those for the anodic peaks. In the range of s for which $E_{p,c}$ becomes logarithmic in s, the peak potentials of C_{Pb5} are linearly dependent on log s over the whole range of potentials in which the peaks can be resolved. However, for the peak potentials of C_{Pb1}, there is deviation from linearity in the Tafel-type plot of E_p vs log s (Figs. 6.11 to 6.13), for the same reasons given for anodic peaks. These effects, coupled with complications due to anion adsorption process, probably explain why the s_o values for the processes associated with the cathodic peaks are generally smaller than those for the corresponding anodic peaks (Table 6.1).

Inspection of Table 6.1 shows that, for any given solvent, the s_o values for the anodic "spike" (A_{Pb5}) are approximately equal to those for the coprresponding cathodic "spike" (C_{Pb5}), although the

values for any given pair vary from solvent to solvent. This indicates that the kinetic reversibility of the 2-dimensional phase-transition, the process commonly attributed to these peaks, is solvent dependent. It is least affected by anion adsorption processes becuse it corresponds already to a coverage θ_{Pb} of ca. 68%. At this coverage, most of the Au surface is already covered by the Pb adatoms so that most of the anions have already been desorbed during the cathodic sweep up to the potential of the "spike". Similarly, on the anodic side, the Au electrode is still extensively covered by Pb adatoms so that few anions can be re-adsorbed.

As observed for the anodic peaks, except for the results in MeOH, the s_o value of the cathodic peak C_{Pb1} is larger than that of C_{Pb5}. Also the s_o values increase with rise in temperature for the same reasons given for the anodic peaks, although the values obtained at 298 K and the next lower temperature are comparable in most cases.

6.8 Slopes of the Tafel-type Relations

In the range of s where E_p is linearly logarithmic in s, Tafel-type slopes, $dE_{p,a}/d\log s$, were estimated and the values obtained are summarized in Table 6.2. Because of the uncompensatable "iR" drop effects, accurate evaluation of the Tafel-type slopes is difficult and hence the values obtained are only approximate. However, within the limits of experimental error, most of the values obtained for the Tafel slopes are actually close to the theoretically expected value, 120 mV/ decade of s, i.e. $2.3\,RT/\beta F$ with $\beta \cong 0.5$. At 298 K, the slopes of the Tafel-type relations for the anodic A_{Pb1} vary from 105 mV/decade in s (in PC) to 170 mV/decade in s in AN and DMF; while for A_{Pb5} the slopes range from 115 mV/decade in s in PC to 140 mV/decade in s in AN. In general, the values obtained in DMF and AN are higher than the corresponding values obtained in PC and MeOH. The higher values could be due to "iR" drop effects at these higher sweep-rates. In most cases, the slope of the plot for A_{Pb1} is higher than that for the plot of A_{Pb5} and this difference could not arise from the "iR" drop effect. The values obtained for the various Tafel slopes are consistent with the theoretically expected slope for a surface process, taking $\beta = 0.5$. Abnormally low Tafel slopes would conventionally indicate that a multi-step mechanism is involved, which is physically

Table 6.2 Estimated Slopes from the Tafel-type Plots for the Adsorption/Desorption of Pb at Au in Various Non-aqueous solvents and at Different Temperatures

Slovent	T/K	$dE_p/d\log[s_{A,C}/V\ s^{-1}]$			
		(A_{Pb1})	(A_{Pb5})	(C_{Pb1})	(C_{Pb5})
AN	273	195	140	-130	-90
	298	170	140	-115	-120
MeOH	268	110	80	-125	
	298	120	140	-125	-115
DMF	278	180	125	-210	
	298	170	125	-135	-125
	318	145	115	-145	-110
PC	298	105	115	-140	-120
	318	120	115	-110	-110

unlikely here, although surface diffusion is one possibility.

In the case of cathodic peaks, the range of peak potentials for which $E_{p,c}$ varies linearly in log s is rather limited and, as with the anodic peaks, there is some deviation from linearity at the higher sweep-rates (Figs. 6.10 to 6.12). Most of the estimated values of the slopes from the Tafel-type plots are close to the theoretically expected value, -120 mV/decade s, i.e. $-2.3RT/\beta F$ for a cathodic surface process with $\beta = 0.5$ again.

It is of interest to note that a process that involves an adsorbed state (of Pb) as reactant or product of ion (Pb^{++}) discharge the value of β is still near 0.5 as it is for many ionic outer-sphere redox reactions where neither product nor reactant are chemisorbed.

CHAPTER 7

TEMPERATURE EFFECTS ON THE UPD OF Pb AT Au

7.1 Entropy of 2-Dimensional Array States of UPD Pb Atoms

One of the principal thermodynamic factors of interest in the formation of 2- dimensional (2-d) lattices of adatoms on metal surfaces is the standard entropy, ΔS°, of formation or desorption of the adatoms (see Section 4.1). In the case of electrochemically formed adatom arrays, submonolayer states can be well resolved and the peak potentials of the cyclic-voltammograms give the Gibbs energies of the distinguishable states, the peak potential, E_p, being a standard potential for half-coverage of the array when the pseudocapacitance vs potential profile is symmetrical. Normally the E_p values are referred to a reference electrode in the same solution; here Pb/Pb^{++} for the non-aqueous solutions or H_2/H^+ in the aqueous solution case. Then from the determinations of the dependence of the E_p values on temperature, we can readily find the corresponding entropies of the states, i.e. $F.dE_p/dT = \Delta S$ or ΔS° for some appropriate standard state conditions.

The ΔS quantities are of considerable interest because, from their values, it can usually be indicated what states of mobility and/or vibrations the adatoms are in, e.g. are there arrays of 2-dimensionally mobile or immobile adatoms, for which cases the ΔS° values are expected to be substantially different as may be calculated from the respective partition functions.

This part of the work is therefore concerned with the evaluation and interpretation of the temperature-dependence of E_p values and calculation of the corresponding entropies of sub-monolayer states of Pb developed at Au in the various solvent systems described earlier in this thesis.

7.2 Problems in Measurement of dE_p/dT in Relation to Derivation of the ΔS_{Pb} Quantities

A general problem arises with derivation of entropy changes for single electrode processes from temperature-dependence of electrode potentials; here the problem arises with evaluation of

dE_p/dT: if E_p values are referred to a reference electrode in the same given solution, at the same temperature as the test electrode (the so-called isothermal cell measurement), then the recorded cell potential measurements at various temperatures includes the normally finite absolute variation of the reference electrode potential with temperature; hence only apparent dE_p/dT values result. Alternatively a non-isothermal cell measurement may be made, with the test electrode held at various temperatures, with the potential being measured against a reference held at constant temperature. This type of cell involves an unavoidable thermal liquid junction potential, E_j, between two solutions at the different temperatures but can be minimized (to ca. 1 mV) by using a salt-bridge thermal liquid junction. This arrangement was employed in the present work. The EMF of such non-isothermal cells also involves a thermoelectric potential difference between the metal wires at the two temperatures but this is negligible over the experimental temperature range used here.

The two possible cell arrangements are indicated below:

a) **isothermal cell**

M_1		M_2
ref. electrode T (varied)	|	test electrode, T varied (same as at M_1)

b) **non-isothermal cell**

M_1		E_j		M_2
ref. electrode at constant potential, 298 K	/	satd. salt thermal junction, 298 K	/	test electrode, T varied

with (b) being used in the present work; the reference electrode M_1 was Pb^{++}/Pb in the non-aqueous solution experiments and $Pt/H_2/H^+$ in the aqueous $HClO_4$ experiments. The "test electrode, M_2" corresponds to adatom states of Pb at Au (almost) in equilibrium with Pb^{++} in solution, giving the E_p potentials which can be recorded on both the cathodic and anodic sweeps.

Non-isothermal cells, such as (b), have been used by Weaver et al. [201] in studies of entropy of single-electrode redox reactions and by a variety of other workers [202 - 204] for evaluation of single-ion partial molar entropies.

7.3 Temperature Effects on the i vs E UPD Profiles

As discussed earlier in Section 1.5, the upd of H or metal adatoms on foreign metal substrates gives rise to electrochemically distinguishable sub-monolayer states below monolayer coverage, as is also observed even on single-crystal surfaces [39,47]; these distinguishable sub-monolayer states have temperature-dependent standard Gibbs energies of deposition and ionization corresponding to the standard entropies, $\Delta S°$, of their formation or desorption. For Pb at Au it has been found that, depending on the "cleaniliness" of the system and, in the present work, depending on the solvent used (see Chapter 4), up to seven sub-monolayer states can be distinguished. By conducting experiments at various temperatures, interesting information on the states of the upd adatoms of Pb at Au can be obtained by evaluating the temperature-dependence of the peak potentials of the i vs E profiles which leads, as shown below, to information on the entropies of the Pb adatoms in the various resolved states, as observed in the several solvents used.

In the present work the experimental study of the dependence of the peak potentials on temperature required, in most cases, evaluation of the temperature-dependence of the potential of the Pb^{++}/Pb reference electrode (for measurements in non-aqueous media) or the Pt/H_2 reference electrode (for experiments in aqueous medium) in which the reference electrode is in the same solution as the working electrode (Au electrode in the case of the present work). An alternative set-up would involve use of an external reference electrode maintained at a fixed temperature; however, this is less desirable because such an arrangement leads to unavoidable temperature-dependent thermal junction potentials.

A series of potentiodynamic i vs E profiles, recorded for the upd of Pb at Au in 0.1M $NaClO_4$ solutions of AN and DMF over a range of temperatures, are shown as examples in Figs. 7.1 and 7.2, respectively, and are representative of the results obtained in the other non-aqueous solvents used. The corresponding upd profiles obtained in aqueous $HClO_4$ at various temperatures are shown in Fig. 7.3.

On examining the upd i vs E profiles obtained in 0.1M $NaClO_4$ solution in AN (Fig. 7.1), it is observed that there are no significant changes in the shape of the cyclic-voltammetry profiles for

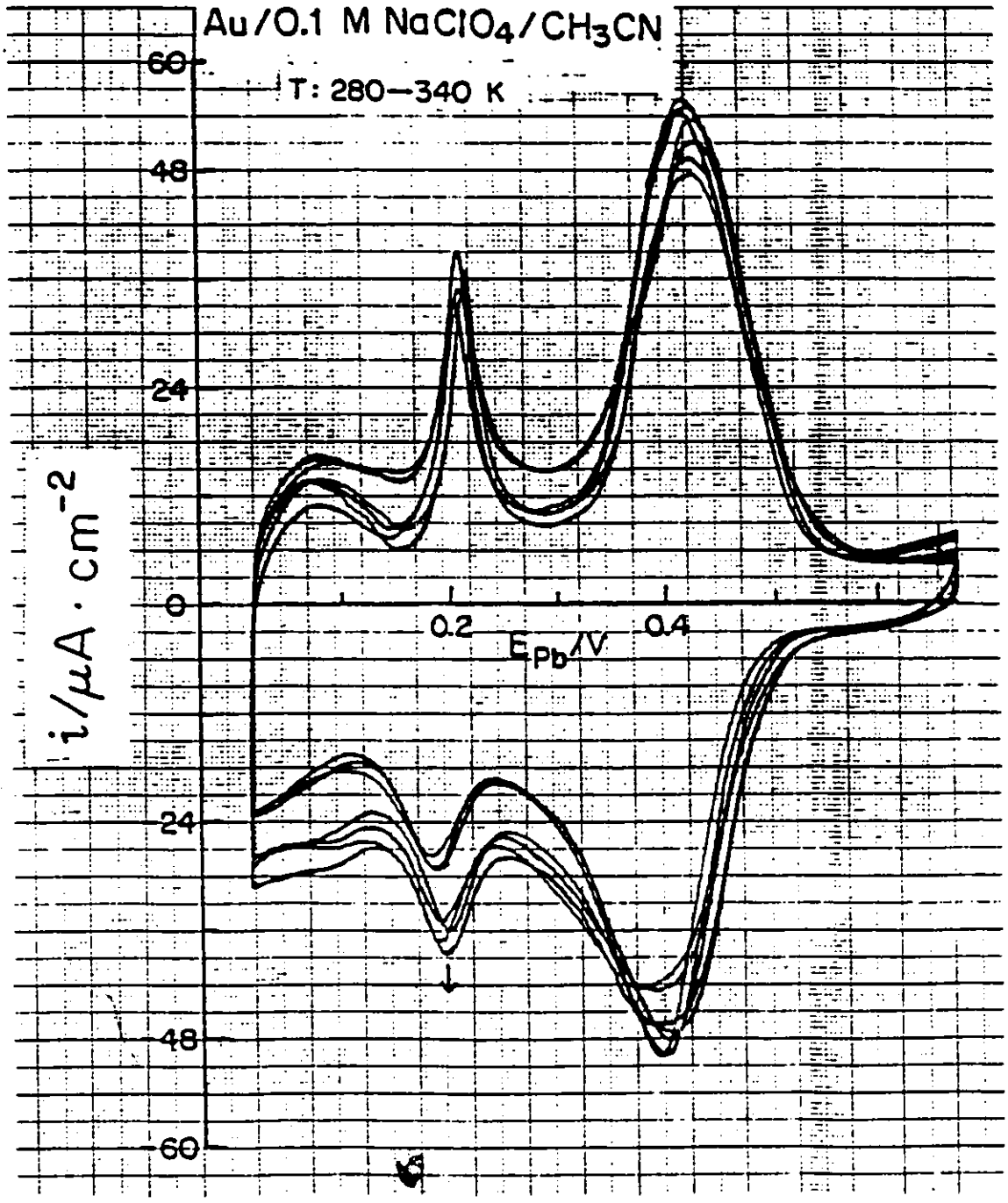

Fig. 7.1 Series of superimposed i vs E upd profiles for Pb upd at Au from 0.1M $NaClO_4$ + 10^{-2}M $Pb(CF_3SO_3)_2$ solution in AN with increasing temperature in the range 280 to 340 K. s = 50 mV s^{-1}.

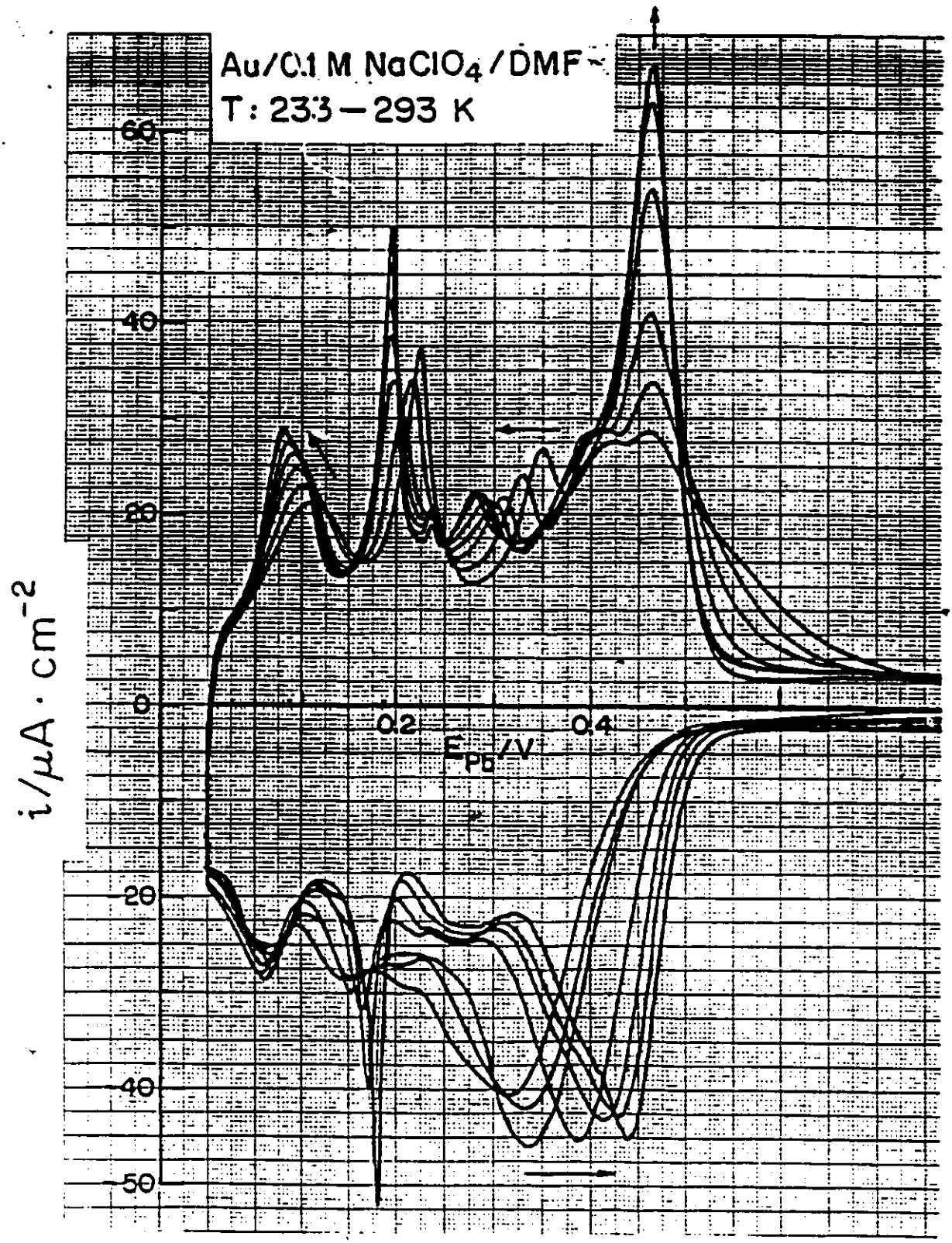

Fig. 7.2 (a) Series of superimposed i vs E upd profiles for Pb upd at au from 0.1M $NaClO_4$ + 10M $Pb(CF_3SO_3)_2$ solution in DMF with increasing temperature in the range 233 to 293 K. Arrows indicate the direction of the shift of the curves with increasing temperature. s = 50 mV s^{-1}.

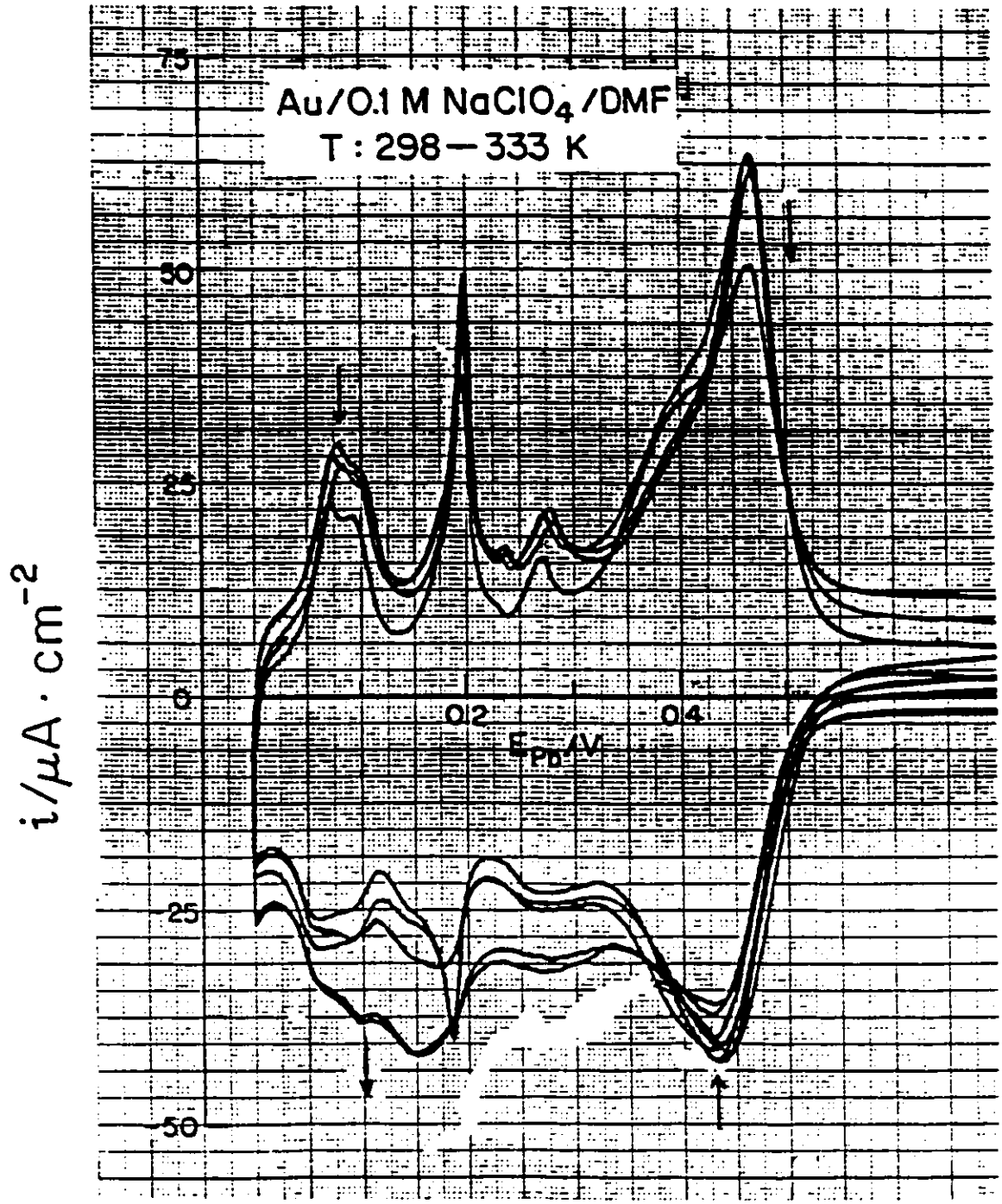

Fig. 7.2 (b) Series of superimposed i vs E upd profiles for Pb upd at au from 0.1M $NaClO_4$ + 10M $Pb(CF_3SO_3)_2$ solution in DMF with increasing temperature in the range 298 to 333 K. Arrows indicate the direction of the shift of the curves with increasing temperature. s = 50 mV s^{-1}.

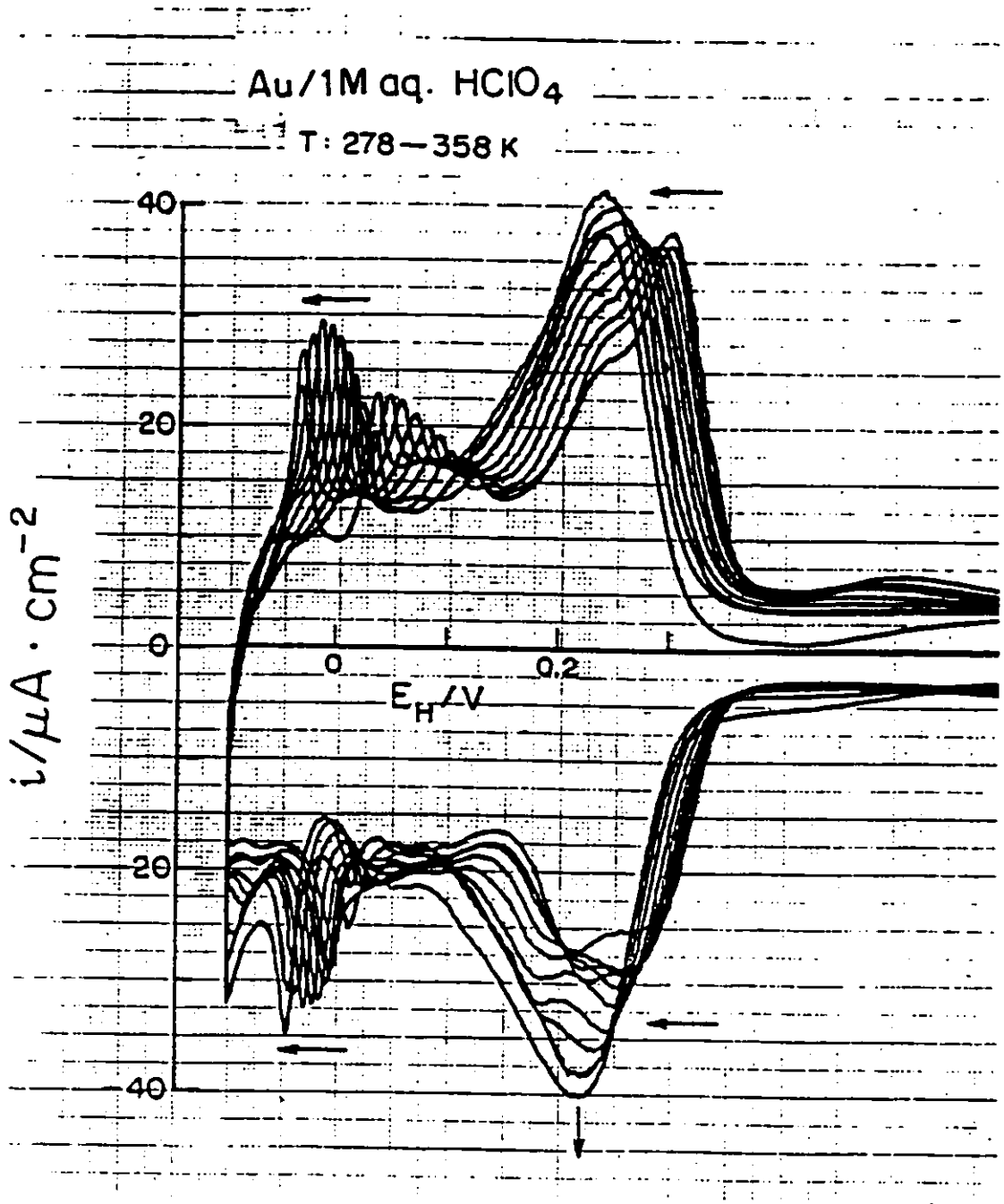

Fig. 7.3 Series of superimposed i vs E upd profiles for Pb upd at Au in aq. 1M $HClO_4$ + 10^{-3}M $Pb(NO_3)_2$ solution with increasing temperature in the range 278 to 358 K. Arrows indicate the direction of the shift of the curves with increasing temperature. s = 50 mV s^{-1}.

Pb deposition or ionization over a 60 K range of temperature. Even down to a temperature of 236 K (the profiles for which are not shown), effects of temperature on the upd profiles are not significant. However, at temperatures below ca. 273 K, both the anodic and cathodic "spikes", also observed in water, become less pronounced. It is interesting to note that over a temperature range of ca. 100 K there is no significant shift of the peak potentials of any of the resolvable cathodic and anodic peaks, in particular the first cathodic peak, in contrast to what is observed in the case of the upd profiles obtained in aq. $HClO_4$ or in the other non-aqueous solvents used (see, for example, Figs. 7.2 and 7.3). In the temperature range ca. 236 - 340 K, it is also seen that temperature has little effect on the resolution of the distinguishable peaks in the upd profiles. The fact that there is no systematic shift of the profiles between the anodic and corresponding cathodic directions of the sweep is an indication that Pb deposition and dissolution processes remain fairly reversible for this solvent (AN) in the temperature range stated above.

With DMF as the solvent, temperature has significant effects on the shape of the cyclic-voltammetry upd profiles for the deposition and dissolution of Pb at Au. At the lowest temperature, 233 K, there is a significant shift of the first cathodic peak to more negative potentials. At this temperature the first cathodic peak is also broad and the "spike" is almost unresolved. This irreversibility at low temperatures could be due to diffusion-limited supply of Pb^{++} ions during the electrodeposition half-cycle. As the temperature is raised, the first cathodic peak (C_{Pb1}) shifts to more positive potentials and, at the same time, becomes sharper. With increase of temperature above ca. 293 K, the peak potential of the first cathodic peak remains fairly constant but the cathodic "spike" (C_{Pb5}) increases in height. There are, however, no significant shifts in the peak potentials with change in temperature.

On the anodic side of the upd profile, the first anodic peak (A_{Pb1}), which is low and broad at low temperatures, becomes sharp and increases in height as the temperature is raised and remains constant at ca. 303 K. The peak potential of the first anodic peak remains constant over a temperature range of ca. 100 K. Unlike the cathodic "spike", which is not pronounced at low temperatures, the anodic "spike" is well developed even at the lowest temperature empolyed in this

system. It shifts slightly to more negative potentials and increases in height with rise in temperature up to ca. 303 K.

The other resolvable peaks on the anodic side of the profile, which are designated as A_{Pb3} and A_{Pb7}, shift progressively to less positive potentials with temperature change from ca. 233 to 283 K. Above 313 K, the cathodic peaks become distorted with a broad peak appearing close to the potential of the "spike".

In MeOH, low temperatures have significant effects on the shape and resolution of the upd profiles. At 219 K, the lowest temperature at which the upd profile was recorded for this system, the upd profile is characterized by one broad cathodic peak (the first cathodic peak and the "spike" have merged to form one peak) significantly shifted to more cathodic potentials and one broad anodic peak, slightly shifted to less anodic potentials.

As was the case for the upd of Pb in DMF, the first cathodic peak shifts to more positive potentials with temperature rise. The usual shape of the peaks and the resolution of the upd profile is restored at ca. 258 K, and further increase in temperature has no significant effects on the shape of the upd profiles.

In PC, the effects of temperature of the upd profiles are quite similar to those observed in MeOH. At low temperatures, there is a large shift of the first cathodic peak to more negative potentials and the whole profile is less resolved than at higher temperatures. As usual, the first cathodic peak shifts to more positive potentials with rise in temperature. From a temperature of ca. 258 K, when the anodic side of the upd profile has regained its usual peak resolution, further increase in temperature has no effect on the shape of the profile or the potentials of the "spike" and the first anodic peak (A_{Pb1}). However, the peak A_{Pb7} shifts to more negative potentials with increase in temperature. Above 318 K, the first cathodic peak becomes broader, as was observed in DMF and probably for the same reason.

The large negative shift of the first cathodic peak observed in the profiles recorded in MeOH and PC could arise, as remarked earlier, because of the diffusion-limited supply of Pb^{++} ions during the cathodic sweep at these low temperatures. Another possibility could be anion adsorption effects

if their adsorbability increases with decrease of temperature.

In the case of experiments conducted in aq. $HClO_4$ (Fig. 7.3), it is observed that although temperature has no significant effects on the shape of the profiles for the upd of Pb at Au, the anodic and cathodic peaks do shift progressively to more negative potentials with increase of temperature from 278 to 358 K. This is in contrast to the behaviour in the non-aqueous solvents where the first cathodic peak shifted to more positive potentials with rise in temperature.

At higher temperatures, bulk Pb deposition commences at less negative potentials relative to the RHE; a similar effect is observed in non-aqueous solvents. Above ca. 328 K, the first cathodic peak becomes sharpened and the cathodic "spike" somewhat more pronounced.

Since the total charge within the i vs E envelopes remains almost constant with temperature, the increase in size of the "spike" and the development of the cathodic peak C_{Pb4} (which is less pronounced at low temperatures) with rise in temperature must be due to the deposition of Pb which was not accommodated in the state corresponding to the first cathodic peak due to its shift to less positive potentials.

7.4 Procedure for Evaluation of True dE_p/dT Values and the Corresponding ΔS_p's

The preferred procedure in most of the work was to make the potential-sweep measurements under isothermal conditions [system (a)] and then correct for the absolute variation of the reference electrode potential with temperature, using non-isothermal reference electrode cells of the type

c) $\quad Pb/Pb^{++}(S) \;/\; E_j \;/\; Pb/Pb^{++}(S)$
$\quad\quad$ T varied $\quad / \quad$ Ref. T = 298 K

for each solvent (S) system, E_j being minimized by use of a salt bridge thermal junction, as mentioned earlier.

In the case of the aqueous solution behaviour, the absolute variation of the H_2/H^+ electrode potential with temperature was taken from the calculation of Conway, Kozlowska and Sharp [127] based on the standard entropies of $H_2/2\ H^+$ ion, taking the entropies of electrons as virtually zero at 298 K. The $dE_{H_2/H^+}/dT$ is found to be 0.84 mV K^{-1}.

The experimentally determined values of the temperature dependence of the Pb/Pb^{++} electrode potential are based on the plots in Fig. 7.4 (p. 193) for $E_{Pb/Pb^{++}}$ vs T, evaluated from measurements on non-isothermal cells of type (c).

From the results of the non-isothermal cell measurements on the Pb/Pb^{++} reference electrode in the various solvents, the absolute temperature coefficient dE_{Pb}/dT for this electrode in the various non-aqueous solvents used is about 1.0 ± 0.03 mV K^{-1}. Details of actual values are given later in Table 7.1 (p. 194). A positive value for the temperature coefficient indicates that the Pb reference electrode potential increases positively with rise in temperature relative to the Pb electrode at the "reference temperature" 298 K.

7.5 Correction of the Observed dE_p/dT Values to Absolute Values Using the Temperature-Dependence of the Reference Electrode Potential

Lead upd peaks whose potentials, relative to the Pb/Pb^{++} electrode in the same solution, increase with temperature must have a larger absolute temperature coefficient, γ, of potential than does the reference electrode itself (coefficient α) (as diagramatically illustrated in Fig. (a) below); then $\gamma = \alpha + \beta$.

a)

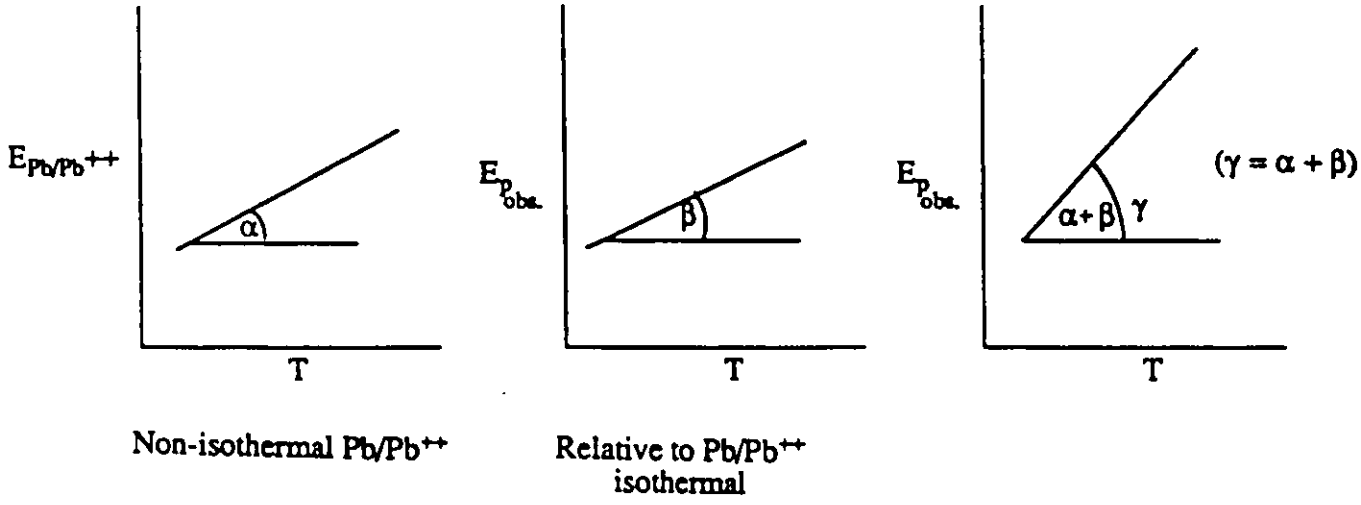

Non-isothermal Pb/Pb^{++}

Relative to Pb/Pb^{++} isothermal

On the other hand, for cases where the E_p, measured isothermally with the Pb/Pb^{++} reference electrode in the same solution, remains <u>independent</u> of T, then the E_p values must have the same absolute variation of potential as that of the reference electrode (as illustrated in Fig. (b) below), i.e. $\gamma = \alpha$.

b)

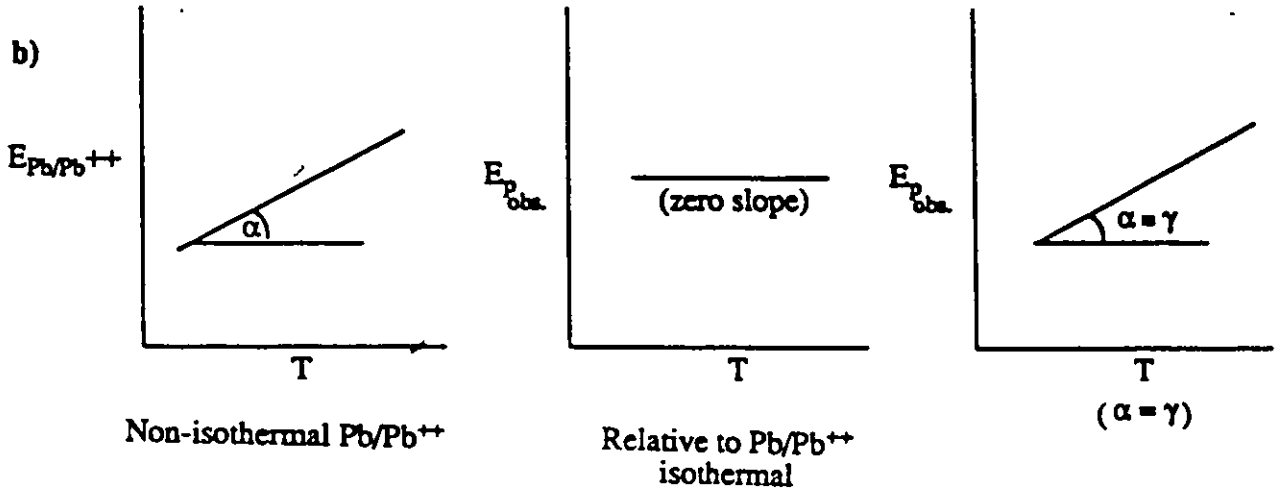

Non-isothermal Pb/Pb^{++}

Relative to Pb/Pb^{++} isothermal

Conversely, if E_p <u>vs</u> T has the opposite sign of slope to that of the reference electrode, then the dE_p/dT values must be <u>subtracted</u>, as illustrated below, giving the absolute $dE_p/dT = \gamma = \alpha - \beta$.

C)

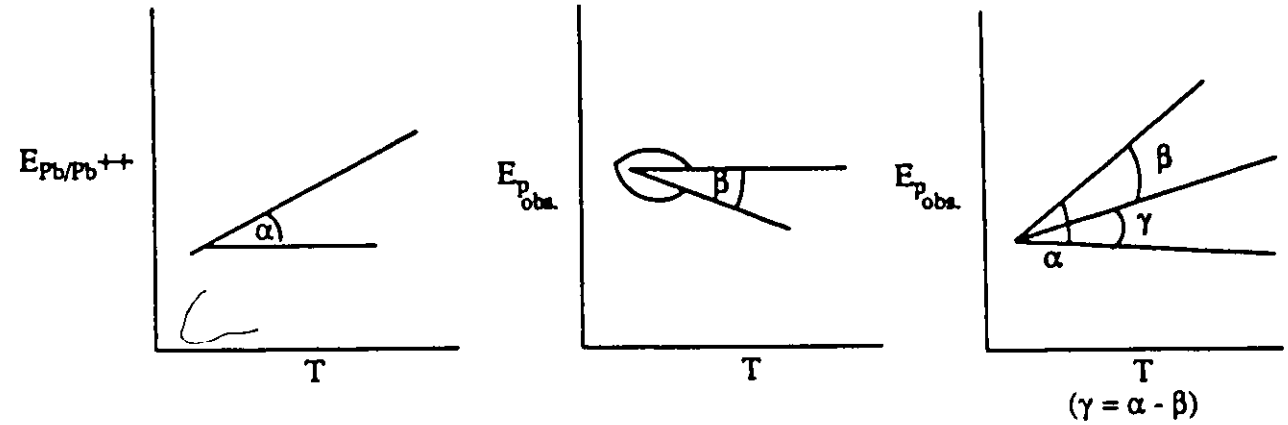

Non-isothermal Pb/Pb^{++}

Relative to Pb/Pb^{++} isothermal

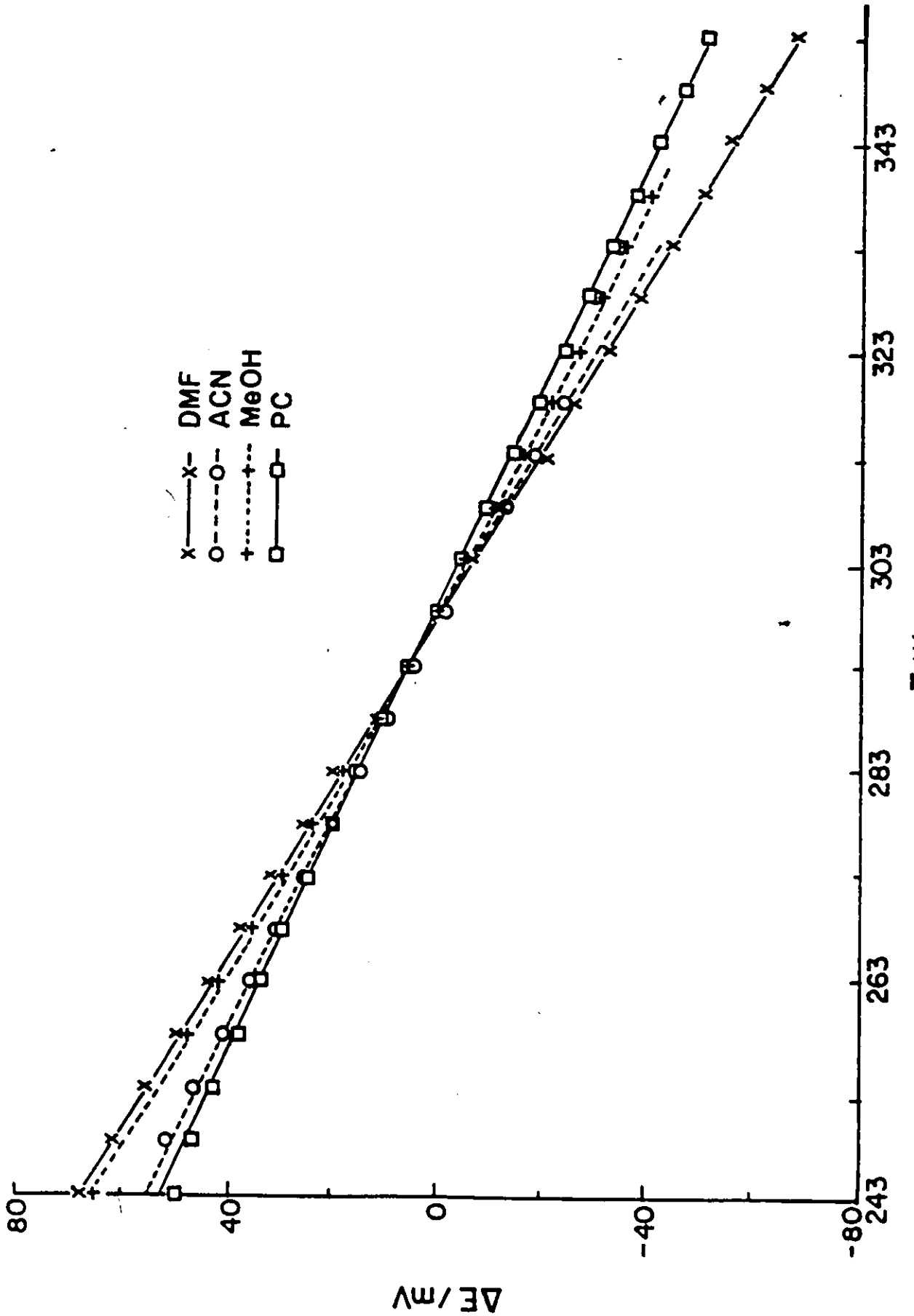

Fig. 7.4 Non-isothermal cell potentials for the Pb^{++}/Pb reference electrode in 0.1M $NaClO_4$ + 10^{-2}M $Pb(CF_3SO_3)_2$ in various non-aqueous solvents referred to 298 K.

Table 7.1 **Temperature Coefficients of Non-isothermal Cell Potentials for Pb/Pb^{++} and H_2/H^+ Reference Electrodes at 298 K**

Solvent	Electrolyte	Reference electrode	$dE_{cell}/dT^{\#} \pm 0.03$ mV K^{-1}
AN	(0.1M $NaClO_4$) 0.01M $Pb(CF_3SO_3)_2$	Pb/Pb^{++}	1.09
MeOH	(0.1M $NaClO_4$) 0.01M $Pb(CF_3SO_3)_2$	Pb/Pb^{++}	1.20
DMF	(0.1M $NaClO_4$) 0.01M $Pb(CF_3SO_3)_2$	Pb/Pb^{++}	1.23
PC	(0.1M $NaClO_4$) 0.01M $Pb(CF_3SO_3)_2$	Pb/Pb^{++}	0.95
H_2O	0.5M H_2SO_4	H_2/H^+	0.84*

* From ref. [127].

Positive when hot electrode is the positive pole.

The experimentally determined temperature dependence, dE/dT, of peak potentials , E_p, measured isothermally w.r.t. the Pb/Pb^{++} electrode, is the derivative $d(E_p - E_{Pb/Pb^{++}})_{isothermal}/dT$, $= (dE_p/dT)_{isothermal}$ $mV\ K^{-1}$.

Then the absolute value of dE_p/dT required for calculation of the entropies of the Pb adatom states is given by

$$(dE_p/dT)_{abs.} = (dE_p/dT)_{isothermal} + (dE_{Pb/Pb^{++}}/dT)_{non\text{-}isothermal} \qquad (7.1)$$
$$= \Delta S_{Pb}/zF$$

The last derivative is determined from the non-isothermal Pb/Pb^{++} cell (or $H_2/2H^+$) cell measurements; hence ΔS_{Pb} is determinable for each solvent system.

7.6 Temperature Dependence of Peak Potentials

7.6.1 General Significance

The potentials (E_P) of peaks for various sub-lattice states of Pb adatoms in the upd i vs E profiles for Pb at Au represent the Gibbs energies of the distinguishable states of adatoms at half-coverage of a given sub-lattice state (in the case where the peaks are symmetrical). When the peak potentials are measured with respect to the potential of a Pb/Pb^{++} reference electrode in the same solution, they correspond to the Gibbs energy of transfer in the process:

$$Pb(\text{crystal lattice}) \rightarrow Pb(\text{adatoms in surface array}) \qquad (7.2)$$

If the temperature dependence of E_P values is determined it will therefore give the respective entropies, ΔS_{Pb}, of the adatom states, relative to the entropy of Pb(crystal lattice): $\Delta S_{Pb} = - d\Delta G_{Pb} / dT = 2F\ (dE_{p,Pb}/dT)$. This entropy quantity is of considerable interest as its value may be employed to determine the state of deposited adatoms in the various distinguishable sub-lattice arrays corresponding to the peaks of the i vs E profiles. In particular, the ΔS_{Pb} values should be able to be associated either with mobile or with immobile states of Pb adatoms on the surface amongst solvent molecules for conditions where $\theta_{Pb} < 1$, taking account of a possible vibrational mode of Pb normal to the surface. (In practice, there will be a complex vibrational coupling between the Pb adatoms and the surface vibrational modes of the Au surface lattice). The

distinction between mobile or immobile adsorption states should be fairly easy to establish as the expected values of ΔS°_{Pb} would be substantially different, as in the case of H at Pt [126] or H_2O or MeOH on Hg [124].

The expected standard entropies of Pb adatoms at Au can be evaluated from the partition function for an immobile film or for a 2-d mobile film, together with the partition function for a vibration normal to the surface as referred to above.

Also, as required, the entropies of processes such as

$$2e + Pb^{++}(S) + Au \bullet \rightarrow Au/Pb(adatom) + S \qquad (7.3)$$

where S represents solvationally bound solvent molecules, could also be evaluated if the partial molar entropy, $S^{\circ}_{Pb^{++}}$, of Pb^{++} ions in solution were known. Such a quantity seems only to be available for Pb^{++} in water [205]. Fortunately, the entropic condition of Pb adatoms can evidently be evaluated adequately through eqn. (7.2) which does not require information on the entropy of solvated Pb^{++} ion in various media.

Earlier, in Section 4.2, it was suggested that Pb adatom deposition at Au is not a simple process, as it would be from gas phase atoms, but involves displacement of adsorbed solvent molecules, S, with development of <u>new</u> interactions between S and the deposited adatoms (Fig. 4.9, p. 94). This, then, will somewhat complicate the interpretation of evaluated ΔS_{Pb} values.

A further complication, to be discussed later, would arise if the Pb adatom deposition required desorption of a previously adsorbed anion (e.g. Cl^-) or neutral molecule (e.g. thiourea, see Chapter 5). This can arise especially in the process corresponding to the first peak of the cathodic sweep, C_{Pb1}, in certain solvents with added surface-active anions or molecules present. However, the T-dependence of peak potentials under such conditions was not investigated, as the interpretation of the anticipated complex behaviour would probably be unproductive.

7.6.2 <u>Experimental Behaviour of E_p Values with Temperature</u>

It was found that various types of behaviour arose in the dependence of the various peak potentials, E_p, for the several solvent systems used. In most cases, E_p values referred to the

reference electrode in the same solution at the given experimental temperature, either decreased with T or remained approximately constant (i.e., in the latter case, the E_p values varied in the same way as the reference electrode potential, with T). In some cases an initial increase of E_p with T was observed.

In order to avoid repetitive description, a tabular summary of the directions of the E_p changes with T is given in Appendix I. The actual experimental plots are shown in Figs. 7.5 to 7.9 and the corresponding entropy changes, ΔS_p, for the process $Pb_{crystal\ lattice} \rightarrow Pb$ (adatoms in surface array) (reaction eqn. 7.2) are shown later in Table 7.2 (p. 206). A variety of behaviours is seen, depending on the electrolyte/solvent systems.

7.7 Evaluation of Entropy Changes in the Electrodeposition and Desorption of Pb at Au

In order to obtain the real variation with temperature of the experimentally measured peak potentials, the experimentally determined dE_p/dT is corrected according to the procedure in 7.4 using the experimentally determined dE_{cell}/dT for the reference electrode used (Section 7.3).

The experimentally determined peak potential as a function of temperature can be written as

$$E_{p(T)} = E_{p(T=0)} \pm aT \qquad (7.4)$$

and the potential of the Pb reference electrode from the non-isothermal measurements can be written similarly as

$$E_{Pb(T)} = E_{Pb(T=0)} \pm bT \qquad (7.5)$$

where a and b are empirical coefficients. Then the real variation of peak potential with temperature will be given by

$$E_{P(T),real} = E_{p(T)} + E_{Pb(T)} \qquad (7.6)$$

The entropy changes of the distinguishable states of Pb at Au referred to bulk Pb must be evaluated using the corrected temperature coefficient of the peak potential, i.e.

$$nF(dE_{p(T),real}/dT) = nF[dE_{p(T)} + dE_{Pb(T)}/dT] = \Delta S_{react} \qquad (7.7)$$

For the evaluation of entropy changes in aqueous $HClO_4$, $E_{Pb(T)}$ in the above equations is replaced by $E_{H(T)}$, the potential of the H_2 reference electrode used.

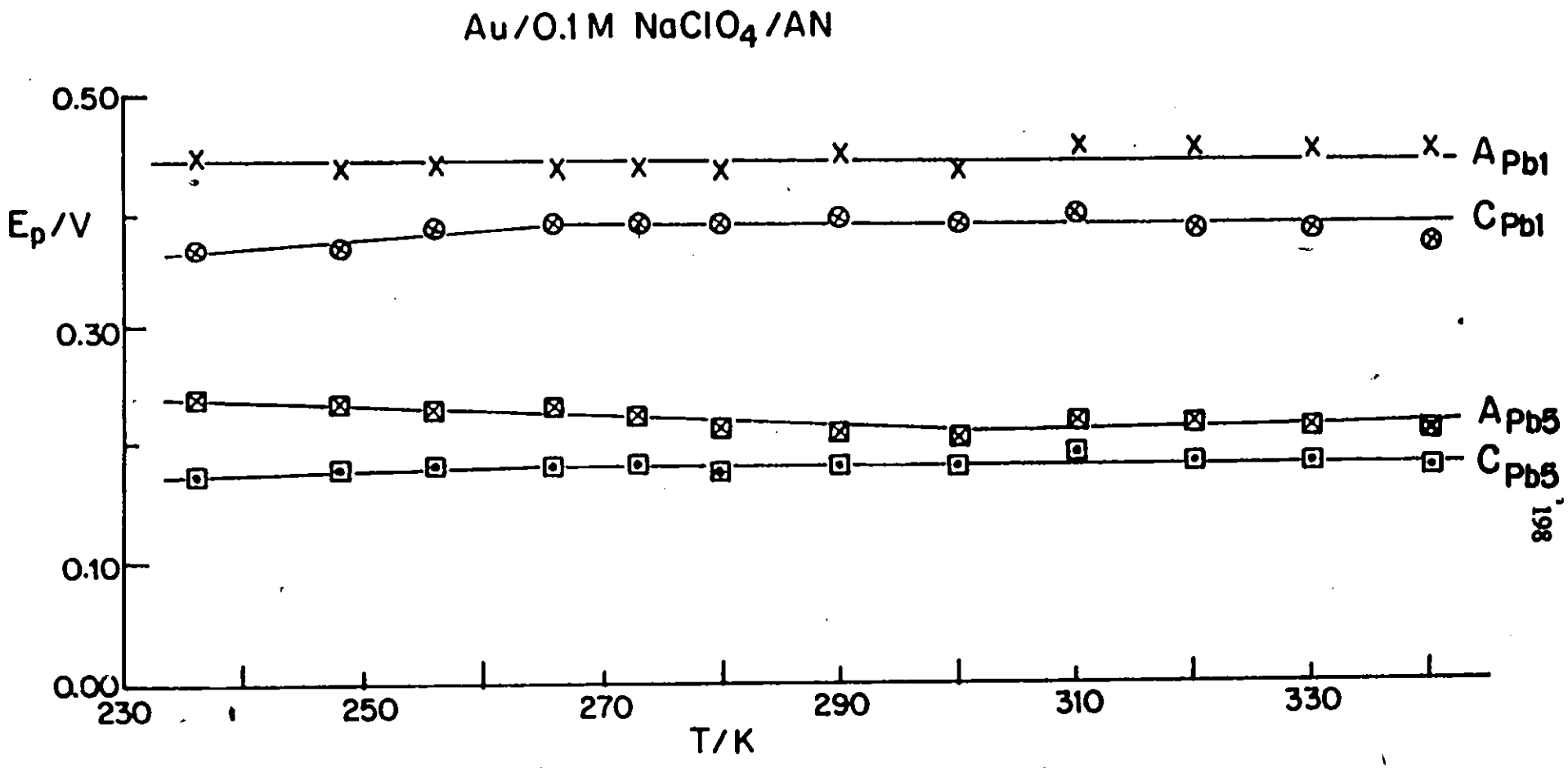

Fig. 7.5 Temperature dependence of Pb apparent peak potentials in the i vs E upd profile for Pb at Au from 0.1M $NaClO_4$ + 10^{-2}M $Pb(CF_3SO_3)_2$ solution in AN.

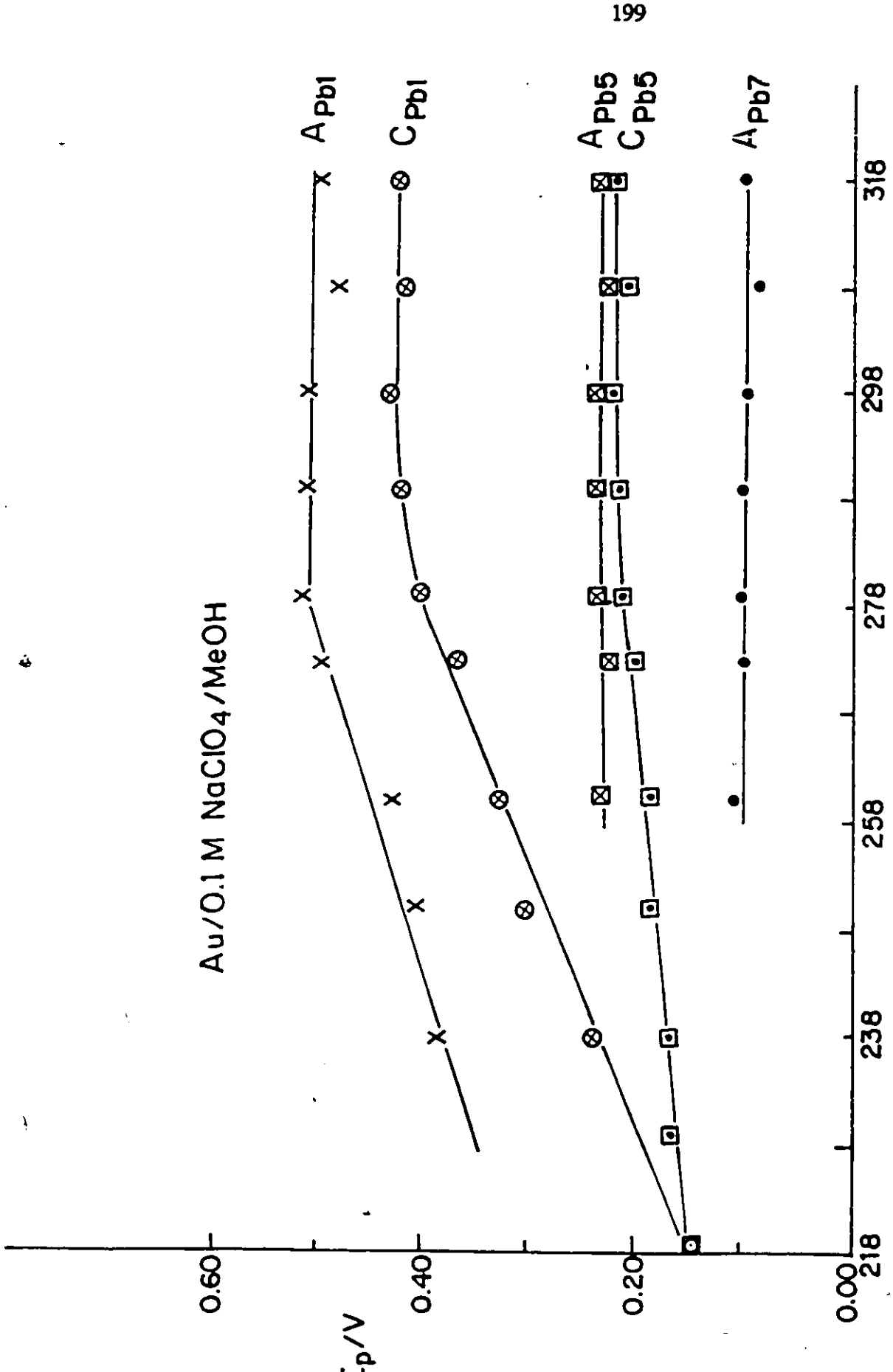

Fg. 7.6 Temperature dependence of Pb apparent peak potentials in the i vs E upd profile for Pb at Au from 0.1M $NaClO_4$ + 10^{-2}M $Pb(CF_3SO_3)_2$ solution in MeOH.

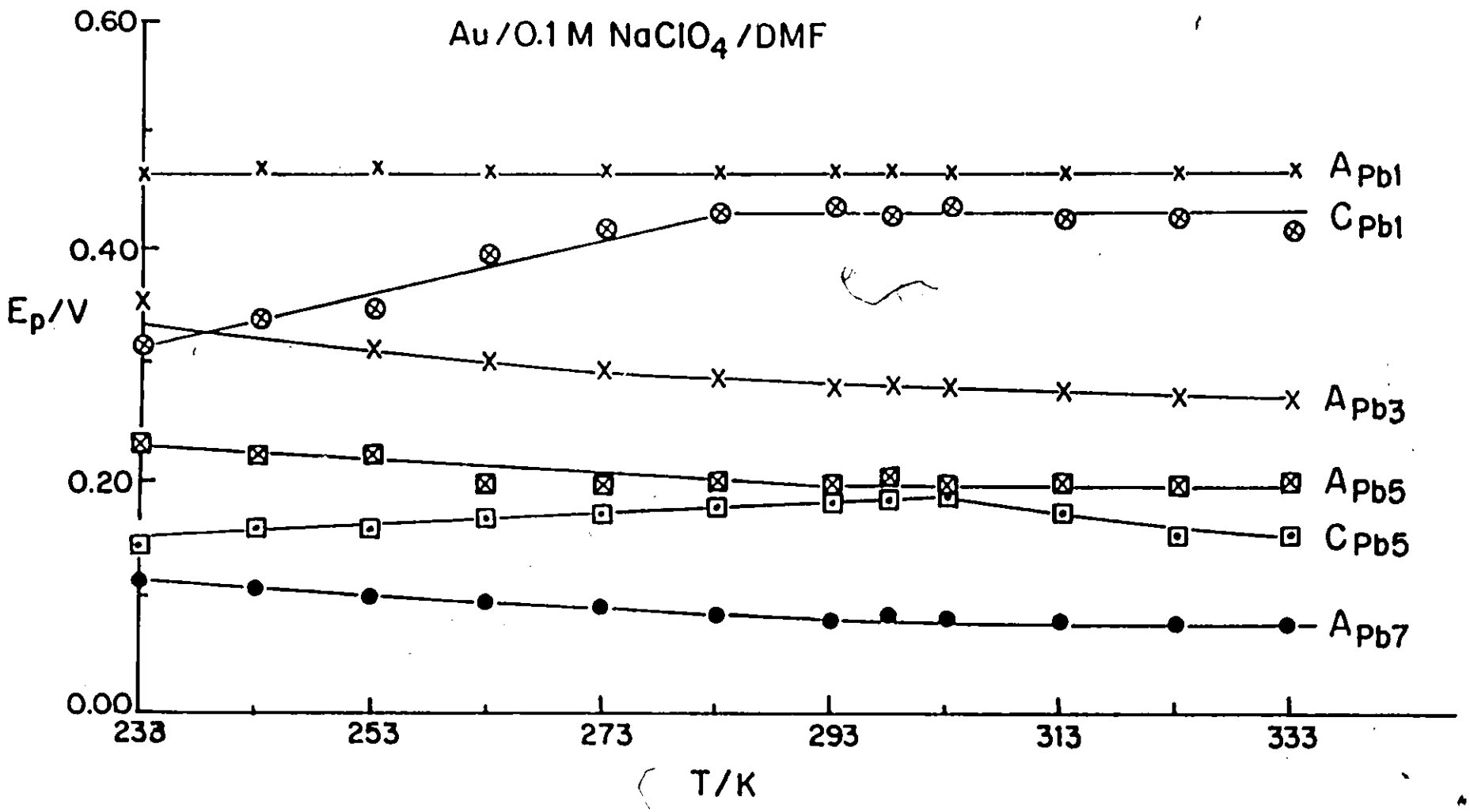

Fig. 7.7 Temperature dependence of Pb apparent peak potentials in the i vs E upd profile for Pb at Au from 0.1M $NaClO_4$ + 10^{-2}M $Pb(CF_3SO_3)_2$ solution in DMF.

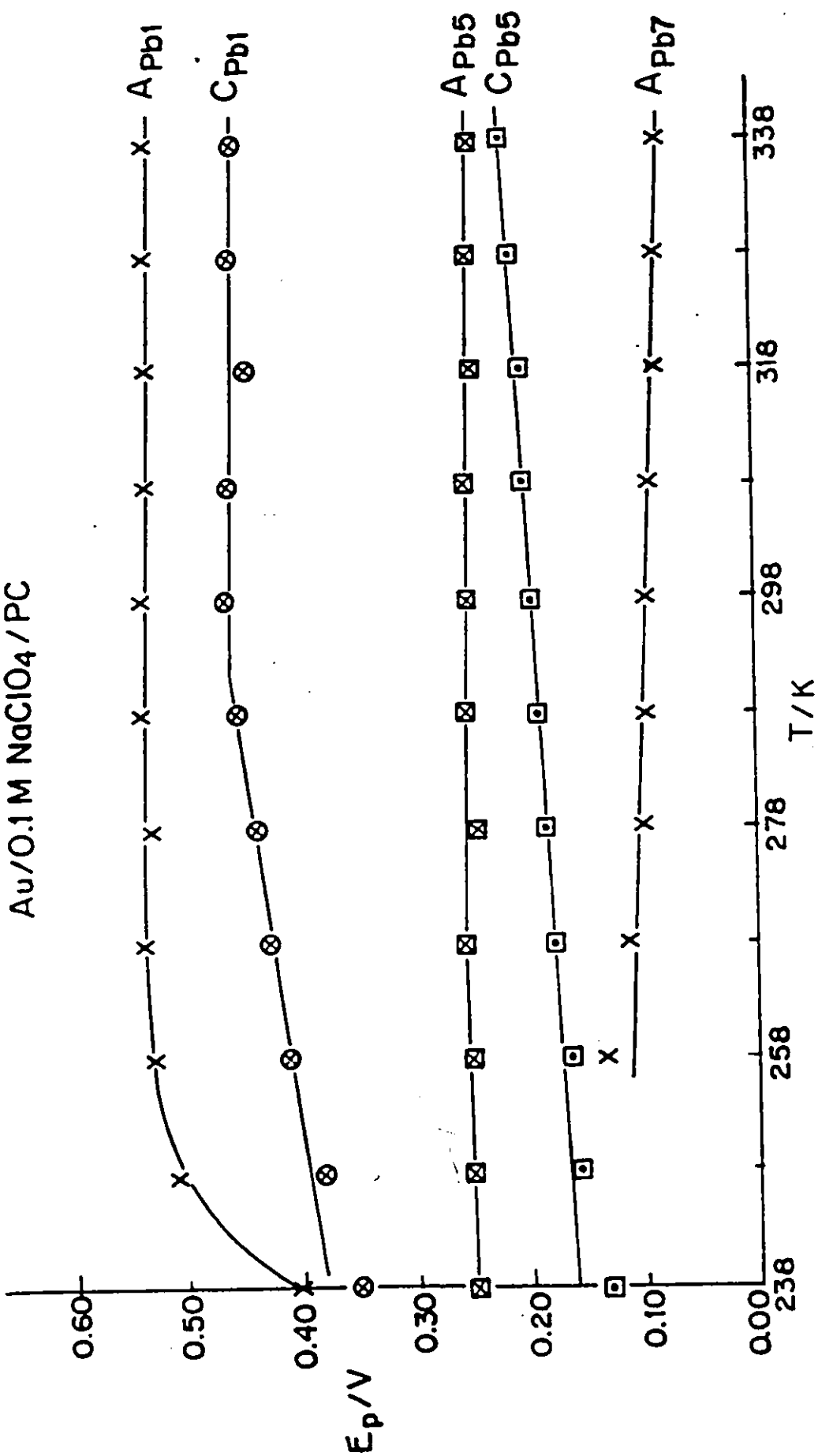

Fig. 7.8 Temperature dependence of Pb apparent peak potentials in the i vs E upd profile for Pb at Au from 0.1M $NaClO_4$ + 10^{-3}M $Pb(CF_3SO_3)_2$ solution in PC.

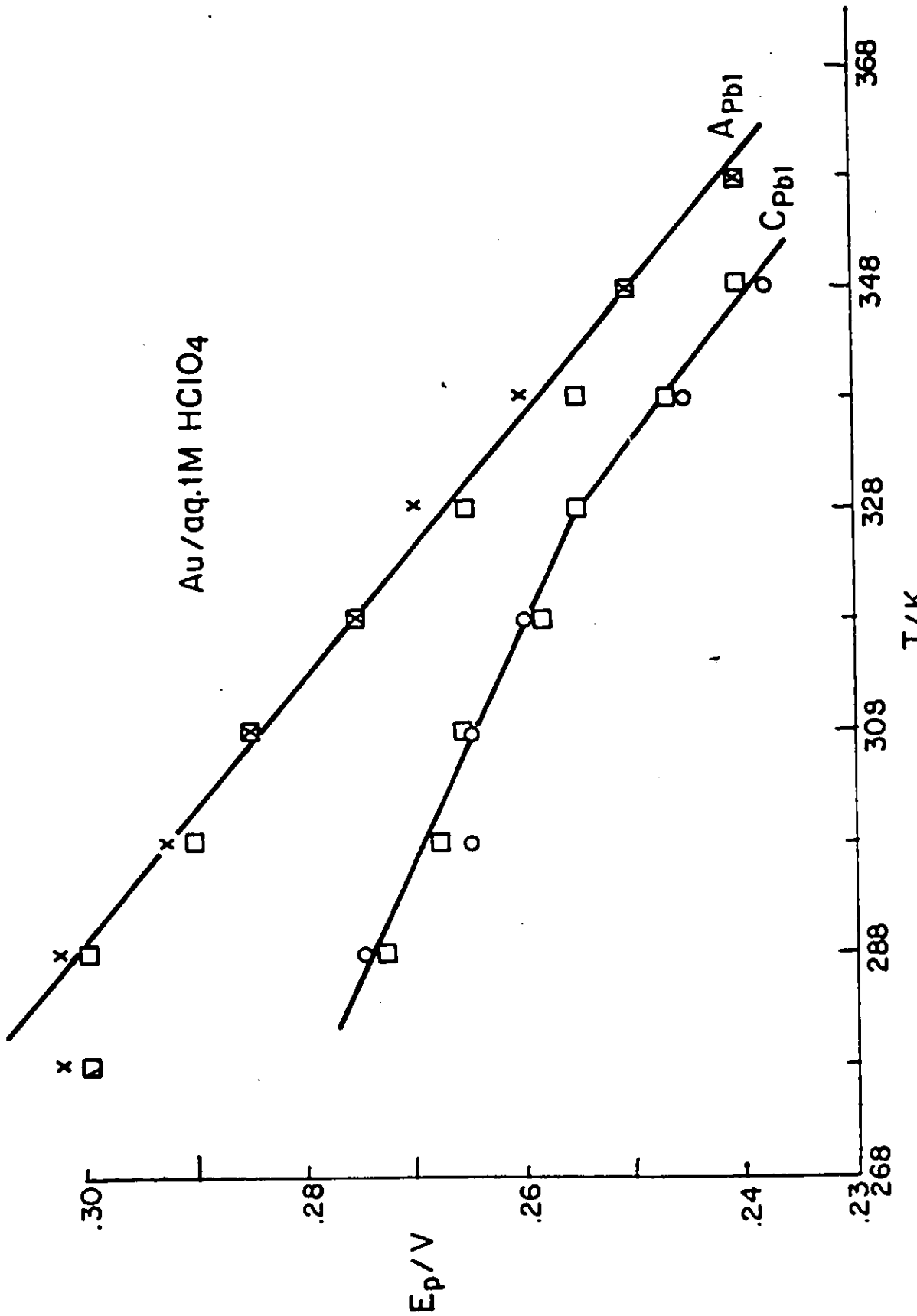

Fig. 7.9 (a) Temperature dependence of Pb apparent peak potentials in the i vs E upd profile for Pb at Au in aq. 1M $HClO_4$ + 10^{-3}M $Pb(NO_3)_2$.

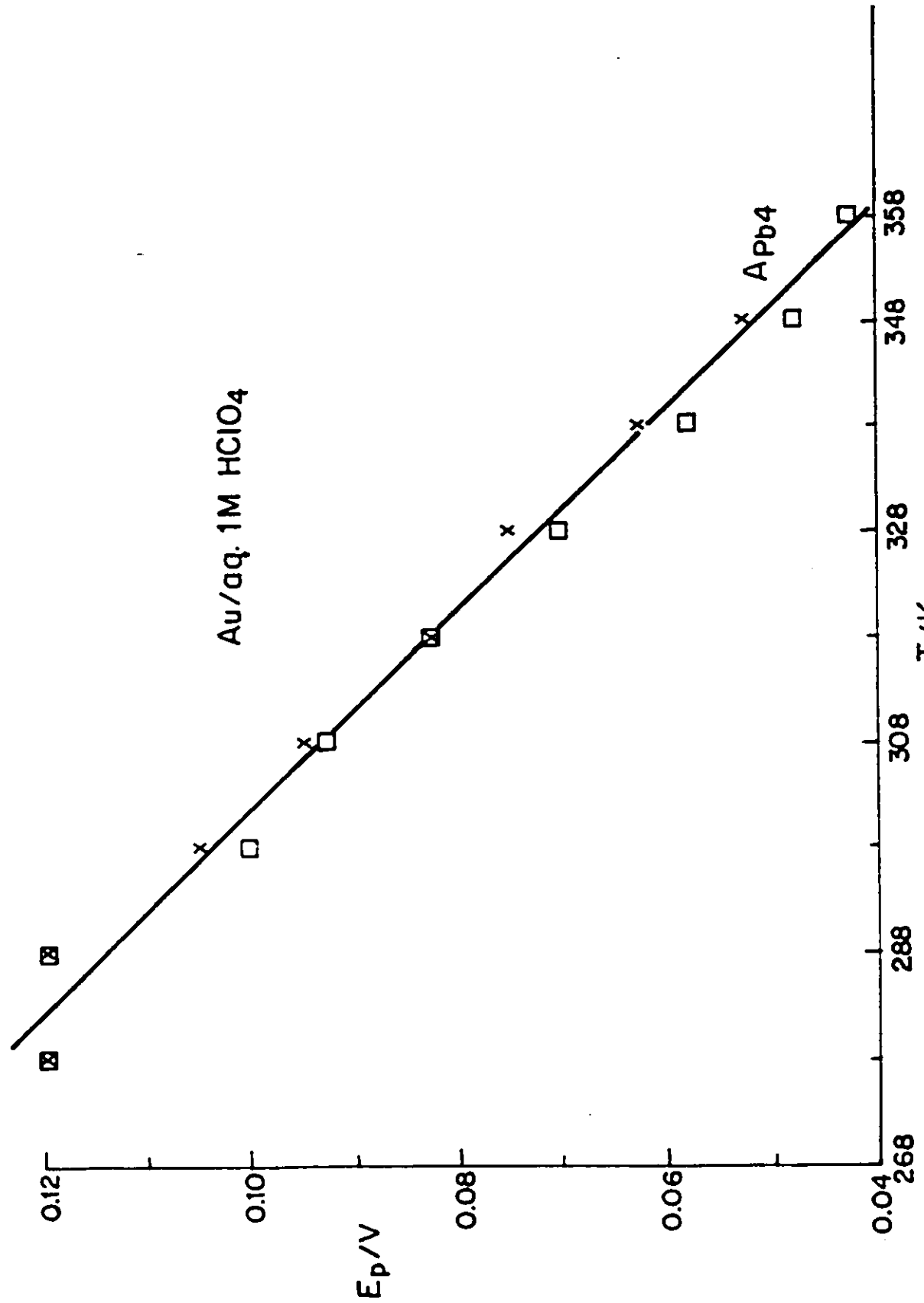

Fig. 7.9 (b) Temperature dependence of Pb apparent peak potential with temperature in the i vs E upd profile for Pb at Au in aq. 1M $HClO_4$ + 10^{-3}M $Pb(NO_3)_2$.

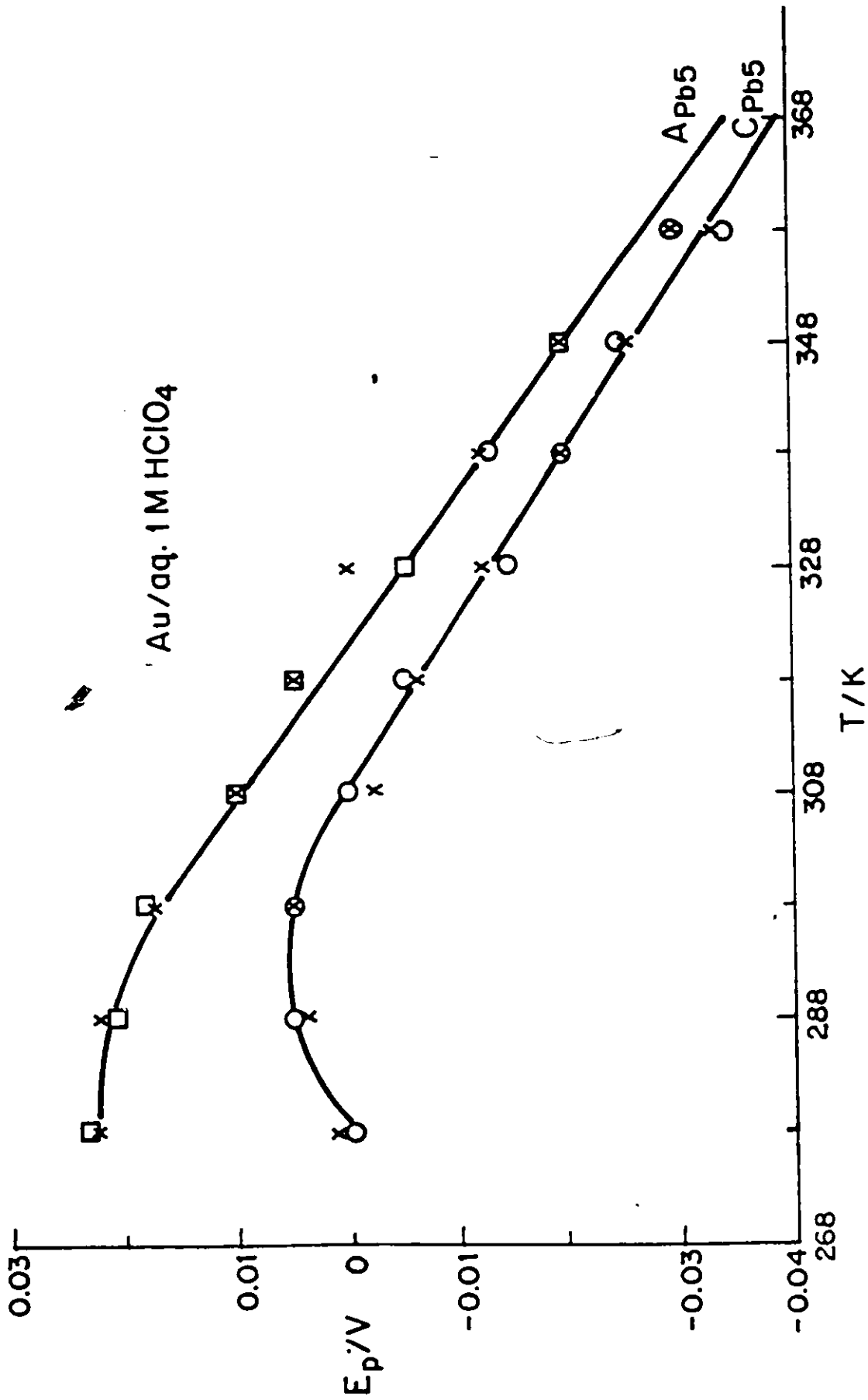

Fig. 7.9 (c) Temperature dependence of Pb apparent peak potentials in the i vs E upd profile for Pb at Au in aq. 1M $HClO_4$ + 10^{-3}M $Pb(NO_3)_2$.

The values of dE_p/dT, $dE_{p(T)_{real}}/dT$ and the evaluated estimates of entropy changes for the various Pb adstates on Au in the various non-aqueous solvents and aqueous $HClO_4$, relative to Pb in the bulk, are given in Table 7.2. The general observations to be made are: (i) the estimated entropy values are solvent-dependent, i.e. they differ significantly for the several solvents used in the present work; thus a given ad-state of Pb at Au, for example the one corresponding to the peak A_{Pb1}, has a different entropy value in different solvents (Table 7.2); (ii) for a given solvent, all the resolvable ad-states of Pb do not necessarily have the same value of the entropy change; (iii) the lowest entropy values are obtained in PC followed by AN, while in DMF, some of the highest values arise; (iv) the entropy values obtained for the aqueous medium seem anomalously small compared to those obtained for the non-aqueous media. The data, as remarked in the footenote (p. 207), are to be experimentally rechecked under different experimental conditions.

The estimated entropy changes corresponding to the various states of adsorbed Pb at Au will be discussed in relation to the standard entropy of Pb in the bulk which, for the crystalline solid (298 K) is 64.85 J mol^{-1} K^{-1}, while that of Pb in water is 21.3 J mol^{-1} K^{-1}.

By referring the E_p values to the potential of the bulk Pb/Pb^{++} ion electrode, the requirement of information on the standard partial molar entropy of the Pb^{++} ion in the non-aqueous solvents used is avoided, as mentioned earlier. This is useful since $S^\circ_{Pb^{++}}$ for such solvents is not available in the literature. Thus, this procedure of measurement gives the ΔS° value for the hypothetical transfer process represented in eqn. 7.2, i.e.

$$\text{Pb(crystal lattice) at 298 K} \xrightarrow{\Delta S^\circ} \text{Pb(adatom in surface array)}$$

Hence the standard entropy of the Pb adatoms* relative to the standard entropy of Pb in bulk crystalline lead can be evaluated without ambiguity, knowing to a good approximation the absolute

---

*The standard states for the Pb adatom arrays are to be taken as half-coverage of each array, i.e. corresponding to the peak potential of reversible surface processes. With the upd profile for Pb at Au, some of the states are not completely resolved from others due to polycrystallinity.

Table 7.2 **dE_p/dT, $(dE_p/dT + dE_{cell}/dT)$ and Estimated $\Delta S°$ Values for Pb Adatom States on Au in Various Solvents**

Solvent	State	dE_p/dT ($mV\ K^{-1}$) (Isothermal)	$dE_p/dT + dE_{cell}/dT$ ($mV\ K^{-1}$)	$\Delta S°$ ($J\ mol^{-1}\ K^{-1}$)
H_2O*	A_{Pb1}	- 0.86	- 0.02	- 4
	A_{Pb4}	- 1.05	- 0.21	- 41
	A_{Pb5}	- 0.67	0.17	33
	C_{Pb1}	- 0.45 to - 0.80	0.39 to 0.04	75 to 8
	C_{Pb5}	- 0.65	0.19	37
AN	A_{Pb1}	0	1.09	210
	A_{Pb5}	0 to - 0.38	1.09 to 0.71	210 to 137
	C_{Pb1}	0 to - 0.75	1.09 to 0.34	210 to 66
	C_{Pb5}	0	1.09	210
MeOH	A_{Pb1}	0 to 3.26	1.20 to 4.46	232 to 861
	A_{Pb5}	0	1.20	232
	A_{Pb7}	0	1.20	232
	C_{Pb1}	0 to 4.20	1.20 to 5.4	232 to 1,042
	C_{Pb5}	0 to 1.20	1.20 to 2.4	232 to 463

Solvent	State	dE_p/dT (mV K^{-1}) (Isothermal)	$dE_p/dT + dE_{cell}/dT$ (mV K^{-1})	$\Delta S°$ (J mol^{-1} K^{-1})
DMF	A_{Pb1}	0	1.23	237
	A_{Pb3}	- 0.31 to - 1.03	0.92 to 0.20	178 to 39
	A_{Pb5}	0 to - 0.50	1.23 to 0.73	237 to 141
	A_{Pb7}	0 to - 0.33	1.23 to 0.90	237 to 174
	C_{Pb1}	0 to 2.43	1.23 to 3.66	237 to 706
	C_{Pb5}	- 1.0 to 0.5	0.23 to 1.73	44 to 334
PC	A_{Pb1}	0	0.95	183
	A_{Pb5}	0	0.95	183
	A_{Pb7}	- 0.43	0.52	100
	C_{Pb1}	0	0.95	183
	C_{Pb5}	0.59	1.54	297

Reference value for Pb(bulk crystal) = 64.5 J mol^{-1} K^{-1} at 298 K. Standard states: Pb crystal at 298 K; adatom states at θ_{Pb} = 0.5 for each sub-lattice array at 298 K.

---

* In relation to the results for $\Delta S°$ for the Pb adatom states generated in the non-aqueous media, the data for aqueous solution seem anomalously small. They were based on potential measurements vs the H_2 electrode in 1M aq. $HClO_4$ as reference, the temperature coefficient of which, vs Pb/Pb^{++}, is taken into account in the calculation of $\Delta S°$. Before publication of those results for the aq. solution, the data are to be experimentally rechecked due to the possibility of contamination of the Pt/H_2 reference electrode by Pb.

temperature coefficient of the Pb/Pb^{++} electrode potential in each solvent, as measured in the present work.

The estimated entropy values in Table 7.2 are all higher than the standard entropy value of Pb in the bulk, which indicates that the Pb adatoms on the Au surface are more mobile than the Pb atoms in the bulk. For Pb in the bulk (i.e. in the crystalline solid), the only contribution to the entropy is the vibrational entropy (the electronic contribution is negligible at ordinary temperatures) and it should be more than zero (positive value) since it is only at the absolute zero that a perfect crystalline solid may have zero entropy.

For the chemisorbed Pb adatoms at a Au electrode surface, their total entropy will be made up of the vibrational entropy (which will depend on the strength of the Au-Pb bond) and the contribution from the 2-dimensional translational entropy (if the ad-layer is mobile). Usually vibrational entropies are much smaller than translational entropies because of the large differences in the respective partition functions or quanta that are involved (the ratio of the translational partition function to that for vibration is of the order 10^{30} : 10). It is probable, therefore, that much of the contribution to the estimated entropy changes of the Pb ad-states is from the 2-dimensional translational mode. The large (positive) values indicate that the Pb ad-layer is mobile on the surface of the Au electrode. However, as indicated earlier, the entropy changes are found to be solvent-dependent; this is probably due to Au-Pb-solvent interactions which should be different for different solvents. It is also possible that these differences could arise from the anion adsorption effects which are also solvent-dependent.

The large positive values of entropy changes associated with the state C_{Pb1} in MeOH and DMF which arise from the high positive values of dE_p/dT observed at low temperatures (shift of the peak potential to more negative values with lowering of temperature) seem rather unexpected. A large positive value of entropy change would imply a more mobile ad-layer of Pb on the Au surface at these low temperatures. This implies that the entropy of the ad-layer increases with lowering of temperature, an unexpected observation since entropy should increase with temperature rise. These values should be omitted on the grounds that the large shift to more negative potentials

at low temperatures must probably be due to anion adsorption effects and/or limited supply of Pb^{++} ions at low temperatures and not due directly to the lowering of temperature, as discussed earlier. The entropy values estimated using the potentials of the peaks observed on the anodic sweep should therefore be more reliable than those on the cathodic sweep, especially the values for the state C_{Pb1} at low temperatures.

In PC, for which low entropy values are observed, the state A_{Pb7} has a ΔS° value of 100 J mol^{-1} K^{-1} which implies that it is the least mobile state of adsorbed Pb on Au. This is inconsistent with the earlier assertion that this state corresponds to the most loosely bound adstate of Pb at Au since it is the state which is desorbed first at the lowest positive potential on the anodic sweep. In MeOH and DMF, where this state is also identifiable, its entropy value is also equal to those of the other states.

For the states the peak potentials of which are independent of temperature, i.e. dE_p/dT is small or zero, the derived values of ΔS° are numerically determined by the temperature coefficients of the reference electrode potentials, which are different for different solvents. It has the lowest value in PC, and hence correspongingly, the lowest ΔS° values (Table 7.2) arise in this solvent.

The estimated ΔS° changes for Pb states at Au in various solvents used in the present study are significantly higher than those calculated for the H at Pt [127] in alkaline and acidic solutions.

The entropy change associated with fusion (i.e. $Pb_{(s)} \rightarrow Pb_{(l)}$) is 7.9 J mol^{-1} K^{-1}, while that for vapourization is 87.9 J mol^{-1} K^{-1}. These values are lower than the derived entropy values for the Pb adstates on Au associated with the process of reaction eqn. 7.2 especially for the experiments conducted in non-aqueous media. These high values are probably, as remarked earlier, due to solvent and/or anion effects especially at low temperatures since anion effects are solvent dependent.

APPENDIX I

SUMMARY OF HOW THE INDIVIDUAL PEAK POTENTIALS CHANGE WITH TEMPERATURE IN VARIOUS SOLVENT SYSTEMS

System	Peak	Direction of dE_p/dT
Au / aq. 1M $HClO_4$	A_{Pb1}	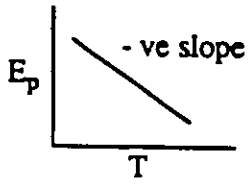
	A_{Pb4}	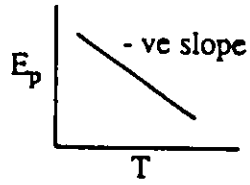
	A_{Pb5}	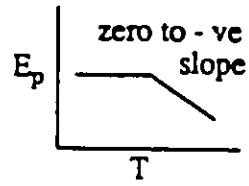
	C_{Pb1}	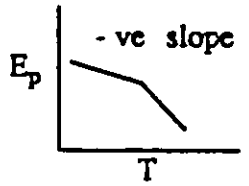
	C_{Pb5}	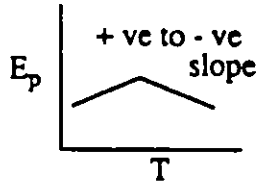

System	Peak	Direction of dE_p/dT
Au / 0.1M $NaClO_4$/MeOH	A_{Pb1}	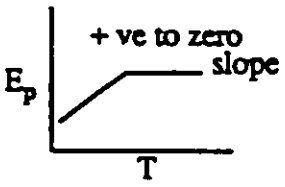
	A_{Pb5}	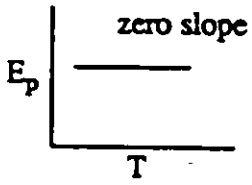
	A_{Pb7}	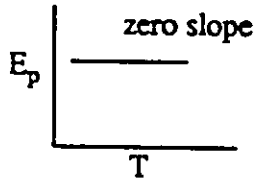
	C_{Pb1}	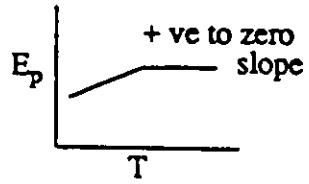
	C_{Pb5}	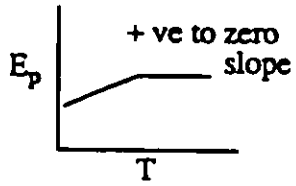
Au / 0.1M $NaClO_4$/ DMF	A_{Pb1}	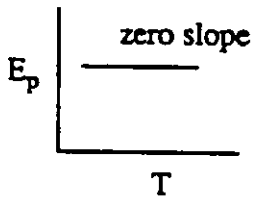

System	Peak	Direction of dE_p/dT
Au / 0.1M $NaClO_4$ / DMF	A_{Pb3}	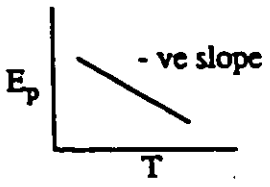
	A_{Pb5}	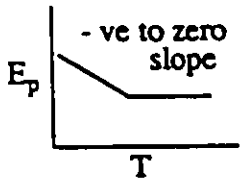
	A_{Pb7}	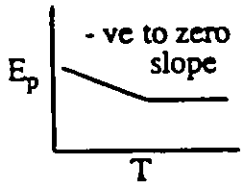
	C_{Pb1}	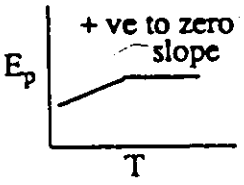
	C_{Pb5}	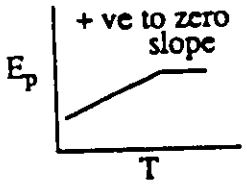
Au / 0.1M $NaClO_4$ / PC	A_{Pb1}	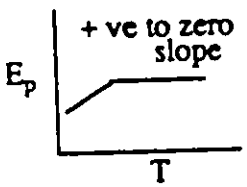

System	Peak	Direction of dE_p/dT
Au / 0.1M $NaClO_4$ / PC	A_{Pb5}	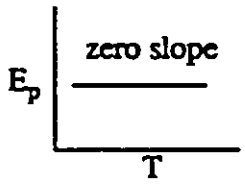
	A_{Pb7}	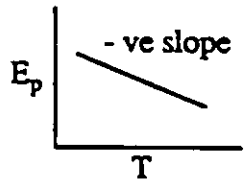
	C_{Pb1}	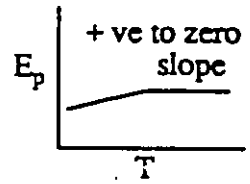
	C_{Pb5}	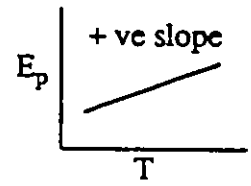
Au / 0.1M $NaClO_4$ / AN	A_{Pb1}	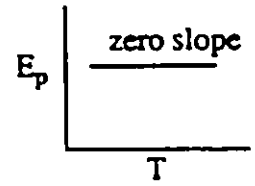
	A_{Pb5}	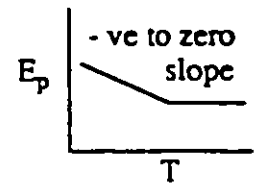

System	Peak	Direction of dE_p/dT
Au / 0.1M $NaClO_4$ / AN	C_{Pb1}	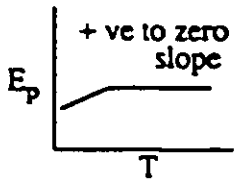
	C_{Pb5}	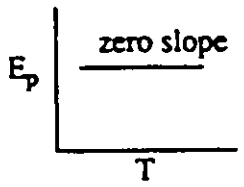

CONTRIBUTIONS TO ORIGINAL RESEARCH

1. The underpotential deposition (upd) of Pb at polycrystalline Au was studied from various protic and aprotic non-aqueous solvents (H_2O, MeOH, AN, DMF, PC) using cyclic-voltammetry. The results from aqueous medium are used for reference purposes. It is demonstrated that regardless of the solvent used (aqueous or non-aqueous), the i vs E cyclic-voltammograms upd profiles are all characterized by five or six (and in some cases up to seven) distinct cathodic and anodic peaks occuring at different potentials as the monolayer of the underpotential-deposited Pb is laid down, as is also found in aqueous medium. This phenomenon, referred to as multiple-state adsorption which corresponds to distinquishable states of adsorbed Pb adatoms on Au, is found to arise over a wide range (ca. 0.6 V) of potentials, although this range is found to be solvent-dependent. Another important and experimentally significant aspect of the result of the present work is that good i vs E profiles are obtained which demonstrate in, most cases, good reversibility in the absence of strongly adsorbing anions.

2. It is demonstrated that the i vs E upd profiles indicate that peak shapes, peak potentials and the overall resolution of the peaks is solvent-dependent, a result which is discussed in terms of the anion adsorption/desorption which is also a solvent dependent process.

3. The solvent effect is most pronounced in the initial stages of Pb adatom deposition. This is to be expected because, before Pb adatom electrodeposition commences, the electrode surface (Au in the present work) is fully covered by the solvent molecules with different Au/solvent molecule interactions for the various solvents.

4. There are also some systematic but significant differences between the peak potentials for corresponding sub-monolayer states as revealed on the cathodic sweeps in comparison with

the anodic sweeps. This is explained as probably being due to some irreversibility in anion adsorption/desorption which is solvent dependent.

5. TEA^+ and NO_3^-, as ions of the supporting electrolyte, are shown to have marked effects on the upd i vs E profiles for Pb at Au. They cause the first cathodic peak to be shifted to more negative potentials, leading to irreversibility between the deposition and the corresponding desorption process, because of their tendency to adsorb strongly on Au. $CF_3SO_3^-$ and ClO_4^-, as anions of the supporting electrolyte or Pb salt, are found to have little or no effects on the upd i vs E upd profile, an indication that they are weakly or non-adsorbing.

6. It is demonstrated that added strongly adsorbing anions (Cl^-, Br^-, I^-) or thiourea (TU) have marked and significant effect on the upd i vs E profiles of Pb at Au starting from very low concentrations (10^{-7} to 10^{-6}M). The general observation is that with increasing concentration of added X^- or thiourea, the peak potential of the first cathodic peak is shifted to more cathodic potentials. The magnitude in shift depends on the species added. The effects are discussed in terms of the extent of charge transfer that arises when the anion or TU chemisorption takes place at the Au electrode surface. However, the most striking result is demonstrated with Cl^-: an extra anodic peak, at potentials more positive than the potentials of the usual first anodic peak is observed. The most interesting thing is that there is no corresponding peak on the cathodic sweep. It is found that the same quantity of Pb is eventually electrodeposited as in the absence of co-adsorbed ions or thiourea, but over a different range of potentials and in different sub-states.

7. The kinetic parameter, s_o, which characterizes the kinetics of Pb desorption or adsorption on the Au electrode surface is evaluated from the plots of shift in peak potential vs log s for the various distinquishable peaks corresponding to various distinguishable states of Pb adatoms. In general, the values of s_o, the sweep-rate at which the surface process just begins to be

kinetically irreversible, obtained in various non-aqueous solvents is about 10 V s^{-1}, to be compared with 100 to 200 V s^{-1} obtained in aq. medium. The low values of s_o in non-aqueous media demonstrate transition from kinetic reversibility to irreversibility at lower sweep-rates in non-aqueous than in aqueous media. The s_o values for the cathodic peaks are found to be lower than the corresponding values for the anodic peaks, possibly due to complications from anion adsorption/desorption and diffusion effects and probably "iR" drop effects also. From the Tafel-type plots, the Tafel-slopes are close to the actually expected value, 120 mV/decade of s, i.e. $2.3RT/\beta F$ with $\beta \equiv 0.5$. It is of interest to note that a process that involves an adsorbed state (of Pb) as reactant or product of ion (Pb^{++}) discharge, the value of (β is still near 0.5 as it is for many ionic outer-sphere redox reactions where neither product nor reactant are chemisorbed.

8. Temperature dependences of E_p values were evaluated and gave the corresponding entropies of sub-monolayer states of Pb developed at Au in the various solvent systems used in the present work. In order to obtain the real variation with temperature of the experimentally measured peak potentials, the experimentally determined dE_p/dT data were corrected using the experimentally determined dE_{cell}/dT for the reference electrode used as evaluated from non-isothermal reference cell measurements under conditions where the thermal junction potential is obtained for the various distinguishable states of Pb adatoms.

REFERENCES

1. D.M. Kolb, in "Adv. Electrochem. and Electrochem. Eng.", Eds. H. Gerischer and C. Tobias, Wiley Interscience, New York, 11 (1978) 125.
2. B.E. Conway and H. Angerstein-Kozlowska, Acc. Chem. Res., 14 (1981) 49.
3. R.R. Adzic, in "Adv. Electrochem. and Electrochem Eng.", Eds. H. Gerischer and C. Tobias, Wiley Interscience, New York, 15 (1985) 159.
4. F.G. Will and C.A. Knorr, Zeit. Elektrochem., 64 (1960) 258.
5. B.E. Conway, in "Ionic Hydration in Chemistry and Biophysics, Elsevier Publ. Co., Amsterdam, 1981.
6. B.E. Conway, Prog. Surf. Sci., 16 (1984) 1.
7. G. Kokkinidis, J. Electroanal. Chem., 201 (1986) 217.
8. G.V. Hevesy, Physik. Z., 13 (1912) 715.
9. K.F. Herzfeld, Physik. Z., 14 (1913) 29.
10. L.B. Rogers, D.P. Krause, J.C. Griess, Jr., and D.B. Ehrlinger, J. Electrochem. Soc., 95 (1949) 33.
11. M. Haissinsky, J. Chim. Phys., 43 (1946) 21.
12. M. Haissinsky, Experientia, 8 (1952) 125.
13. M.M. Nicholson, J. Amer. Chem. Soc., 79 (1957) 7.
14. M.M. Nicholson, Anal. Chem., 32 (1960) 1058.
15. T. Millis and G.M. Wills, J. Electrochem. Soc., 100 (1953) 452.
16. E. Schmidt and H.R. Gygax, Chimia, 16 (1962) 165.
17. E. Schmidt and N. Wüthrich, J. Electroanal. Chem., 34 (1972) 377.
18. E. Schmidt and S. Stucki, J. Electroanal. Chem., 43 (1973) 425.
19. S. Bruckenstein and D.T. Napp, J. Amer. Chem. Soc., 90 (1958) 6303.
20. V.A. Vicente and S. Bruckenstein, Anal. Chem., 44 (1972) 297.
21. V.A. Vicente and S. Bruckenstein, Anal. Chem., 45 (2973) 2036.
22. J.W. Shultze and F.D. Koppitz, Electrochim. Acta, 21 (1976) 327., 337.
23. K.J. Vetter and J.W. Schultze, Ber. Bunsenges, Phys. Chem., 76 (1972) 920.
24. J.W. Schultze and K.J. Vetter, Electrochim. Acta, 19 (1973) 63.

25. J.W. Schultze, Ber. Bunsenges. Phys. Chem., 74 (1970) 705.

26. W.J. Lorenz, H.D. Hermann, N. Wüthrich, and F. Hilbert, J. Elctrochem. Soc., 121 (1974) 1167

27. B.J. Bowles, Electrochim. Acta, 15 (1970) 589, 737.

28. T. Takamura, K. Takamura, W. Nippe and E. Yeager, J. Electrochem. Soc., 117 (1970) 626.

29. R. Adzic, E. Yeager and B.D. Cahan, J. Electrochem. Soc., 121 (1974) 474.

30. D.M. Kolb, Ber. Bunsenges, Phys. Chem., 77 (1973) 891.

31. D.M. Kolb, M. Przasnyski and H. Gerischer, J. Electroanal. Chem., 54 (1978) 25.

32. I. Fried and H. Barak, J. Electroanal. Chem., 30 (1971) 279.

33. D.M. Kolb and H. Gerischer, Surf. Sci., 51 (1975) 323.

34. M.M. Nicholson, J. Electrochem. Soc., 121 (1974) 734.

35. J.O. Besenhard and H.P. Fritz, Electrochim. Acta, 20 (1975) 513.

36. B.E. Conway, K. Tellefsen and S. Marshall in J. D. E. McIntyre, M.J. Weaver and E.B. Yeager, Eds. Proc. of the Symposium on the Chemistry and Physics of Electrocatalysis, ECS, Princeton, NJ, 1984, P. 15.

37. Xue-Kun Xing, P. Abel, R. McIntyre and D. Scherson, J. Electroanal. Chem., 216 (1987) 261.

38. E. Schmidt and H.R. Gygax, J. Electroanal. Chem., 13 (1967) 378.

39. K. Engelsman, E.J . Lorenz and E. Schmidt, J. Electroanal. Chem., 114 (1980) 1.

40. T. Takamura and M. Sakamoto, J. Electroanal. Chem., 56 (1974) 249.

41. T. Takamura, F. Wanatabe and K. Takamura, Electrochim. Acta, 19 (1974) 933.

42. J.D.E McIntyre and D.E. Aspnes, Surf. Sci. 24 (1971) 417.

43. T. Takamura, Y. Sato and K. Takamura, J. Electroanal. Chem., 41 (1973) 31.

44. J.D.E. McIntyre, in " Adv. Electrochem. and Electrochem. Eng.", Ed. R.H. Muller, Wiley Interscience, New York, 9 (1973) 939.

45. J. Horkans, B.D. Cahan and E. Yeager, J. Electrochem. Soc., 122 (1975) 1585.

46. J.W. Schultze and D. Dickertmen, Surf. Sci., 54 (1976) 489.

47. A. Hamelin, J. Electroanal. Chem., 165 (1984) 167.

48. A.N. Frumkin and B. Slygin, Acta Physicochim. URSS., 3 (1935) 791.

49. A.N. Frumkin and B. Slygin, Acta Physicochim. URSS., 5 (1936) 819.

50. B.E. Conway, H. Angerstein-Kozlowska, W.B.A. Sharp and E. Criddle, Anal. Chem., 45 (1973) 133.

51. B.E. Conway, H. Angerstein-Kozlowska and W.B.A. Sharp, Symposium on Electrocatalysis, The Electrochemical Society, San Francisco, 1973, p. 94.

52. W.B.A. Sharp, Ph.D. Thesis, University of Ottawa, 1976.

53. J. Clavilier, J. Electroanal. Chem., 107 (1980) 211.

54. D.M. Newns, J. Chem. Phys., 50 (1969) 4572.

55. T.L. Einstein, Surf. Sci., 83 (1979) 141.

56. J. Koutecky, Phys. Rev., 108 (1957) 13.

57. A. Bewick, K. Kunimatsu, J. Robinson and J.W. Russell, J. Electroanal. Chem., 119 (1981) 175.

58. G.A. Sormarjai, in "Principles of Surface Chemistry", p. 36, Prentice Hall, N.J., (1972).

59. J.R. Smith, Ed., Topics in Current physics, Springer-Verlag, 19 (1980) 1.

60. J.H. Van Vleck., Rev. Mod. Phys., 34 (1962) 681.

61. N.R. Burke, Surf. Sci., 58 (1976) 349.

62. M.C. Desjonqueres and D. Spanjaard, J. Phys. C: Solid State Phys., 15 (1982) 4007.

63. P.M. Marcus, J.E. Demuth and D.W. Jepsen, Surf. Sci., 53 (1975) 501.

64. J.E. Demuth, D.W. Jepsen and P.M. Marcus, Phys. Rev. Lett., 31 (1973) 540.

65. M.A. Van Hove and S.Y. Tong, J. Vac. Sci. Technol., 12 (1978) 230.

66. J.N. Brønsted and N.L. Ross-Kane, J. Am. Chem. Soc., 53 (1931) 3624.

67. B.E. Conway and E. Gileadi, Trans. Far. Soc., 58 (1962) 2493.

68. J.P. Biberian and G.A. Somarjai, J. Vac. Sci. Technol., 16 (1979) 2073.

69. J.P. Biberian, Surf. Sci., 74 (1978) 437.

70. J.P. Biberian and M. Huber, Surf. Sci., 55 (1976) 259.

71. M. Huber and J. Oudar, Surf. Sci., 47 (1975) 605.

72. T.E. Madey and J.T. Yates, Jr., Chem. Phys., Lett., 51 (1977) 77.

73. M.W. Breiter, Electrochim. Acta, 8 (1963) 925.

74. V.S. Bagotzky, Y.B. Vasillyev, J. Weber and J.N. Pirtskhaleva, J. Electroanal. Chem., 27 (1970) 31.

75. D.M. Novak and B.E. Conway, J. Chem. Soc., Far. Trans. 1, 77 (1981) 2341.

76. H. Angerstein-Kozlowska, B.E. Conway, B. Barnett and J. Mozota, J. Electroanal. Chem., 100 (1977) 417.

77. Khr. Iv. Noninski and E.M. Lazarova, Elektrokhimiya, 9 (1979) 673.

78. E. Schmidt, P. Moser and W. Riesen, Helv. Chim. Acta, 46 (1963) 2285.

79. E. Schmidt and N. Wüthrich, J. Electroanal. Chem., 28 (1970) 349.

80. R.J. Watts-Tobin, Philos. Mag., 6 (1961) 133.

81. J.O'M. Bockris, M.A.V. Devanathan and K. Müller, Pro. Roy. Soc., London, A274 (1963) 55.

82. S.L. Marshall and B.E. Conway, J. Chem. Phys., 81 (1984) 923.

83. B.E. Conway and H.P. Dhar, Croat. Chim. Acta, 45 (1973) 173.

84. A.N. Frumkin. Z. Phys. Chem., 103 (1923) 43.

85. D.C. Grahame, Z. Elektrochem., 59 (1955) 740.

86. R. Payne, in "Adv. Electrochem. and Electrochem. Eng.", Eds., H. Gerischer and C. Tobias, Wiley Interscience, New York, 7 (1970) 1.

87. R. Parsons, Electrochim. Acta, 21 (1976) 681.

88. S. Minc, J. Jastrzebska and M. Brzostowska, J. Electrochem. Soc., 108 (1961) 1160.

89. R. Payne, J. Phys. Chem., 71 (1967) 1548.

90. W.R. Fawcett and R.O. Loutfy, Can. J. Chem., 51 (1973) 230.

91. D.C. Grahame, J. Electrochem. Soc., 98 (1951) 343.

92. S. Minc, and M. Brzostowska, Rocz. Chem., 34 (1960) 1109.

93. W.R. Fawcett and M.D. Mackey, J. Chem. Soc. Far. Trans. 1, 69 (1973) 634.

94. Z. Borkowska and W.R. Fawcett, Can. J. Chem., 59 (1981) 710.

95. R. Payne, J. Amer. Chem. Soc., 89 (1967) 489.

96. G.J. Hills and R.M. Reeves, J. Electroanal. Chem., 38 (1972) 1.

97. Z. Borkowska and W.R. Fawcett, Can. J. Chem., 60 (1982) 1787.

98. L.M.G. Gordon and B.E. Conway, J. Phys. Chem., 73 (1969) 3609.

99. W.R. Fawcett, J. Phys. Chem., 82 (1978) 1385.

100. R. Payne, J. Electroanal. Chem., 47 (1973) 265.

101. V.D. Bezugly and L.A. Korshikov, Elektrokhimiya, 1 (1965) 1422; 3 (1967) 309.

102. H.C. Nguyen, A. Jenard and H. D. Hurwitz, J. Electroanal. Chem., 103 (1979) 399.

103. R.J. Watts-Tobin and N.F. Mott, Electrochim. Acta, 4 (1961) 79.

104. S. Levine, G.M. Bell and A.L. Smith, J. Phys. Chem., 73 (1969) 3534.

105. J.O'M. Bockris and M.A. Habib, J. Electroanal. Chem., 65 (1975) 423.

106. R. Parsons, J. Electroanal. Chem., 8 (1964) 93.

107. B.B. Damaskin, Elektrokhimiya, 1 (1965) 63.

108. B.B. Damaskin and A.N. Frumkin, Electrochim. Acta, 19 (1974) 173.

109. R. Parsons, J. Electroanal. Chem., 59 (1975) 229.

110. J.R. Macdonald and C.A. Barlow, Jr., J. Chem. Phys., 36 (1962) 3062.

111. W.R. Fawcett and R.M. de Nobriga, J. Phys. Chem., 86 (1982) 371.

112. C. Herring and M.H. Nicholas, Rev. Mod. Phys., 21 (1949) 185.

113. M.S. Metsik, V.D. Perevertaev, V.A. Liopo, G.T. Timoshtchenko and A.B. Kiselev, J. Colloid Interface Sci., 43 (1973) 662.

114. G.E. Van Gils, J. Colloid Interface Sci., 30 (1969) 272.

115. E. Gileadi, in "Electrosorption", Plenum Press, New York, 1967.

116. J.A. Butler, J. Phys. Chem., 34 (1932) 2286.

117. R.G. Barradas and B.E. Conway, J. Electroanal. Chem., 6 (1963) 314.

118. E. Gileadi, J. Electroanal. Chem., 11 (1966) 137.

119. T. Bejerano, Ch. Forgacs and E. Gileadi, J. Electroanal. Chem., 27 (1970) 69.

120. E. Gileadi, Collect. Czech. Chem. Comm., 36 (1971) 464.

121. E. Gileadi and B.E. Conway, in "Modern Aspects of Electrochemistry, Vol. 3, Chapter 5, Eds. J.O'M. Bockris and B.E. Conway, Butterworths, London, 1974.

122. E. Gileadi and G. Stoner, J. Electrochem. Soc., 118 (1971) 1316.

123. C. Kemball, Proc. Roy. Soc., London, A187 (1946) 73.

124. C. Kemball, Proc. Roy. Soc., London, A187 (1946) 117.

125. B.E. Conway, J. Solution Chem., 7 (1978) 721.

126. B.E. Conway, W.B.A. Sharp and H. Angerstein-Kozlowska, J. Chem. Soc., Far. Trans. 1, 74 (1978) 1373.

127. H. Angerstein-Kozlowska and B.E. Conway, J. Electroanal. Chem., 95 (1979) 1.

128. B. Barnett, Ph.D. Thesis, Uninersity of Ottawa, 1981.

129. N.P. Berezina and N.V. Nikolaeva-Fedorovich, Elektrokhimiya, 3 (1967) 255.

130. M.Z. Hassan and S. Brückenstein, Analytical Chem., 46 (1974) 1962.

131. R.A. Bonewitz and G.M. Schmid, J. Electrochem. Soc., 117 (1970) 1367.

132. J. Horkans, B.D. Cahan and E. Yeager, Surf. Sci., 46 (1974) 1.

133. J.N. Gaur and G.M. Schmid, J. Electroanal. Chem., 24 (1970) 279.

134. H. Angerstein-Kozlowska, in "Comprehensive Treatise of Electrochem. Vol. 9 Eds. E. Yeager, J. O'M. Bockris, B.E. Conway and S. Sarangapani, Plenum Publish., 1984, p. 15.

135. K. Tellefsen, Ph.D. Thesis, University of Ottawa, 1988.

136. B.E. Conway, Proc. Roy. Soc., London, A256 (1960) 128.

137. D.J. Ives and G.J. Janz, in "Reference Electrodes, Theory and Practice", Academic Press, New York, 1961.

138. A.M. Feltham and M. Spiro, Chem. Revs., 71 (1971) 177.

139. M.W. Breiter, Trans. Far. Soc., 61 (1965) 749.

140. M.W. Breiter, Electrochim. Acta, 10 (1965) 543.

141. D.A.J. Rand and R. Woods, J. Electroanal. Chem., 35 (1972) 209.

142. D.F. Untereker and S. Bruckenstein, J. Electrochem. Soc., 121 (1974) 360.

143. T. Fujinaga and S. Sakamoto, Pure and Appl. Chem., 52 (1980) 1387.

144. R. De Levie and J.C. Kreuser, J. Electroanal. Chem., 38 (1972) 239.

145. E.R. Gonzalez and S. Srinivasan, Electrochim. Acta, 27 (1982) 1425.

146. T. Gramstad and R.M. Haszeldine, J. Chem. Soc., Part III (1957) 4069.

147. B.E. Conway and D.F. Tessier, Int. J. Chem. Kin., 13 (1981) 925.

148. T. Fujinaga and I. Sakamoto, J. Electroanal. Chem., 73 (1976) 235.

149. D.W. Wilkison, Ph.D. Thesis, University of Ottawa, 1987.

150. B.E. Conway, H. Angerstein-Kozlowska, F.C. Ho, J. Klinger, B. Macdougall and S. Gottesfeld, Far. Disc. Chem. Soc., 56 (1973) 199.

151. T. Bielgler, D.A.J. Rand and R. Woods, J. Electroanal. Chem., 29 (1971) 269.

152. A.A. Michiri, A.G. Pshchenichnikov and R.Kh. Burshtein, Elektrokhimiya, 8 (1972) 364.

153. S. Srinivasan and E. Gileadi, Electrochim. Acta, 11 (1966) 321.

154. E. Laviron, J. Electroanal. Chem., 34 (1972) 333, 463; 39 (1972) 1; 52 (1974) 355, 395.

155. H. Angerstein-Kozlowska, J. Klinger and B.E. Conway, J. Electroanal. Chem., 75 (1977) 45.

156. J.E.B. Randles, Trans. Faraday Soc., 44 (1948) 327.

157. A. Sevick, Coll. Czech. Chem. Comm., 13 (1948) 349.

158. P. Delahay and G. Perkins, J. Phys. Coll. Chem., 55 (1951) 586; 1146.

159. R.S. Nicholson and I. Shain, Anal. Chem., 36 (1964) 706.

160. S. Srinivasan and E. Gileadi, Electrochim. Acta, 11 (1966) 321.

161. D.C.W. Kannangara, Ph.D. Thesis, University of Ottawa, 1985.

162. G.A. Garwood, Jr., and A.T. Hubbard, Surf. Sci., 118 (1982) 223.

163. D.C. Grahame, Chem. Rev., 41 (1947) 441.

164. S. Trasatti, J. Chem. Soc., Far. Trans., 68 (1974) 229.

165. S. Trasatti, J. Electroanal. Chem., 54 (1974) 437.

166. W.R. Fawcett, B.M. Ikeda and J.B. Sellan, Can. J. Chem., 57 (1979) 2268.

167. A. De Battisti and S. Trasatti, J. Electroanal. Chem., 48 (1973) 213.

168. T.E. Crum, Ph.D. Thesis, University of Massachusettes, 1971.

169. H. Angerstein-Kozlowska, B. Macdougall and B.E. Conway, J. Electroanal. Chem., 39 (1972) 287.

170. T. Fujinaga and I. Sakamoto, J. Electroanal. Chem., 67 (1976) 201.

171 I.S. Perelygin, Optics and Spectrosc., 13 (1962) 198.

172. Z. Kecki, Roczniki Chem., 44 (1970) 847.

173. C. Nguyen Van Huong, J. Electroanal. Chem., 194 (1985) 131.

174. R. Gambert and H. Baumgartel, J. Electroanal. Chem., 183 (1985) 315.

175. J.F. Coetzee and G.P. Cunningham, J. Am. Chem. Soc., 87 (1965) 2529.

176. C.H. Springer, J.F. Coetzee and R.L. Kay, J. Phys., Chem., 73 (1969) 471.

177. R. Zana, G. Perron and J.E. Desnoyers, J. Solut. Chem., 8 (1979) 729.

178. R.L. Kay, J. Amer. Chem. Soc., 82 (1960) 2099.

179. J.D. Garnish and R. Parsons, Trans. Far. Soc., 63 (1967) 1754.

180. A.N. Dey, J. Electrochem. Soc., 114 (1967) 823.

181. B. Burrows and S. Kirkland, J. Electrochem. Soc., 11 (1968) 1164.

182. V.S. Bagotzky, Y.B. Vasillyev, J. Weber and J.N. Pirtskaleva, J. Electroanal. Chem., 27 (1970) 31.

183. M. Girgis, E. Ghali and A. Wieckowski, Electrochim. Acta, 31 (1986) 681.

184. E. Ghali and B. Dandapani, The metallurgical Transactions, 15B (1984) 605.

185. J.R. Vilche and K. Jüttner, Electrochim. Acta, 32 (1987) 1567.

186. B.C. Schardt, J.L. Stickney, D.A. Stern, A. Wieckowski, D.C. Zaplen and A.T. Hubbard, Surf. Sci., 175 (1986) 520.

187. A.M. Frumkin, Ergebn. Exakt. Naturwiss., 7 (1928) 235.

188. F.W. Schapink, M. Oudeman, K.W. Leu and J.N. Hell, Trans. Far. Soc., 56 (1960) 415.

189. R. Parsons and P.C. Symons, Trans. Far. Soc., 64 (1968) 1077.

190. W. Lorenz and G. Krüger, Z. Phys. Chem., 221 (1962) 231.

191. N.B. Grigor'ev, V.P. Kuprin and Yu.M. Loshkarev, Elektrokhimiya, 11 (1975) 638.

192. N.B. Grigor'ev, and D.N. Machavariani, Elektrokhimiya, 6 (1975) 89.

193. H. Wroblowa and M. Green, Electrochim. Acta, 8 (1963) 679.

194. R.F. Lane and A.T. Hubbard, J. Phys. Chem., 79 (1975) 808.

195. K.J. Vetter and D. Berndt, Zeit. Elektrochem., 62 (1958) 378.

196. K.J. Vetter and J.W. Schultze, J. Electroanal. Chem., 43 (1972) 131; 141.

197. R. Parsons, J. Electroanal. Chem., 21 (1969) 35.

198. P. Stonehart, H. Angerstein-Kozlowska and B.E. Conway, Proc. Roy. Soc., London, A310 (1969) 541.

199. L. Rouillier and E. Laviron, J. Electroanal. Chem., 157 (1983) 193.

200. T.E. Tessier and B.E. Conway, Electrochim. Acta, 30 (1985) 1703.

201. E.L. Yee, R.J. Cave, K.L. Guyer, P.D. Tyma and M.J. Weaver, J. Amer. Chem. Soc., 101 (1979) 1131.

202. M.J. Weaver, J. Phys. Chem., 83 (1979) 1748.

203. J.N. Agar, in "Adv. Electrochem. and Electrochem. Eng.", Eds. P. Delahay and C.W. Tobias, Wiley Interscience, New York, 3 (1963) 31.

204. A.J. deBethune, T.S. Licht and N. Swendeman, J. Electrochem. Soc., 106 (1959) 616.

205. B.G. Cox and A.J. Parker, J. Amer. Chem. Soc., 95 (1973) 6879.